

**Studies into solid core drug delivery system using
haemoglobin as a model drug and supercritical fluid
processing for encapsulation**

Ruchir Bhomia (M. Pharm)

A thesis submitted to the University of Greenwich in partial fulfilment of the
requirements for the degree of Doctor of Philosophy

June 2015



University of Greenwich
School of Science
Chatham Maritime
Kent, ME4 4TB, UK

DECLARATION

I certify that this work has not been accepted in substance for any degree, and is not concurrently being submitted for any degree other than that of Doctor of Philosophy being studied at the University of Greenwich. I also declare that this work is the result of my own investigations except where otherwise identified by references and that I have not plagiarised the work of others.

Signature (Candidate) _____

Date: _____

Signature (Supervisor) _____

Date: _____

Acknowledgements

I would like to express gratitude to my supervisors, Dr Vivek Trivedi and Dr Nicola Coleman for their patient guidance, constructive criticism and encouragement throughout my research work. A very special thanks to Professor John Mitchell for funding my research and providing me great experience towards industry based projects. I wish to acknowledge the help provided by Dr. Ian Slipper towards the SEM and XRD measurements and to Samuel Owusu-Ware for DSC analysis. I am also thankful to Dr. Bruce Alexander along with other members of the School of Science for giving me the opportunity to enhance my scientific skills.

I am particularly grateful to Livia Pagnan and Yash Joshi for helping me with protein desorption studies along with Mehak Rafiq, Shashi Rudrangi, Hai Pham, Andrew Hurt and Darren Pink, my fellow colleagues and friends for making this journey so pleasant.

I would like to convey my genuine appreciation for Professor Steve Wicks and all the staff and students in Medway Centre for Pharmaceutical Sciences for making me feel so welcome, particularly George Vine, Joanna Thorne, Marie Pettit and Tammy Savage.

Thanks also to my family and friends for all their words of encouragement and support throughout.

Abstract

The aim of this project was to formulate a solid core drug delivery system for oral delivery of proteins using silica as core material, haemoglobin as model drug and supercritical fluid processing as encapsulation technique. Silica particles of different morphology were used as a carrier material for protein immobilisation and fatty acids coating was performed using supercritical carbon dioxide (CO₂) as a processing media.

The melting behaviour of saturated fatty acids (lauric, myristic, palmitic and stearic acid) and pluronics (F-38, F-68, F-77, F-127 and F-108) were studied under pressurised CO₂ to identify the coating parameters. These excipients showed a melting point depression in the range of 10 to 20 °C in pressurised CO₂. In the case of fatty acids the decrease in melting point was inversely proportional to the carbon chain length and directly related to the polarity of carbonyl group. Whereas, melting point depression for all pluronics was similar and was attributed to the high cohesive energy density of these polymers. This phenomenon was used to encapsulate the thermolabile protein molecules in pressurised CO₂ at low temperatures.

The stability of bovine haemoglobin (bHb) was studied by ultraviolet-visible and circular dichroism spectroscopy. Thermal, storage and agitation stability were studied to identify the processing parameters for the storage, adsorption and desorption processes.

Three morphologically different silica particles were studied as potential inorganic carrier for the protein. The particles were characterised by nitrogen adsorption and scanning electron microscopy and the maximum protein adsorption and kinetics was determined at pH 6. The bHb adsorption on silica was found to be irreversible, hence application of pluronics as a displacer was also studied.

Finally, the bHb adsorbed particles were coated with fatty acids by supercritical fluid processing and solvent evaporation methods. The highest bHb release was obtained from S_{FP} (Syloid FP-244) silica in comparison to other silica particles in pH 6.8 phosphate buffer. S_{FP} based formulation also showed a trend in the protein release which was dependent on the solubility of fatty acids in the release media. The highest release was obtained from myristic acid coated solid core drug delivery system (SCDDS) followed by palmitic and stearic acid. Lauric acid coated S_{FP} formulations led to changes in protein conformations, hence omitted from these studies. The release studies of myristic acid based SCDDS in simulated gastric and intestinal fluids showed that fatty acid coating provided enteric properties to the formulation. It can be concluded from these studies that SCDDS prepared using mesoporous silica as core and fatty acids as coating material can be an effective drug delivery system for the oral delivery of biomolecules.

TABLE OF CONTENTS

Declaration	i
Acknowledgements	ii
Abstract	iii
Table of contents	iv-viii
List of abbreviations.....	ix-xi
List of tables and figures	xii-xvii
Chapter 1 Introduction.....	1-38
1.1 Protein and peptides	1
1.2 Biologics market	4
1.3 Protein formulation and delivery	5
1.3.1 Invasive delivery	6
1.3.2 Non-invasive delivery	7
1.4 Supercritical fluids	11
1.4.1 SCF technology in pharmaceutical research.....	13
1.5 Haemoglobin.....	17
1.5.1 Haemoglobin structure and function.....	18
1.6 Solid core drug delivery system.....	20
1.7 Aim and objectives.....	22
References	24
Chapter 2 Instrumentation and theory of experimental techniques	39-56
2.1 Ultraviolet-visible spectrophotometry	39
2.2 Circular dichroism spectroscopy	41
2.3 Differential scanning calorimetry.....	44
2.4 Powder X-ray diffraction	45
2.5 Supercritical phase monitor.....	48

2.6 Scanning electron microscopy	49
2.7 Brunauer, Emmett and Teller and Barrett, Joyner and Halenda models	52
2.8 Supercritical fluid instrument.....	53
References	55
Chapter 3 Materials and methods	57-64
3.1 Materials.....	57
3.2 Methods.....	58
3.2.1 Melting and solidification point determination in supercritical phase monitor	58
3.2.2 Differential scanning calorimetry	60
3.2.3 Powder X-ray diffraction	60
3.2.4 Phosphate buffer solutions	60
3.2.5 Procedure for thermal stability studies of bHb by UV spectroscopy.....	61
3.2.6 Procedure for thermal stability studies of bHb by CD spectroscopy	61
3.2.7 Procedure for six-hours stability of bHb	61
3.2.8 Procedure for inter-day stability of bHb	62
3.2.9 Procedure for agitation stability of bHb	62
3.2.10 Adsorption of bHb on silica particles	62
3.2.11 BET studies on silica particles	63
3.2.12 SEM analysis of silica particles	64
3.2.13 Phosphate buffer pH 6.8 (USP).....	64
Chapter 4 Supercritical fluid processing of excipients	65-90
4.1 Introduction	65
4.1.1 Fatty acids	65
4.1.2 Pluronics.....	67
4.2 Materials and Methods	69
4.2.1 Materials	69
4.2.2 Melting point determination by supercritical phase monitor	69

4.2.3 Differential scanning calorimetry	69
4.2.4 Powder X-ray diffraction	69
4.3 Results and discussion	69
4.3.1 Effect of pressure and melting point depression of fatty acids in CO ₂	70
4.3.2 Solidification of fatty acids in CO ₂	73
4.3.3 Effect of pressure and melting point depression of pluronics in CO ₂	75
4.3.4 Differential scanning calorimetric analysis.....	80
4.3.5 Powder X-ray diffraction analysis	82
4.4 Conclusions	84
References	85
Chapter 5 Stability of bovine haemoglobin	91-115
5.1 Introduction	91
5.2 Thermal stability of bHb	92
5.2.1 Analysis by UV spectroscopy	92
5.2.2 Analysis by CD spectroscopy	96
5.2.3 Discussion	99
5.3 Six hours stability of bHb	102
5.4 Inter-day stability of hemoglobin.....	104
5.4.1 Analysis by UV spectroscopy	104
5.4.2 Analysis by CD spectroscopy	106
5.4.3 Discussion	109
5.5 Agitation stability.....	111
5.6 Conclusions	112
References	113
Chapter 6 Characterisation of silica particles & adsorption of bHb.....	116-138
6.1 Introduction	116
6.2 Characterisation of silica particles	116

6.2.1 Materials and methods	116
6.2.2 Results and discussion.....	117
6.3 Adsorption of bHb on silica particles	126
6.3.1 Materials and methods	128
6.3.2 Results and discussion.....	128
6.4 Conclusions	134
References	136
Chapter 7 Effect of pluronics on desorption of bHb from silica particles	139-160
7.1 Introduction	139
7.2 Materials and methods	140
7.2.1 Materials.....	140
7.2.2 Adsorption protocol.....	140
7.2.3 Desorption procedure	140
7.2.4 Effect of pluronics on bHb conformation	140
7.3 Results	140
7.3.1 Desorption from S _{LP} particles	141
7.3.2 Desorption from S _S particles	144
7.3.3 Desorption from S _{FP} particles	148
7.3.4 Effect of pluronics on bHb conformation	152
7.4 Discussion	154
7.5 Conclusions	158
References	160
Chapter 8 Coating and release studies	161-183
8.1 Introduction	161
8.2 Coating of silica particles with FAs	161
8.2.1 Materials and methods	162
8.3 Results	164

8.3.1 <i>In-vitro</i> release studies at pH 6.8.....	164
8.3.2 <i>In-vitro</i> release studies at pH 1.2 and 6.8.....	173
8.3.3 Conformation of bHb released from S _{FP} formulation	175
8.4 Discussion	177
8.5 Conclusions.....	181
References.....	182
Chapter 9 Summary and future work.....	184-188
9.1 Summary	184
9.2 Future work	186
References.....	188
Appendix.....	189-206
A) Thermal stability of bHb	189
A.1) UV spectra	189
A.2) CD spectra	192
B) Six hours stability of bHb	195
B.1) UV spectra	194
B.2) CD spectra.....	196
C) Inter-day stability of bHb	198
C.1) UV spectra	198
C.2) CD spectra.....	201
D) Publications.....	204

List of Abbreviations

Symbol	Description
°C	Degree celcius
µm	Micrometer
2, 3 BPG	2, 3-bisphosphoglycerate
2	Diffraction angle
A	Absorbance
Å	Angstrom
ABPR	Automatic back pressure regulator
BET	Brunauer, Emmett and Teller
bHb	Bovine haemoglobin
BJH	Barrett, Joyner and Halenda
CD	Cyclodextrin
CD	Circular dichroism
CDNN	Circular dichroism neural network
cm	Centimeter
CO ₂	Carbon dioxide
CPP	Cell penetrating peptides
Cu	Copper
dL	Deciliter
DSC	Differential scanning calorimetry
ELISA	Enzyme linked immunosorbant assay
FA	Fatty acids
g	Gram
GAS	Gaseous anti-solvent
GRAS	Generally regarded as safe
Hb	Haemoglobin
HbA	Human haemoglobin
HbS	Sickel cell haemoglobin
HIV	Human immunodeficiency virus
ICDD	International centre for diffraction data
kcal	Kilocalorie

KH ₂ PO ₄	Potassium hydrogen phosphate
kV	Kilovolt
l	Litre
LA	Lauric acid
LAL	Limulus ameocyte lysate
LCP	Left circularly polarised
m	Meter
m°	Millidegrees
MA	Myristic acid
mg	Milligram
Mins	Minutes
ml	Mililiter
mm	Millimeter
Na ₂ HPO ₄	Disodium hydrogen phosphate
Ni	Nickel
nm	Nanometer
O ₂	Oxygen
PA	Palmitic acid
PAGE	Polyacrylamide gel electrophoresis
P _c	Critical pressure
PEG	Polyethylene glycol
PEM	Photoelastic modulator
PEN	Pentane
PEO	Poly-ethyleneoxide
PGSS	Particles from gas saturated solution
pI	Iso-electric point
PPO	Poly-propyleneoxide
PXRD	Powder X-ray diffraction
RBC	Red blood cells
RCP	Right circularly polarised
RESS	Rapid expansion of supercritical solution
RP-HPLC	Reverse phase-High performance liquid

	chromatography
rpm	Rotations per minute
s	Second
SA	Stearic acid
SAS	Supercritical anti-solvent
SCCO ₂	Supercritical carbon dioxide
SCDDS	Solid core drug delivery system
SCF	Supercritical fluid processing
SDS	Sodium dodecyl sulphate
SEM	Scanning electron microscopy
S _{FP}	FP-244 syloid silica
SGF	Simulated gastric fluid
SIF	Simulated intestinal fluid
S _{LP}	Large particle silica
SPM	Supercritical phase monitor
S _S	Spherical silica
T	Temperature
TAT	Transactivating transcriptional activator
T _c	Critical temperature
T _m	Melting temperature
USP	United states pharmacopoeia
UV	Ultraviolet
UV/Vis	Ultraviolet-visible
	Ellipticity

LIST OF TABLES AND FIGURES

List of tables

Table 1.1 List and structure of amino acids	2-3
Table 1.2 A selective list of some functional roles for proteins.....	4
Table 1.3 Possible formulation options for therapeutic peptides/proteins	5-6
Table 1.4 Critical conditions of some compounds	11
Table 1.5 Density, viscosity and diffusivity comparison of different fluids	12
Table 3.1 Chemical reagents	57-58
Table 3.2 Phosphate buffer preparation	60
Table 4.1 Physical properties of saturated fatty acids	66
Table 4.2 Physical properties of pluronics	68
Table 4.3 Melting point depression of fatty acids	70
Table 4.4 Melting point of MA, PA and SA in pressurised CO ₂	71
Table 4.5 Solidification point of MA, PA and SA in CO ₂ at different pressure	73
Table 4.6 Difference in melting and solidification point of FAs at various pressure	74
Table 4.7 Melting point of pluronics in pressurised CO ₂	76
Table 6.1 Characteristics of silica particles by nitrogen sorption	124
Table 6.2 Comparison of BET results before and after adsorption of bHb.....	134
Table 8.1 Parameters for silica coating by SCF processing	163
Table 8.2 Dissolution data for F1 and F2 calculations	174
Table 8.3 Percentage content of secondary structures of untreated bHb and bHb released from MA coated S _{FP} formulations	176
Table 8.4 Adsorbed and desorbed amount of bHb from different silica particles with their physical characteristics.....	178
Table 8.5 Solubility of fatty acids in water at 20 °C	179

List of figures

Figure 1.1 Basic structure of amino acid..... 1

Figure 1.2 Three forms of alanine occurring between pH 2 and 12..... 1

Figure 1.3 Phase diagram of pure carbon dioxide..... 11

Figure 1.4 Structure of haemoglobin..... 18

Figure 1.5 Structure of heme..... 18

Figure 1.6 X-ray crystal structure of Hb from protein database 19

Figure 1.7 (a) R state and (b) T state of dimeric Hb 20

Figure 1.8 Schematic diagram of SCDDS preparation 22

Figure 2.1 Absorption of UV light by sample..... 39

Figure 2.2 Schematic diagram of a double beam UV spectrophotometer..... 41

Figure 2.3 Left (L) and right (R) circularly polarised components of plane polarised radiation:
[I] The two components have the same amplitude; [II] the components are of different
magnitude and the resultant (dashed line) is elliptically polarised. 42

Figure 2.4 Schematic diagram of CD Spectrometer..... 43

Figure 2.5 Schematic diagram of a heat flux DSC..... 45

Figure 2.6 Schematics of PXRD instrument 46

Figure 2.7 Schematics of X-ray tube..... 47

Figure 2.8 Schematic diagram of supercritical phase monitor 48

Figure 2.9 Diagram of sample holder..... 49

Figure 2.10 Schematics of SEM..... 50

Figure 2.11 Diagram showing electron beam through the condenser lens and aperture..... 51

Figure 2.12 Applications of SEM 51

Figure 2.13 Schematic presentation of SCF instrument..... 54

Figure 3.1 Various stages of the experiment (Pluronic F-68) 59

Figure 4.1 Structure of FAs a) Lauric acid, b) Linoleic acid 65-66

Figure 4.2 Generalised structure of a pluronic molecule.	68
Figure 4.3 P- T diagram (melting) of MA, PA and SA	72
Figure 4.4 P-T diagram (solidification) of FAs	74
Figure 4.5 P-T diagram of pluronics	77
Figure 4.6 Comparison of melting point depression of pluronics with PPO units.....	78
Figure 4.7 Comparison of melting point depression of pluronics with molecular weight	79
Figure 4.8 Thermograms of processed and unprocessed FAs	80
Figure 4.9 Thermograms of CO ₂ processed and unprocessed pluronics	81
Figure 4.10 Diffractograms of processed and unprocessed FAs	82
Figure 4.11 Diffractograms of processed and unprocessed pluronics	83
Figure 5.1 Analytical methods for protein characterisation	91
Figure 5.2 UV spectrum of bHb in pH 6 phosphate buffer	93
Figure 5.3 Thermal stability of bHb in pH 6 buffer (Absorbance at 405 and 274 nm)	94
Figure 5.4 Thermal stability of bHb in pH 7 buffer (Absorbance at 405 and 274 nm)	95
Figure 5.5 Thermal stability of bHb in pH 8 buffer (Absorbance at 405 and 274 nm)	96
Figure 5.6 Thermal stability of bHb in pH 6 buffer (Secondary structure content).....	97
Figure 5.7 Thermal stability of bHb in pH 7 buffer (Secondary structure content).....	98
Figure 5.8 Thermal stability of bHb in pH 8 buffer (Secondary structure content).....	99
Figure 5.9 : Six hours stability of bHb at pH 6, 7 and 8 (Absorbance at 405 and 274 nm) ..	102
Figure 5.10: Six hours stability (secondary structure content) of bHb at pH 6 (A), pH 7 (B) and pH 8 (C).....	103
Figure 5.11: Inter-day stability of bHb at pH 6 stored at 23 °C (A) and 4 °C (B)	104
Figure 5.12: Inter-day stability of bHb at pH 7 stored at 23 °C (A) and 4 °C (B)	105
Figure 5.13: Inter-day stability of bHb at pH 8 stored at 23 °C (A) and 4 °C (B)	106
Figure 5.14: Secondary structure content of bHb at pH 6 stored at 23 °C (A) and 4 °C (B) ..	107
Figure 5.15: Secondary structure content of bHb at pH 7 stored at 23 °C (A) and 4 °C (B) ..	108
Figure 5.16: Secondary structure content of bHb at pH 8 stored at 23 °C (A) and 4 °C (B) ..	108
Figure 5.17: Agitation stability of bHb UV results.....	111

Figure 6.1: Complete BET isotherm of S_{LP}	117
Figure 6.2: Types of sorption isotherms and hysteresis loops	118
Figure 6.3: Pore size distribution of S_{LP}	119
Figure 6.4: Cumulative pore volume of S_{LP}	120
Figure 6.5: BET isotherm of S_S	120
Figure 6.6: Pore size distribution of S_S by BJH model	121
Figure 6.7: Cumulative pore volume of S_S by BJH model	121
Figure 6.8: BET isotherm of S_{FP}	122
Figure 6.9: Pore size distribution of S_{FP} by BJH model	123
Figure 6.10: Cumulative pore volume of S_{FP} by BJH model	123
Figure 6.11: SEM micrographs of S_S at low and high magnification	124
Figure 6.12: SEM micrographs of S_{LP} at low and high magnification	125
Figure 6.13: SEM micrographs of S_{FP} particles	126
Figure 6.14: Adsorption isotherm of bHb on S_{LP}	129
Figure 6.15: Adsorption isotherm of bHb on S_S	129
Figure 6.16: Adsorption isotherm of bHb on S_{FP}	129
Figure 6.17: Adsorption kinetics of 2 mg/ml bHb solution on S_{LP}	131
Figure 6.18: Adsorption kinetics of 1 mg/ml bHb solution on S_S	131
Figure 6.19: Adsorption kinetics of 8 mg/ml bHb solution on S_{FP}	131
Figure 6.20: Inverse relationship between surface area and protein adsorption	132
Figure 6.21: Comparison of adsorbed protein with pore volume and pore diameter.....	133
Figure 7.1: bHb desorption from S_{LP} particles using F-38 as a displacer	141
Figure 7.2: bHb desorption from S_{LP} particles using F-68 as a displacer	142
Figure 7.3: bHb desorption from S_{LP} particles using F-77 as a displacer	143
Figure 7.4: bHb desorption from S_{LP} particles using F-127 as a displacer	143
Figure 7.5: bHb desorption from S_{LP} particles using F-108 as a displacer	144
Figure 7.6: bHb desorption from S_S particles using F-38 as a displacer	145

Figure 7.7: bHb desorption from S_S particles using F-68 as a displacer 145

Figure 7.8: bHb desorption from S_S particles using F-77 as a displacer 146

Figure 7.9: bHb desorption from S_S particles using F-127 as a displacer 147

Figure 7.10: bHb desorption from S_S particles using F-108 as a displacer 147

Figure 7.11: bHb desorption from S_{FP} particles using F-38 as a displacer 148

Figure 7.12: bHb desorption from S_{FP} particles using F-68 as a displacer 149

Figure 7.13: bHb desorption from S_{FP} particles using F-77 as a displacer 149

Figure 7.14: bHb desorption from S_{FP} particles using F-127 as a displacer 150

Figure 7.15: bHb desorption from S_{FP} particles using F-108 as a displacer 151

Figure 7.16: bHb desorption from S_{LP} particles by 1 mg/ml of pluronics 151

Figure 7.17: bHb desorption from S_{FP} particles by 1 mg/ml of pluronics 152

Figure 7.18: bHb desorption from S_S particles by 1 mg/ml of pluronics 152

Figure 7.19: UV spectra of bHb with various concentrations of pluronics F-127 153

Figure 7.20: Effect of F-127 concentration on bHb secondary structures 154

Figure 7.21: Pluronic adsorbed at hydrophilic surface in a pancake formation 157

Figure 7.22: Schematics of protein desorption by pluronics 157

Figure 8.1: Schematic diagram of coating by SCF processing 162

Figure 8.2: bHb release from S_{LP} based SCDDS with LA coating 165

Figure 8.3: bHb release from S_{LP} based SCDDS with MA coating 166

Figure 8.4: bHb release from S_{LP} based SCDDS with PA coating 166

Figure 8.5: bHb release from S_{LP} based SCDDS with SA coating 167

Figure 8.6: bHb release from S_S based SCDDS with LA coating 168

Figure 8.7: bHb release from S_S based SCDDS with MA coating 168

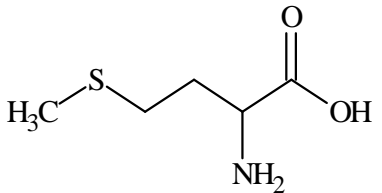
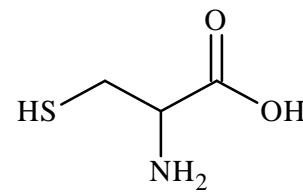
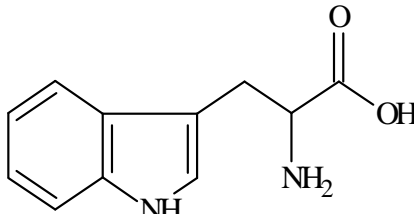
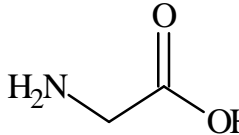
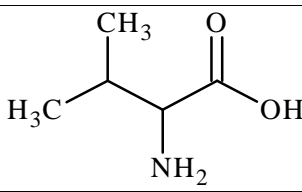
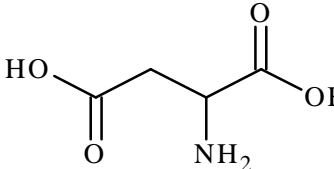
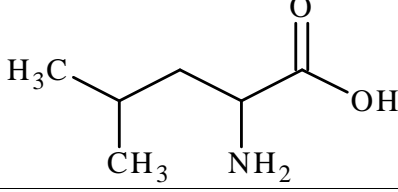
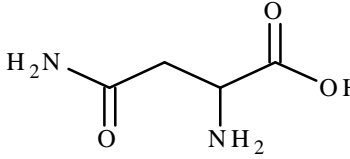
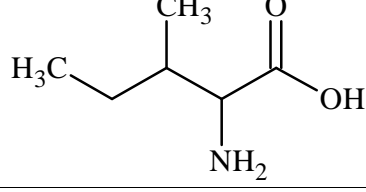
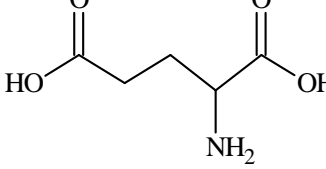
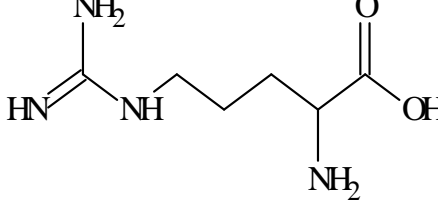
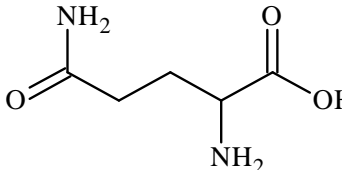
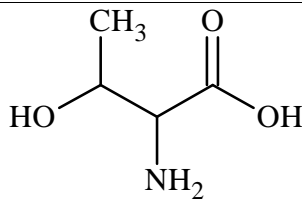
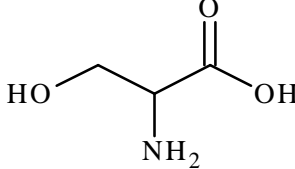
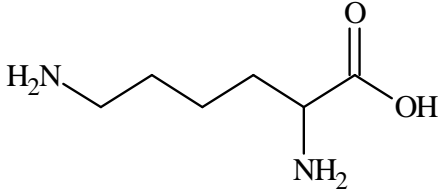
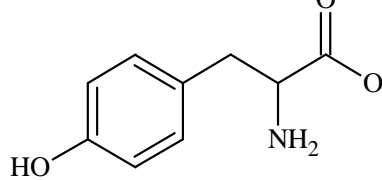
Figure 8.8: bHb release from S_S based SCDDS with PA coating 169

Figure 8.9: bHb release from S_S based SCDDS with SA coating 170

Figure 8.10: bHb release from S_{FP} based SCDDS with MA coating 171

Figure 8.11: bHb release from S_{FP} based SCDDS with PA coating 172

Figure 8.12: bHb release from S _{FP} based SCDDS with SA coating	172
Figure 8.13: Release studies from MA coated S _{FP} based SCDDS at pH 1.2 and 6.8.....	173
Figure 8.14: UV spectra of untreated bHb and bHb released from LA coated S _{FP} formulations	175
Figure 8.15: UV spectra of untreated bHb and bHb released from MA coated S _{FP} formulations	175

Amino Acid	Structure (Essential)	Amino Acid	Structure (Non-Essential)
Methionine		Cysteine	
Tryptophan		Glycine	
Valine		Aspartic Acid	
Leucine		Asparagine	
Isoleucine		Glutamic Acid	
Arginine		Glutamine	
Threonine		Serine	
Lysine		Tyrosine	

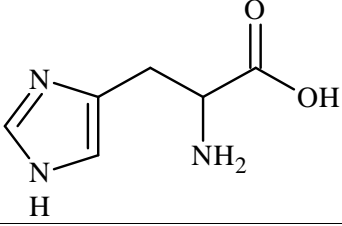
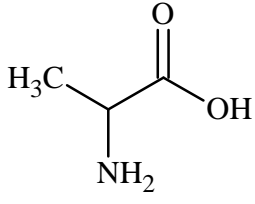
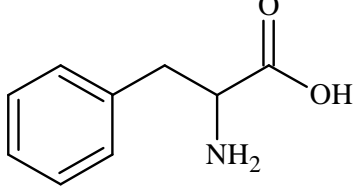
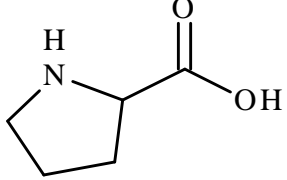
Histidine		Alanine	
Phenyl alanine		Proline	

Table 1.1: List and structure of amino acids [3]

The amino acids link together with a covalent peptide bond to form a long chain described as the primary structure of protein. The primary structure gives rise to secondary structure as a result of the spatial arrangements of amino acid residues in the primary sequence. The three basic units of the secondary structure are helix, strand and random coils [2]. In helix, the protein chain twists like a coiled spring where each turn contains 3.6 amino acid residues with the side chains pointing out from the helix [4]. In sheet conformation, the protein backbone is fully extended and based on the direction of two interacting strands which can be either parallel or antiparallel. Lastly, the residual fraction of amino acid sequence which cannot be classified under either helix or sheet is categorised as random coils. The overall packing of the various elements of secondary structure results in the tertiary structure of a protein. Finally, these separate protein chains (subunits or monomers) combine to form a well-defined structure known as the quaternary structure where subunits are held together by non-covalent forces *viz.* hydrophobic interactions, hydrogen bonds, or van der Waals interactions. This 3-dimensional quaternary structure is important for protein function which could be lost with any changes to the protein conformation [5]. Proteins perform a variety of functions within living organisms, including catalysing metabolic reactions, replicating DNA, responding to stimuli and as a carrier in transporting molecules from one location to another. Table 1.2 lists some functional roles of proteins.

Proteins	Function
Trypsin, DNA polymerases and ligases.	Enzymes or catalysis
Actin, myosin, tubulin.	Contraction
Collagen, keratin.	Structural and cytoskeletal
Insulin, growth factor, thyroid stimulating hormone.	Effectors
Immunoglobulin, thrombin.	Defence
Cytochrome oxidase, ferredoxin.	Electron transfer
Ferritin.	Storage
Haemoglobin.	Transport

Table 1.2: A selective list of some functional roles for proteins [2]

It is estimated that there are approximately 25,000 to 40,000 different genes in the human genome which can produce a large number of structurally and functionally different proteins. Therefore, disease may occur if these proteins contain any mutations and/or present in abnormally high/low concentrations [6]. Therapeutically active proteins and peptides, also known as biopharmaceuticals or biologics have emerged as promising candidates for the treatment of diseases such as diabetes, cancer and autoimmune diseases *etc.* [7]. The protein/peptide based molecules have also become highly important in recent years especially due to the advent of recombinant DNA technology to produce genetically modified biopharmaceuticals on a large scale [8].

1.2 Biologics market

There are more than 100 native and modified therapeutic proteins approved for the clinical use in the European Union and USA [9]. The 2010 sales of biologics was USD 108 billion with monoclonal antibodies accounting for almost half (48%) of the sales [9]. The biologics market is expected to be of USD 143.4 billion by 2015 and 220 billion by 2019 [10], [11].

This increase in the market of biologics has also intensified the development of innovative delivery strategies [12]. A literature review on various formulations for therapeutic proteins has been discussed in the next section.

1.3 Protein formulations and delivery

Parenteral administration is the most common route for therapeutic peptide/protein delivery but patient compliance and cost make it less favourable [13]. Therefore, a lot of research is being conducted towards the non-invasive administration of biomolecules. The development of drug delivery systems for biologics is a complex process and cannot be compared to small molecules [14]. A detailed knowledge of pharmacology, physicochemical properties and the therapeutic application of the protein is necessary in order to successfully prepare a novel drug delivery system for these molecules [14]. Table 1.3 lists possible formulation options for therapeutic peptides/proteins based on the key issue in protein therapy [15].

Key issues		Nano (nm)	Micron (μm)	Millimetre (mm)
Non-invasive delivery (across mucosal barrier)	Protein solution with permeability enhancers.	nano-carriers (polymeric, complexes, liposomes, solid lipid) surface modified for mucosal translocation (paracellular or transcellular /transcytosis)	micro-carriers and matrices for oral protein delivery.	
Intracellular delivery	protein conjugates with cell penetrating peptides or ligands for receptor mediated endocytosis; fusion proteins; stimuli responsive protein polymer conjugates	nano-carriers (polymeric, complexes, liposomes and solid lipid) surface modified with ligands for internalising receptors	micro-carriers for uptake by phagocytic cells; micro-carriers for lung deposition	

Biodistribution/ delivery across barriers	<p>protein conjugates for improved distribution (<i>e.g.</i> pegylated proteins/antibodies).</p> <p>protein conjugates or fusion proteins to cross biological barriers.</p>	<p>nano-carriers surface modified for improved distribution (pegylation and/or targeting ligands) nano-carriers surface modified (with ligands) to cross biological barriers.</p>		
Sustained release			<p>injectable microcarriers (polymeric liposomes, solid lipid)</p>	<p>implants: polymeric implants or scaffolds</p> <p>stimuli responsive matrices</p>

Table 1.3: Possible formulation options for therapeutic peptides/proteins [15]

Overall, large molecules formulations can be divided into two main categories *viz.* invasive and non-invasive which are discussed in next section.

1.3.1 Invasive delivery

The parenteral route is currently the main mode of protein delivery but lack of patient compliance requires development of sustained formulations. Current developments include; formulations based on encapsulation of protein into lipid based microparticles [16] or a polymeric matrix to control the release and achieve prolonged effect. Since the matrix remains in the body for a considerable period of time, materials used to formulate them must have non-toxic degradation products. Polyesters, polyanhydrides, and naturally occurring materials including gelatine, alginate and chitosan are amongst the most commonly used polymers to develop sustained release protein formulations [17]. Different methods to formulate the drug loaded polymeric microparticles include; solvent emulsification methods [18], spray drying and supercritical fluid processing [19]. The injectable sustained release formulations are appropriate for biologics which are present in the circulation and the therapy requires systemic exposure of the protein. A number of approved products such as Decapeptyl a LHRH (luteinising hormone

releasing hormone) analogue for prostate cancer and Nutropin (growth hormone) are available in the market [15]. The main disadvantages of microencapsulation are low loading capacity and exposure of proteins to harsh processing conditions such as high shear stress and organic-water solvent interface which may lead to structural changes in proteins. Alternative approaches such as preparation of spherical particles formulated by gradual dialysis of the solution against precipitating agents [20], or by cooling of a pre-heated supersaturated solution [21] have shown to maintain the conformation of some proteins [21]. In the dialysis method; a concentrated crystallisation buffer is allowed to pass slowly through the dialysis membrane, where it equilibrates with less concentrated solution containing protein. This process gradually increases the effective concentration of protein resulting in the formation of spherical protein particles of 0.04 to 200 microns [20]. Microsphere formation by cooling a preheated solution involves use of polyethylene glycol at a pH near to protein's isoelectric point to promote rapid nucleation and particle growth. Particles formed by this process were found to be uniformly spherical and of 1-2 μm [21]. Another way to make an injectable sustained release delivery system is to form *in situ* polymeric implants or microparticle systems [22]. Kranz & Bodmeier reported *in situ* phase inversion microencapsulation of small drug molecules in polylactide/glycolide or its copolymers with polyethylene oxide [23]. Polymer solution was prepared in an acceptable organic solvent such as N-methyl-2-pyrrolidone or dimethylsulfoxide which resulted in precipitation of polymer leading to encapsulation of the active component upon injection due to the dilution by *in vivo* aqueous environment. This strategy has been applied by many marketed formulations such as Lupron DepotTM which contains Leuprolide acetate and used in the treatment of prostate cancer [24].

1.3.2 Non- invasive delivery

There are very few peptides/proteins which are administered through a route other than parenteral. Examples of marketed non-parenteral protein formulations include Fortical® (nasal calcitonin spray) for the treatment of post-menopausal osteoporosis and Oralyn® (buccal insulin formulation) for terminally ill patients [25]. Therefore, finding alternatives to parenteral delivery still remains a challenge due to issues related to other potential routes *e.g.* oral as summarised below [26] :-

- a.) Denaturation of proteins by the acidic environment of stomach.
- b.) Protein degradation by the proteolytic enzymes present in stomach and intestine.
- c.) Mucocilliary clearance.
- d.) Impermeability of macromolecules across the intestinal wall.

Oral delivery of biomolecules requires protection from enzymatic degradation and pH for example a hydrogel based system with pH-dependent swelling behaviour claims to prevent protein denaturation and promote release in intestine [27]. Hydrogels are polymeric three-dimensional networks capable of imbibing large amounts of water. The hydrophilic environment of hydrogels, beneficial for protein's active conformation and their bioadhesive nature in intestine has shown to increase the bioavailability of insulin by approximately 8% in rats [28] [29]. Hydrogels such as cross linked tetra-PEG have shown tuneable drug release and degradation rates [30]. The biomolecule can be easily attached to the hydrogels using self-cleaving linkers without the application of excessive stress or energy. These linkers undergo -eliminative cleavage to release the drug with predictable half-lives ranging from a few hours to over 1 year [30]. Hydrogels comprised of poly(methacrylic acid) grafted with poly(ethylene glycol) were characterised and examined for their potential as oral insulin carriers by Tuesca *et al.* [29]. They observed that the total absorption of insulin was dependent on both the amount of polymer and concentration of insulin present in hydrogels. Formulations based on hydrogels are also being studied as a potential sustained protein delivery systems after parenteral administration [31], [32]. The role of hydrogels in the biopharmaceutical market is likely to expand in the near future due to their advantageous properties and continuous progress in this field [33].

The mucocilliary clearance is an initial barrier and a major factor responsible for low absorption of therapeutic agents in the gut. Mucoadhesive materials such as polyacrylic acid derivatives, chitosan or thiolated polymers have been used to prolong the residence time of the delivery system by the non-specific binding to the mucus layer [34]. The above mentioned formulations have shown promising *in vitro* results but poor *in vivo* correlation after oral administration. The primary reason for this is the rapid replenishment of mucosal layer in the intestine resulting in limited mucoadhesion [35].

A second generation approach to increase the residence time is based on bioadhesion [36]. A bioadhesive is generally made of plant lectins which binds specifically to the sugar moieties of glycocalyx on the intestinal epithelia. These formulations are known to be resistant to digestion and is not affected by mucus turnover [37]. Moreover, bioadhesion also presents a possibility of inducing transcytosis and endocytic uptake by intestinal epithelial cells [38].

Another approach of transporting large proteins and peptides across the intestinal epithelial cell lining is by paracellular route. The mucosal epithelial cells are connected by tight junctions with paracellular space of 10 to 50 Å which makes it difficult for particles larger than 30 Å to pass through them [39]. However, use of permeation enhancers in formulations has shown promising results in increasing the membrane permeability [40]. These agents increase the permeability by mechanisms such as increase in membrane fluidity by surfactants, decrease in mucus viscosity by mucolytic agents and disruption of tight junctions by chelating agents and polymers e.g. chitosan [41]. The main drawbacks of this approach include; potential uptake of toxic substances other than the target molecules through these junctions and adverse effects on the intestinal epithelium with long-term use [42].

The activity of therapeutic proteins can be extended by changing their pharmacokinetics in the body. Chemical modifications, such as PEG-ylation, glycosylation and amino acid alterations are known to prolong the systemic circulation. PEG-ylation is the most common chemical modification studied in the biopharmaceutical industry, primarily due to its GRAS (generally regarded as safe) status and biodegradability [43]. PEG (polyethylene glycol) is a non-ionic and hydrophilic molecule which protects its conjugates from recognition by the patient's immune system and reduces the clearance *via* steric shielding and effective increase in the size of the biomolecule [44].

A new strategy which also presents a possibility for the oral delivery of proteins is to use specific cell-penetrating peptides (CPPs) [45]. A number of peptides largely derived from viral or bacterial origin have shown to cross the cell membrane e.g. trans-activating transcriptional activator (TAT) peptide from human immunodeficiency virus (HIV-1) protein. TAT and other CPPs, attached to nanoparticles, polymers and

liposomes carrying the therapeutic drug have shown their efficient cellular internalization [46]. The actual mechanism of cell penetration by the CPPs is still under discussion with evident differences in the literature. Some reports advocate the direct entry of the CPP and conjugated cargo into the cytosol while others emphasize on endocytotic pathway [47]. For example, Gupta *et.al* showed that TAT peptide were able to deliver proteins such as α -galactosidase, horseradish peroxidase, RNase A, and domain III of *Pseudomonas* exotoxin A , into the cytoplasm of different cell types in vitro [47].

Similarly, the application of nanoparticles for the delivery of biomolecules is also an extensive area of research [48]. The nano-carriers generally made of polymers, complexes or liposomes with surface modification by mucoadhesive agents and permeability enhancers are of particular interest [49]. The absorption of proteins through intestinal epithelia, especially through Peyer's patches is largely influenced by the size, surface charge and the nature of the nano-carriers [50]. Surface modified nanoparticles are known to enhance transcellular transport of protein *e.g.* vitamin B-12 modified nanoparticles are reported to protect incorporated protein/peptide from proteolytic enzymes and result in higher bioavailability [51], [52]. Recently, Mohanraj *et.al* designed a silica nanoparticle coated liposomal system which increased protein encapsulation and provided protection against enzymatic degradation [53].

These are some of the recent strategies studied by the formulators to deliver biologics through various routes. The preferred route of protein delivery today is *via* injections which leads to poor patient compliance especially for those on long term medication and require frequent administration. The available formulations are also unaffordable to the large proportion of population; hence one of the major aims of this work is to design an affordable oral drug delivery system for biomolecules. The first step towards the formulation of this protein delivery system is to find a processing technique which prevents the denaturation of these sensitive molecules and supercritical fluid processing can be the answer to this problem.

1.4 Supercritical fluids

Supercritical fluid (SCF) is the defined state of a compound, mixture or element above its critical pressure (P_c) and critical temperature (T_c) [54]. Critical conditions of few commonly used supercritical solvents are presented in Table 1.4 [55].

Compound	Critical Temperature (°C)	Critical Pressure (bar)
Water	374.1	220.5
Ammonia	132.5	112.8
Acetone	235.0	46.9
Ethylene	9.2	50.4
Ethanol	243.0	63.8
Nitrous oxide	36.4	72.5

Table 1.4: Critical conditions of some compounds

The effect of temperature and pressure can be explained by the phase diagram of carbon dioxide (CO_2), as shown in Figure 1.3.

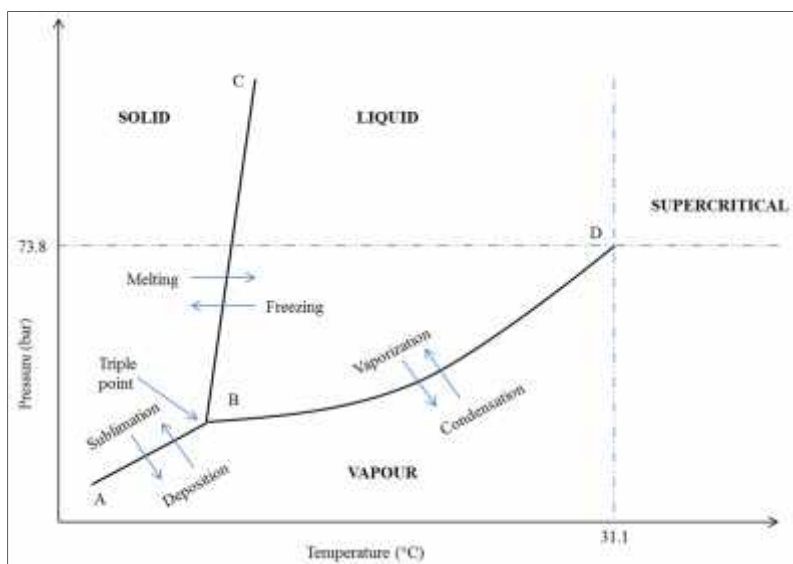


Figure 1.3: Phase diagram of pure carbon dioxide [56]

Curve ABC denotes the melting boundary and curve ABD signifies the boiling. The point B on the phase diagram represents triple point where CO_2 exists in all three states.

CO₂ reaches to the supercritical state at 73.8 bar and 31.1 °C. The supercritical state also signifies the disappearance of the distinction between liquid and vapour boundary.

SCFs have properties intermediate to liquid and gases *i.e.* gas like viscosity and liquid like densities [57]. A comparison between some physical properties of SCF, liquid and gas is shown in Table 1.5.

Mobile Phase	Density (g/cm ³)	Viscosity (Poise)	Diffusivity (cm ² /s)
Gas	0.001	0.5-3.5 x 10 ⁻⁴	0.01-1.00
SCF	0.2-0.9	0.2-1.0 x 10 ⁻³	0.1-3.3 x 10 ⁻⁴
Liquid	0.8-1.0	0.3-2.4 x 10 ⁻²	0.5-2.0 x 10 ⁻⁵

Table 1.5: Density, viscosity and diffusivity comparison of different fluids [57], [58]

The density of SCF can be easily tuned within the critical region by small changes in pressure and temperature [59]. SCFs have various advantages over common organic solvents because of the above mentioned unique properties. The advantages of SCFs can be summarised as following [57], [60] :-

- a) SCFs with higher diffusivities and lower viscosities are desirable due to solvating power similar to organic solvents.
- b) The ability to rapidly vary solvent strength allows SCFs to be used as both solvent and anti-solvent in many pharmaceutical operations.
- c) SCFs are effective media for particle formation due to their easily tuneable density and diffusivity.
- d) Commonly used SCFs (e.g. CO₂) are economical, safe and easily available.
- e) Unlike organic solvents, SCFs are environmentally benign, easy to dispose and recycle.
- f) SCFs such as SCCO₂ can be used to process thermolabile substances due to low T_c and P_c.

The main disadvantages of SCFs are the use of relatively high pressures and complex thermodynamics [61]. There are numerous applications of SCFs in pharmaceutical industry, few of which are discussed in the following section.

1.4.1 Supercritical fluid technology in pharmaceutical research

The main features of the SCFs are high compressibility and diffusivity along with high evaporation rate and the possibility of fine tuning of the solvent power through density modulation (temperature and/or pressure variation) [62]. There are certain important characteristics that govern the solubility of a compound in CO₂. The first main attribute is the presence of CO₂ interacting functional groups. These can be electron donating or accepting groups which promote Lewis acid-base interactions with CO₂ [63]. However, the strong solute-solute interactions due to the presence of hydrogen-bonding functionalities in a compound may result in weak solute-CO₂ interactions. The second characteristic is the polarity, where CO₂ soluble compounds should be slightly polar to allow the interaction with the quadrupole moment of CO₂. Conversely, high dipole moment is undesirable as it may lead to stronger solute-solute interactions. Another significant feature for CO₂ solubility is the molecular architecture, especially in the case of large compounds such as polymers. The presence of large free volume and high degree of flexibility are necessary for stronger CO₂ interactions [64]. Finally, a balance between the enthalpy and entropy of mixing of a compound is also important for its interaction with CO₂ [65].

A SCF can be used as solute, anti-solvent or solvent and there are number of processes which utilise these properties as discussed in the following sections.

1.4.1.1 Rapid Expansion of Supercritical Solution (RESS)

RESS requires saturation of SCF with a solute followed by rapid depressurisation through a heated nozzle at supersonic speed [66]. The depressurisation results in a rapid nucleation of the solute to form small particles of uniform size [67]. Moreover, particle formation by this technique avoids additional drying steps and issues related to residual solvent. For example, micronisation of carbamazepine by RESS produced particles of 0.4 to 0.9 microns which were 60 times smaller than the unprocessed particles [68]. The main factors affecting the particle size in RESS process include [69]:-

- a) Processing temperature and pressure conditions,
- b) Substance solubility in SCCO₂,

- c) Diameter of nozzle, and
- d) Expansion vessel dimensions.

Advantages of RESS comprise easily controlled process parameters and organic solvent free operation. Common disadvantages include; difficulty in scale-up, possible particle aggregation and nozzle blockage. Furthermore, SCFs such as SCCO₂ are although excellent solvents for small, non-polar molecules but poor solubility of numerous pharmaceutically important compounds is a major limitation of this process [70]. The addition of a suitable co-solvent can address this issue to an extent but may give rise to the problem of residual solvent in the product [71].

1.4.1.2 Sterilisation

Sterilisation by pressurised CO₂ has been studied by some researchers [72], [73] and is already applied in the food industry. This approach can also be used in the pharmaceutical field to sterilise polymeric materials and fine particles [74]. Several hypothesis about microbial inactivation by SCCO₂ have been proposed such as cytoplasmic acidification, modification of cell membrane, extraction of cell wall lipids, cell rupture due to fast depressurisation, inactivation of key enzymes for cell metabolism and extraction of intracellular substances [72]. The SCF sterilisation seems to have a promising future as a green technology and is a better alternative to classical approaches as it avoids the issues such as thermal degradation during heat sterilisation, radiolysis during irradiation and unwanted reactions with sterilising chemicals (ethylene oxide, hydrogen peroxide, *etc.*) [75].

1.4.1.3 SCF as an anti-solvent

The application of SCFs as anti-solvent is of great importance for the compounds with limited solubility in the media. Here, the solute is first dissolved in an organic solvent and then introduced in a chamber containing pressurised CO₂. The CO₂ diffuses into organic solvent and lowers its solvent power resulting in the solute precipitation. The efficacy of this approach depends upon the ability of organic solvent to dissolve a large quantity of SCF and poor solubility of solute in the SCF [62]. The main anti-solvent techniques are known as GAS (Gaseous anti-solvent) and SAS (Supercritical anti-

solvent). In GAS, the solute dissolved in organic solvent is placed in the precipitation chamber and then a dense gas such as CO₂ is introduced into the vessel till the final pressure is reached [76]. Whereas in SAS, SCCO₂ is first pumped into the vessel until the system reaches the desired pressure followed by the spraying of organic solution through a nozzle [77]. Recent example includes formation of vinblastine nanoparticles by SAS process with a mean diameter of 121 nm where *N*-methyl-2-pyrrolidone was used as a solvent and SCCO₂ as an antisolvent [78].

1.4.1.4 Particles from gas saturated solutions (PGSS)

In this process, the compressed fluid (supercritical or liquid) is dissolved into a melted material to obtain a gas saturated solution before a rapid expansion of this mixture through a nozzle. This phenomenon leads to the formation of particles due to an extremely rapid temperature decrease caused by the fluid expansion known as the Joule-Thomson effect [79]. PGSS is suitable for the processing of excipients such as polymers and lipids which solubilise large amounts of dense gas leading to a melting point depression effect [80]. The extent of the melting point depression depends upon the molecular interaction of dissolved SCF and the substance of interest. The determination of solid-liquid transition of the desired excipient in pressurised system is essential to gain information on the pressure and temperature conditions required for the micronisation and particle engineering [81]. The main advantages of PGSS include; use of lower pressures than RESS, quantity of compressed fluid required is relatively less, organic solvent free operation and the possibility to work in continuous mode. Whereas, the poor control on particle size is the main limitation of this process [62].

1.4.1.5 Foams /scaffolds

A foam has a porous arrangement formed by empty cells of diameter about 10 microns or less and has a cell density greater than 10⁹ cells/cm³ [82]. Foams made from biodegradable polymers have vast applications from drug delivery to tissue engineering as they provide a temporary support for cells to adhere and grow *in vivo* [83]. SCFs have a great ability to create porous materials at relatively low temperatures and without the use of any organic solvents [84]. The foams or scaffolds are produced by saturating the material (polymer) with SCF at constant temperature and pressure

followed by depressurisation. The pressure decrease leads to supersaturation resulting in phase separation and growth of pores [85]. SCCO₂ has been used to produce foams of up to 97% porosity with uniform distribution of macropores (10-100 μm) [86]. The main factors affecting porosity and pore structure are the amount of gas dissolved in the polymer (which depends upon gas pressure and temperature), the diffusion of gas molecules through the polymer, equilibration time and the rate of gas nucleation [86], [87]. It has been reported in various studies that amorphous polymers are highly suitable for porous foam formation as they absorb/solubilise large quantities of CO₂ in comparison to crystalline polymers [88].

1.4.1.6 Cyclodextrins inclusion complexes

The application of SCCO₂ in drug-cyclodextrin (CD) complexation has also been studied by various authors [89], [90]. CDs are cyclic oligosaccharides containing six (α-CD), seven (β-CD) or eight (γ-CD) glycopyranose units connected by α-1, 4-linkages. They have an outer hydrophilic surface and inner hydrophobic cavity. CDs are known to form inclusion complexes with many drugs by taking up a whole or part of the drug molecule into the cavity. This type of encapsulation affects many physicochemical properties of drugs including their aqueous solubility and the rate of dissolution [90]. Conventional methods for the preparation of drug-CD inclusion complexes include kneading, co-precipitation, co-evaporation, co-grinding, freeze and spray-drying [91]. Most of these methods require large volumes of aqueous or organic solvents. SCF processes in the formulation of drug-CD inclusion complexes to avoid disadvantages related to the conventional processes are widely reported in the literature [89], [92]. An inclusion complex between β-cyclodextrin, piroxicam and L-lysine was obtained using SCCO₂ in 1:2:1.5 molar ratio which had an improved dissolution rate than physical mixture [93]. Another example includes application of SAS process to prepare simvastatin and hydroxypropyl-β-cyclodextrin inclusion complex where CO₂ was used as an antisolvent [94].

1.4.1.7 Coating/Encapsulation

Particles are generally coated by conventional coating techniques such as spray drying, fluid bed coating, coacervation, extrusion and milling either for aesthetic/handling

purposes or controlled release applications [95]. These techniques have various limitations such as the difficulty of maintaining aseptic conditions, inability to coat small particles due to electrostatic charges, risk of forming explosive vapour phase mixtures when organic solvents are used with air as the fluidizing medium and adverse environmental effects of volatile organic compound emissions [96]. Tsutsumi *et al.* described a fluidised-bed coating process based on RESS technique which consists of 3 basic steps: extraction, expansion and fluidisation [97], [98]. In a typical coating experiment coating material is melted in an extraction column in the presence of CO₂ which is then expanded through a nozzle into the CO₂ filled fluidised bed followed by the separation of encapsulated particles by a cyclone and filters [99]. Key process parameters include; temperature, pressure, fluidisation gas velocity and solidification kinetics of the coating material [100]. Moreover, such processes also enable the encapsulation of sensitive materials like proteins and peptides due to the absence of organic solvents and relatively low temperatures and pressures [101].

The conventional coating techniques are not safe for the processing of biomolecules due to the requirement of high temperatures and shear stress and use of organic solvents. Hence, encapsulation by SCF technology as discussed in this section provides solution to many of the stated limitations. SCCO₂ was used in this study to coat protein adsorbed silica particles with saturated fatty acids. The model protein used in this work was haemoglobin, properties of which are discussed in the following section.

1.5 Haemoglobin

Haemoglobin (Hb) is an oxygen carrying transport protein which is nearly 95% of the intracellular proteins in the red blood cells (RBC). The Hb content of whole blood is given in grams of Hb per decilitre which ranges from 14–18 g/dL in males and 12–16 g/dL in females [102]. The quaternary structure of Hb is important for it to function as an oxygen carrier. The structure and function of Hb are discussed in the following section.

1.5.1 Haemoglobin structure and function

Hb molecules have complex quaternary structures (Figure 1.4 and 1.6) where each molecule is a tetramer comprised of two α and two β -globin chains. These chains are bound to each other by hydrogen bonding, salt bridges and hydrophobic effect. The molecular weight of Hb is 64.5 kDa with linear dimensions of 5.3-5.4-6.5 nm [103]. Each chain in the Hb is a globular protein subunit which resembles structurally to the myoglobin in skeletal and cardiac muscle cells. All these chains are known to be in α -helix form and contain a non-protein haem group which is made of iron held in a porphyrin ring (Figure 1.5). The haem group is also attached to the nitrogen atom of histidine group which helps in its stability within each subunit [104], [105].

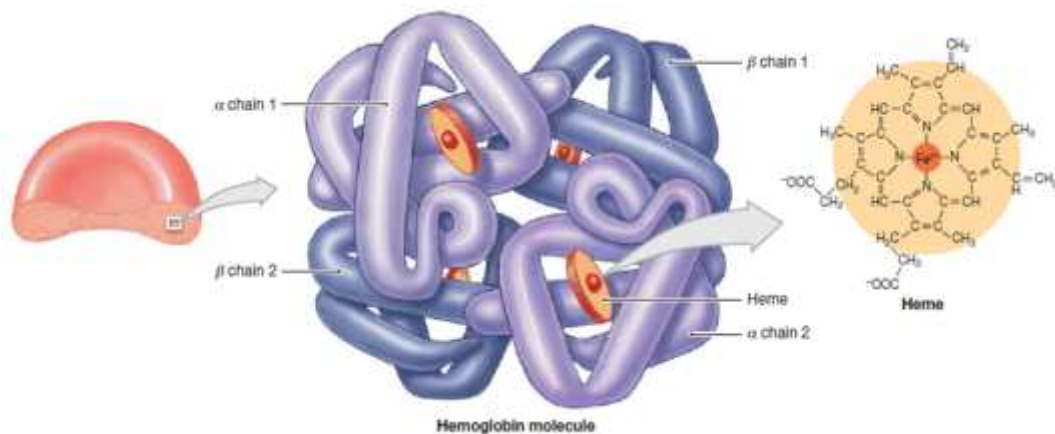


Figure 1.4: Structure of Hb [106]

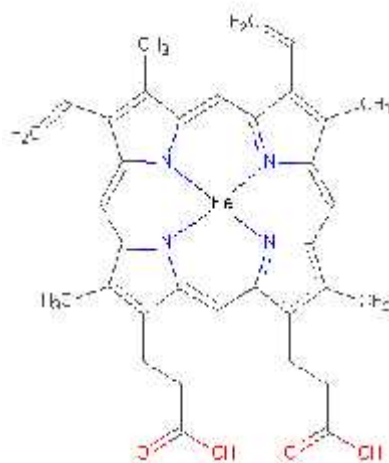


Figure 1.5: Structure of haem [2]

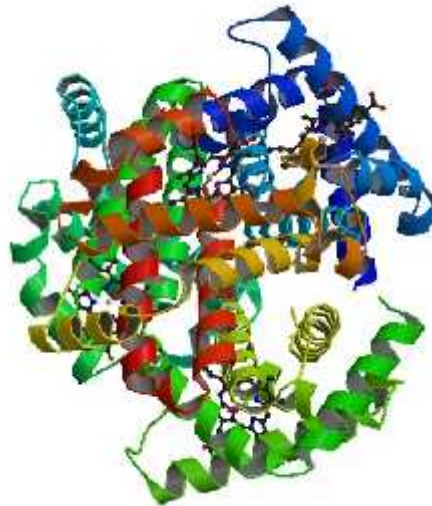


Figure 1.6: X-ray crystal structure of Hb from protein database [107]

Each haem group interacts with an oxygen molecule and forms oxyhemoglobin which is facilitated by the orientation of iron inside haem unit. This iron–oxygen interaction is weak and the reaction can be reversed without damaging the haem or the oxygen molecule. Furthermore, binding of oxygen to haem pulls the iron into the plane of porphyrin ring causing a minor conformational shift which boosts oxygen binding to the three remaining haems within the haemoglobin making oxygen binding cooperative [108]. This phenomenon facilitates the transport of oxygen to the cells.

One RBC holds about 280 million Hb molecules and one Hb molecule contains four haem units, this means that a single RBC can potentially carry more than a billion oxygen molecules. The amount of oxygen bound to Hb depends mostly on the oxygen content of the plasma. Hb exists in two forms, a *taut (tense) form* (T) and a *relaxed form* (R) as shown in Figure 1.7. The factors such as low pH, high CO₂ and 2, 3-bisphosphoglycerate (2, 3 BPG) at tissue levels favour taut form with low O₂ affinity. Conversely, a high pH, low CO₂ and low 2, 3 BPG favours the relaxed form which has higher oxygen binding capacity [109]. The partial pressure of the system also affects O₂ affinity for example, the relaxed state is favoured at high partial pressures of oxygen in lungs and the tense state is favoured when the partial pressure of O₂ is low at peripheral capillaries [110].

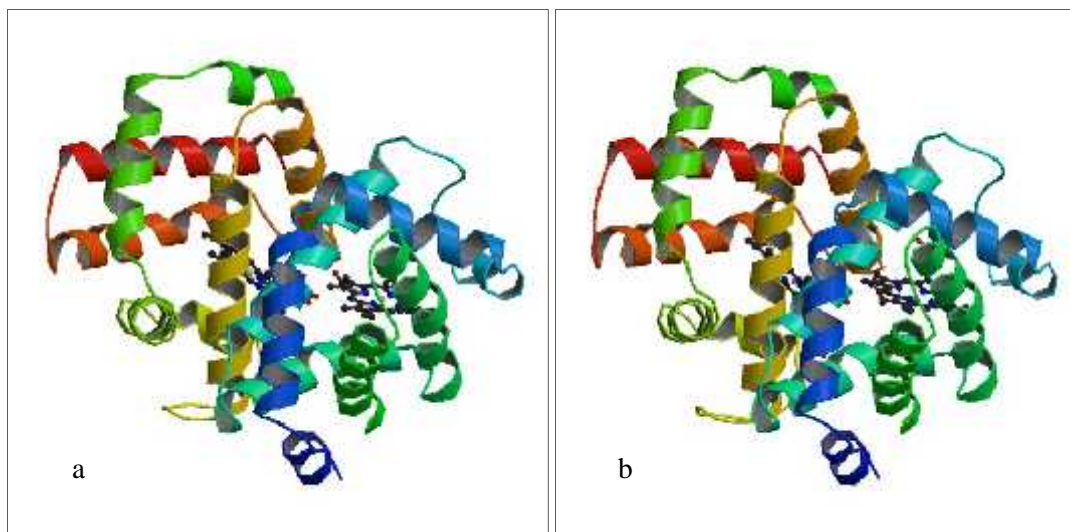


Figure 1.7: (a) R state and (b) T state of dimeric Hb [111]

Hb is a popular model protein in drug delivery research and is used to develop a solid core drug delivery system (SCDDS) for the biomolecules in the present study [112], [113]. This is primarily because of its stable quaternary structure over a broad pH range (4-7), along with its inability to form associates in solution and easy photometric quantification at 400 nm [103].

1.6 Solid Core Drug Delivery System

As discussed earlier, proteins and peptides are regularly used in the treatment of various ailments including diabetes and autoimmune diseases. The favoured route of their delivery is parenteral mainly because biomolecules are sensitive to gastric pH and proteolytic enzymes. Moreover, these also have a tendency to form aggregates inside the body or accumulate in non-targeted tissues, if not delivered precisely to the target site [114].

The development of protein biopharmaceuticals is undoubtedly more complex than traditional pharmaceutical drug development. The key determinants of their delivery route are their physical size and sensitivity towards degradation [25]. The main challenges towards the use of proteins as drug molecules can be summarised as follows [115], [116] :-

- a) Large molecular size and hydrophilic nature lead to their poor intrinsic permeability.
- b) High tendency towards structural modification or conformation due to changes in environmental factors such as pH, temperature and ionic strength.
- c) Rapid clearance from the body due to enzymatic degradation and immune system processing.
- d) Immunogenicity or antigenicity.

Most of the protein drug delivery systems are based on biodegradable polymeric nanoparticles, liposomes and dendrimers [117]. The controlled release is obtained from these materials upon structural degradation of the carrier triggered by various chemical factors such as pH and temperature [117]. However, premature release of drugs still remains an issue in these systems. The use of inorganic materials has been investigated by many researchers to overcome the problem of premature release and to provide a sustained delivery. Among many stable biocompatible excipients, silica is generally the material of choice and has been studied in many drug delivery systems [118]. The properties such as biocompatibility, hydrophilicity and protection to internal payload makes mesoporous (pore size 2-50 nm) silica particles a perfect candidate for drug delivery. Moreover, the release rate can also be controlled by tailoring the size and shape of these particles [119]. Another important advantage of mesoporous silica particles is the ease of its surface modification to optimise the drug loading and release kinetics [120]. Silica is also considered to have better biocompatibility in comparison with other metal oxides such as titanium and iron oxide [120]. Artificial implants of silica and its composites are known to have osteogenic properties [121]. It has also been shown that silica is able to store and gradually release drugs like antibiotics and other small molecules [117]. Moreover, it is also known that the biocompatibility of several drug delivery systems such as biopolymers, micelles and magnetic nanoparticles can be enhanced by the use of silica [122]–[124]. Hence, silica can be an excellent carrier for biomolecules and is used as a core material for the protein immobilisation in the present study.

The preparation of SCDDS involves protein immobilisation on a solid surface followed by coating to control the drug release [125]. It has been reported in literature that the

adsorption of proteins on a surface may enhance their stability [126]. Furthermore, systems containing protein adsorbed mesoporous particles with a further coating have been reported to provide sustained release [127]. A number of fatty acids, fats and polymers have been reported to protect the protein from gastric pH and control the release [128]. Mesoporous silica and fatty acid as core and coating materials respectively were chosen to develop SCDDS in the current study as presented in Figure 1.8.

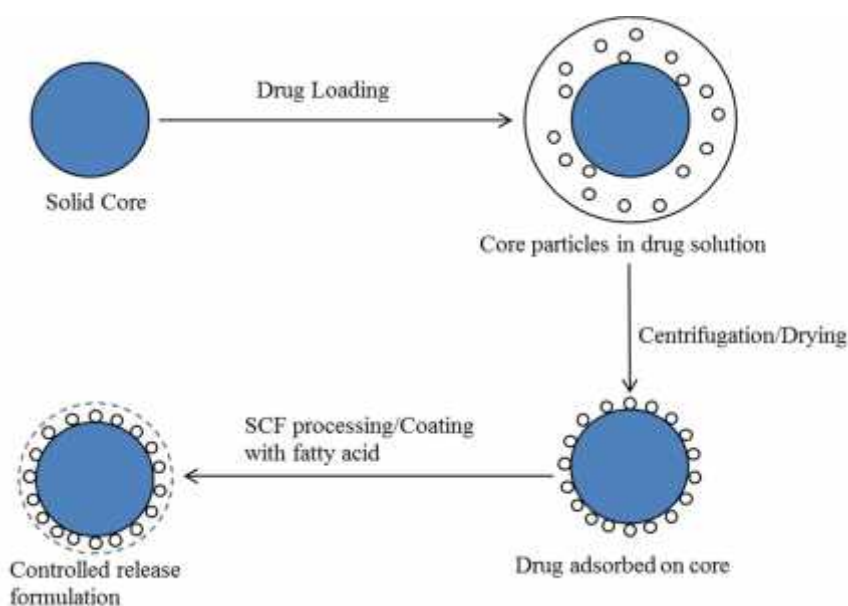


Figure 1.8: Schematic diagram of SCDDS preparation

First step in this process allows the protein molecules from aqueous solution to be adsorbed on the carrier surface which is then centrifuged and dried. The second step includes coating of protein adsorbed particles with fatty acids *via* SCF processing. The rationale behind using fatty acid coating is to protect the protein from gastric media due to its limited solubility in acidic conditions and to promote drug release in intestinal environment.

1.7 Aim and objectives

The aim of this project is to formulate an oral drug delivery system using haemoglobin as a model protein, silica as a core material and pressurised CO₂ as a media for fatty acid coating. The rationale behind this work is to find a cost effective oral drug delivery

system for proteins and peptides. This project involved investigation of the following parameters in order to achieve the abovementioned aim:-

a) Phase behaviour of coating materials in pressurised CO₂

The effect of pressurised CO₂ on melting point of excipients (fatty acids and pluronics) was investigated. The parameters identified here were used in encapsulation/coating of silica particles.

b) Identification of a suitable core

Three morphologically different silica particles were characterised and used to immobilise bovine haemoglobin.

c) To determine stability of the model protein

Storage, thermal and agitation stability of bovine haemoglobin was studied in different pH buffer solutions.

d) Adsorption and desorption studies of protein on core particles

Adsorption and desorption conditions of bovine haemoglobin were identified. These experiments also established the protein loading capacity, kinetics and stability of protein during the process.

e) Coating of the particles or encapsulation

Encapsulation of protein adsorbed particles with fatty acids was performed by SCF processing and solvent evaporation.

f) *In-vitro* drug release studies from the formulation

The release of model protein from the various formulations was determined in simulated gastric and intestinal fluids without enzymes.

References

- [1] L. W. Janson and M. E. Tischler, *Medical biochemistry: the big picture*, 1st ed. New York, USA: McGraw-Hill, 2012.
- [2] D. Whitford, *Proteins: structure and function*. West Sussex, England: John Wiley & Sons, Ltd, 2005.
- [3] E. Buxbaum, *Fundamentals of Protein Structure and Function*. Portsmouth, Dominica: Springer, 2007.
- [4] A. Banga, *Therapeutic peptides and proteins: formulation, processing and delivery systems*, 2nd ed. CRC Press, 2005.
- [5] M. P. Ratnaparkhi, S. P. Chaudhari, and V. A. Pandya, 'Peptides and proteins in pharmaceuticals', *Int. J. Curr. Pharm. Res.*, vol. 3, no. 2, pp. 1–9, 2011.
- [6] B. Leader, Q. J. Baca, and D. E. Golan, 'Protein therapeutics: a summary and pharmacological classification.', *Nat. Rev. Drug Discov.*, vol. 7, no. 1, pp. 21–39, 2008.
- [7] G. Muller, 'Oral delivery of protein drugs: driver for personalized medicine.', *Curr. Issues Mol. Biol.*, vol. 13, no. 1, pp. 13–24, 2011.
- [8] D. A. Eppstein and J. P. Longenecker, 'Alternative delivery systems for peptides and proteins as drugs.', *Crit. Rev. Ther. Drug Carrier Syst.*, vol. 5, no. 2, pp. 99–139, Jan. 1988.
- [9] D. S. Dimitrov, *Therapeutic Proteins*, 2nd ed., vol. 899. Totowa, NJ: Humana Press, 2012.
- [10] 'Global Protein Therapeutics Market Forecast to 2015', *RNCOS E-Services Pvt. Ltd.*, 2012. [Online]. Available: http://marketpublishers.com/report/medicine_pharmaceuticals_biotechnology/dr

ugs_biotechnology/global_protein_therapeutics_market_forecast_to_2015.html.
[Accessed: 31-Mar-2013].

- [11] ‘Biologics and Biosimilars World Markets’, *TriMark Publications, LLC*, 2013. [Online]. Available: <http://www.trimarkpublications.com/biologics-and-biosimilars-world-markets/>. [Accessed: 09-Sep-2013].
- [12] D. S. Pisal, M. P. Kosloski, and S. V Balu-Iyer, ‘Delivery of therapeutic proteins.’, *J. Pharm. Sci.*, vol. 99, no. 6, pp. 2557–75, 2010.
- [13] S. B. Andrade. F, Antunes. F, Nascimento. A.V, da Silva. S.B, das Neves. J, Ferreira. D, ‘Chitosan formulations as carriers for therapeutic proteins’, *Curr. Drug Discov. Technol.*, vol. 8, no. 3, pp. 157–72, 2011.
- [14] J. L. Cleland, A. Daugherty, and R. Mrsny, ‘Emerging protein delivery methods’, *Curr. Opin. Biotechnol.*, vol. 12, no. 2, pp. 212–9, 2001.
- [15] S. Stolnik and K. Shakesheff, ‘Formulations for delivery of therapeutic proteins.’, *Biotechnol. Lett.*, vol. 31, no. 1, pp. 1–11, 2009.
- [16] S. Martins, B. Sarmento, D. C. Ferreira, and E. B. Souto, ‘Lipid-based colloidal carriers for peptide and protein delivery--liposomes versus lipid nanoparticles.’, *Int. J. Nanomedicine*, vol. 2, no. 4, pp. 595–607, 2007.
- [17] M. Yang, S. K. Lai, Y. Wang, W. Zhong, C. Happe, M. Zhang, J. Fu, and J. Hanes, ‘Biodegradable nanoparticles composed entirely of safe materials that rapidly penetrate human mucus.’, *Angew. Chem. Int. Ed. Engl.*, vol. 50, no. 11, pp. 2597–600, 2011.
- [18] V. R. Sinha and A. Trehan, ‘Biodegradable microspheres for protein delivery’, *J. Control. Release*, vol. 90, no. 3, pp. 261–80, 2003.
- [19] M. J. Whitaker, J. Hao, O. R. Davies, G. Serhatkulu, S. Stolnik-Trenkic, S. M. Howdle, and K. M. Shakesheff, ‘The production of protein-loaded microparticles

- by supercritical fluid enhanced mixing and spraying.’, *J. Control. Release*, vol. 101, no. 1–3, pp. 85–92, 2005.
- [20] K. Yakovlevsky, M. Shamashkin, N. Khalaf, C. P. Govardhan, and C. W. Jung, ‘Spherical protein particles and methods for making and using them’, US 2004/0219224 A1, 2004.
- [21] L. Bromberg, J. Rashba-Step, and T. Scott, ‘Insulin particle formation in supersaturated aqueous solutions of poly(ethylene glycol).’, *Biophys. J.*, vol. 89, no. 5, pp. 3424–33, 2005.
- [22] E. Yapar, Ö. nal, Y. Özkan, and T. Baykara, ‘Injectable in situ forming microparticles: a novel drug delivery system’, *Trop. J. Pharm. Res.*, vol. 11, no. 2, pp. 307–318, 2012.
- [23] H. Kranz and R. Bodmeier, ‘A novel in situ forming drug delivery system for controlled parenteral drug delivery.’, *Int. J. Pharm.*, vol. 332, no. 1–2, pp. 107–14, 2007.
- [24] R. R. S. Thakur, H. L. McMillan, and D. S. Jones, ‘Solvent induced phase inversion-based in situ forming controlled release drug delivery implants.’, *J. Control. Release*, vol. 176, no. 2014, pp. 8–23, 2014.
- [25] L. R. Brown, ‘Commercial challenges of protein drug delivery.’, *Expert Opin. Drug Deliv.*, vol. 2, no. 1, pp. 29–42, 2005.
- [26] M. R. Rekha and C. P. Sharma, ‘Oral delivery of therapeutic protein/peptide for diabetes--future perspectives.’, *Int. J. Pharm.*, vol. 440, no. 1, pp. 48–62, 2013.
- [27] R. Gong, C. Li, S. Zhu, Y. Zhang, Y. Du, and J. Jiang, ‘A novel pH-sensitive hydrogel based on dual crosslinked alginate/N- -glutaric acid chitosan for oral delivery of protein’, *Carbohydr. Polym.*, vol. 85, no. 4, pp. 869–874, 2011.

- [28] C.-C. Lin and A. T. Metters, 'Hydrogels in controlled release formulations: network design and mathematical modeling.', *Adv. Drug Deliv. Rev.*, vol. 58, no. 12–13, pp. 1379–408, 2006.
- [29] A. Tuesca, K. Nakamura, M. Morishita, J. Joseph, N. Peppas, and A. Lowman, 'Complexation hydrogels for oral insulin delivery: effects of polymer dosing on in vivo efficacy.', *J. Pharm. Sci.*, vol. 97, no. 7, pp. 2607–18, 2008.
- [30] G. W. Ashley, J. Henise, R. Reid, and D. V. Santi, 'Hydrogel drug delivery system with predictable and tunable drug release and degradation rates', *Proc. Natl. Acad. Sci. U. S. A.*, vol. 110, no. 6, pp. 2318–23, 2013.
- [31] N. Sahu, P. Gils, D. Ray, and P. Sahoo, 'Biodegradable hydrogels in controlled drug delivery', *Adv. Polym. Sci. Technol.*, vol. 3, no. 2, pp. 22–30, 2013.
- [32] T. Ito, I. P. Fraser, Y. Yeo, C. B. Highley, E. Bellas, and D. S. Kohane, 'Anti-inflammatory function of an in situ cross-linkable conjugate hydrogel of hyaluronic acid and dexamethasone.', *Biomaterials*, vol. 28, no. 10, pp. 1778–86, 2007.
- [33] T. Vermonden, R. Censi, and W. E. Hennink, 'Hydrogels for protein delivery.', *Chem. Rev.*, vol. 112, no. 5, pp. 2853–88, 2012.
- [34] A. Bernkop-Schnürch, 'Thiomers: a new generation of mucoadhesive polymers.', *Adv. Drug Deliv. Rev.*, vol. 57, no. 11, pp. 1569–82, 2005.
- [35] K. Vinod, T. R. Reddy, S. Sandhya, and V. D. Banji, 'Critical review on mucoadhesive drug delivery systems', *Hygeia J. drugs Med.*, vol. 4, no. 1, pp. 7–28, 2012.
- [36] J. Woodley, 'Bioadhesion: new possibilities for drug administration?', *Clin. Pharmacokinet.*, vol. 40, no. 2, pp. 77–84, 2001.

- [37] E. Haltner, J. H. Easson, and C.-M. Lehr, 'Lectins and bacterial invasion factors for controlling endo- and transcytosis of bioadhesive drug carrier systems', *Eur. J. Pharm. Biopharm.*, vol. 44, no. 1, pp. 3–13, 1997.
- [38] M. A. Jepson, M. A. Clark, and B. H. Hirst, 'M cell targeting by lectins: A strategy for mucosal vaccination and drug delivery', *Adv. Drug Deliv. Rev.*, vol. 56, no. 4, pp. 511–525, 2004.
- [39] W. Rubas, M. E. Cromwell, Z. Shahrokh, J. Villagran, T. N. Nguyen, M. Wellton, T. H. Nguyen, and R. J. Mersny, 'Flux measurements across Caco-2 monolayers may predict transport in human large intestinal tissue.', *J. Pharm. Sci.*, vol. 85, no. 2, pp. 165–9, 1996.
- [40] A. Alexander and M. Ajazuddin, 'Polymers and permeation enhancers: Specialized components of mucoadhesives', *Stamford J. Pharm. Sci.*, vol. 4, no. 1, pp. 91–95, 2011.
- [41] M. Kondoh and K. Yagi, 'Tight junction modulators: promising candidates for drug delivery.', *Curr. Med. Chem.*, vol. 14, no. 23, pp. 2482–8, 2007.
- [42] H. J. R. Lemmer and J. H. Hamman, 'Paracellular drug absorption enhancement through tight junction modulation.', *Expert Opin. Drug Deliv.*, vol. 10, no. 1, pp. 103–14, 2013.
- [43] S. N. S. Alconcel, A. S. Baas, and H. D. Maynard, 'FDA-approved poly(ethylene glycol)-protein conjugate drugs', *Polym. Chem.*, vol. 2, no. 7, p. 1442, 2011.
- [44] P. Caliceti and F. M. Veronese, 'Pharmacokinetic and biodistribution properties of poly(ethylene glycol)-protein conjugates.', *Adv. Drug Deliv. Rev.*, vol. 55, no. 10, pp. 1261–77, 2003.
- [45] J. S. Wadia and S. F. Dowdy, 'Transmembrane delivery of protein and peptide drugs by TAT-mediated transduction in the treatment of cancer.', *Adv. Drug Deliv. Rev.*, vol. 57, no. 4, pp. 579–96, 2005.

- [46] Y. S. Nam, J. Y. Park, S. Han, and I. Chang, 'Intracellular drug delivery using poly (D , L -lactide-co-glycolide) nano- particles derivatized with a peptide from a transcriptional activator protein of HIV-1', *Biotechnol. Lett.*, pp. 2093–2098, 2002.
- [47] B. Gupta, T. S. Levchenko, and V. P. Torchilin, 'Intracellular delivery of large molecules and small particles by cell-penetrating proteins and peptides.', *Adv. Drug Deliv. Rev.*, vol. 57, no. 4, pp. 637–51, 2005.
- [48] M. Morishita and N. A. Peppas, 'Is the oral route possible for peptide and protein drug delivery?', *Drug Discov. Today*, vol. 11, no. 19–20, pp. 905–910, 2006.
- [49] H. Takeuchi, H. Yamamoto, and Y. Kawashima, 'Mucoadhesive nanoparticulate systems for peptide drug delivery.', *Adv. Drug Deliv. Rev.*, vol. 47, no. 1, pp. 39–54, 2001.
- [50] H. J. Lee, 'Protein drug oral delivery: the recent progress.', *Arch. Pharm. Res.*, vol. 25, no. 5, pp. 572–584, 2002.
- [51] P. L. Tuma and A. L. Hubbard, 'Transcytosis: crossing cellular barriers.', *Physiol. Rev.*, vol. 83, no. 3, pp. 871–932, 2003.
- [52] S. M. Clardy, D. G. Allis, T. J. Fairchild, and R. P. Doyle, 'Vitamin B12 in drug delivery: breaking through the barriers to a B12 bioconjugate pharmaceutical.', *Expert Opin. Drug Deliv.*, vol. 8, no. 1, pp. 127–40, 2011.
- [53] V. J. Mohanraj, T. J. Barnes, and C. A. Prestidge, 'Silica nanoparticle coated liposomes: A new type of hybrid nanocapsule for proteins', *Int. J. Pharm.*, vol. 392, no. 1–2, pp. 285–293, 2010.
- [54] A. McNaught and A. Wilkinson, *International union of pure and applied chemistry: compendium of chemical terminology (gold book)*. 2012.
- [55] D. R. Lide and W. Haynes, Eds., *CRC handbook of chemistry and physics*, 90th ed. New York, USA: CRC Press, 2003.

- [56] P. J. Ginty, M. J. Whitaker, K. M. Shakesheff, and S. M. Howdle, 'Drug delivery goes supercritical', *Mater. today*, vol. 8, no. 8, pp. 42–48, 2005.
- [57] M. Mukhopadhyay, *Natural extracts using supercritical carbon dioxide*. Boca raton, USA: CRC Press, 2000.
- [58] V. Goodship and E. Oqur, 'Polymer processing with supercritical fluids', *Rapra Rev. reports*, vol. 15, no. 8, p. 148, 2005.
- [59] S. P. Nalawade, F. Picchioni, and L. P. B. M. Janssen, 'Supercritical carbon dioxide as a green solvent for processing polymer melts: processing aspects and applications', *Prog. Polym. Sci.*, vol. 31, no. 1, pp. 19–43, 2006.
- [60] B. Subramaniam, R. A. Rajewski, and K. Snavely, 'Pharmaceutical processing with supercritical carbon dioxide', *J. Pharm. Sci.*, vol. 86, no. 8, pp. 885–890, 1997.
- [61] A. Martín and M. J. Cocero, 'Micronization processes with supercritical fluids: Fundamentals and mechanisms', *Adv. Drug Deliv. Rev.*, vol. 60, no. 3, pp. 339–350, 2008.
- [62] I. Pasquali and R. Bettini, 'Are pharmaceuticals really going supercritical?', *Int. J. Pharm.*, vol. 364, no. 2, pp. 176–87, 2008.
- [63] J. C. Meredith, K. P. Johnston, J. M. Seminario, S. G. Kazarian, and C. A. Eckert, 'Quantitative Equilibrium Constants between CO₂ and Lewis Bases from FTIR Spectroscopy', *J. Phys. Chem.*, vol. 100, no. 26, pp. 10837–10848, 1996.
- [64] D. L. Tomasko, H. Li, D. Liu, X. Han, M. J. Wingert, L. J. Lee, and K. W. Koelling, 'A Review of CO₂ Applications in the Processing of Polymers', *Ind. Eng. Chem. Res.*, vol. 42, no. 25, pp. 6431–6456, 2003.
- [65] T. Sarbu, T. Styranec, and E. Beckman, 'Non-fluorous polymers with very high solubility in supercritical CO₂ down to low pressures', *Nature*, vol. 405, no. 6783, pp. 165–8, 2000.

- [66] P. G. Debenedetti, J. W. Tom, X. Kwauk, and S. D. Yeo, 'Rapid expansion of supercritical solutions (ress): fundamentals and applications', *Fluid Phase Equilib.*, vol. 82, pp. 311–321, 1993.
- [67] E. Phillips and V. Stella, 'Rapid expansion from supercritical solutions: application to pharmaceutical processes', *Int. J. Pharm.*, vol. 94, 1993.
- [68] D. Bolten and M. Türk, 'Micronisation of carbamazepine through rapid expansion of supercritical solution (RESS)', *J. Supercrit. Fluids*, vol. 62, pp. 32–40, 2012.
- [69] H. R. Satvati and M. N. Lotfollahi, 'Effects of extraction temperature, extraction pressure and nozzle diameter on micronization of cholesterol by RESS process', *Powder Technol.*, vol. 210, no. 2, pp. 109–114, 2011.
- [70] P. York, 'Strategies for particle design using supercritical fluid technologies.', *Pharm. Sci. Technol. Today*, vol. 2, no. 11, pp. 430–440, 1999.
- [71] A. Taberner, E. M. Martín del Valle, and M. A. Galán, 'Supercritical fluids for pharmaceutical particle engineering: Methods, basic fundamentals and modelling', *Chem. Eng. Process. Process Intensif.*, vol. 60, pp. 9–25, 2012.
- [72] S. Spilimbergo and A. Bertucco, 'Non-Thermal Bacteria Inactivation with Dense CO₂', *Biotechnol. Bioeng.*, vol. 84, no. 6, pp. 627–638, 2003.
- [73] A. White, D. Burns, and T. W. Christensen, 'Effective terminal sterilization using supercritical carbon dioxide.', *J. Biotechnol.*, vol. 123, no. 4, pp. 504–15, 2006.
- [74] A. Dillow, R. Langer, N. Foster, and J. Hrkach, 'Supercritical fluid sterilization method', *US Pat. 6,149,864*, 2000.
- [75] M. Perrut, 'Sterilization and virus inactivation by supercritical fluids (a review)', *J. Supercrit. Fluids*, vol. 66, pp. 359–371, 2012.

- [76] J. Fages, H. Lochard, J. J. Letourneau, M. Sauceau, and E. Rodier, 'Particle generation for pharmaceutical applications using supercritical fluid technology', *Powder Technol.*, vol. 141, no. 3, pp. 219–226, 2004.
- [77] P. York, U. Kompella, and B. Shekunov, *Supercritical fluid technology for drug product development*. New York, USA: Marcel Dekker, Inc, 2004.
- [78] X. Zhang, X. Zhao, Y. Zu, X. Chen, Q. Lu, Y. Ma, and L. Yang, 'Preparation and physicochemical properties of vinblastine microparticles by supercritical antisolvent process.', *Int. J. Mol. Sci.*, vol. 13, no. 10, pp. 12598–607, 2012.
- [79] F. Graser and G. Wickenhaeuser, 'Conditioning of finely divided crude organic pigments', *US Pat. 4,451,654*, pp. 1–5, 1984.
- [80] E. Weidner, 'High pressure micronization for food applications', *J. Supercrit. Fluids*, vol. 47, no. 3, pp. 556–565, 2009.
- [81] A. V. M. Nunes and C. M. M. Duarte, 'Dense CO₂ as a Solute, Co-Solute or Co-Solvent in Particle Formation Processes: A review', *Materials (Basel)*, vol. 4, pp. 2017–2041, 2011.
- [82] D. F. Baldwin and C. B. Park, 'A microcellular processing study of poly (ethylene terephthalate) in the amorphous and semicrystalline states. Part I: microcell nucleation', *Polym. Eng. Sci. Sci.*, vol. 3, no. 11, pp. 1437–1445, 1996.
- [83] O. R. Davies, A. L. Lewis, M. J. Whitaker, H. Tai, K. M. Shakesheff, and S. M. Howdle, 'Applications of supercritical CO₂ in the fabrication of polymer systems for drug delivery and tissue engineering.', *Adv. Drug Deliv. Rev.*, vol. 60, no. 3, pp. 373–87, 2008.
- [84] X. Liao, H. Zhang, and T. He, 'Preparation of porous biodegradable polymer and its nanocomposites by supercritical CO₂ foaming for tissue engineering', *J. Nanomater.*, vol. 2012, pp. 1–12, 2012.

- [85] D. J. Mooney, D. F. Baldwin, N. P. Suh, J. P. Vacanti, and R. Langer, 'Novel approach to fabricate porous sponges of poly(D,L-lactic-co-glycolic acid) without the use of organic solvents.', *Biomaterials*, vol. 17, no. 14, pp. 1417–22, 1996.
- [86] S. Goel and E. Beckman, 'Generation of microcellular polymeric foams using supercritical carbon dioxide. I: Effect of pressure and temperature on nucleation', *Polym. Eng. Sci.*, vol. 3, no. 74, pp. 1137–1147, 1994.
- [87] I. Tsivintzelis, E. Pavlidou, and C. Panayiotou, 'Porous scaffolds prepared by phase inversion using supercritical CO₂ as antisolvent', *J. Supercrit. Fluids*, vol. 40, no. 2, pp. 317–322, 2007.
- [88] S. Siripurapu, Y. J. Gay, J. R. Royer, J. M. DeSimone, R. J. Spontak, and S. A. Khan, 'Generation of microcellular foams of PVDF and its blends using supercritical carbon dioxide in a continuous process', *Polymer (Guildf)*, vol. 43, no. 20, pp. 5511–5520, 2002.
- [89] S. R. S. Rudrangi, R. Bhomia, V. Trivedi, G. J. Vine, J. C. Mitchell, B. D. Alexander, and S. R. Wicks, 'Influence of the preparation method on the physicochemical properties of indomethacin and methyl- β -cyclodextrin complexes.', *Int. J. Pharm.*, 2015.
- [90] R. Singh and N. Bharti, 'Characterization of cyclodextrin inclusion complexes—a review', *J. Pharm. Sci. Technol.*, vol. 2, no. 3, pp. 171–183, 2010.
- [91] M. E. Brewster and T. Loftsson, 'Cyclodextrins as pharmaceutical solubilizers.', *Adv. Drug Deliv. Rev.*, vol. 59, no. 7, pp. 645–66, 2007.
- [92] T. Irie and K. Uekama, 'Cyclodextrins in peptide and protein delivery.', *Adv. Drug Deliv. Rev.*, vol. 36, no. 1, pp. 101–123, 1999.

- [93] M. Sauceau, E. Rodier, and J. Fages, 'Preparation of inclusion complex of piroxicam with cyclodextrin by using supercritical carbon dioxide', *J. Supercrit. Fluids*, vol. 47, no. 2, pp. 326–332, 2008.
- [94] S. W. Jun, M. S. Kim, J. S. Kim, H. J. Park, S. Lee, J. S. Woo, and S. J. Hwang, 'Preparation and characterization of simvastatin/hydroxypropyl-beta-cyclodextrin inclusion complex using supercritical antisolvent (SAS) process.', *Eur. J. Pharm. Biopharm.*, vol. 66, no. 3, pp. 413–21, 2007.
- [95] A. K. Anal and H. Singh, 'Recent advances in microencapsulation of probiotics for industrial applications and targeted delivery', *Trends food Sci. Technol.*, vol. 18, no. 5, pp. 240–251, 2007.
- [96] F. Niu, J. Haslam, R. Rajewski, and B. Subramaniam, 'A fluidized-bed coating technology using near-critical carbon dioxide as fluidizing and drying medium', *J. Supercrit. Fluids*, vol. 66, pp. 315–320, 2012.
- [97] A. Tsutsumi, S. Nakamoto, T. Mineo, and K. Yoshida, 'A novel fluidized-bed coating of fine particles by rapid expansion of supercritical fluid solutions', *Powder Technol.*, vol. 85, no. 3, pp. 275–278, 1995.
- [98] T. J. Wang, A. Tsutsumi, H. Hasegawa, and T. Mineo, 'Mechanism of particle coating granulation with RESS process in a fluidized bed', *Powder Technol.*, vol. 118, no. 3, pp. 229–235, 2001.
- [99] H. Kröber and U. Teipel, 'Microencapsulation of particles using supercritical carbon dioxide', *Chem. Eng. Process. Process Intensif.*, vol. 44, no. 2, pp. 215–219, 2005.
- [100] C. Vogt, R. Schreiber, G. Brunner, and J. Werther, 'Fluid dynamics of the supercritical fluidized bed', *Powder Technol.*, vol. 158, no. 1–3, pp. 102–114, 2005.

- [101] K. Rosenkranz, M. M. Kasper, J. Werther, and G. Brunner, 'Encapsulation of irregularly shaped solid forms of proteins in a high-pressure fluidized bed', *J. Supercrit. Fluids*, vol. 46, no. 3, pp. 351–357, 2008.
- [102] B. Katzung, S. Masters, and A. Trevor, *Basic & clinical pharmacology*, 12th ed. McGraw-Hill, 2012.
- [103] L. F. Atyaksheva, I. V. Dobryakova, I. I. Ivanova, E. E. Knyazeva, R. a. Ovsyannikov, and E. S. Chukhrai, 'Adsorption properties of hemoglobin', *Russ. J. Phys. Chem. A*, vol. 86, no. 3, pp. 468–474, 2012.
- [104] F. DeVenuto, 'Stability of hemoglobin solution during extended storage.', *J. Lab. Clin. Med.*, vol. 92, no. 6, pp. 946–52, 1978.
- [105] S. Bettati, C. Viappiani, and A. Mozzarelli, 'Hemoglobin, an "evergreen" red protein.', *Biochim. Biophys. Acta*, vol. 1794, no. 9, pp. 1317–24, 2009.
- [106] F. H. Martini, J. L. Nath, and E. F. Bartholomew, *Fundamentals of anatomy and physiology*, 9th ed. San Francisco, USA: Benjamin Cummings, 2011.
- [107] M. Paoli, R. Liddington, J. Tame, A. Wilkinson, and G. Dodson, 'Crystal structure of T State haemoglobin with oxygen bound at all four haems', *J. Mol. Biol.*, vol. 256, no. 4, pp. 775–792, 1996.
- [108] K. C. Chou, 'Low-frequency resonance and cooperativity of hemoglobin', *Trends Biochem. Sci.*, vol. 14, no. 6, p. 212, 1989.
- [109] M. W. King, 'Hemoglobin and Myoglobin', 2013. [Online]. Available: <http://themedicalbiochemistrypage.org/hemoglobin-myoglobin.php#hemoglobin>. [Accessed: 19-May-2013].
- [110] S. Pin, B. Alpert, and A. Michalowicz, 'An investigation by iron K-edge spectroscopy of the oxidation state of iron in hemoglobin and its subunits.', *FEBS Lett.*, vol. 147, no. 1, pp. 106–10, 1982.

- [111] J. Choi, S. Muniyappan, J. T. Wallis, W. E. Royer, and H. Ihee, 'Protein conformational dynamics of homodimeric hemoglobin revealed by combined time-resolved spectroscopic probes.', *Chemphyschem*, vol. 11, no. 1, pp. 109–14, 2010.
- [112] F. Höök, M. Rodahl, B. Kasemo, and P. Brzezinski, 'Structural changes in hemoglobin during adsorption to solid surfaces: effects of pH, ionic strength, and ligand binding.', *Proc. Natl. Acad. Sci. U. S. A.*, vol. 95, no. 21, pp. 12271–6, 1998.
- [113] A. K. Bajpai and R. Sachdeva, 'Study on the adsorption of hemoglobin onto bentonite clay surfaces', *J. Appl. Polym. Sci.*, vol. 85, no. 8, pp. 1607–1618, 2002.
- [114] W. Wang, S. K. Singh, N. Li, M. R. Toler, K. R. King, and S. Nema, 'Immunogenicity of protein aggregates-concerns and realities.', *Int. J. Pharm.*, vol. 431, no. 1–2, pp. 1–11, 2012.
- [115] R. Solaro, F. Chiellini, and A. Battisti, 'Targeted Delivery of Protein Drugs by Nanocarriers', *Materials (Basel)*, vol. 3, no. 3, pp. 1928–1980, 2010.
- [116] S. Mitragotri, P. A. Burke, and R. Langer, 'Overcoming the challenges in administering biopharmaceuticals: formulation and delivery strategies.', *Nat. Rev. Drug Discov.*, pp. 1–18, 2014.
- [117] I. I. Slowing, J. L. Vivero-Escoto, C. W. Wu, and V. S. Y. Lin, 'Mesoporous silica nanoparticles as controlled release drug delivery and gene transfection carriers.', *Adv. Drug Deliv. Rev.*, vol. 60, no. 11, pp. 1278–88, 2008.
- [118] R. Roggers, S. Kanvinde, S. Boonsith, and D. Oupický, 'The practicality of mesoporous silica nanoparticles as drug delivery devices and progress toward this goal.', *AAPS PharmSciTech*, vol. 15, no. 5, pp. 1163–71, 2014.

- [119] C. Barbe, J. Bartlett, L. Kong, K. Finnie, H. Q. Lin, M. Larkin, S. Calleja, A. Bush, and G. Calleja, 'Silica Particles: A Novel Drug-Delivery System', *Adv. Mater.*, vol. 16, no. 21, pp. 1959–1966, 2004.
- [120] S. Kwon, R. K. Singh, R. A. Perez, E. A. Abou Neel, H. W. Kim, and W. Chrzanowski, 'Silica-based mesoporous nanoparticles for controlled drug delivery.', *J. Tissue Eng.*, vol. 4, 2013.
- [121] S. Areva, V. Aäritalo, S. Tuusa, M. Jokinen, M. Lindén, and T. Peltola, 'Sol-Gel-derived TiO₂-SiO₂ implant coatings for direct tissue attachment. Part II: Evaluation of cell response.', *J. Mater. Sci. Mater. Med.*, vol. 18, no. 8, pp. 1633–42, 2007.
- [122] Q. Huo, J. Liu, L. Wang, Y. Jiang, T. N. Lambert, and E. Fang, 'A new class of silica cross-linked micellar core-shell nanoparticles.', *J. Am. Chem. Soc.*, vol. 128, no. 19, pp. 6447–53, 2006.
- [123] J. Allouche, M. Boissire, C. Helary, J. Livage, and T. Coradin, 'Biomimetic core-shell gelatine/silica nanoparticles: a new example of biopolymer-based nanocomposites', *Journal of Materials Chemistry*, vol. 16, no. 30. p. 3120, 2006.
- [124] M. Arruebo, M. Galán, N. Navascués, C. Téllez, C. Marquina, M. R. Ibarra, and J. Santamaría, 'Development of Magnetic Nanostructured Silica-Based Materials as Potential Vectors for Drug-Delivery Applications', *Chem. Mater.*, vol. 18, no. 7, pp. 1911–1919, 2006.
- [125] J. C. Mitchell and V. Trivedi, 'Pharmaceutical nanomaterials: The preparation of solid core drug delivery systems (SCDDS)', *J. Pharm. Pharmacol.*, vol. 62, no. 10, pp. 1457– 1458, 2010.
- [126] Y. Urabe, T. Shiomi, T. Itoh, A. Kawai, T. Tsunoda, F. Mizukami, and K. Sakaguchi, 'Encapsulation of hemoglobin in mesoporous silica (FSM)-enhanced thermal stability and resistance to denaturants.', *Chembiochem*, vol. 8, no. 6, pp. 668–74, 2007.

- [127] T. Cerchiara, B. Luppi, F. Bigucci, M. Petrachi, I. Orienti, and V. Zecchi, 'Controlled release of vancomycin from freeze-dried chitosan salts coated with different fatty acids by spray-drying.', *J. Microencapsul.*, vol. 20, no. 4, pp. 473–478, 2003.
- [128] M. W. Pettit, P. D. R. Dyer, J. C. Mitchell, P. C. Griffiths, B. Alexander, B. Cattoz, R. K. Heenan, S. M. King, R. Schweins, F. Pullen, S. R. Wicks, and S. C. W. Richardson, 'Construction and physiochemical characterisation of a multi-composite, potential oral vaccine delivery system (VDS).', *Int. J. Pharm.*, vol. 468, no. 1–2, pp. 264–71, 2014.

CHAPTER 2

Instrumentation and Theory of Experimental Techniques

Instrumentation and theory of all the major techniques used in this project are briefly discussed in this chapter.

2.1 Ultraviolet-visible spectrophotometry

Ultraviolet-visible (UV/Vis) spectrophotometry is one of the most frequently used techniques in pharmaceutical analysis. It measures the amount of ultraviolet (190-380 nm) and/or visible (380-800 nm) radiation absorbed by the substance in a solution. Absorption occurs when the energy of the incident light matches with the energy required to induce the electronic transitions and its associated rotational and vibrational transitions of the absorbing species as shown in Figure 2.1 [1]. According to Beer and Lambert, this absorption is proportional to the concentration of the solution and pathlength of cuvette used.

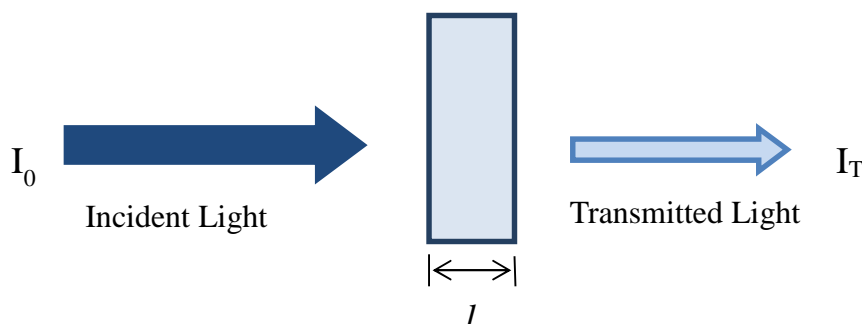


Figure 2.1: Absorption of UV light by sample

The absorbance and transmittance of UV from a sample can be presented as follows where I_0 and I_T are incident and transmitted lights respectively;

$$T \quad (T) = \frac{I_T}{I_0} \quad (E) \quad 2.1$$

$$A \quad (A) = -\log T \quad (E) \quad 2.2$$

According to the Lambert's law, the intensity of a beam of parallel monochromatic radiation decreases exponentially with the thickness or length of the cell which can be presented as follows [1].

$$A = \frac{k \cdot b}{2.303} \quad (E \quad 2.3)$$

Where, k is a constant, b is thickness or pathlength.

According to Beer's law (equation 2.4), the intensity of a beam of parallel monochromatic radiation decreases exponentially with the number of absorbing molecules [1].

$$A = \frac{k' \cdot c}{2.303} \quad (E \quad 2.4)$$

Where, k' is a constant and c is concentration.

A combination of the two laws yields the Beer-Lambert law as follows;

$$A = l \epsilon \frac{I_0}{I_T} = a \quad (E \quad 2.5)$$

Where, ' a ' is absorptivity. The name and value of ' a ' depends on the units of concentration. For example, when ' c ' is in moles per litre the constant is called molar absorptivity and has the symbol ' ϵ '. The equation then becomes

$$A = \epsilon \cdot b \cdot c \quad (E \quad 2.6)$$

The ϵ depends on the wavelength of the light and on the compound's structure, orientation and environment. At a particular wavelength, the absorbance increases with increase in concentration of absorbing species. Figure 2.2 presents a schematic diagram of a typical double beam UV spectrophotometer.

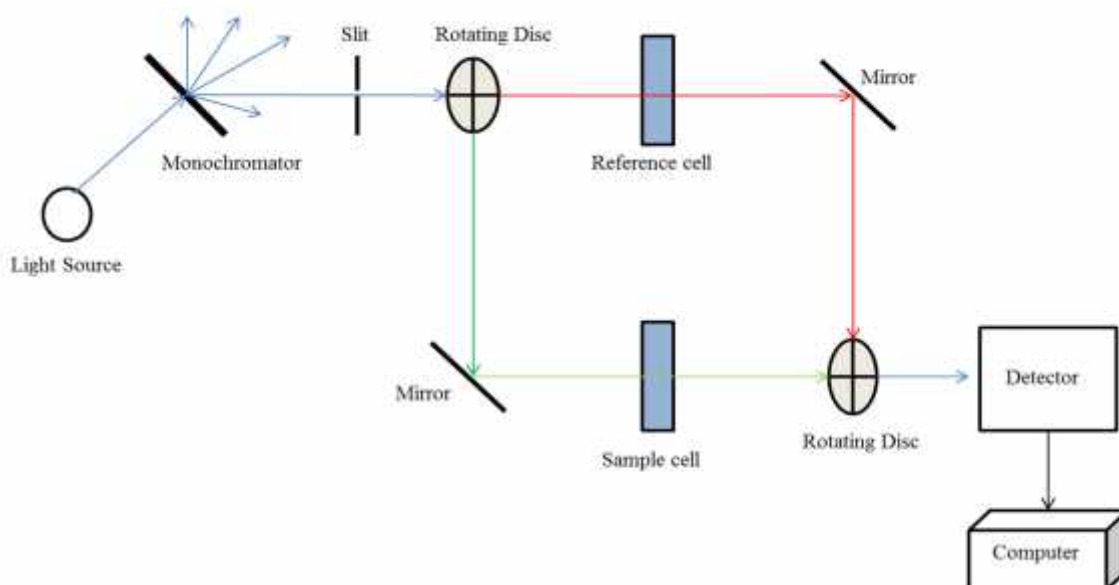


Figure 2.2: Schematic diagram of a double-beam UV spectrophotometer.

The light from the tungsten or deuterium source is focused on a monochromator to obtain a monochromatic beam which then passes through a narrow slit so that light of only a specific wavelength reaches to the rotating disc or beam splitter. The rotating disc has half reflecting and half transmitting sides which along with the help of mirrors allow the incident light to pass through reference and sample cells. The light after passing through the respective cells is detected by a photomultiplier and analysed by the software. The quality of spectrophotometric measurements depends on the intensity of stray light and sample conditions *i.e.* solvent, concentration, pathlength and instrumental parameters such as wavelength, slit width and scan speed [2]. The UV/vis spectra of most compounds have limited value in qualitative analysis and have been largely superseded by the more definitive infrared and mass spectroscopy techniques. However, it is one of the most widely used spectrophotometric technique for the quantitative analysis of chemical substances as pure materials and components of dosage forms in the pharmaceutical industry [3].

2.2 Circular Dichroism spectroscopy

Circular dichroism (CD) is a variant of electronic absorption spectroscopy which uses circularly polarised light instead of normal plane polarised light to detect molecules with chiral chromophore. This technique also allows detection in aqueous environment

which makes it easy to monitor changes in secondary structures of proteins caused by the alterations in pH, salt concentration, temperature and ligand binding [4]. The incident beam in CD is split into right (RCP) and left (LCP) circularly polarised components by passing through a modulator. A sample which does not absorb RCP and LCP or absorbs both to the same extent produces resultant radiations on the original plane. However, an elliptically polarised radiation is obtained when one component is absorbed to a greater extent than the other as shown in Figure 2.3 [5].



Figure 2.3: Left (L) and right (R) circularly polarised components of plane polarised radiation: [I] The two components have the same amplitude; [II] the components are of different magnitude and the resultant (dashed line) is elliptically polarised.

In practice, the CD instrument detects the LCP and RCP light separately and then displays the dichroism at a given wavelength as the difference in the absorbance of two components as shown in equation 2.7 [6]:-

$$\Delta A = A_L - A_R \quad (E \quad 2.7)$$

Where, A_L and A_R is the absorption of left and right circular polarised light respectively.

CD can also be expressed in degrees of ellipticity (θ) as;

$$\theta = t \cdot 10^{-1} (b/a) \quad (E \quad 2.8)$$

Where, a and b are major and minor axes of the resultant ellipse.

The numeric relationship between ΔA and θ can be presented as follows [6]:-

$$\theta = \Delta A \quad (E \quad 2.9)$$

It must be noted that due to the small size of many measurements, θ is often quoted as millidegrees (m°) or 1/1000 of a degree. The main advantage of CD over other protein structure determining techniques *e.g.* X-ray crystallography and nuclear magnetic resonance is that CD measurements can be carried out rapidly where a good quality spectrum can be obtained within minutes [7]. Other advantages include small sample requirements and non-destructive nature of the technique. Moreover, possibility of using cells of different pathlengths also allow samples to be studied in a wide range of concentrations [7]. CD provides reliable secondary structure content of a protein but it does not designate different regions of a protein with specific structural type [7]. However, the value of CD information can be enhanced by secondary structure prediction algorithms. The limitations of CD include; low resolution structural data and no information on the quaternary structure of proteins.

The schematic diagram of a CD spectrometer is shown in Figure 2.4.

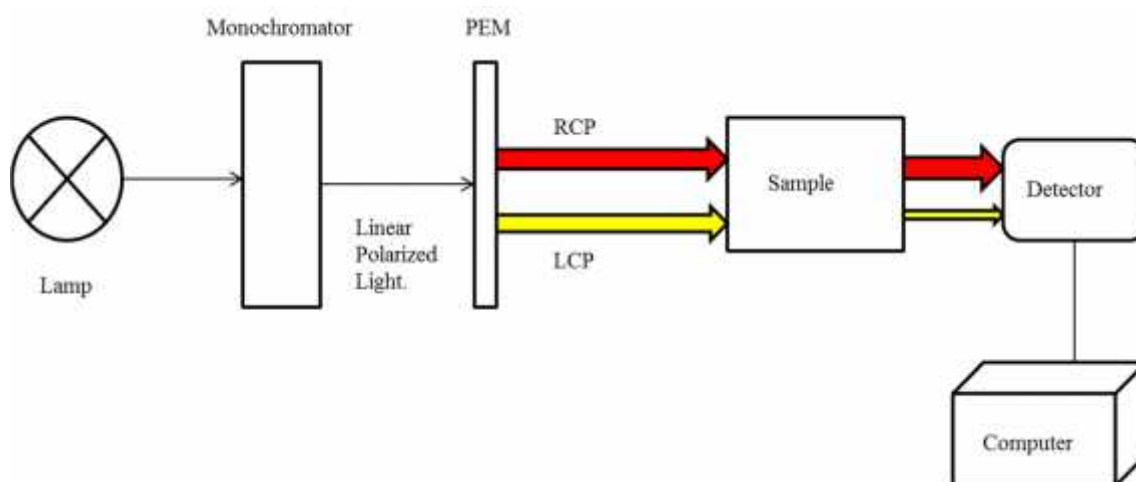


Figure 2.4: Schematic diagram of CD Spectrometer

In CD, a non-polarised light from the lamp is made linearly polarised by a monochromator which is then transformed into circularly polarised light by photoelastic modulator (PEM). The incident beam reaching to the sample switches between LCP/RCP lights and the difference in the absorption of these two components is

recorded by the detector. A plot between the wavelength and CD signal provides important information such as characteristic spectrum of a protein.

2.3 Differential Scanning Calorimetry

Differential scanning calorimetry (DSC) is one of the most commonly used thermal analysis techniques due to its availability, speed and simplicity. DSC measures the temperature and heat flow associated with thermal events (melting, glass transitions, crystallisation and decomposition) as a function of time and temperature in a controlled atmosphere [8]. There are mainly two types of DSCs; power compensated and heat flux [9]. Figure 2.6 presents a schematic of heat flux DSC used in this study. In heat flux DSC, the difference in the heat flow between reference and sample is measured while both are heated by the same unit. The heat to the sample and reference materials is carried by a thermoelectric disk made of Constantan (an alloy of Copper and Nickel) as shown in the Figure 2.5. The stage on which the sample and reference pans are located is made of Chromel disks. The differential heat flow between the sample and reference material is monitored by the thermocouple formed at the junction of constantan platform and the chromel disks. The heat flow from heating furnace to each crucible can be given by equation 2.10 for this type of DSC.

$$\frac{d}{dt} = \frac{\Delta T}{R} \quad (E \quad 2.10)$$

Where, ' Q ' is heat, ' t ' is time, ' T ' is the temperature difference between furnace and crucible and ' R ' is thermal resistance of the path between furnace and crucible [8].

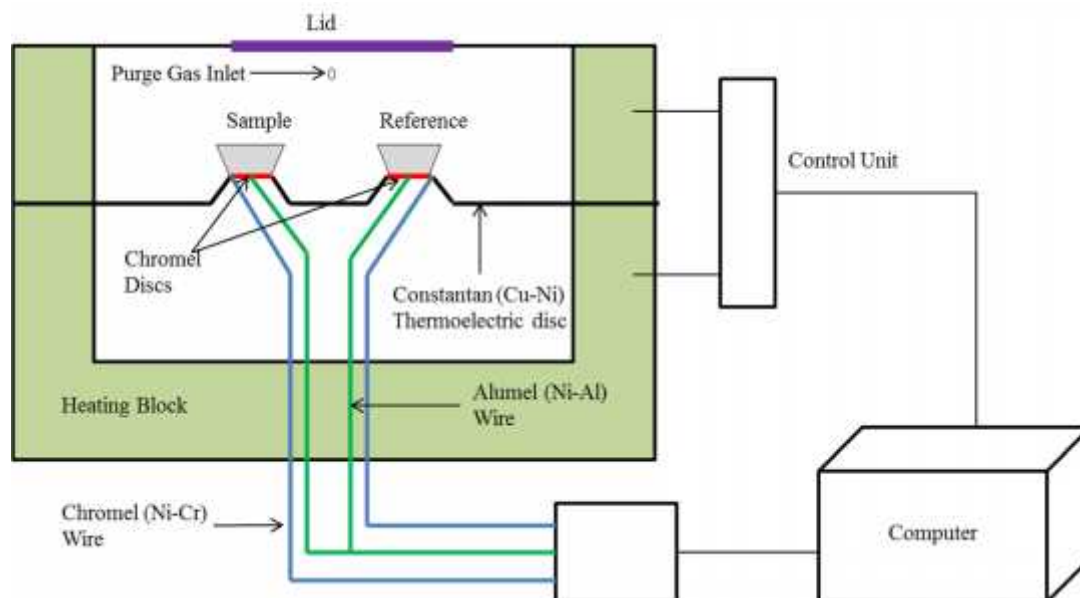


Figure 2.5: Schematic diagram of a heat flux DSC

In a power compensated DSC, the sample and reference temperature is controlled independently using separate but identical furnaces. The exothermic or endothermic changes in the samples are compensated by applying power or energy to either one or both the furnaces and therefore a ‘thermal null’ state is maintained at all times. The difference in power required by the sample and reference furnace is then measured as a function of temperature. Other DSCs such as modulated DSC use the same cell arrangement as heat-flux instrument but the temperature programme is modulated by superimposing a sinusoidal function to produce a micro heating and cooling cycle independent of the overall heating and cooling cycles [9].

These methods of analysis can be used to evaluate compound purity, polymorphism, solvation, degradation, drug–excipient compatibility, and a wide variety of other thermal characteristics [10].

2.4 Powder X-ray Diffraction

Powder X-ray Diffraction (PXRD) is a widely used technique for the characterisation of crystalline materials. Traditionally, this method has been used for phase identification, quantitative analysis and determination of structural imperfections [11].

Microcrystalline materials such as inorganic, organic and pharmaceutical compounds, minerals, catalysts, metals and ceramics can also be characterised using PXRD [11]. Schematic diagram of PXRD is shown in Figure 2.6.

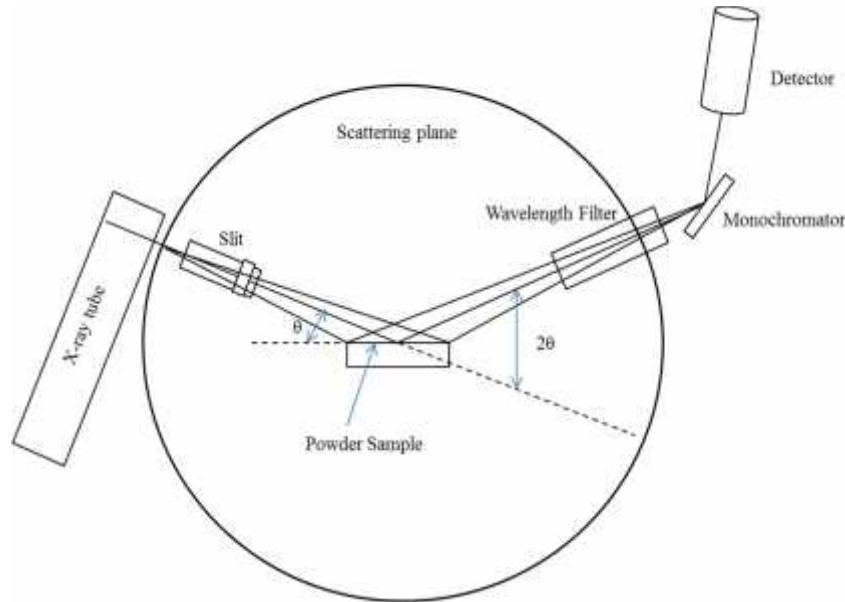


Figure 2.6: Schematics of PXRD instrument [12]

In XRD, crystalline samples containing regular repeating arrays of atoms are irradiated by a monochromatic beam of X-rays. These radiations undergo diffraction and result in an unique fingerprint of the material in the form of diffraction peaks [13]. The intensities of these peaks are measured to obtain information on crystalline components of the sample. The diffraction phenomenon can be explained by Bragg's law [14]

$$n\lambda = 2d \sin \theta \quad (E \quad 2.11)$$

Where,

' n ' is an integer, ' λ ' is wavelength of the X-rays, ' d ' is inter-planar spacing of parallel lattice planes and 2θ is the diffraction angle

Bragg's law states that the reflection of X-rays from the parallel lattice planes of a crystalline material is similar to that of visible light from a mirror. However, unlike visible light, X-rays can penetrate deep inside the material and undergo a number of additional reflections. The reflected X-rays go through constructive interference and

give rise to sharp intensity maxima which are characteristic to the sample and used for its identification [14]. The major components of PXRD instrument are X-ray tube, collimator or slits, filters, monochromator and detector. A schematic of X-ray tube is shown in Figure 2.7 where X-rays are generated. It is made of an evacuated glass tube (encased in lead shield and a steel jacket) containing cathode (wire filament) and anode (pure metal) with a Beryllium window. The cathode gives off electrons (thermoemission) upon electrical heating which accelerate towards the nearby anode and release energy in the form of X-radiations upon striking it. These radiations are directed towards the sample after passing through a collimator.

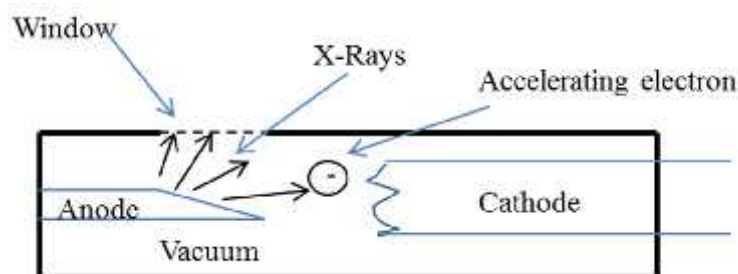


Figure 2.7: Schematics of X-ray tube

Multiple tube or multiple slit collimator arrangements are used to make the X-rays a parallel beam. Commonly, collimators are placed before the sample and detector. The use of collimator increases the wavelength resolution, cuts down stray X-ray emission and reduces background noise [15]. X-ray detectors convert photon energy into electric pulses which are counted in a period of time and are generally expressed as counts per second. The three major classes of X-ray detectors used are; gas-filled, scintillation and semiconductor detectors. In a gas filled detector, the X-rays ionize the gas into positive ions and free electrons. The electric field applied across the chamber records the movement of the free electrons and measures the current produced. On the other hand, scintillation detectors work by converting the X-rays into optical photons using materials such as sodium iodide and then detecting the light by photomultiplier tubes. Whereas, semiconductor detectors employ devices made of silicon or germanium. The interaction of X-rays with these semiconductor devices generate electrons and holes which are then measured to obtain the signal.

X-ray powder diffraction has many applications, few of which are listed here [11]:-

- a) Qualitative identification and characterisation of single phase materials.
- b) Quantitative determination of distinct crystalline phases in a sample.
- c) Determination of crystallite size and its microstructural imperfections.
- d) Identification of structural and microstructural changes as a function of an external constraint (temperature, atmosphere, pressure, electric field, etc.)
- e) Determination of crystal structure and refinement.

2.5 Supercritical Phase Monitor

The supercritical phase monitor (SPM) is an analytical tool to determine the solubility parameters and phase behaviour of compounds and mixtures in sub and supercritical fluids. It provides direct, visual observation of materials under precisely controlled conditions. A schematic diagram of SPM is presented in Figure 2.8.

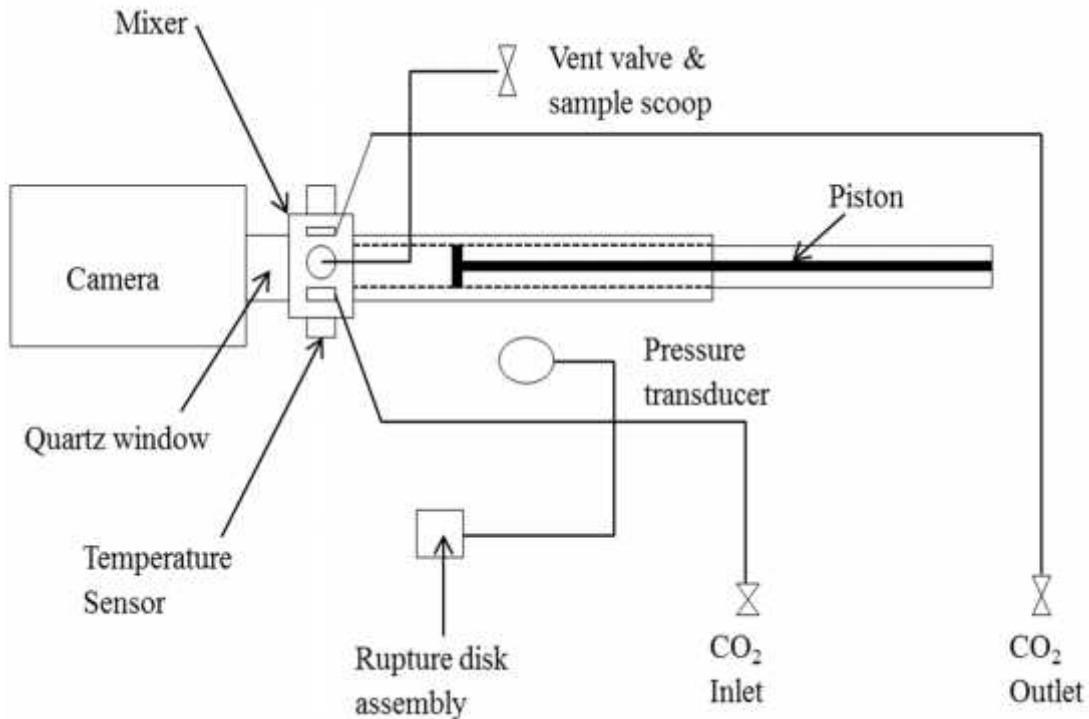


Figure 2.8: Schematic diagram of supercritical phase monitor

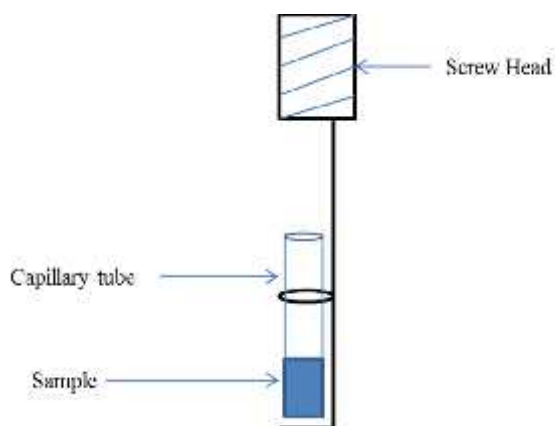


Figure 2.9: Diagram of sample holder

The main components of SPM include; sample holder, reaction chamber and a manually controlled syringe pump. A sample filled capillary tube is held securely in an optimal viewing position for solubility and melting point studies in the captive holder as shown in Figure 2.9. The reaction vessel on SPM is a 20 ml steel flask with a syringe pump and quartz windows. The heating of this vessel is controlled and maintained by an internally mounted resistance temperature detector with a precision of 0.2 °C and the desired pressure can be achieved by manually rotating the syringe pump. The reaction chamber is illuminated by a variable intensity, fibre optic light source through a quartz window. Visual observations on samples in the reaction vessel are carried out by a variable focus, charged-couple device camera attached to the second quartz window. The main advantages of SPM are the ability to monitor experiments live and small sample requirements. SPM was used in the present study to determine the effect of pressure on the phase behaviour of excipients in liquid or SCCO₂.

2.6 Scanning Electron Microscopy

Scanning electron microscopy (SEM) is a powerful analytical tool to obtain detailed images of a sample using concentrated beam of high energy electrons. The SEM analysis can provide information on the external morphology (texture), crystalline structure and chemical compositions of the sample. A conventional SEM regime i.e. magnification range from 20X to 30,000X and spatial resolution of 50 to 100 nm can examine approximately 5 µm to 1 cm area in width and provide qualitative and

quantitative information. The main components of SEM include electron gun, lenses, sample stage, detectors and data output devices. The schematic diagram of a typical SEM instrument is shown in Figure 2.10.

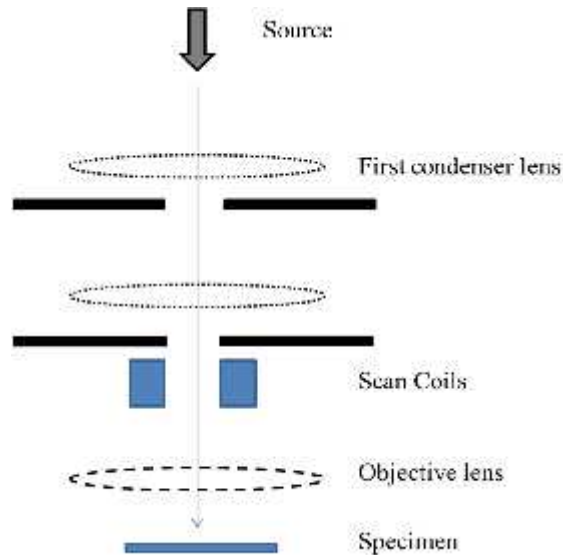


Figure 2.10: Schematics of SEM

In SEM, a monochromatic beam is produced by the electron source or electron gun which should have adjustable energy, small spot size, less energy dispersion and greater stability with high current. The older SEM systems used tungsten “hairpin” or lanthanum hexaboride cathodes but the modern SEMs prefer field emission sources which offer lower energy dispersion and enhanced current. The instrument used in this project ‘Hitachi SU8030 series’ has the emission gun as an electron source and provides a resolution of 1.1 nm at 1 kV and 0.8 nm at 15 kV. The beam from the emission source is passed through a set of condenser lenses to avoid divergence and keep it parallel. The condenser is a magnetic lens consisting of two rotationally symmetric iron pole pieces with a copper winding which provide adjustable magnetic field to control the focal point of the electron beam [19]. A second condenser lens is also used in modern SEM devices to provide additional control on the fast moving electrons. Figure 2.11 describes the use of condenser lens and aperture to focus the electrons into a desired area at the sample surface.

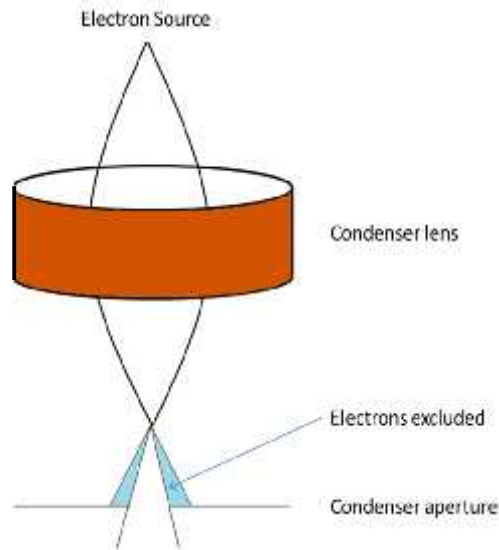


Figure 2.11: Diagram showing electron beam through the condenser lens and aperture.

The complex interactions between fast moving electrons and sample can provide different morphological, compositional and structural information as shown in Figure 2.12.

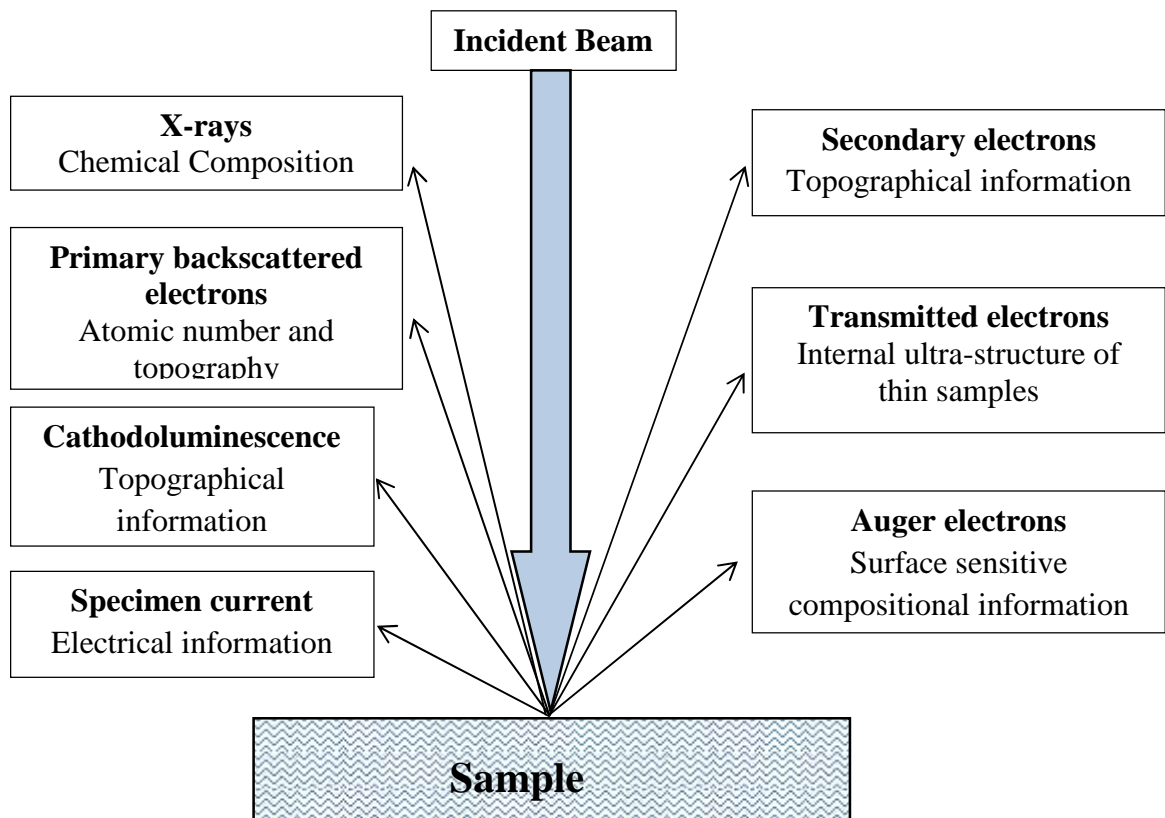


Figure 2.12: Applications of SEM [16]

Though the entire range of above mentioned signals are present in SEM, not all of them are generally used for analysis. Most commonly used signals are the secondary electrons for topographical, X-rays for compositional and backscattered electrons for atomic number and structural information.

2.7 Brunauer, Emmett and Teller and Barrett, Joyner and Halenda models

Stephen Brunauer, Paul Hugh Emmett and Edward Teller (BET) published the first article about the BET theory in 1938. This theory explains the multilayer physisorption of gases on solid surfaces and helps in calculating the specific surface area of porous materials. The BET equation as shown in equation 2.12 assumes multilayer formation and an increase in adsorbate-adsorbent binding with the increase in the concentration of adsorbate molecules. [17].

$$\frac{V}{V_m} = \frac{c \cdot x}{(1 - x)[1 + (c - 1)x]} \quad (E \quad 2.12)$$

Where,

' V ' is volume/moles adsorbed at standard temperature and pressure (STP), ' V_m ' is volume/moles adsorbed when surface is completely covered or monolayer is formed at STP, ' c ' is the BET constant (indicates the relative strength of adsorption to the surface and condensation of pure adsorbate) and ' x ' is P/P_0 (P is the pressure of the gas and P_0 is the saturated equilibrium vapour pressure)

The BET equation can also be presented in a different form as shown in equation 2.13 to enable the estimation of V_m and c [18].

$$\frac{x}{V(1 - x)} = \frac{1}{c \cdot V} + \frac{(c - 1)x}{c \cdot V} \quad (E \quad 2.13)$$

The above equation resembles a straight line equation and a plot between $x / V(1 - x)$ and ' x ' provides values of ' c ' and ' V_m ' from the intercept and slope respectively. The specific surface area or area per gram of adsorbent available for adsorbate is calculated using the experimental values of ' V_m ' in the equation 2.14.

$$\Sigma = V \cdot \sigma \cdot \rho \quad (E \quad 2.14)$$

Where,

Σ is specific surface area, ' σ ' is area per adsorption site (cm^2 per molecule) and ' ρ ' is number of gas molecules per cm^3

Barrett- Joyner- Halenda (BJH) model is used to calculate the pore size and volume distribution of a sample. It uses the Kelvin equation (equation 2.15) to relate the amount of adsorbate removed from pores of a material when the relative pressure (P/P_0) is decreased from a high to low value [19].

$$R.T.ln \frac{P}{P_c} = -2\sigma \frac{V}{r_k} \quad (E \quad 2.15)$$

Where,

' V_m ' is molar volume of nitrogen, ' r_k ' is Kelvin radius, ' σ ' is surface tension of liquid nitrogen, ' P ' is the pressure at which the pore of Kelvin radius is filled, ' P_0 ' is saturation pressure of adsorbate at temperature T and ' R ' is the gas constant

This method is extremely useful in determining parameters such as pore volume, specific surface area and pore size distribution. One major drawback of this technique can be the time required for measurements. Although, measurements can be done automatically but single analysis can take up to hours. The pore diameter range that can be determined is from 0.3 to 300 nm, which is not completely covered by mercury porosimetry [20]. The samples are also required to be kept cold (-196°C) using liquid nitrogen which can have untoward effect on sensitive analytes [20].

2.8 Supercritical fluid processing instrument

The coating of protein adsorbed silica particles was performed on the instrument presented in Figure 2.13.

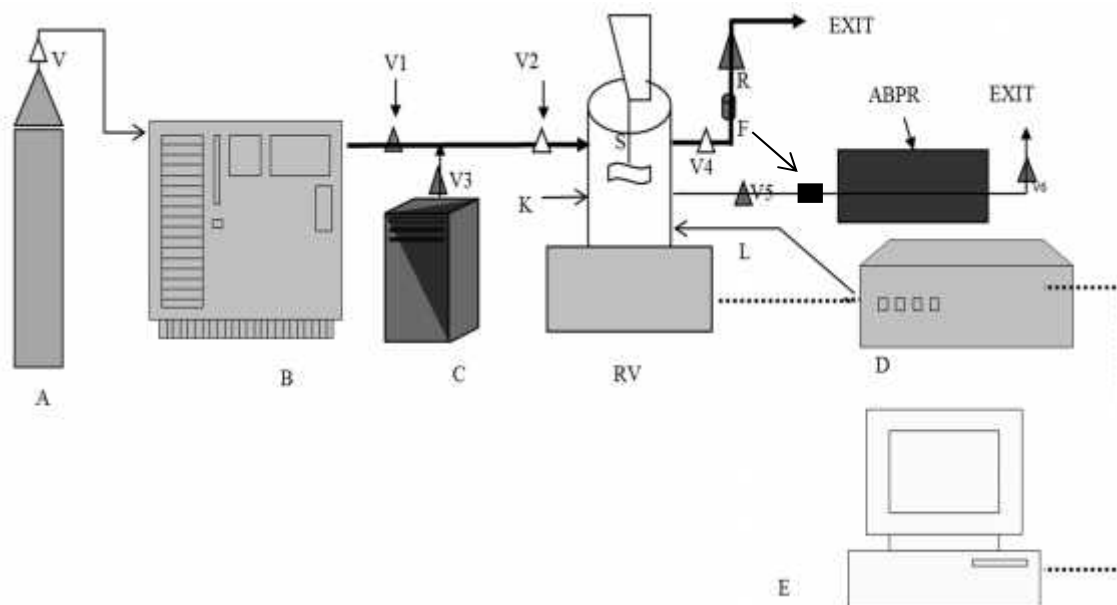


Figure 2.13: Schematic presentation of SCF instrument

The supercritical fluid (SCF) instrument mainly consists of a CO₂ cylinder (A), chilling unit (B), CO₂ pump (C), reaction vessel (RV), automatic back pressure regulator (ABPR), controller (D) and display unit (E). The chilling unit helps to maintain the pump heads and the CO₂ from the cylinder at 6 °C throughout the transit. The RV is a temperature controlled, 150 ml, 3.5 cm thick stainless steel cylinder with sapphire windows where the experiments are carried out. It consists of two parts where the lid or head can be removed to place the sample inside the chamber. A variable speed stirrer is also attached to the lid for the efficient mixing of the contents. The maximum working temperature and pressure for the current setup is 100 °C and 450 bar. Interior of the RV is illuminated by a light source (L) which allows the process to be monitored live using a camera (K) directly attached to the vessel *via* sapphire window. An automated back pressure regulator (ABPR) attached to the RV provides additional control over depressurisation process. The desired pressure and temperature values can be assigned and monitored from a control unit (D). The rate of CO₂ addition and evacuation along with the live feed from the camera can be monitored on the computer (E). There is an alternate exit valve attached directly to the RV which can be used in the case of quick uncontrolled depressurisation. There is also a possibility of addition of second RV which can be used as an expansion chamber for the generation of fine particles through PGSS process.

References

- [1] A. H. Beckett and J. B. Stenlake, *Practical pharmaceutical chemistry: part 2*. London: Continuum International Publishing Group Ltd., 1988.
- [2] W. Parson, *Modern optical spectroscopy: with exercises and examples from biophysics and biochemistry*. New York: Springer, 2007.
- [3] L. Ohannesian and A. Streeter, *Handbook of pharmaceutical analysis*. New York, USA: Marcel Dekker, Inc, 2001.
- [4] J. Johnson WC, “Secondary structure of proteins through circular dichroism spectroscopy,” *Annu. Rev. Biophys. Biophys. Chem.*, vol. 17, pp. 145–166, 1988.
- [5] S. M. Kelly, T. J. Jess, and N. C. Price, “How to study proteins by circular dichroism.,” *Biochim. Biophys. Acta*, vol. 1751, no. 2, pp. 119–39, 2005.
- [6] “CD Units & Conversions,” *Photophysics, Applied*, 2011. [Online]. Available: <http://www.photophysics.com/tutorials/circular-dichroism-cd-spectroscopy/7-cd-units-conversions>. [Accessed: 25-Dec-2012].
- [7] S. Kelly and N. Price, “The Use of Circular Dichroism in the Investigation of Protein Structure and Function,” *Curr. Protein Pept. Sci.*, vol. 1, no. 4, pp. 349–384, 2000.
- [8] D. Craig and M. Reading, *Thermal analysis of pharmaceuticals*. Boca raton, US: CRC Press, 2010.
- [9] D. Skoog, F. Holler, and T. Nieman, *Principles of instrumental analysis*. Canada: Thomson Brooks/Cole, 1998.
- [10] S. Ahuja and N. Jespersen, *Modern instrumental analysis*. Oxford, UK: Elsevier, 2006.

- [11] T. Wenzel, *Encyclopedia of spectroscopy and spectrometry: part 2.*, vol. 2. Elsevier, 2000.
- [12] R. Gilles, D. Mukherji, M. Hoelzel, P. Strunz, D. M. Toebbens, and B. Barbier, “Neutron and X-ray diffraction measurements on micro- and nano-sized precipitates embedded in a Ni-based superalloy and after their extraction from the alloy,” *Acta Mater.*, vol. 54, no. 5, pp. 1307–1316, 2006.
- [13] J. H. Reibenspies, *Principles and applications of powder diffraction*. Chichester, UK: John Wiley & Sons, Ltd, 2009.
- [14] R. Dinnebier and S. Billinge, *Powder diffraction: theory and practice*. Cambridge, UK: RSC Publishing, 2008.
- [15] J. Robinson, E. Frame, and G. M. Frame II, *Undergraduate instrumental analysis*, 6th ed. New York, USA: Marcel Dekker, Inc, 2004.
- [16] W. Zhou, R. P. Apkarian, and Z. L. Wang, “Fundamentals of Scanning Electron Microscopy,” in *Scanning Microscopy for Nanotechnology*, W. Zhou and Z. L. Wang, Eds. New York, NY: Springer New York, 2006, pp. 1–40.
- [17] P. C. Wankat, *Rate-Controlled Separations*, 1st ed. Indiana, USA: Springer, 1994.
- [18] D. Freifelder, *Physical Chemistry for Students of Biology and Chemistry*. Boston, Massachusetts: Science Books International, Inc, 1982.
- [19] E. P. Barrett, L. G. Joyner, and P. P. Halenda, “The Determination of Pore Volume and Area Distributions in Porous Substances. I. Computations from Nitrogen Isotherms,” *J. Am. Chem. Soc.*, vol. 73, no. 1, pp. 373–380, 1951.
- [20] S. Westermarck, “Use of Mercury Porosimetry and Nitrogen Adsorption in Characterisation of the Pore Structure of Mannitol and Microcrystalline Cellulose Powders, Granules and Tablets,” University of Helsinki, Finland, 2000.

CHAPTER 3

Materials and methods

All reagents used in the project along with the standard methods for melting point determination, DSC and PXRD analysis, UV and CD procedures etc. are discussed in this chapter.

3.1 Materials

The chemicals used in this work are listed in Table 3.1. All excipients were stored at room temperature except bovine haemoglobin (4-8 °C) and used as supplied without any further purification.

Chemical Name	CAS no.	Batch no.	Source	Purity
Stearic acid	57-11-4	A0215983	Acros organics (USA)	97.0 %
Palmitic acid	51-10-3	A0166845001	Acros organics (USA)	98.0 %
Myristic acid	544-63-8	0001349933	Fluka analytical (Germany)	98.0 %
Lauric acid	143-07-7	MKBF0916	Sigma-Aldrich (USA)	98.0 %
Liquid CO ₂	124-38-9	NA	BOC ltd (U.K.)	99.9 %
Pluronic F-127	9003-11-6	086K0026	Sigma (USA)	NA
Pluronic F-77	9003-11-6	WPDA559B	BASF (USA)	NA
Pluronic F-38	9003-11-6	WPMB554B	BASF (USA)	NA
Pluronic F-68	9003-11-6	BCBD6489V	Sigma life science (USA)	NA
Pluronic F-108	9003-11-6	0001375698	Fluka analytical (France)	NA
Sodium hydrogen phosphate	7558-79-4	10126289	Alfa Aesar (USA)	98.0 %

Potassium dihydrogen phosphate	7778-77-0	13C120034	VWR (Belgium)	99.5 %
Bovine haemoglobin (bHb)	9008-02-0	010K7618V, SLBF3496V	Sigma (USA)	NA
Sodium hydroxide	1310-73-2	SZBD1220V	Sigma (Sweden)	98.0 %
Hydrochloric acid	7647-01-0	1340652	Fischer scientific (U.K.)	37 % w/v
Large particle silica (S _{LP})	7631-86-9	J16T039	Alfa Aesar (USA)	NA
Spherical silica (S _S)	7631-86-9	TQ25K-NK	TCI Ltd. (Japan)	NA
FP-244 silica (S _{FP})	7631-86-9	1000259186	Grace Davison (U.K.)	NA
Pentane	109-66-0	STBD5077V	Sigma (Germany)	99.0 %

Table 3.1: Chemical reagents (NA-not available)

3.2 Methods

The standard methods used throughout this project for the formulation of SCDDS are discussed in this section. Specific methods such as desorption process, coating of silica particles by SCF processing and solvent evaporation, protein release from coated particles and *in-vitro* release studies at pH 1.2 and 6.8 are detailed in sections 7.2.3, 8.2.1.2, 8.2.1.3, 8.2.1.4 and 8.2.1.5 respectively.

3.2.1 Melting and solidification point determination by supercritical phase monitor

Manufacturer- Supercritical fluid technologies (New Jersey, USA)

Instrument- Supercritical phase monitor

Capillaries- Marienfeld, 1.5 mm internal diameter

Instrument was calibrated prior to the experiments using naphthalene as standard. 1 to 3 mg of powdered sample was filled in the glass capillary and placed in the captive holder which was then firmly positioned inside the reaction chamber. Liquid CO₂ was released into the vessel and the desired pressure was achieved and maintained by manually

rotating the syringe pump. The temperature was increased slowly by the increments of 0.2 °C until the complete melt was observed (except in the case of lauric acid which melted at room temperature). This was repeated at each predetermined pressure value between 70 to 500 bar in the case of fatty acids and from 20 to 500 bar in the case of pluronics. The phase change of the excipients was monitored live *via* camera attached to the quartz window on the reaction vessel and values for the complete melt were recorded. Figure 3.1 presents an example of Pluronic F-68 at various stages of the experiment. The analysis was carried out in triplicates for all samples.

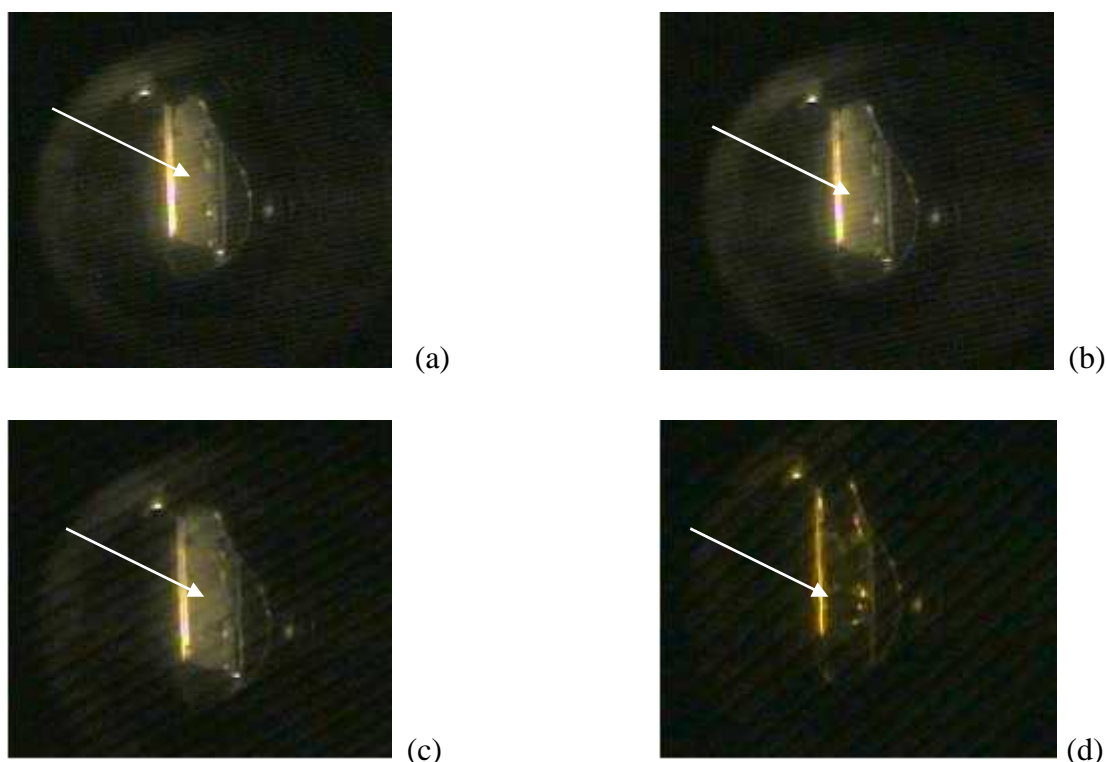


Figure 3.1: Various stages of the experiment [Pluronic F-68 at the; (a) Beginning of the experiment (b) After the introduction of CO₂ (c) Start of melting (d) Complete melt]

Solidification pressure and temperature were also determined for fatty acids. For solidification, heating on the reaction vessel was turned off and the chamber was allowed to cool down. The temperature and pressure values at which gradual expulsion of CO₂ from the sample matrix induced solidification occurred were noted in triplicates for each fatty acid. These experiments were omitted from pluronics study primarily due to the lack of precise control over the cooling rate.

3.2.2 Differential scanning calorimetry

Manufacturer- TA Instruments (Hertfordshire, U.K.)

Model number- Q2000

3-5 mg of sample was weighed in a T-zero aluminium pan (40 μ l) which was then sealed using a crimper. The sealed pans were placed inside the instrument and heated from 25 to 100 °C at a rate of 10 °C per minute. The thermograms obtained were analysed by Star Evaluation software.

3.2.3 Powder X-ray diffraction

Manufacturer- Bruker (Massachusetts, USA)

Diffractometer- D8 Advanced

Software- Diffrac.Suite

X-ray diffraction patterns were obtained at room temperature for all samples. The dry powder was sandwiched between two layers of Mylar film and placed in the sample holder. Diffractograms were collected in transmission mode using Cu K α radiations at a scan rate of 0.02°/sec from 2.5 to 50° 2 θ values by rotating the sample cell at 15 rpm. The results obtained were compared with the reference database values published by the international centre for diffraction data (ICDD) in 2008.

3.2.4 Phosphate buffer solutions

Phosphate buffers of desired pH were prepared by mixing 0.133 M disodium hydrogen phosphate (Na₂HPO₄) and 0.133 M potassium hydrogen phosphate (KH₂PO₄) as described in Table 3.2.

pH	Na ₂ HPO ₄ (ml)	KH ₂ PO ₄ (ml)
6	12.0	88.0
7	50.0	50.0
8	94.5	5.5

Table 3.2: Phosphate buffer preparation

3.2.5 Procedure for thermal stability studies of bHb by UV spectroscopy

Manufacturer- Shimadzu (Kyoto, Japan)

Instrument- UV-2550

Software- UV Probe

0.1 mg/ml bHb solution was prepared in 6, 7 and 8 pH phosphate buffer. Each of these solutions were taken in a 1 cm pathlength quartz cuvette and subjected to a temperature ramp from 25 to 65 °C in the UV spectrophotometer and cooled back to 25 °C. The temperature was increased or decreased by 5 °C at a time and sample was allowed to equilibrate for 10 minutes before every measurement. Absorbance spectrum was recorded between 200 to 700 nm after every 5 °C increase/decrease in the temperature.

3.2.6 Procedure for thermal stability studies of bHb by CD spectroscopy

Manufacturer- Applied photophysics (Surrey, U.K.)

Software- Chirascan and CDNN

The bHb solutions prepared in pH 6, 7 and 8 phosphate buffers were subjected to heating and cooling cycle similar to UV experiments. Samples were heated in 1 mm pathlength cylindrical quartz cuvette from 25 to 65 °C and then cooled back to 25 °C. The sample was allowed to equilibrate for 10 minutes before every measurement. The CD spectrum was recorded in the far UV region between 190 to 260 nm with a bandwidth of 1 nm and sampling time of 2 seconds per point. The CD spectra obtained were then deconvoluted using CDNN software supplied by applied photophysics.

3.2.7 Procedure for six hour stability of bHb

0.1 mg/ml solutions of bHb were prepared in phosphate buffers of pH 6, 7 and 8. Three separate sets of samples were stored at room temperature (23 ± 2 °C) and their stability was analysed by CD and UV spectroscopy after 0, 1, 2, 4 and 6 hours. The CD and UV spectra were collected according to the methods described in sections 3.2.5 and 3.2.6.

3.2.8 Procedure for inter-day stability of bHb

Three sets of 0.1 mg/ml solutions of bHb were prepared in pH 6, 7 and 8 phosphate buffers and stored at 23 ± 2 °C and 4 ± 1 °C. The stability of these samples were analysed by collecting the CD and UV spectra according to the methods described in sections 3.2.5 and 3.2.6 after 0, 1, 2, 3 and 40 days.

3.2.9. Procedure for agitation stability of bHb

Protein solution of 0.1 mg/ml concentration in pH 6 phosphate buffer was stirred in a 10 ml volumetric flask at 250 rpm for 5 hours. UV and CD analysis was performed after 0, 1, 2, 3, 4 and 5 hours to determine conformation changes due to stirring at room temperature (23 ± 2 °C).

3.2.10 Adsorption of bHb onto silica particles

The following sections contain protocols employed to establish maximum protein adsorption and bHb adsorption kinetics on three morphologically different silica used in this study.

3.2.10.1 Maximum adsorption of bHb on silica particles

The adsorption experiments were carried out only for 4 hours due to protein stability issues. 0.5, 1, 2 and 4 mg/ml protein solutions in pH 6 phosphate buffer were prepared and 10 ml of each solution was transferred in a volumetric flask. 400 mg of silica was added to each flask and the contents were stirred at 250 rpm at room temperature. After 4 hours, the supernatant was collected, filtered and analysed by UV spectrophotometer. The quantity of bHb adsorbed was calculated using an indirect method *i.e.* by subtracting the remaining amount of bHb in the solution from the initial content. The bHb concentrations used for the adsorption experiments on S_{FP} were 8, 12 and 16 mg/ml due to its higher adsorption capacity. The adsorption experiments were conducted in triplicates for all three silica particles.

3.2.10.2 Kinetic measurements of bHb adsorption on silica particles

The kinetic measurements were conducted using 1, 2 and 8 mg/ml protein concentrations for S_S , S_{LP} and S_{FP} respectively. These concentrations were selected by studying the results obtained from experiments mentioned in section 3.2.10.1. For kinetic measurements, 10 ml of the above mentioned protein concentrations were taken in 9 volumetric flasks (one for each time point) of 10 ml capacity and 400 mg of silica was added to each of them. The contents were stirred at 250 rpm and UV measurements were taken after 15, 30, 45, 60, 90, 120, 180 and 240 minutes in the case of S_S and also after 300 minutes for S_{LP} and S_{FP} . The experiments were conducted at ambient conditions and readings were recorded in triplicates.

3.2.10.3 Adsorption protocol for further studies

This adsorption protocol used throughout the formulation development is based on the findings from the experiments discussed in sections 3.2.10.1 and 3.2.10.2. Protein solutions of 1, 2 and 8 mg/ml concentrations were prepared in pH 6 phosphate buffer for bHb adsorption on S_S , S_{LP} and S_{FP} respectively. 400 mg of silica was added to each of these solutions and the mixture was stirred at 250 rpm for 4 hours at 23 ± 2 °C. After this, particles were separated from the media either by allowing the suspension to stand for 15 minutes (S_S and S_{LP}) or centrifugation (S_{FP}) at 2000 rpm for 2 mins. The supernatant was decanted and the remaining protein adsorbed silica particles were freeze dried to remove any residual solvent.

3.2.11 BET studies on silica particles

Manufacturer- Micromeritics instrument corporation (Hertfordshire, U.K.)

Instrument- Gemini 2380

BET analysis was performed on all three silica particles before and after protein adsorption to determine the specific surface area, pore volume and pore distribution. 10-16 mg of silica particles were weighed in the sample tube and degassed with nitrogen in order to remove any moisture or adsorbed gases. The degas conditions used for pure and protein adsorbed silica were 100 °C for 4 hours and 40 °C for 8 hours respectively.

Sample and reference tubes were then placed firmly inside the instrument and were dipped in liquid nitrogen. The air in the tubes was evacuated at the rate of 50-100 mmHg/min for 5 minutes. Complete BET adsorption and desorption isotherms were obtained at P/P_0 from 0.05 to 1. Pore sizes were calculated using BJH model.

3.2.12 SEM analysis of silica particles

Manufacturer- Hitachi (Texas, USA)

Instrument- SU8030

These experiments were conducted to determine the morphology of different types of silica studied in this work. Approximately 1-2 mg of silica particles were placed on the sample stub and the excess/loose particles were removed. The stub was then mounted onto the sample holder and placed inside the SEM. The focus and stigmatism of the microscope were adjusted and the micrographs were collected using upper detector. The voltages used to accelerate the electrons were 1.0 and 0.5 kV and the working distance was approximately 2.3 mm.

3.2.13 Simulated intestinal fluid /Phosphate buffer pH 6.8 (USP)

Phosphate buffer was prepared by mixing 50 ml of 0.2 M monobasic potassium phosphate solution with 22.4 ml of 0.2 M sodium hydroxide solution in a 200 ml volumetric flask. The de-ionised water was used to make up the volume to 200 ml. This solution was used as simulated intestinal fluid (without pancreatin) for bHb release from SCDDS.

CHAPTER 4

Supercritical fluid processing of excipients

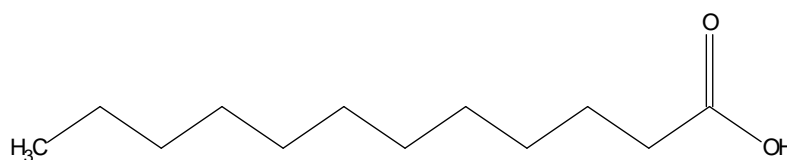
This chapter discusses the effect of pressure on the phase behaviour of saturated fatty acids (FAs) and pluronics in the pressurised carbon dioxide (CO₂). The temperature and pressure values for the maximum depression in melting temperature of these excipients were determined in liquid or supercritical carbon dioxide (SCCO₂) and the information was utilised in the formulation of SCDDS. FAs studied in this work were lauric acid (LA), myristic acid (MA), palmitic acid (PA) and stearic acid (SA). Pluronic used in this study were F-127, F-77, F-38, F-68 and F-108.

4.1 Introduction

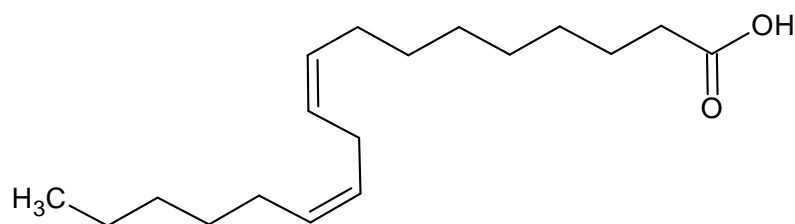
FAs and pluronics are amongst the most commonly used excipients in the food and pharmaceutical industries as they are non-toxic and widely available. These excipients have also been studied in the development of various novel drug delivery systems [1], [2]. The physical properties and applications of FAs and pluronics are discussed in this section.

4.1.1 Fatty acids

FAs are carboxylic acids with long hydrocarbon side chain, which are divided into two major groups, saturated and unsaturated. Saturated FAs contain only single bonds in the hydrocarbon chain whereas unsaturated FAs have one or more carbon-carbon double/triple bonds. Figure 4.1 shows examples of saturated and unsaturated FAs [3].



a.) Lauric acid (Saturated fatty acid)



b.) Linoleic acid (Unsaturated fatty acid)

Figure 4.1: Structure of FAs a) Lauric acid, b) Linoleic acid

Physical properties of the saturated FAs studied in this work are listed in Table 4.1.

Fatty acid	Lauric acid (LA)	Myristic acid (MA)	Palmitic acid (PA)	Stearic acid (SA)
Molecular weight (g/mol)	200.32	228.38	256.43	284.48
Melting point (°C)	44.0- 46.0	52.0-54.0	61.0-62.5	69.0-71.0
Boiling point (°C) (at 100 mm Hg)	225.0	250.0	271.5	361.0
Density at 25°C (g/cm ³)	0.880	0.862	0.852	0.840
Water solubility at 25°C (mg/l)	55.0	2.4	0.83	0.34

Table 4.1: Physical properties of saturated FAs [4]–[8].

The physical properties such as boiling and melting points of FAs are dependent upon the carbon chain length of the molecule as shown in Table 4.1. For example, melting point of FAs increases with the increase in carbon chain length and molecular weight. Similarly, polarity of FAs decreases with the increase in the number of carbon atoms in the molecule with an overall effect on their aqueous solubility. In general, FAs are poorly soluble in water and their solubility decreases with the decrease in carbonyl group polarity or increase in carbon chain length. For example, solubility of SA is approximately 160 times lower than LA in water at 20 °C [9]. However, their solubility in water improves with pH *e.g.* the solubility of LA increases from 55 mg/l at neutral conditions to 200 mg/l in pH 7.4 phosphate buffer [3], [10]. Similarly, the solubility of FAs in CO₂ also increases with the decrease in carbon chain length and there are

numerous studies which discuss this phenomenon but the information regarding the effect of pressure on the melting behaviour of these excipients in CO₂ is scarce [11]–[14].

FAs have found numerous applications in pharmaceutical and food industry as they are biologically inert, nontoxic and biocompatible [1]. These excipients are used in the development of several drug delivery systems such as FA implants containing insulin [15], ofloxacin-loaded PA solid lipid nanoparticles [16], SA nanoparticles loaded with cyclosporine A [17], encapsulation of paclitaxel into LA based micelles [18] and cefuroxime-axetil containing SA microparticles [19].

4.1.2 Pluronic

Pluronic or poloxomers (non-proprietary name) are tri block copolymers consisting of hydrophilic poly (ethylene oxide) [PEO] and hydrophobic poly (propylene oxide) [PPO] segments in a PEO-PPO-PEO arrangement. The general structure of a pluronic molecule is presented in Figure 4.2. Pluronic nomenclature includes one alphabet followed by two or three digit number. The alphabet represents the physical form of the product, where ‘F’ stands for flakes/solid, ‘L’ for liquid and ‘P’ for paste. The first digit (*e.g.* 3 in the case of F-38) or two digits (*e.g.* 12 in the case of F-127) multiplied by 300 provide the molecular mass of the central hydrophobe or PPO. Whereas, the last digit of the code represents the percentage weight content of PEO when multiplied by 10. For example, pluronic F-77 is a solid with PPO block’s approximate molecular weight of 2100 (7 x 300) and PEO content of 70% [20].

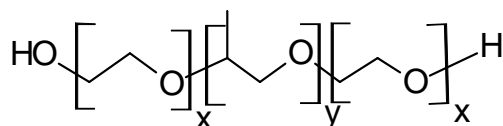


Figure 4.2: Generalised structure of a pluronic molecule; where x and y are positive integers

Pluronic are manufactured by sequential polymerisation in the presence of an alkaline catalyst such as sodium hydroxide where the PPO block is synthesised followed by the growth of PEO chains at both ends of it [21]. Pluronic are large polymers with high average molecular weight therefore commercially available pluronic may have the

admixtures of PPO homopolymer along with di and tri-block copolymers [20]. The physical properties along with the number of EO and PO units of the pluronics studied in this work are presented in Table 4.2.

Pluronic	Average molecular weight (g/mol)	Melting point (°C)	Weight EO	Weight PO	EO (units) x/2	PO (units) y
F38	4600	48	3680	920	84	16
F68	8400	52	6720	1680	152	30
F108	14600	57	11680	2920	266	50
F77	6600	48	4620	1980	106	34
F127	12600	56	8820	3780	202	65

Table 4.2: Physical properties of pluronics

Pluronic are commonly used pharmaceutical excipients listed in United States and British pharmacopoeia and have found variety of applications in drug delivery. They are widely used as emulsifying, dispersion, solubilisation, thickening, coating, and wetting agents [2]. Pluronic display surfactant properties including the ability to interact with hydrophobic surfaces and biological membranes due to their amphiphilic nature [22]. The incorporation of drugs into pluronic micelles is known to increase the solubility and stability of drugs [23]. Pluronic have shown to modify the biological response by overcoming drug resistance in cancer and promoting drug transport across cellular barriers [2], [24]. Pluronic-polyacrylic acid copolymers also demonstrated the potential for the oral administration of chemotherapeutic agents such as camptothecin [25].

Similar to FAs, the solubility of low molecular weight pluronics (upto 3738 g/mol) in CO₂ has been discussed in the literature but data on large pluronics is difficult to find. In general, the solubility of (L) pluronics decreases with an increase in the PEO/PPO ratio for a given molecular weight and increases with the increasing molecular weight for polymers with constant PEO/ PPO ratio [26], [27].

As discussed earlier, the interactions of saturated FAs and high molecular weight pluronics with CO₂ are either unknown or scarcely described in literature. The study discussed in this chapter evaluated the effect of the increase in carbon chain length of saturated FAs and the influence of PPO/PEO ratio and molecular weight of pluronics on the S-L (solid-liquid) transitions of these excipients with respect to pressure in liquid or supercritical CO₂.

4.2 Materials and methods

This section discusses the methods used for the SCF processing of FAs and pluronics.

4.2.1 Materials

Refer to section 3.1

4.2.2 Melting point determination by supercritical phase monitor

Refer to section 3.2.1

4.2.3 Differential scanning calorimetry (DSC)

Refer to section 3.2.2

4.2.4 Powder X-ray diffraction

Refer to section 3.2.3

4.3 Results and discussion

An effect of the molecular weight/carbon chain length on the melting behaviour was observed for all studied FAs. Whereas, pluronics did not show any such correlations in terms of molecular weight or PPO/PEO content. A detailed discussion on the melting behaviour of FAs and pluronics in pressurised CO₂ is presented in the following sub-sections.

4.3.1 Effect of pressure on melting point depression of FAs in CO₂

FAs melted 10.7 to 19.5 °C below their actual melting point in pressurised CO₂. This depression in melting temperature was inversely proportional to the carbon chain length of FAs *i.e.* the longer the carbon chain length, the lower the depression in melting point. The minimum melting temperatures of FAs in pressurised CO₂ are presented in Table 4.3.

FA	T _m at 1 bar (°C)*	T _m in CO ₂		T (°C)
		T _m (°C)	P (bar)	
LA	44.5	25.0 ± 0.0	70	19.5
MA	54.4	41.2 ± 0.2	100	13.2
PA	63.0	51.1 ± 1.1	150	11.9
SA	69.9	58.9 ± 0.2	150	10.7

Table 4.3: Melting point depression of FAs (* Determined by DSC)

As shown in Table 4.3, MA melted at 41.2 °C and 100 bar in CO₂ which was 13.2 °C lower than its actual melting point of 54.4 °C. Similarly, PA and SA showed a decrease of 11.9 and 10.7 °C respectively at 150 bar. The depression in melting temperature of 19.5 °C was largest for LA amongst all studied FAs where S-L transition took place at 25 °C and 70 bar in pressurised CO₂.

It is known that the impregnation of CO₂ in the crystalline or amorphous matrix is the main cause of the melting point and glass transition depression respectively [28]. However, the extent of CO₂ permeation in an excipient is dependent upon the interactions between CO₂ molecules and the functional groups present in the compound [29]. The CO₂ molecule does not have a dipole moment but quadrupole moment in the molecule causes a charge separation such that the oxygen atom carries more electron density than carbon atom. This charge separation favours Lewis acid-base interactions between CO₂ molecules and functional groups with high electron density such as carboxylic acids, aldehydes and ketones [30], [31]. It is known that the interaction

between CO₂ and a compound (*i.e.* CO₂-philicity) increases with the availability and accessibility of electron accepting/donating groups such as carboxyl and amino groups [32]. The inverse relationship between the melting point depression and carbon chain length arises from the favoured interaction of CO₂ with the polar carboxylic acid group of FAs. The increase in carbon chain length decreases the overall CO₂-philicity of the molecule leading to weaker interactions with CO₂ and lower decrease in melting temperature.

The CO₂-excipient interactions are also known to be affected by the processing conditions *i.e.* pressure and temperature [33]. The effect of pressure on the S-L transition of FAs is presented in Table 4.4 and Figure 4.3. These studies were conducted only on MA, PA and SA. LA was excluded from this study as it melted at 25 °C in CO₂ and it was not possible to conduct experiments below room temperature on the available setup.

Pressure (bar)	Melting point mean (°C) ± Standard deviation (n=3)		
	Myristic Acid	Palmitic Acid	Stearic Acid
70	44.3 ± 0.4	55.6 ± 0.3	62.7 ± 0.5
100	41.2 ± 0.2	52.3 ± 0.3	60.0 ± 0.2
150	41.8 ± 0.5	51.1 ± 0.5	58.9 ± 0.2
200	41.8 ± 0.5	51.7 ± 0.3	59.7 ± 0.0
250	42.5 ± 0.2	52.4 ± 0.2	60.4 ± 0.6
300	42.7 ± 0.2	53.2 ± 0.4	60.9 ± 0.4
428	43.9 ± 0.2	54.2 ± 0.2	61.7 ± 0.4
500	45.1 ± 0.2	55.2 ± 0.3	62.6 ± 0.3

Table 4.4: Melting point of MA, PA and SA in pressurised CO₂

It is evident from the results shown in Table 4.4 that the melting points of FAs vary as a function of the operating pressure. An initial increase in the pressure led to the rapid decrease in the melting temperature of MA, PA and SA. However, the melting point of FAs started to rise again with the further increase in the pressure after reaching to a minimum at 150 bar for PA, SA and 100 bar for MA. The melting trend of all three FAs

in pressurised CO₂ was alike with similar melting temperatures at the lowest (70 bar) and highest (500 bar) pressure values studied in this work.

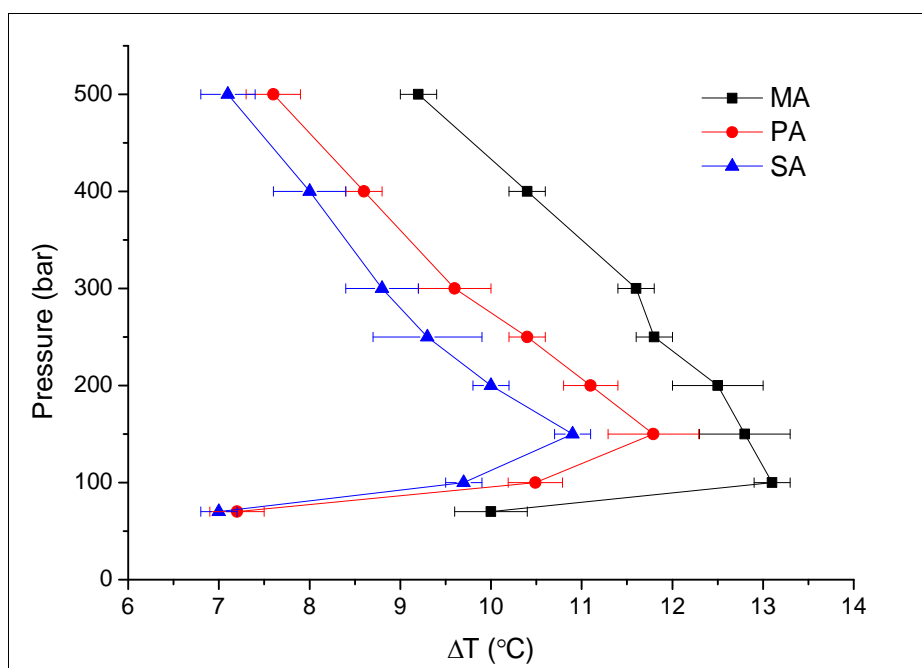


Figure 4.3: P- T diagram (melting) of MA, PA and SA

The trend in melting temperature presented in Figure 4.3 was similar to the studies reported by other researchers for MA [34], PA [34], [35] and SA [35], [36]. However, the phase behaviour of FAs above 300 bar was previously not reported in the literature. Moreover, there is variability in stated melting point data from study to study; for example, the minimum melting temperature of SA reported by Uchida *et al.* [36] was 55.5 °C at 125 bar, whereas Bertakis *et al.* reported a value of 51.5 °C at 156 bar [37]. The minimum S-L transition temperature for SA was 58.9 °C at 150 bar in this study which was slightly higher than the earlier reported values. These differences in the results could be due to various reasons such as purity of the samples, source of the samples, method of melting measurements (onset or complete) and interpersonal variations.

This trend in the melting point depression with pressure can be attributed to the solubility/sorption behaviour of CO₂ in FAs. The P- T diagram presented in Figure 4.3 clearly suggests that the solubility of CO₂ increases with the initial increase in the pressure. However, at higher values this pressure dependence on the solubility of CO₂

in a substance becomes smaller and leads to either no change or an increase in the melting temperature [37]. This can be explained by the dominance of “pressure effect” over the “solubility effect” at higher pressures [38]. Additionally, factors such as density and diffusivity of CO₂ also play an important role in this phenomenon. For example, increase in the density of CO₂ at higher pressures leads to the decrease in its diffusivity which could be attributed to the higher melting temperatures [39]. However, CO₂-excipient interaction is a complex phenomenon where more than one factor may work simultaneously to produce discussed outcomes.

4.3.2 Solidification of FAs in CO₂

Ideally, a pure substance is expected to melt and solidify at the same temperature but this is not the case for FAs studied in pressurised CO₂ as shown in Table 4.5 and Figure 4.4. The solidification of FAs always took place several degrees below their melting temperature. The solidification temperature of MA was in the range of 35 to 40 °C. Whereas, PA and SA showed a solidification range of 45-50 and 54-58 °C respectively.

Myristic Acid		Palmitic Acid		Stearic Acid	
P (bar)	T _s (°C)	P (bar)	T _s (°C)	P (bar)	T _s (°C)
68.0	37.4 ± 0.7	69.4	49.3 ± 0.3	68.8	57.7 ± 0.7
94.1	35.9 ± 0.5	97.2	47.4 ± 0.3	98.1	56.1 ± 0.1
141.9	36.2 ± 0.3	143.7	46.9 ± 0.7	142.6	55.7 ± 0.4
180.2	35.2 ± 0.2	188.9	47.1 ± 0.4	190.5	54.7 ± 0.3
226.0	36.3 ± 0.5	232.2	45.7 ± 1.0	236.5	54.0 ± 0.4
265.3	35.6 ± 0.1	284.8	47.5 ± 0.1	281.2	54.3 ± 0.9
398.6	38.1 ± 0.5	408.1	48.8 ± 0.3	405.5	56.9 ± 0.3
475.3	39.8 ± 0.9	477.1	49.7 ± 0.4	469.4	57.7 ± 0.1

Table 4.5: Solidification point of MA, PA and SA in CO₂ at different pressure; and temperatures reported are mean ± SD (n=3)

The solidification trend of FAs presented in Figure 4.4 was also similar to their melting point trends, *i.e.* solidification temperature decreased initially and then increased after

reaching to a minimum. For example, MA solidified at 37.4 °C at 68 bar in comparison to 35.2 °C at 180 bar.

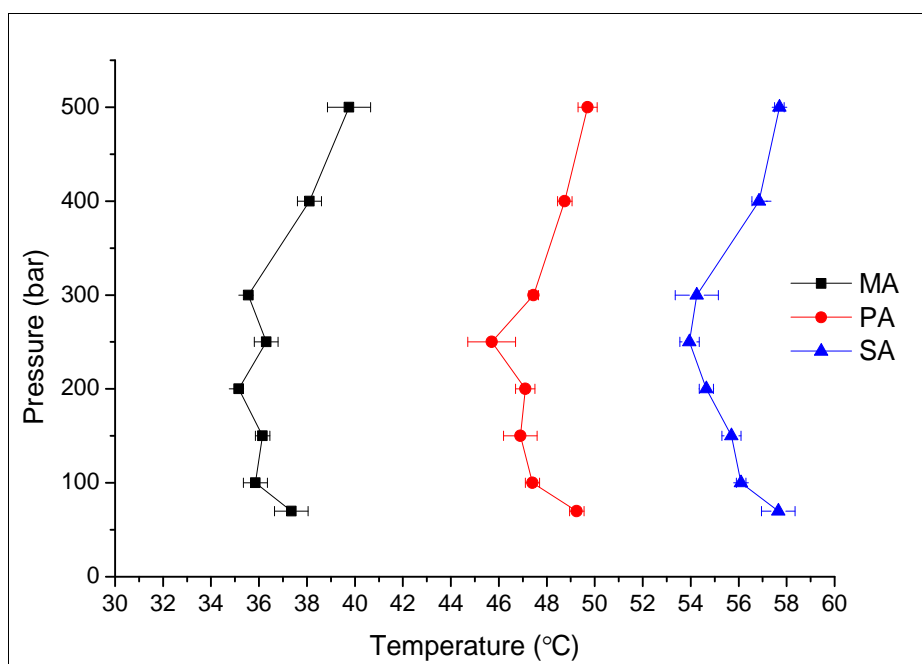


Figure 4.4: P-T diagram (solidification) of FAs

The difference between melting and solidification temperature of FAs in pressurised CO₂ are presented in Table 4.6.

Mean difference in solidification and melting temperature (°C) ± Standard deviation (n=3)			
Pressure (bar)	Myristic acid	Palmitic acid	Stearic acid
70	7.0 ± 1.0	6.4 ± 0.3	5.1 ± 0.2
100	5.4 ± 0.7	5.0 ± 0.8	4.5 ± 0.1
150	5.7 ± 0.8	4.2 ± 0.4	3.3 ± 0.3
200	6.7 ± 0.7	4.7 ± 0.6	5.1 ± 0.3
250	6.3 ± 0.6	6.7 ± 0.2	6.5 ± 0.2
300	7.2 ± 0.2	5.8 ± 0.6	6.7 ± 1.3
400	5.8 ± 0.6	5.5 ± 0.3	4.9 ± 0.2
500	5.4 ± 1.0	5.5 ± 1.0	5.0 ± 0.4

Table 4.6: Difference in melting and solidification point of FAs at various pressure values

Solidification of a substance at slightly below its melting temperature is a common phenomenon primarily due to the presence of impurities [40]. However, solidification of FAs in CO₂ occurred at several degrees below their melting point; MA solidified in the range of 35 to 40 °C, which was 5-7 °C below its melting temperature. Similarly, PA and SA solidified at 4-7 °C and 3-7 °C respectively below their melting points in pressurised CO₂. In general, a larger drop in temperature was observed for the solidification of MA followed by PA and SA.

It is worth mentioning that liquid to solid (L-S) transition in these cases occurred primarily due to the expulsion of CO₂ from the FA melt. The rate of CO₂ exclusion from the melt was mainly dependent upon the operating temperature/ pressure conditions and the affinity of the CO₂ towards the compound. Moreover, it was a closed system and any changes to the established equilibrium took place only consequently to the slow reduction in temperature of the reaction chamber. Hence, the rate of expulsion of CO₂ from the melt was relatively slow which resulted in a delayed solidification of FAs at the studied pressure range. These experiments provided a comprehensive data regarding pressure and temperature conditions for the processing of FAs. However, studies with controlled cooling rate would be beneficial to understand this phenomenon in detail.

4.3.3 Effect of pressure and melting point depression of pluronics in CO₂

Similar to FAs, the purpose of this study was to understand the phase behaviour of pluronics F-127, F-77, F-108, F-68 and F-38 in liquid or SCCO₂ and to determine the effect of pressure on their melting temperature. The melting point of pluronics at atmospheric pressure was determined using DSC and compared with the values at higher pressures in CO₂. The melting points of pluronics with respect to pressure are presented in Table 4.7.

Mean melting temperature (°C) ± standard deviation (n=3)					
Pressure (bar)	F-77	F-127	F-38	F-68	F-108
1	46.4 ± 0.2	54.0 ± 0.2	49.3 ± 0.2	52.0 ± 0.2	57.7 ± 0.2
20	44.8 ± 0.2	52.4 ± 0.3	47.4 ± 0.3	50.9 ± 0.2	55.2 ± 0.2
40	39.8 ± 0.3	48.5 ± 0.2	42.3 ± 0.3	46.1 ± 0.4	50.8 ± 0.2
60	33.9 ± 0.3	42.9 ± 0.6	35.3 ± 0.3	41.1 ± 0.3	45.7 ± 0.2
80	28.8 ± 0.6	38.8 ± 0.9	30.6 ± 0.7	34.8 ± 0.3	41.4 ± 0.6
100	29.2 ± 0.3	37.2 ± 0.7	31.4 ± 0.6	35.0 ± 0.5	40.0 ± 0.5
150	28.9 ± 0.4	37.0 ± 0.4	31.6 ± 0.4	35.0 ± 0.9	38.2 ± 0.7
200	27.2 ± 0.2	37.0 ± 0.8	31.7 ± 0.6	33.9 ± 0.2	38.8 ± 0.3
300	26.9 ± 0.2	35.9 ± 0.7	30.3 ± 0.4	32.1 ± 0.7	39.0 ± 0.6
400	27.3 ± 0.2	36.2 ± 0.9	30.3 ± 0.2	32.5 ± 0.6	39.3 ± 0.6
500	27.9 ± 0.2	36.6 ± 0.4	30.7 ± 0.2	32.8 ± 0.5	39.5 ± 0.2

Table 4.7: Melting point of pluronics in pressurised CO₂

The pluronics in pressurised CO₂ melted at a temperature range of 18.1 to 19.3 °C below their actual melting point. The melting temperature minimum for pluronic F-108 in CO₂ was 38.2 °C at 150 bar. Whereas, pluronic F-77, F-127, F-38 and F-68 showed a S-L transition minimum at 26.9, 35.9, 30.3 and 32.1 °C respectively at 300 bar.

The pressure-temperature diagram presented in Figure 4.5 showed two distinct regions where, almost linear decrease in melting point with increase in pressure could be seen in 'region A', followed by no significant change in melting temperature with pressure in 'region B'. This type of melting trend has been previously reported for other polymers such as polycaprolactone and poly (butylene succinate) in the pressure range of 1 to 276 bar and 1 to 207 bar respectively [41]. The initial decrease in the melting temperature as shown in Figure 4.5 could be accredited to the solubility/permeation effect and any increase in melting point at higher pressure was considered to be due to the pressure effect.

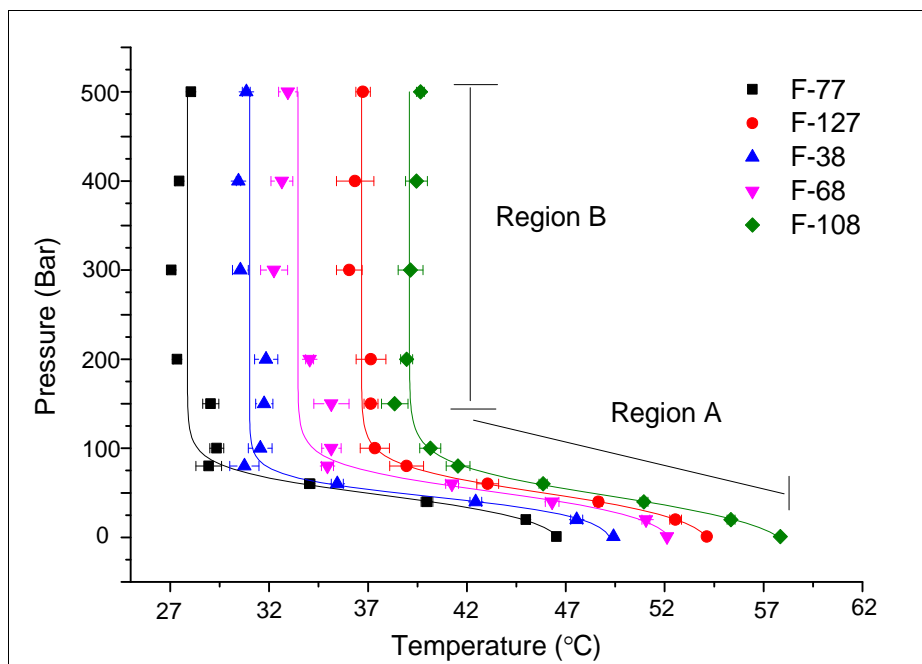


Figure 4.5: P-T diagram of pluronics

The depression in melting point of polymers is widely accepted to occur due to the increase in free volume and segment mobility caused by the impregnation of CO₂ in the molecular matrix [42]. The extent of this depression generally depends upon the ability of CO₂ to interact with CO₂-philic functional groups present in the polymer [43]. It has been shown that similar to carbonyl groups, presence of ether linkages in a polymer also promotes Lewis acid-base type interactions to encourage CO₂-polymer mixing. These interactions are dependent on both the number of available ether linkages and on the accessibility of ether oxygen [27], [29]. For example, PPO is considered relatively more CO₂-philic than PEO due to the presence of an extra methyl group per monomer unit. This weakens the intermolecular forces and improves the accessibility of CO₂ to the ether oxygen in a PPO molecule [44]. The solubility behaviour of small and medium molecular weight (up to 3738 g/mol) pluronics in CO₂ can be easily explained by this assumption where increase in the PEO content results in the decreased solubility of the polymer [27], [44]. Therefore, it could be proposed that pluronics with higher PPO content would show larger depression in the melting point in the current study. However, no such relationship was found for the pluronics studied in this work as shown in Figure 4.6. This suggested that CO₂-pluronic interactions were independent of

PPO/PEO ratio and the PPO content in the polymer as pluronics with both 20% and 30% PPO showed similar depression in the melting point in the pressurised CO₂.

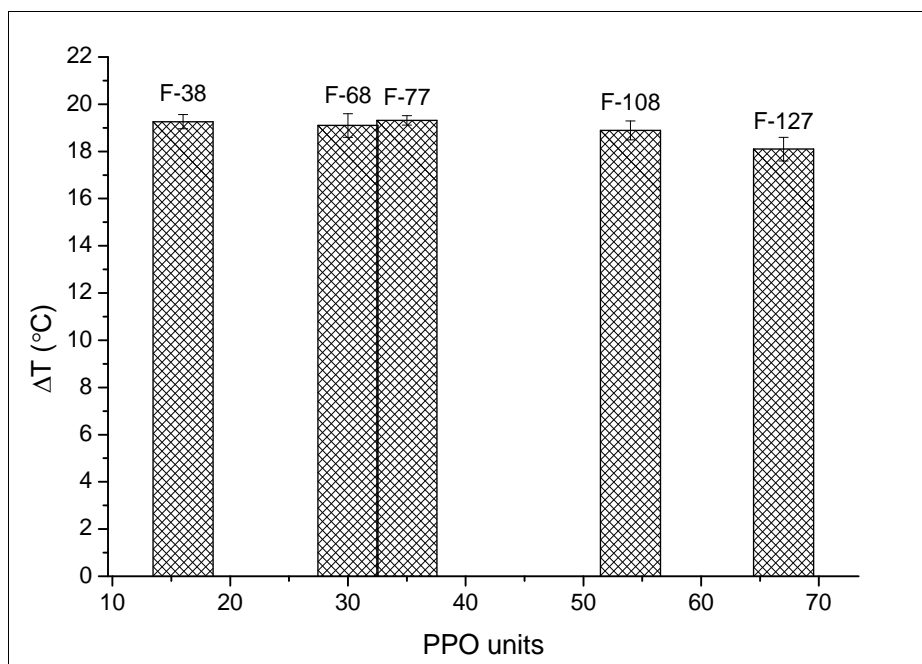


Figure 4.6: Comparison of melting point depression of pluronics with PPO units where, ($\Delta T = T_m$ measured by DSC – T_m at 300 bar).

The solubility or interaction of pluronics with CO₂ is also known to improve with their molecular weight for a fixed PPO/PEO ratio due to enhanced free volume [39]. As stated earlier, solubility of pluronics (up to 3738 g/mol) increases with the increase in the molecular weight for a particular PPO/PEO ratio. The Figure 4.7 presents a graph between the molecular weight of pluronics and their melting point depression in pressurised CO₂, which does not show any such correlations.

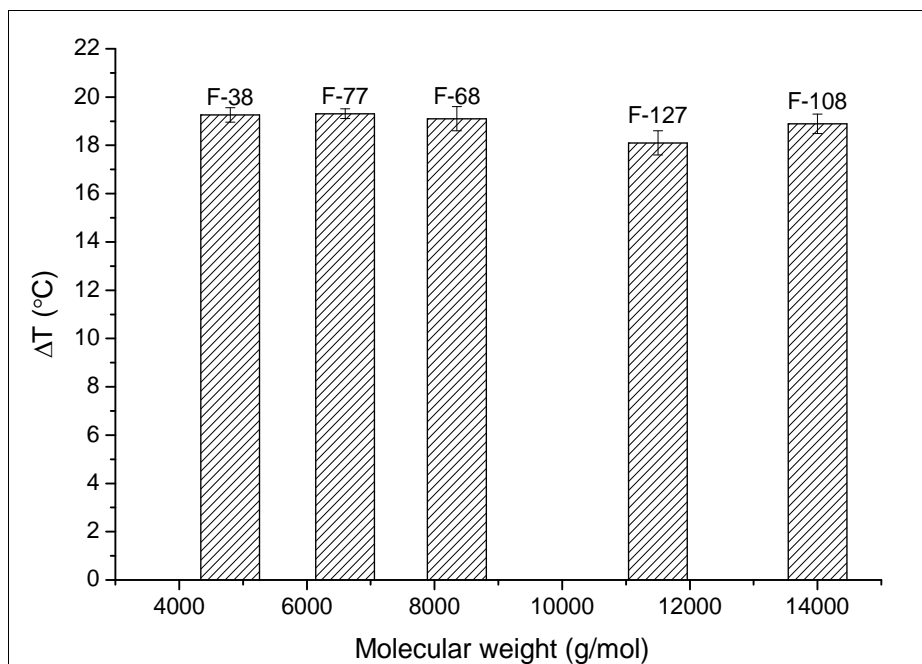


Figure 4.7: Comparison of melting point depression of pluronics with molecular weight where, ($T = T_m$ measured by DSC – T_m at 300 bar).

This behaviour of large molecular weight pluronics in pressurised CO_2 can be explained by the cohesive energy density (CED) of polymers, which is defined as the amount of energy required to completely remove a unit volume of molecules from their neighbours. Mathematically, it is the ratio of heat of vaporisation of the polymer divided by its molar volume in condensed phase [45]. In addition, it has also been reported that the increase in the number of CO_2 -philic components in a polymer results in the favourable enthalpy of mixing [46]. However, this increase in CO_2 interacting monomers can decrease the entropy of mixing by hindering the segmental motion. Hence, the increase in CO_2 -philic monomer units can enhance the CED of the copolymer only to an extent after which further incorporation of these monomers may no longer favour the enthalpy of mixing [46]. Therefore, as pluronics used in this study have large numbers of CO_2 -polymer interacting groups (ether linkages/ PPO units) which correspond to the high CED, such that the enthalpy of mixing is no longer favoured. This phenomenon explains why increase in PPO content in studied pluronics did not show higher melting point depression in pressurised CO_2 .

Nonetheless, it is also important to note that the interaction of CO_2 with polymers is a complex phenomenon which depends upon numerous factors such as number and ease

of accessibility of CO₂-philic functionalities, molecular weight of polymer, intermolecular bonding, structural regularity, chain flexibility and copolymerisation [47]. Hence, studies similar to this work at even higher pressures would be helpful to deduce the phase behaviour of pluronics in the pressurised CO₂.

4.3.4 Differential scanning calorimetric analysis

DSC analysis was performed on the unprocessed and CO₂ processed FAs and pluronics to understand the effect of CO₂ processing. The thermograms of FA and pluronics are presented in Figures 4.8 and 4.9 respectively.

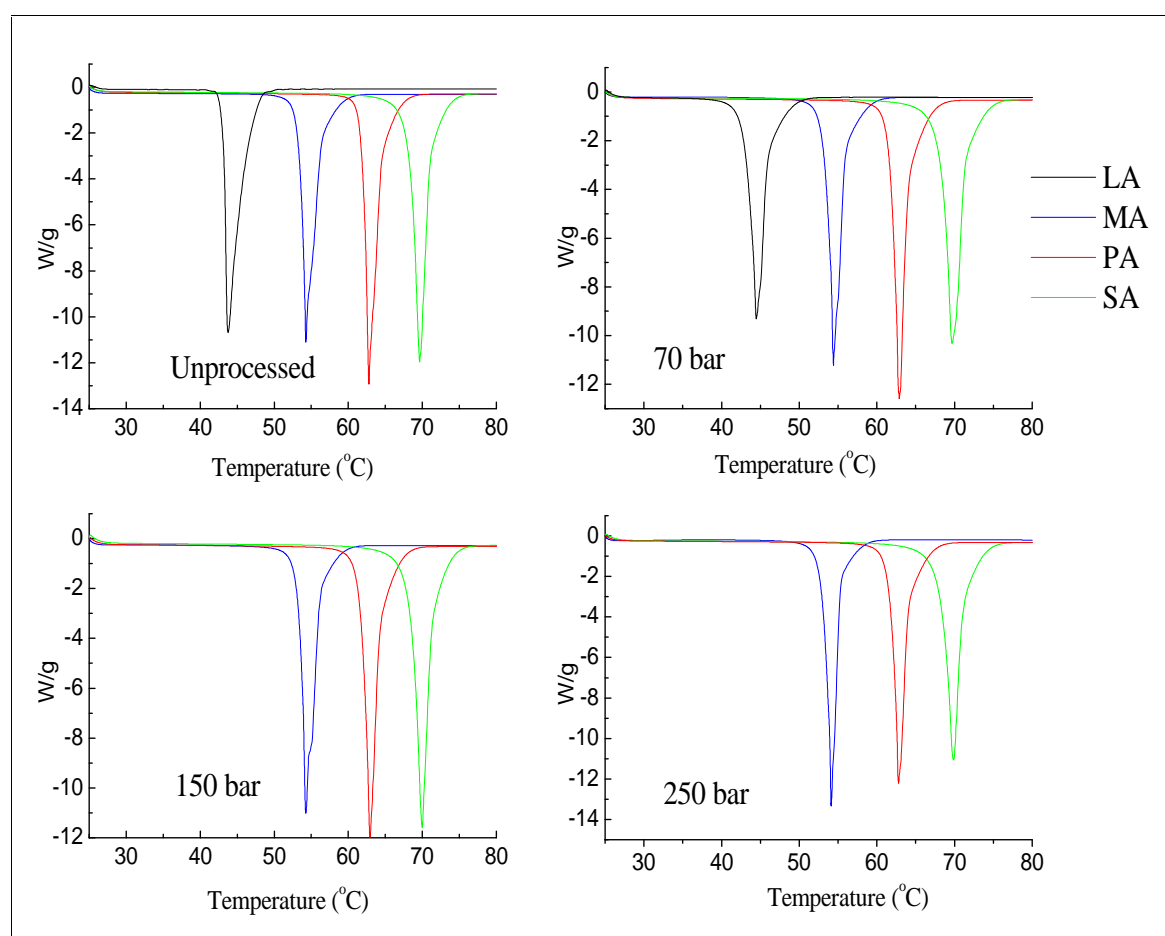


Figure 4.8: Thermograms of processed and unprocessed FAs

FA samples treated with CO₂ at (70, 150 and 250) bar were used for DSC analysis. This covered the range from lowest pressure point to when the melting temperature started to rise again. The thermograms of FAs (Figure 4.8) showed single identical melting peak

irrespective of their processing regime suggesting that CO₂ processing had not affected the thermal properties of these compounds.

Similarly, DSC analysis was performed on unprocessed pluronics and samples processed at 300 bar in CO₂. Unlike FAs, samples used here were processed only at 300 bar because all pluronics had reached to their minimum melting temperature at this pressure value. The thermograms presented in Figure 4.9 show similar onsets of melting/melting peaks for all pluronics.

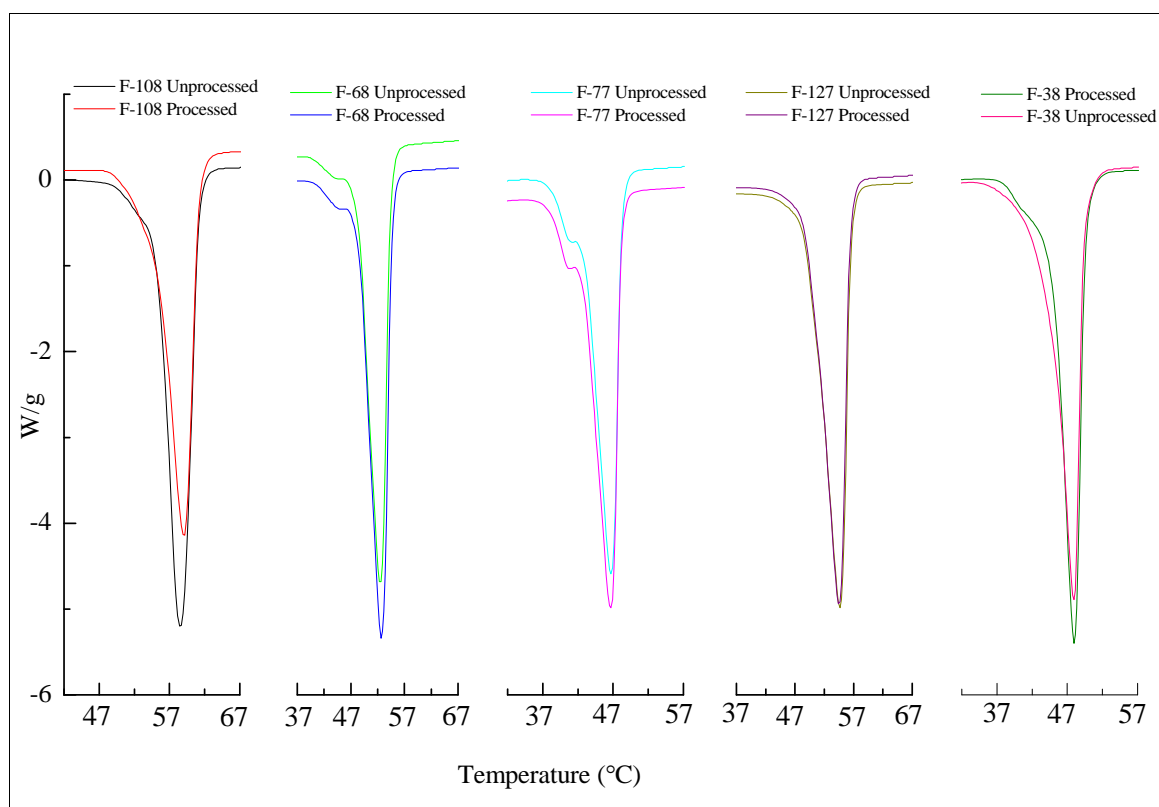


Figure 4.9: Thermograms of CO₂ processed (300 bar) and unprocessed pluronics

Any appearances of shoulder in the peaks was due to the presence of admixtures of PPO homopolymer with di or tri block copolymers [20]. Similar to the FAs, the DSC analysis of pluronics also indicated that CO₂ processing had no effect on the thermal properties of the polymers and any differences in the peak heights were due to variability in the sample size.

4.3.5 Powder X-ray diffraction analysis

Similar to the DSC experiments PXRD analysis was also performed on the unprocessed and processed samples to understand the effect of CO₂ processing on these excipients. The diffractograms of FAs and pluronics are presented in Figures 4.10 and 4.11 respectively.

PXRD analysis was performed on FAs samples treated with CO₂ at 70, 150 and 250 bar. The diffractograms of processed and unprocessed FAs as shown in Figure 4.10 suggested that no changes in the crystal structure occurred due to the CO₂ processing.

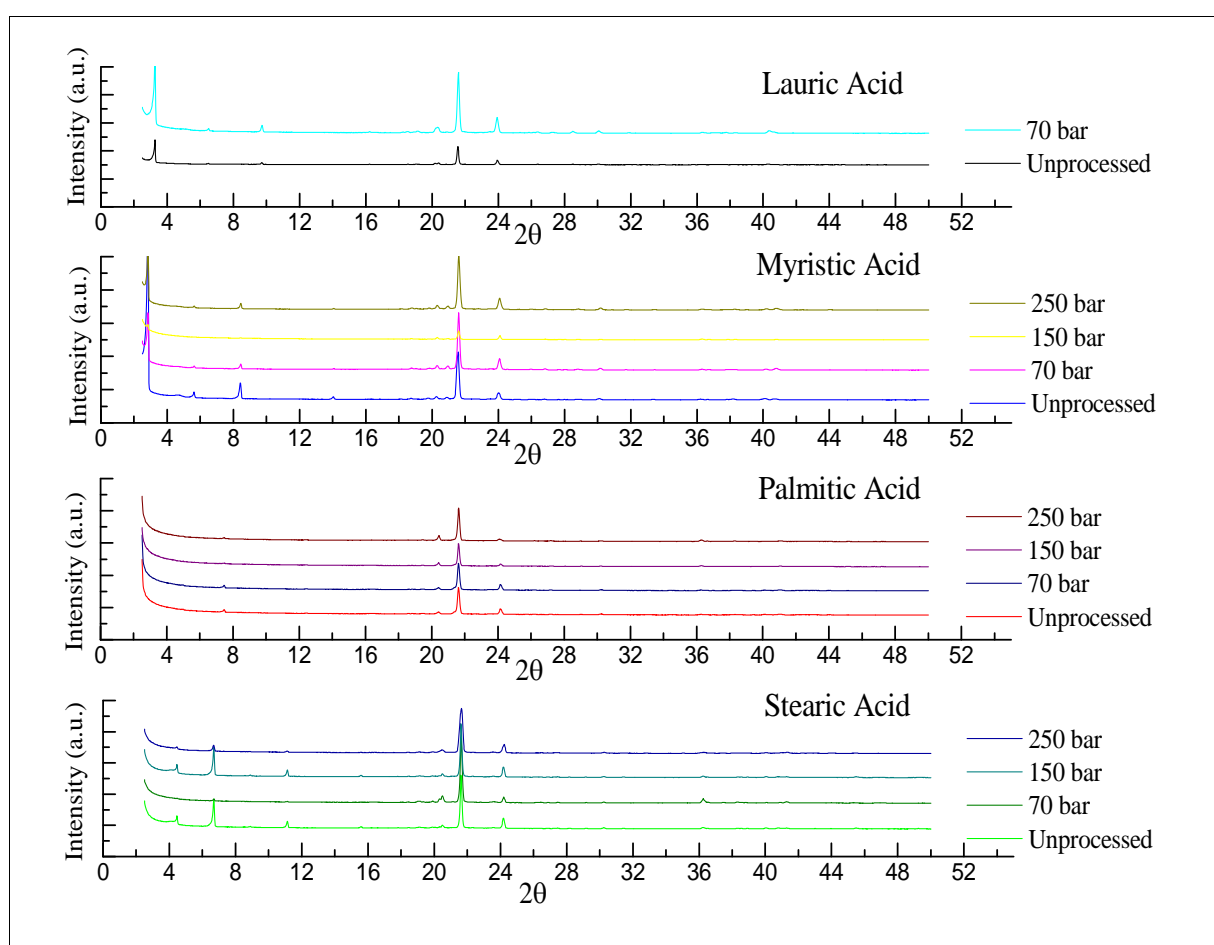


Figure 4.10: Diffractograms of processed and unprocessed FAs

The diffraction patterns obtained were compared with the reference database published by international centre for diffraction data (ICDD) in 2008, which suggested that the FAs used in this study were of polymorphic form. The minor differences in

diffractograms of the unprocessed and processed samples were possibly due the different orientation of the exposed crystals caused by the sample preparation.

Similarly, the PXRD analysis was also performed on processed and unprocessed pluronics to identify the occurrence of any changes in the crystal structure due to CO₂ processing. Peaks at 2θ values of 19 and 23° were present for all processed and unprocessed samples as shown in Figure 4.11. Pluronics are semi-crystalline in nature due to PEO fraction and the peaks observed match with the published standard PXRD pattern of PEO in ICDD database (file number 49-2201). The halo effect in the diffractograms was due to the amorphous PPO fraction.

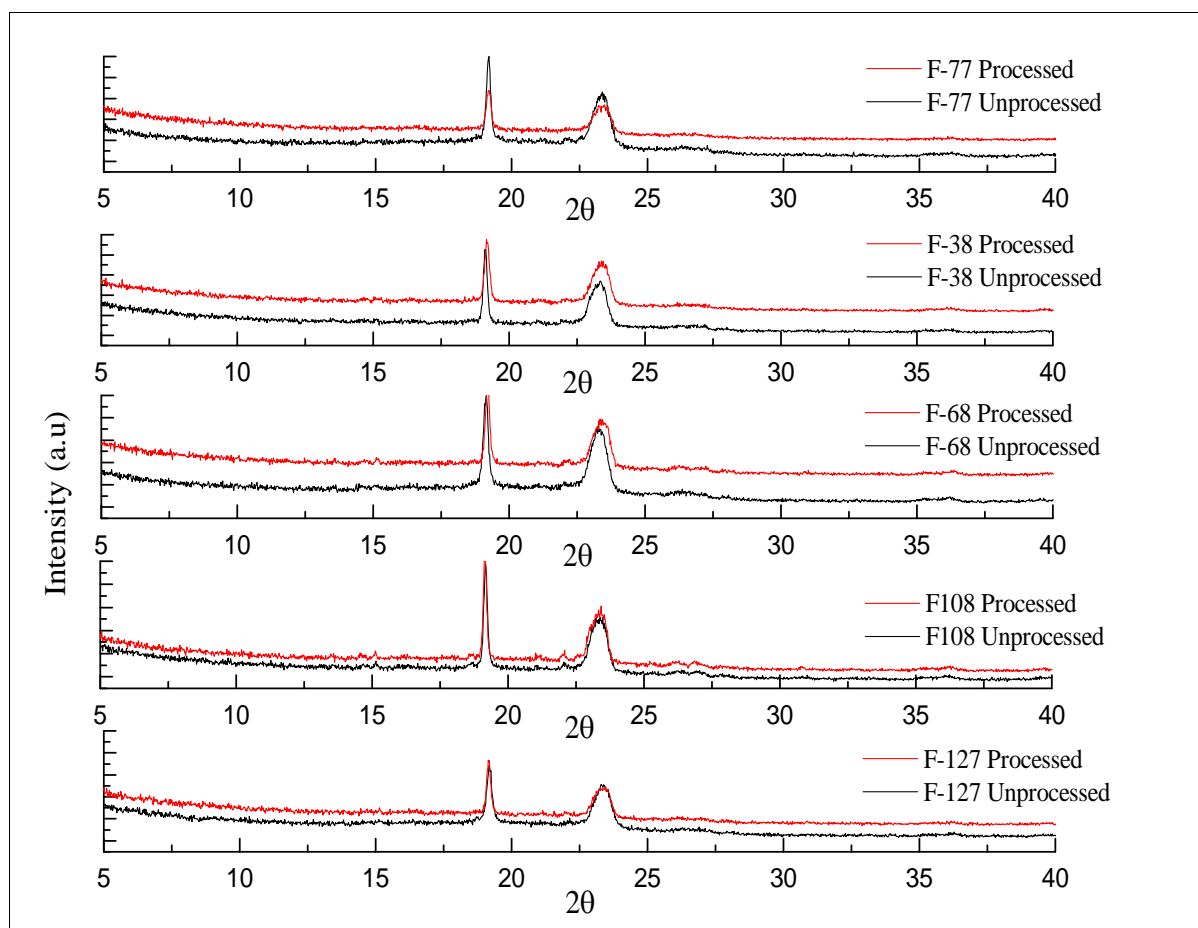


Figure 4.11: Diffractograms of processed and unprocessed pluronics

These PXRD studies further support the DSC analysis and confirm that the CO₂ processing did not cause any changes to the crystal structure of the studied excipients.

4.4 Conclusions

It was concluded from the present study that FAs and pluronics could be melted below their actual melting point in pressurised CO₂. The melting point depression in FAs was between 10.7 to 19.5 °C whereas pluronics melted between 18.1 to 19.3 °C below their actual melting points. The melting behaviour of saturated FAs in CO₂ was inversely proportional to the carbon chain length of the studied molecules. The effect of pressure on the melting point of these excipients was also studied and it was observed that in the case of FAs the melting point initially decreased with the increase in pressure and then increased after reaching to a minimum. The melting behaviour of pluronics in CO₂ was independent of their molecular weight and PPO content. Unlike FAs, the melting temperature of pluronics decreased with the initial increase in the pressure and then remained constant after reaching the minimum under the studied conditions. DSC and PXRD analysis performed on the processed and unprocessed excipients indicated no physical changes due to CO₂ processing.

This data on melting point depression could be utilised in the particle engineering at low temperatures and coating of thermolabile substances such as proteins/peptides. In this project, the minimum melting temperature and pressure conditions of excipients in pressurised CO₂ identified here would be used in designing the coating experiments to develop SCDDS.

References

- [1] I. Pasquali and R. Bettini, "Are pharmaceuticals really going supercritical?," *Int. J. Pharm.*, vol. 364, no. 2, pp. 176–87, 2008.
- [2] A. V. Kabanov, E. V. Batrakova, and V. Y. Alakhov, "Pluronic® block copolymers as novel polymer therapeutics for drug and gene delivery," *J. Control. Release*, vol. 82, pp. 189–212, 2002.
- [3] A. C. Rustan and C. A. Drevon, "Fatty Acids : Structures and Properties," *Encyclopedia of life sciences*. John Wiley & Sons, Ltd, pp. 1–7, 2005.
- [4] Sigma-aldrich, "Lauric acid-Material safety data sheet." 2012.
- [5] K. S. Markley, "Lipids," in *Practical Handbook of Biochemistry and Molecular Biology*, G. . Fasman, Ed. Boca raton, US: CRC Press, 1989, p. 523.
- [6] Sigma-aldrich, "Myristic acid-Material safety data sheet." pp. 1–7, 2012.
- [7] Sigma-Aldrich, "Palmitic acid-Material safety data sheet." pp. 1–7, 2012.
- [8] Sigma-aldrich, "Stearic acid-Material safety data sheet," pp. 6–11, 2012.
- [9] C. W. Hoerr, R. S. Sedgwick, and A. W. Ralston, "The solubilities of the normal saturated fatty acids. III," *J. Org. Chem.*, vol. 11, no. 5, pp. 603–609, 1946.
- [10] H. Vorum, R. Brodersen, U. Kragh-Hansen, and A. O. Pedersen, "Solubility of long-chain fatty acids in phosphate buffer at pH 7.4," *Biochim. Biophys. Acta - Lipids Lipid Metab.*, vol. 1126, no. 2, pp. 135–142, 1992.
- [11] T. Bamberger, J. C. Erickson, C. L. Cooney, and S. K. Kumar, "Measurement and model prediction of solubilities of pure fatty acids, pure triglycerides, and mixtures of triglycerides in supercritical carbon dioxide," *J. Chem. Eng. Data*, vol. 33, no. 3, pp. 327–333, 1988.

- [12] C. Garlapati and G. Madras, "Solubilities of palmitic and stearic fatty acids in supercritical carbon dioxide," *J. Chem. Thermodyn.*, vol. 42, no. 2, pp. 193–197, 2010.
- [13] P. Maheshwari, Z. L. Nikolov, T. M. White, and R. Hartel, "Solubility of fatty acids in supercritical carbon dioxide," *J. Am. oil Chem. Soc.*, vol. 69, no. 11, pp. 1069–1076, 1992.
- [14] Z.-R. Yu, B. Singh, S. S. H. Rizvi, and J. A. Zollweg, "Solubilities of fatty acids, fatty acid esters, triglycerides, and fats and oils in supercritical carbon dioxide," *J. Supercrit. Fluids*, vol. 7, no. 1, pp. 51–59, 1994.
- [15] B. U. Killen and O. I. Corrigan, "Factors influencing drug release from stearic acid based compacts," *Int. J. Pharm.*, vol. 228, no. 1–2, pp. 189–98, 2001.
- [16] S. Xie, L. Zhu, Z. Dong, Y. Wang, X. Wang, and W. Zhou, "Preparation and evaluation of ofloxacin-loaded palmitic acid solid lipid nanoparticles.," *Int. J. Nanomedicine*, vol. 6, pp. 547–55, 2011.
- [17] Q. Zhang, G. Yie, Y. Li, Q. Yang, and T. Nagai, "Studies on the cyclosporin A loaded stearic acid nanoparticles.," *Int. J. Pharm.*, vol. 200, no. 2, pp. 153–9, 2000.
- [18] J. P. Nam, S. C. Park, T. H. Kim, J. Y. Jang, C. Choi, M. K. Jang, and J. W. Nah, "Encapsulation of paclitaxel into lauric acid-O-carboxymethyl chitosan-transferrin micelles for hydrophobic drug delivery and site-specific targeted delivery.," *Int. J. Pharm.*, vol. 457, no. 1, pp. 124–135, 2013.
- [19] H. J. Robson, D. Q. Craig, and D. Deutsch, "An investigation into the release of cefuroxime axetil from taste-masked stearic acid microspheres. Part 1: the influence of the dissolution medium on the drug release profile and the physical integrity of the microspheres.," *Int. J. Pharm.*, vol. 190, no. 2, pp. 183–92, 1999.

- [20] A. V. Kabanov, P. Lemieux, S. Vinogradov, and V. Alakhov, "Pluronic block copolymers: novel functional molecules for gene therapy.," *Adv. Drug Deliv. Rev.*, vol. 54, no. 2, pp. 223–33, 2002.
- [21] I. R. Schmolka, "A review of block polymer surfactants," *J. Am. oil Chem. Soc.*, vol. 54, no. 3, pp. 110–116, 1977.
- [22] E. V. Batrakova and A. V. Kabanov, "Pluronic block copolymers: evolution of drug delivery concept from inert nanocarriers to biological response modifiers.," *J. Control. Release*, vol. 130, no. 2, pp. 98–106, 2008.
- [23] Y. Kadam, U. Yerramilli, and A. Bahadur, "Solubilization of poorly water-soluble drug carbamezapine in Pluronic micelles: Effect of molecular characteristics, temperature and added salt on the solubilizing capacity," *Colloids Surfaces B Biointerfaces*, vol. 72, no. 1, pp. 141–147, 2009.
- [24] A. V. Kabanov, E. V. Batrakova, and V. Y. Alakhov, "Pluronic block copolymers for overcoming drug resistance in cancer.," *Adv. Drug Deliv. Rev.*, vol. 54, no. 5, pp. 759–79, 2002.
- [25] L. Bromberg, T. A. Hatton, R. Barreiro-Iglesias, C. Alvarez-Lorenzo, and A. Concheiro, "Controlled release camptothecin tablets based on pluronic and poly(acrylic acid) copolymer. Effect of fabrication technique on drug stability, tablet structure, and release mode.," *Drug Dev. Ind. Pharm.*, vol. 33, no. 6, pp. 607–615, 2007.
- [26] S. Takishima, "Solubility of block copolymer surfactants in compressed CO₂ using a lattice fluid hydrogen-bonding model," *Ind. Eng. Chem. Res.*, pp. 2821–2833, 1997.
- [27] F. Rindfleisch, T. P. DiNoia, and M. A. McHugh, "Solubility of polymers and copolymers in supercritical CO₂," *J. Phys. Chem.*, vol. 100, no. 38, pp. 15581–15587, 1996.

- [28] F. Kusmanto, M. Billham, and P. Hornsby, "Polymer plasticization using supercritical carbon dioxide," *J. Vinyl Addit. Technol.*, vol. 14, no. 4, pp. 163–166, 2008.
- [29] C. Drohmann and E. J. Beckman, "Phase behavior of polymers containing ether groups in carbon dioxide," *J. Supercrit. Fluids*, vol. 22, no. 2, pp. 103–110, 2002.
- [30] J. C. Meredith, K. P. Johnston, J. M. Seminario, S. G. Kazarian, and C. A. Eckert, "Quantitative equilibrium constants between CO₂ and lewis bases from FTIR spectroscopy," *J. Phys. Chem.*, vol. 100, no. 26, pp. 10837–10848, 1996.
- [31] S. G. Kazarian, M. F. Vincent, F. V. Bright, C. L. Liotta, and C. A. Eckert, "Specific intermolecular interaction of carbon dioxide with polymers," *J. Am. Chem. Soc.*, vol. 118, no. 7, pp. 1729–1736, 1996.
- [32] O. S. Fleming and S. G. Kazarian, "Supercritical Carbon Dioxide," M. F. Kemmere and T. Meyer, Eds. Weinheim, FRG: Wiley-VCH Verlag GmbH & Co. KGaA, 2005, pp. 205–211.
- [33] R. Bhomia, V. Trivedi, J. C. Mitchell, N. J. Coleman, and M. J. Snowden, "Effect of Pressure on the Melting Point of Pluronics in Pressurized Carbon Dioxide," *Ind. Eng. Chem. Res.*, vol. 53, no. 26, pp. 10820–10825, 2014.
- [34] H. Uchida and T. Kamijo, "Measurement and correlation of the solid–liquid–gas equilibria for carbon dioxide+normal chain saturated aliphatic hydrocarbon systems," *J. Supercrit. Fluids*, vol. 51, no. 2, pp. 136–141, 2009.
- [35] E. Bertakis, I. Lemonis, S. Katsoufis, E. Voutsas, R. Dohrn, K. Magoulas, and D. Tassios, "Measurement and thermodynamic modeling of solid–liquid–gas equilibrium of some organic compounds in the presence of CO₂," *J. Supercrit. Fluids*, vol. 41, no. 2, pp. 238–245, 2007.

- [36] H. Uchida and T. Kamijo, "Measurement and correlation of the solid–liquid–gas equilibria for carbon dioxide + octadecanoic acid (stearic acid) and carbon dioxide + 1-octadecanol (stearyl alcohol) systems," *J. Chem. Eng. Data*, vol. 55, no. 2, pp. 925–929, 2010.
- [37] R. Dohrn, E. Bertakis, O. Behrend, E. Voutsas, and D. Tassios, "Melting point depression by using supercritical CO₂ for a novel melt dispersion micronization process," *J. Mol. Liq.*, vol. 131–132, pp. 53–59, 2007.
- [38] E. Weidner, V. Wiesmet, Ž. Knez, and M. Škerget, "Phase equilibrium (solid-liquid-gas) in polyethyleneglycol-carbon dioxide systems," *J. Supercrit. Fluids*, vol. 10, no. 3, pp. 139–147, 1997.
- [39] V. Trivedi, R. Bhomia, J. C. Mitchell, N. J. Coleman, D. Douroumis, and M. J. Snowden, "Study of the effect of pressure on melting behavior of saturated fatty acids in liquid or supercritical carbon dioxide," *J. Chem. Eng. data*, vol. 58, no. 6, pp. 1861–1866, 2013.
- [40] Y. Yuan, N. Zhang, W. Tao, X. Cao, and Y. He, "Fatty acids as phase change materials: A review," *Renew. Sustain. Energy Rev.*, vol. 29, pp. 482–498, 2014.
- [41] Z. Lian, S. A. Epstein, C. W. Blenk, and A. D. Shine, "Carbon dioxide-induced melting point depression of biodegradable semicrystalline polymers," *J. Supercrit. Fluids*, vol. 39, no. 1, pp. 107–117, 2006.
- [42] I. Kikic, F. Vecchione, P. Alessi, A. Cortesi, F. Eva, and N. Elvassore, "Polymer Plasticization Using Supercritical Carbon Dioxide: Experiment and Modeling," *Ind. Eng. Chem. Res.*, vol. 42, no. 13, pp. 3022–3029, 2003.
- [43] S. Kilic, S. Michalik, Y. Wang, J. K. Johnson, R. M. Enick, and E. J. Beckman, "Phase Behavior of Oxygen-Containing Polymers in CO₂," *Macromolecules*, vol. 40, no. 4, pp. 1332–1341, 2007.

- [44] M. O’neill, Q. Cao, and M. Fang, “Solubility of homopolymers and copolymers in carbon dioxide,” *Ind. Eng. Chem. Res.*, vol. 5885, no. 98, pp. 3067–3079, 1998.
- [45] M. D. Dadmun, W. A. Van Hook, D. W. Noid, Y. B. Melnichenko, and B. G. Sumpter, Eds., *Computational Studies, Nanotechnology, and Solution Thermodynamics of Polymer Systems*. Boston, MA: Springer US, 2002.
- [46] T. Sarbu, T. Styranec, and E. Beckman, “Non-fluorous polymers with very high solubility in supercritical CO₂ down to low pressures,” *Nature*, vol. 405, no. 6783, pp. 165–8, 2000.
- [47] R. Ebewele, *Polymer science and technology*. CRC Press, 2000.

CHAPTER 5

Stability of bovine haemoglobin

5.1 Introduction

The aim of this study was to determine the thermal, storage and agitation stability of bHb in aqueous solution. The experiments conducted here provided a better understanding of the stability and robustness of bHb in a range of buffered solutions. These studies were also essential to establish important processing parameters for the development of SCDDS.

Proteins are sensitive molecules and prone to degradation by many pathways which are dependent on parameters such as pH, temperature and ionic strength. Different proteins show unique combination of these degradation pathways and dependencies; therefore a wide range of methods are required to analyse their properties such as stability, purity, activity, safety and structural integrity. The main techniques used to study various properties of proteins are summarised in Figure 5.1 [1].

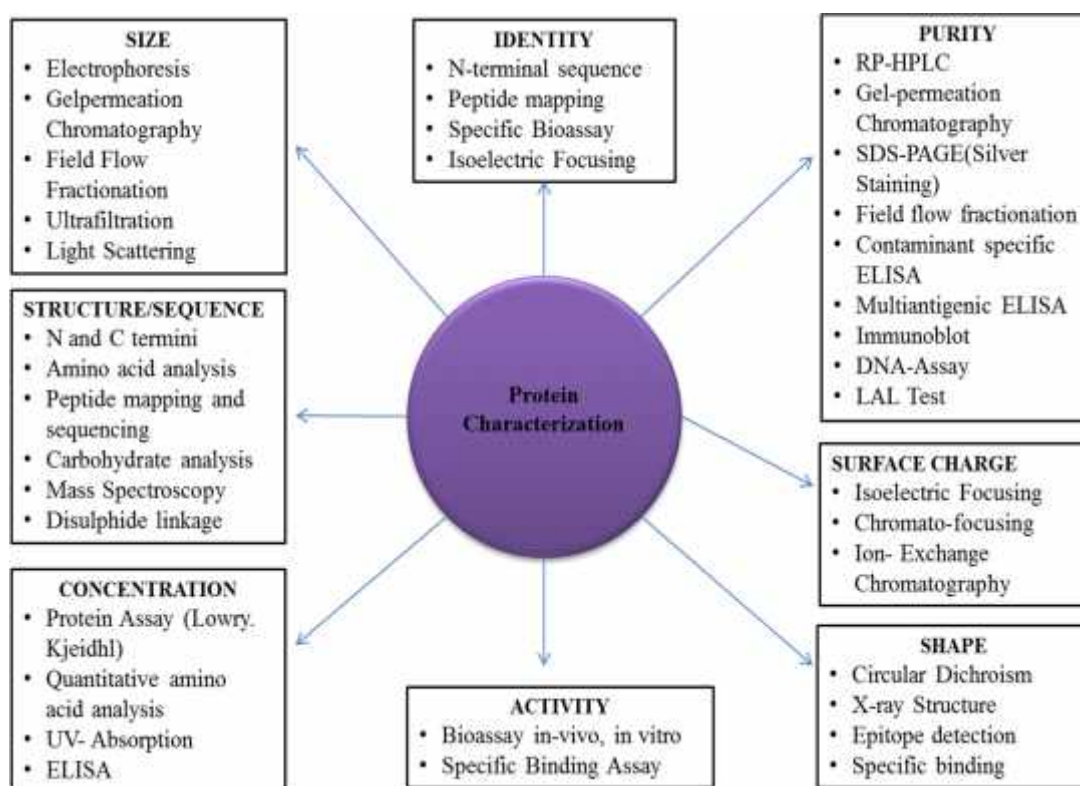


Figure 5.1: Analytical methods for protein characterisation [1]

The stability of bHb in this work was analysed by quantitation and monitoring of conformational transitions using UV/vis and CD spectroscopy. Direct photometric method for quantitative measurement of bHb was chosen because of its small sample requirements, cost effectiveness, ease of availability and quick and non-destructive nature. Additionally, the maximum UV absorption of bHb at 405 nm due to the presence of haem moiety allowed the protein quantification at low concentrations (20 ng/ml) using this technique with ease.

There are several techniques available to study the conformation of proteins such as XRD and nuclear magnetic resonance but CD was the technique of choice in this work. Similar to UV, CD spectroscopy also have various advantages including non-destructive nature, use of small sample size and quick measurements. Additionally, different size of cuvettes can be used which allows a wide range of concentrations to be analysed [2].

5.2 Thermal stability of bHb

Along with pH, temperature is also an essential parameter which affects the stability of protein therefore it is important to identify the optimum temperature required to maintain the structural integrity of bHb. These studies were conducted using UV and CD spectroscopy where spectra were collected after every 5 °C increase/decrease in temperature between 25 to 65 °C.

5.2.1 Analysis by UV spectroscopy

The bHb solutions in pH 6, 7 and 8 phosphate buffers were subjected to a temperature ramp from 25 to 65 °C in the UV spectrophotometer. The sample was also cooled in the similar fashion to 25 °C. Absorbance was recorded at 405 and 274 nm after every 5 °C increase/decrease in temperature.

5.2.1.1 Procedure for thermal stability studies of bHb by UV spectroscopy

Refer to section 3.2.5

5.2.1.2 Results

The general absorption spectrum of bHb is presented in Figure 5.2 which consists of major peaks at 274 and 405 nm. The absorption maximum at 274 nm is a characteristic peak to most of the proteins due to the presence of tyrosine and tryptophan amino acids in the molecule [3].

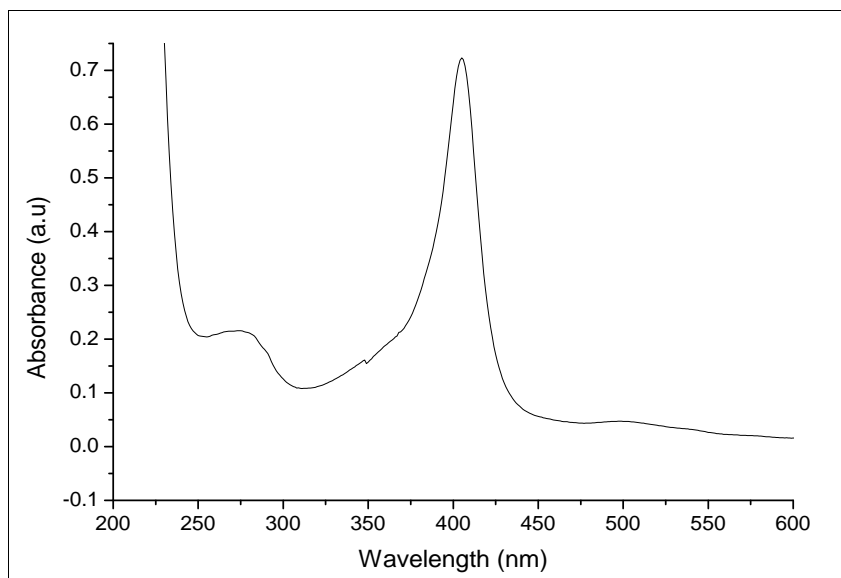
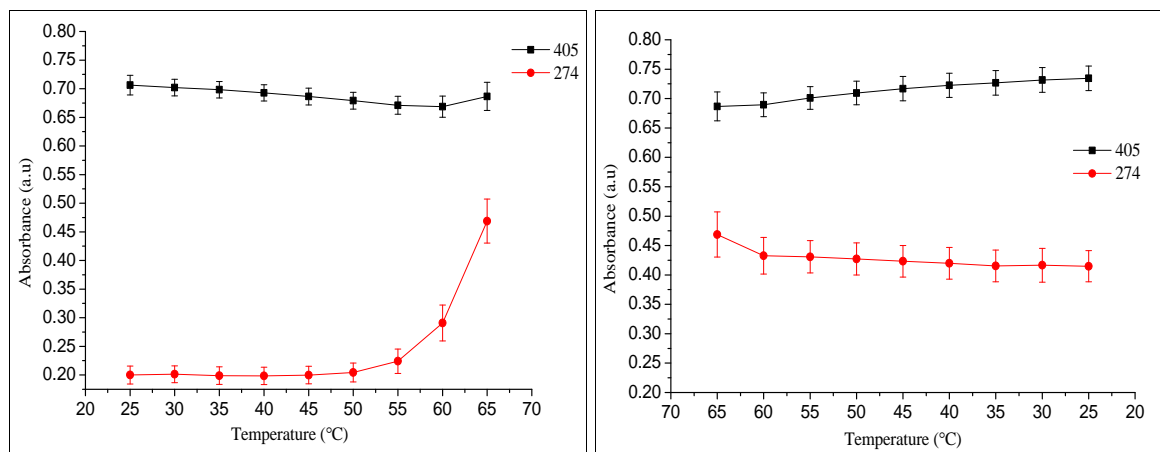


Figure 5.2: UV spectrum of bHb in pH 6 phosphate buffer

The sharp peak at 405 nm known as Soret band is because of the absorption by haem (porphyrin) moiety of the bHb protein [4]. The large absorption at around 210 nm is due to the peptide bonds in the molecule and was not monitored in the current study. The thermal degradation of bHb was examined by collecting UV spectrum at 274 and 407 nm with respect to increase or decrease in the temperature. The full UV spectra of the study are shown in Appendix A.1.

The UV results obtained from thermal stability studies are presented in Figures 5.3, 5.4 and 5.5. Figure 5.3 present changes in the absorbance of bHb solution in pH 6 buffer with respect to temperature. The absorbance at 405 nm (Figure 5.3 A) remained largely unchanged during the heating cycle suggesting negligible effect on the haem moiety due to the increase in temperature to 65 °C. However, values at 274 nm increased substantially above 50 °C possibly due to the breakage of hydrogen bonds and exposure

of aromatic side chains to the solvent. Absorbance values during the cooling cycle (65-25 °C) suggested a slight gain in absorbance at 405 nm and drop at 274 nm especially between 65-60 °C. The absorbance values at 274 nm remained constant thereafter and showed no further decrease upon cooling from 60-25 °C.



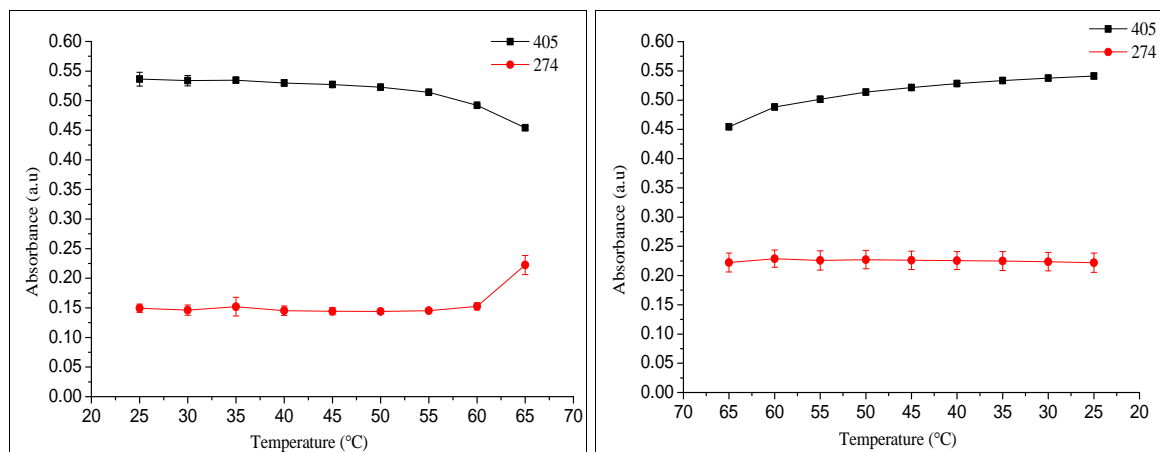
(A): Heating ramp (25 to 65 °C)

(B): Cooling ramp (65 to 25 °C)

Figure 5.3: Thermal stability of bHb in pH 6 buffer (Absorbance at 405 and 274nm)

These results showed that the alterations in absorbance due to the heating and cooling were lower at 405 nm in comparison with the 274 nm. Also, most of the changes in absorbance took place at temperatures above 50 °C which demonstrated the sensitivity of bHb solution to thermal degradation. It is also worth noting that any changes to the protein conformation at higher temperatures were not fully reversible as seen with the values at 274 nm.

Similar to pH 6, changes in protein conformation due to the heating and cooling of bHb solution at pH 7 was also studied by recording the absorbance at 405 and 274 nm (Figure 5.4). Figure 5.4 (A), presents changes in absorbance due to the heating of bHb solution at pH 7 where, values at 405 nm were found to be constant till 50 °C before decreasing with the further increase in temperature.



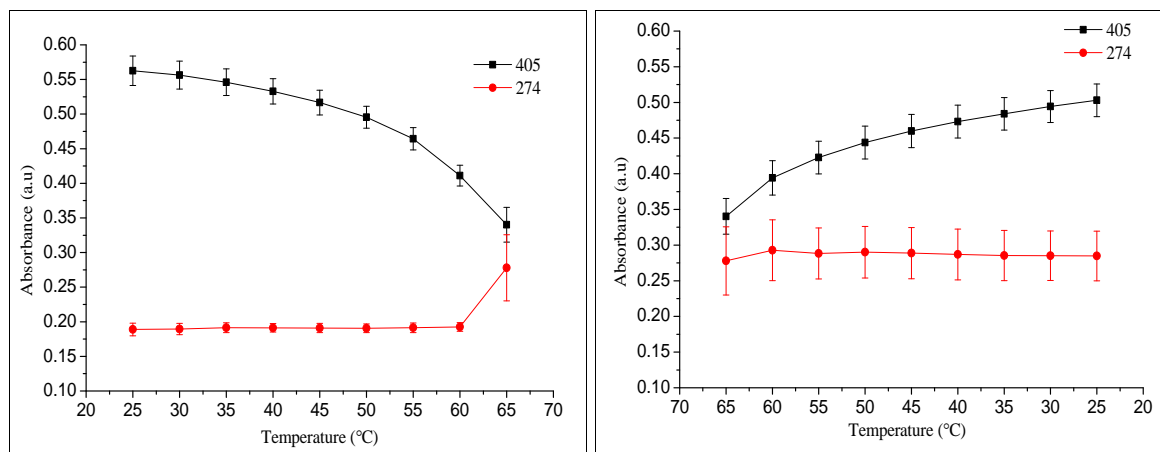
(A): Heating ramp (25 to 65 °C)

(B): Cooling ramp (65 to 25 °C)

Figure 5.4: Thermal stability of bHb in pH 7 buffer (Absorbance at 405 and 274 nm)

Whereas, the absorbance at 274 nm remained mostly unchanged till 60 °C and increased only by 0.05 absorbance units when heated to 65 °C. The hyperchromic shift at 274 nm was a lot smaller at pH 7 than the pH 6. Figure 5.4 (A) also suggested that the conformational changes caused primarily by the exposure of aromatic groups occurred at comparatively lower temperature in pH 6 than 7. Cooling of the protein solution from 65 to 25 °C (Figure 5.4 B) showed an increase in absorbance at 405 nm by approximately 0.1 absorbance units. Similar to pH 6, protein conformation was not fully reversible at higher temperatures as seen with the values at 274 nm which suggested permanent changes in the structure of protein molecule.

The results of heating and cooling experiments on bHb solution in pH 8 buffer are presented in Figure 5.5. Similar to pH 7, the absorbance at 274 nm was stable till 60 °C and increased only at 65 °C during the heating cycle. On the other hand, the absorbance at 405 nm showed steady decrease with the increase in temperature. The total decrease of 0.2 absorbance units at 405 nm was highest amongst all solutions of various pH studied here. This indicated that the temperature sensitivity of the haem group was higher at pH 8 in comparison to pH 6 and 7. The absorbance at 405 nm increased substantially during the cooling cycle but there was negligible drop in the values at 274 nm.



(A): Heating ramp (25 to 65 °C)

(B): Cooling ramp (65 to 25 °C)

Figure 5.5: Thermal stability of bHb in pH 8 buffer (Absorbance at 405 and 274 nm)

This indicated that the changes in absorbance while heating were not completely reversible suggesting the permanent changes to the protein conformation.

The results from UV spectroscopy provided important information on the temperature sensitivity of bHb solution at studied pH. It could also be clearly seen that the protein was prone to conformational changes at temperatures above 50 °C regardless of the solution pH. In addition, haem group was found to be extremely sensitive to temperature at pH 8 and the aromatic side chains appeared to be easily exposed by thermal energy at pH 6.

5.2.2 Analysis by CD spectroscopy

The thermal stability of bHb was also analysed by CD spectroscopy to determine specific changes in its secondary structures due to pH and temperature. The protein solution was prepared in pH 6, 7 and 8 phosphate buffers and subjected to heating and cooling cycles similar to UV experiments between 25 and 65 °C. Similar to UV spectroscopy, CD spectrum was collected after every 5 °C increase/decrease in the temperature.

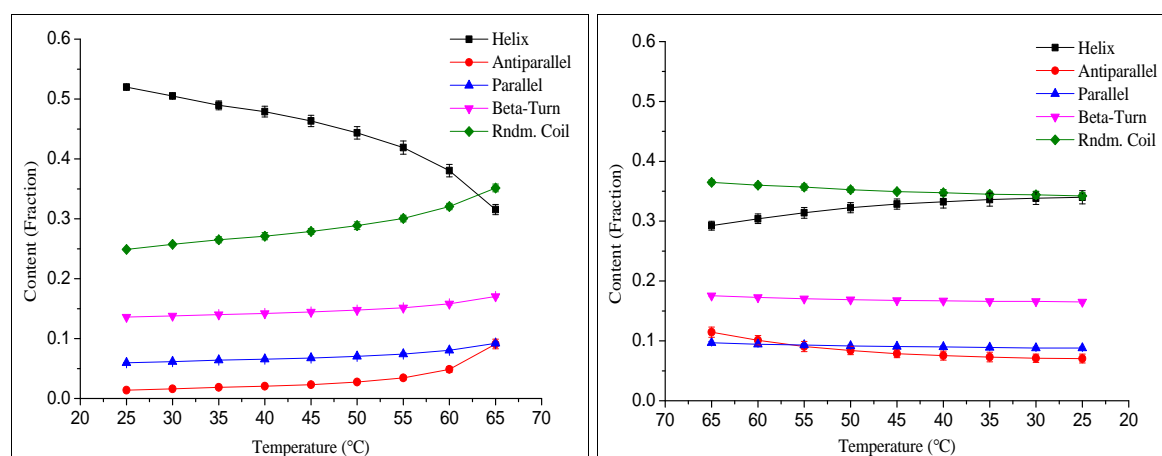
5.2.2.1. Procedure for thermal stability studies of bHb by CD spectroscopy

Refer to section 3.2.6

5.2.2.2 Results

The CD spectra obtained from the instrument were processed by the CDNN software. This software was developed by Dr. Gerald Böhm (Institut für Biotechnologie, Martin-Luther Universität Halle-Wittenberg). CDNN deconvolutes the CD data by cross referencing the sample spectrum with already installed reference spectra. The output is given in the fraction content of different secondary structure of the protein. The original CD spectra of all samples obtained in this study are shown in Appendix A.2

The change in the fraction content of various secondary structures of bHb in pH 6 buffer due to the heating and cooling are shown in Figure 5.6. A decrease of 20.5% was observed in the alpha helix content of the protein during the heating cycle as shown in Figure 5.6 (A). Conversely, the content of beta turn, anti-parallel, parallel and random coil increased by 3.5, 7.7, 3.3 and 10.3% respectively upon heating of protein solution to 65 °C.



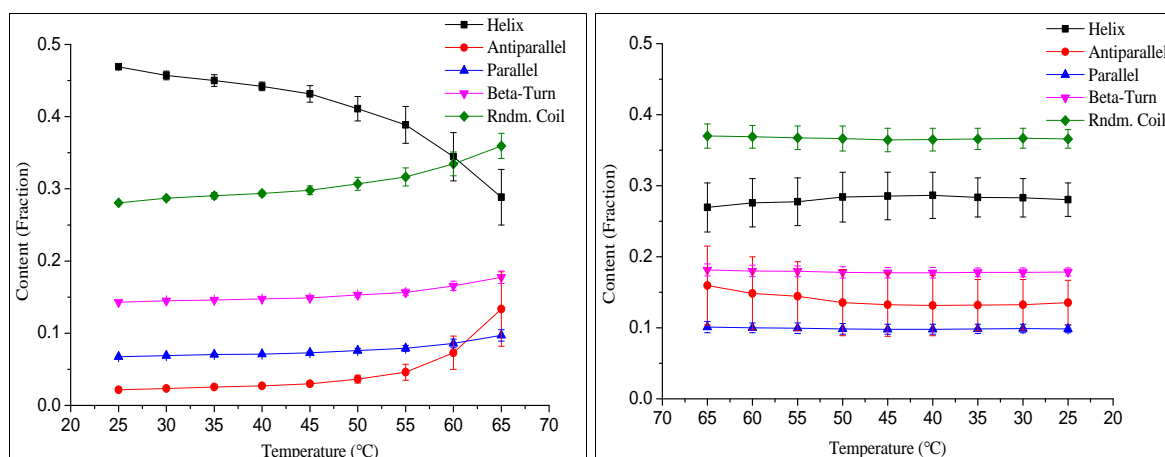
(A): Heating ramp (25 to 65 °C)

(B): Cooling ramp (65 to 25 °C)

Figure 5.6: Thermal stability of bHb in pH 6 buffer (Secondary structure content)

On the other hand, cooling of the same sample resulted in the increase of alpha helix content only by 4.8%. The decrease in the other secondary structure fractions was also minimal *i.e.* random coil (2.3%), antiparallel (4.4%), parallel (1.0%) and beta turn (1.0%). This supports findings from UV spectroscopy of irreversible changes in the secondary structure of bHb due to heating.

The results of heating and cooling on bHb solution at pH 7 are shown in Figure 5.7. The loss of alpha helicity for bHb at pH 7 was found to be 18.1% which was 2.4% less than the pH 6 sample. Whereas, the fraction content of the rest of the secondary structures viz. beta-turn, anti-parallel, parallel, and random coil increased by 3.5, 11.2, 2.3, and 7.9% respectively.



(A): Heating ramp (25 to 65 °C)

(B): Cooling ramp (65 to 25 °C)

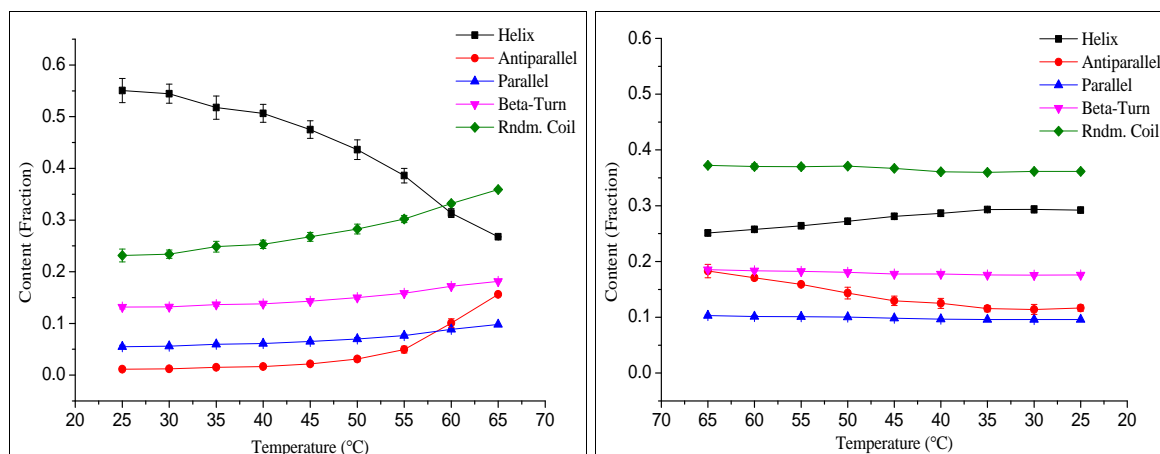
Figure 5.7: Thermal stability of bHb in pH 7 buffer (Secondary structure content)

The changes to the secondary structure contents of bHb at pH 7 were insignificant upon cooling as presented in Figure 5.7 (B). The cooling of protein solution from 65-25 °C resulted in an increase of only 1.1% in alpha-helicity and the decrease of 2.4% (antiparallel), 0.3% (parallel), 0.3% (beta-turn) and 0.4% (random coil) in other secondary structures.

This showed that the overall loss of alpha-helix on heating was slightly less at pH 7 (18.1%) as compared to pH 6 (20.8%) whereas, the reversibility of the protein conformation was marginally better at pH 6 than at pH 7.

Similar to pH 6 and 7, protein solution prepared in pH 8 buffer was also subjected to the heating and cooling cycle in the CD spectrophotometer. The fraction content of the secondary structures obtained after deconvolution of CD spectra is presented in Figure 5.8. Alpha helix content at pH 8 decreased by 28.3% and was greater than the decrease observed at pH 6 and 7. The highest decrease in alpha helicity at pH 8 suggested that

bHb molecule was more sensitive to heating in alkaline environment. Additionally, the content of beta-turn, antiparallel, parallel, and random coil showed an increase of 5.0, 14.4, 4.3, and 12.7% respectively while heating which was also higher than at pH 6 or 7.



(A): Heating ramp (25 to 65 °C)

(B): Cooling ramp (65 to 25 °C)

Figure 5.8: Thermal stability of bHb in pH 8 buffer (Secondary structure content)

The cooling of the sample resulted in slight gain in alpha helix content (4.1%) and loss in beta-turn antiparallel, parallel, and random coil by 0.9, 6.7, 0.7, and 1.1% respectively.

CD results supported the findings from UV spectroscopy that conformation of bHb undergoes change upon heating the samples above 50 °C. Samples prepared at all 3 different pH showed loss in alpha-helicity upon heating but it was highest at pH 8 compared to pH 6 and 7.

5.2.3 Discussion

In the present study, the stability of bHb was assessed at pH 6, 7 and 8 to cover the intestinal pH range as the intended target site was small intestine for the delivery for SCDDS. Whereas, the rationale behind the selection of temperature range (25–65 °C) was to investigate the degree of bHb denaturation during SCF processing. Hb denatures when exposed to heat and as it consists of four sub-units the denaturation is found to be a cooperative transition. Differential scanning microcalorimetry showed that in pH 7.4

phosphate buffer, carboxyhemoglobin denatured at 82 °C, oxyhemoglobin at 71 °C and methemoglobin at 67 °C [5]. Additionally, Michnik *et al* showed that human methemoglobin denatured at 62 °C in pH 6.5 buffer [6]. Furthermore, G.M Artmann used CD spectroscopy to evaluate structural changes in human haemoglobin (HbA) and sickle cell haemoglobin (HbS) upon heating. Authors confirmed that thermal denaturation curves obtained were non-linear and the protein showed accelerated denaturation between 35 to 39 °C. However, the transition was reversible below 39 °C and was independent of solution pH (6.8-7.8) [7].

It is known that proteins fold to attain a conformation that is essential for their biological activity [8]. Thermodynamically or in terms of free energy, native configuration is only 5-20 kcal/mole more stable than the unfolded confirmation [8]. This small conformational stability of proteins is a result of large stabilising and destabilising forces and any changes in external variables (*i.e.* temperature, pH, salt *etc.*) potentially cause destabilisation of the protein molecules to induce unfolding. The major stabilising forces in a protein molecule are hydrogen bonding and hydrophobic effect whereas the major destabilising force is known to be its conformational entropy [9]. These fundamentals are important to understand the UV and CD findings obtained in this work.

The UV results indicated that bHb remained unchanged when heated till 50 °C at pH 6 and 7. However at pH 8, a hypochromic shift in absorbance at 405 nm was observed during the heating cycle. This confirmed that Soret band in UV spectrum of bHb was more resistant to heat at pH 6 and 7 than at pH 8. This phenomenon can be explained by the thermal disruption of forces stabilising the native structure of a protein molecule. It is known that forces such as hydrogen bonding, hydrophobic and van der Waals interactions play a major role in stabilising the secondary and tertiary structure of proteins [8]. Heat provided the energy required to break these interactions and in this case, led to the loss of haem moiety as suggested by the hypochromic shift at 405 nm. On the other hand, the absorbance at 274 nm increased at higher temperatures for all solutions and was not completely reversible on cooling. The increase in absorbance at 274 nm was seen only after 55 °C at pH 6 and after 60 °C at pH 7 and 8. The increase in

absorbance or hyperchromic shift at 274 nm can be explained by the exposure of non-polar side chains at higher temperatures. It is known that approximately 81% of non-polar side chains (Alanine, valine, isoleucine, leucine, methionine, phenylalanine, tryptophan and cysteine) remain buried in the interior of a protein molecule while it attains its native structure at favourable conditions [9]. However, protein unfolding due to the unfavourable atmosphere such as temperatures above 55 °C in this case force these deeply buried side chains to come in contact with the solvent and result in the increase in absorption at 274 nm. This phenomenon of aromatic side chain exposure was more prominent at slightly acidic conditions (pH 6) as compared to neutral and basic pH values (7 and 8). This could be due to the several factors such as the overall charge & charge density on protein molecule, ionic strength of the buffer and protein concentrations [8].

UV studies helped in understanding the effect of temperature on haem group and aromatic side chains whereas CD analysis provided information about the secondary structures of protein with respect to the change in conditions. It was evident from the results that alpha helix was most sensitive to heat amongst all secondary structures studied. Maximum decrease of 28.3% was seen at pH 8 followed by 20.1% and 18.1% at pH 6 and pH 7. Interestingly, this loss in alpha-helicity was reversible to an extent for all samples during the cooling cycle. The increase in alpha helix content upon cooling was found to be 4.8, 4.1 and 1.1% at pH 6, 8 and 7 respectively. Inversely, the fraction content of the rest of the secondary structures increased with increase in temperature and decreased slightly with cooling. The decrease in alpha helix content at higher temperature could be explained by the thermal breakage of the stabilising hydrogen bonds. Initially, when the energy is applied to a protein molecule, the hydrogen bonds are weakened and the molecule becomes flexible exposing the side chain groups to the solvent [10]. If heating is stopped at this stage most proteins readily refold to their native configuration but if the heating is continued then these hydrogen bonds break. Moreover, this causes irreversible changes to the protein's conformation due to the formation of new bonds between water, amide nitrogen and carbonyl oxygen in a molecule. This breakage and formation of hydrogen bonds results in the exposure of

hydrophobic groups to the solvent [10] and explains the hyperchromic shift at 274 nm and decrease in alpha helicity.

These studies confirm that bHb solution can withstand temperatures up-to 50 °C irrespective of the studied pH and major irreversible changes occur only at higher temperatures. Although these findings are valuable in the process of developing SCDDS but they do not provide information on the storage conditions of the protein solution. Further studies were designed to understand the effect of storage period on bHb solution at different pH and temperatures.

5.3 Six hours stability of bHb

The stability of bHb was determined by CD and UV spectroscopy for a period of 6 hours at room temperature. The protein solutions were prepared in pH 6, 7 and 8 phosphate buffer and stored at room temperature (23 ± 2 °C). UV and CD data were collected for each solution after 0, 1, 2, 4 and 6 hours of storage (please refer to Appendix B for full spectra). The UV absorbance of protein solution was monitored at 274 and 405 nm to identify any changes in haem moiety and intra-molecular hydrogen bonding. The results presented in Figure 5.9 showed that the UV absorption at both wavelengths remained largely unchanged for the duration of six hours irrespective of the solution pH suggesting no changes to the bHb conformation during this period.

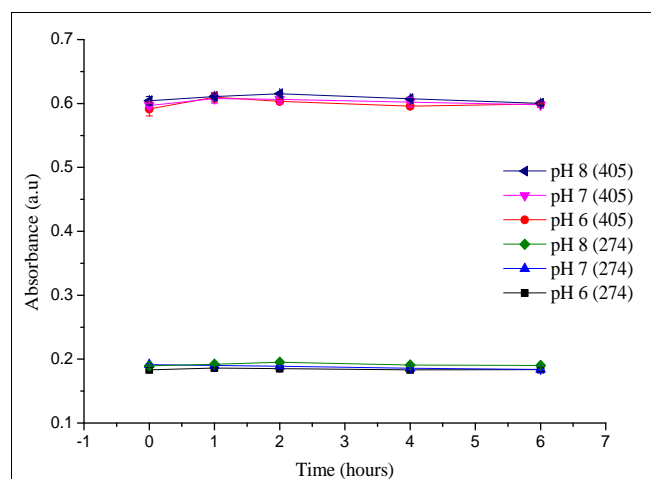


Figure 5.9: Six hours stability of bHb at pH 6, 7 and 8 (Absorbance at 405 and 274 nm)

The deconvoluted CD spectra by CDNN software are presented in Figures 5.10. The CD results showed that the fraction content of various secondary structures of bHb at all studied pH also remained unchanged for the duration of experiment. Similar to UV results, CD data also suggested no change in the protein conformation due to the storage at 23 °C for six hours.

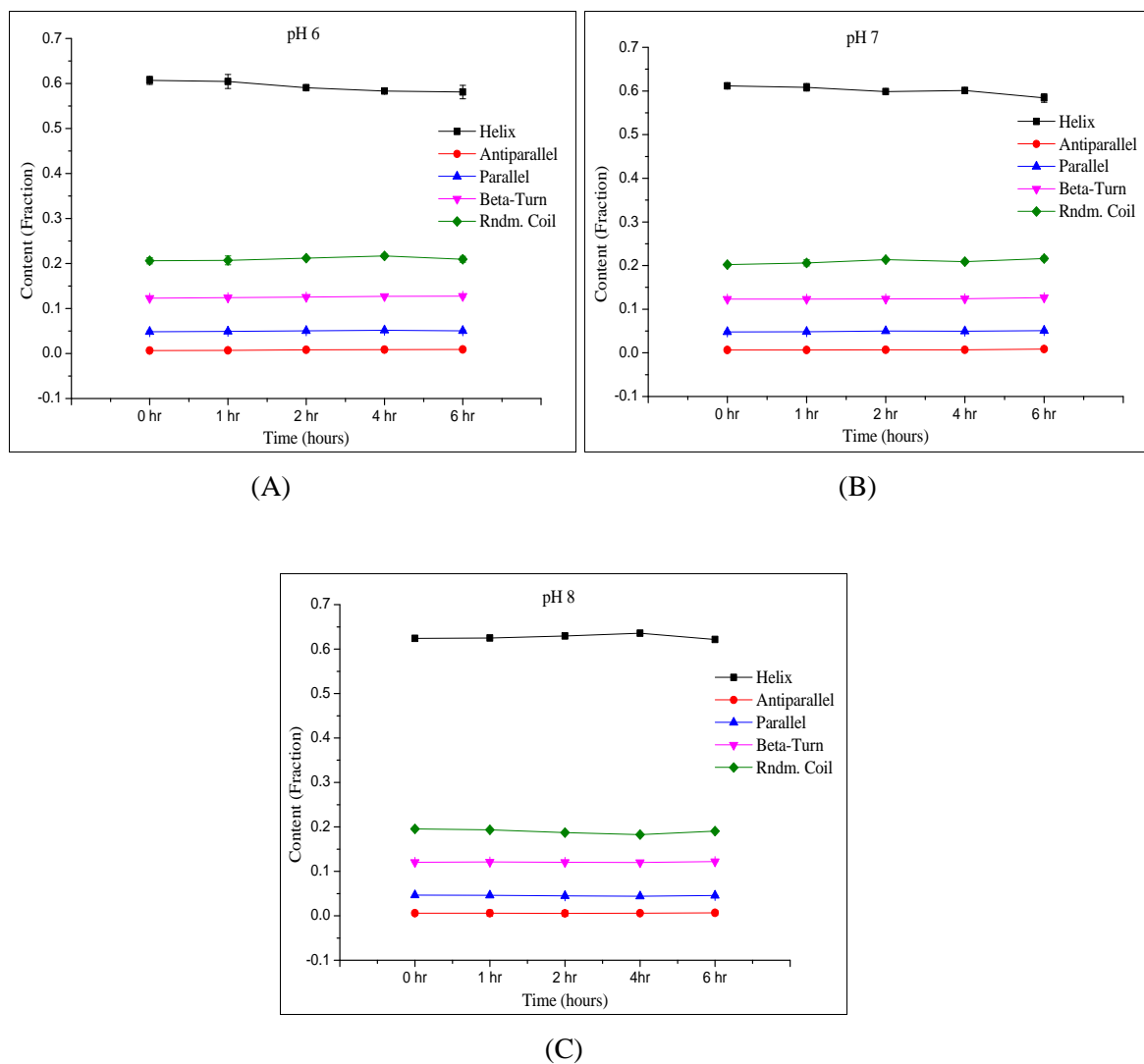


Figure 5.10: Six hour stability (secondary structure content) of bHb at pH 6 (A), pH 7 (B) and pH 8 (C)

The results presented in this section confirmed minimal or no effect on the stability of bHb solution during the short term storage at studied conditions. Hence, these studies were extended to long term storage where conformational changes were monitored after 1, 2, 3 and 40 days at 23 and 4 °C.

5.4 Inter-day stability of bHb

The aim of these experiments was to compare the stability of bHb at 23 °C and at lower temperature (4 °C) in order to determine an appropriate storage time and conditions for the protein solution.

5.4.1 Analysis by UV spectroscopy

Similar to previous experiments, changes in the absorbance at 274 and 405 nm were examined with respect to time and storage conditions. The complete spectra are shown in Appendix C.1 and the results obtained are discussed in this section.

5.4.1.1 Procedure for inter-day stability of bHb

Refer to section 3.2.8

5.4.1.2 Results

The inter-day stability of bHb was studied in buffer solutions of pH 6, 7 and 8 at 23 and 4 °C. The absorbance of pH 6 protein solutions at studied wavelengths for samples stored at 23 and 4 °C is shown in Figure 5.11.

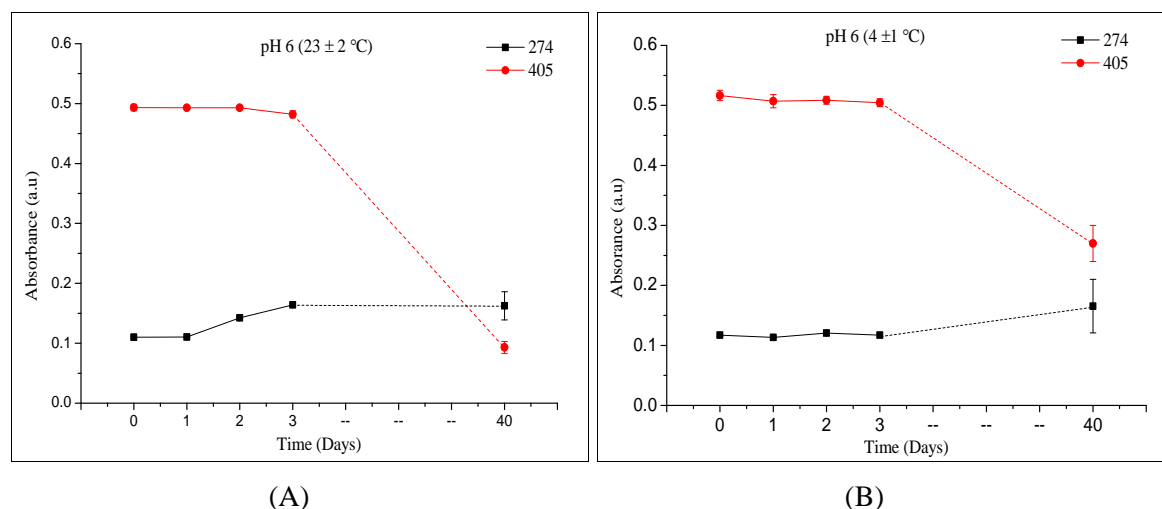


Figure 5.11: Inter-day stability of bHb at pH 6 stored at 23 °C (A) and 4 °C (B)

It was observed that the absorbance at 405 nm did not change for 3 days at both storage temperatures. Whereas, values at 274 nm started to increase after the day 1 of storage at

23 °C but remained constant for the sample stored at 4°C. Data presented in Figure 5.11 also indicated that the hypochromic shift at 405 nm was greater for samples stored at 23 than 4 °C after 40 days. This suggested an almost complete loss of the haem group at higher temperature in comparison with cold conditions in this period.

Conversely, decrease in absorbance at 405 nm (Figure 5.12) was observed from the day 1 for samples prepared in pH 7 buffer and stored at 23 °C. Similarly, the absorbance at 274 nm (Figure 5.12 A) increased after day 1 unlike at pH 6 where values remained constant for the first 24 hours.

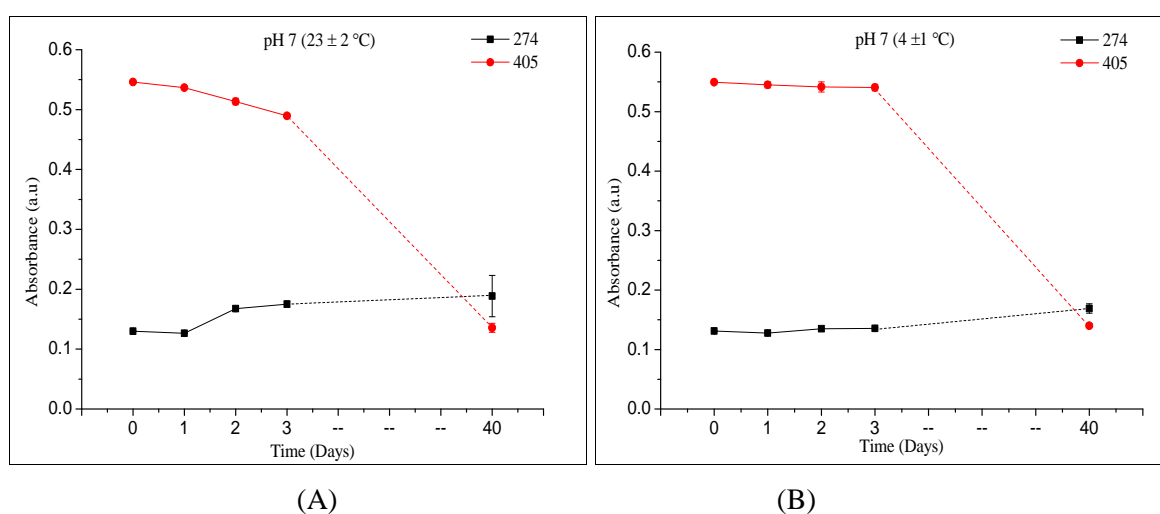


Figure 5.12 Inter-day stability of bHb at pH 7 stored at 23 °C (A) and 4 °C (B)

Protein solution stored at 4 °C showed no change in absorbance at studied wavelengths over the period of 3 days as presented in Figure 5.12 (B). However, loss of the soret band was similar for the samples stored at both temperatures after day 40.

The maximum decrease in absorbance at 405 nm was observed for pH 8 samples kept at 23 °C, where loss of haem group was very quick and started from the day one. The absorbance due to soret band decreased to 0.4 from 0.65 in first 3 days leading to maximum loss by the end of day 40.

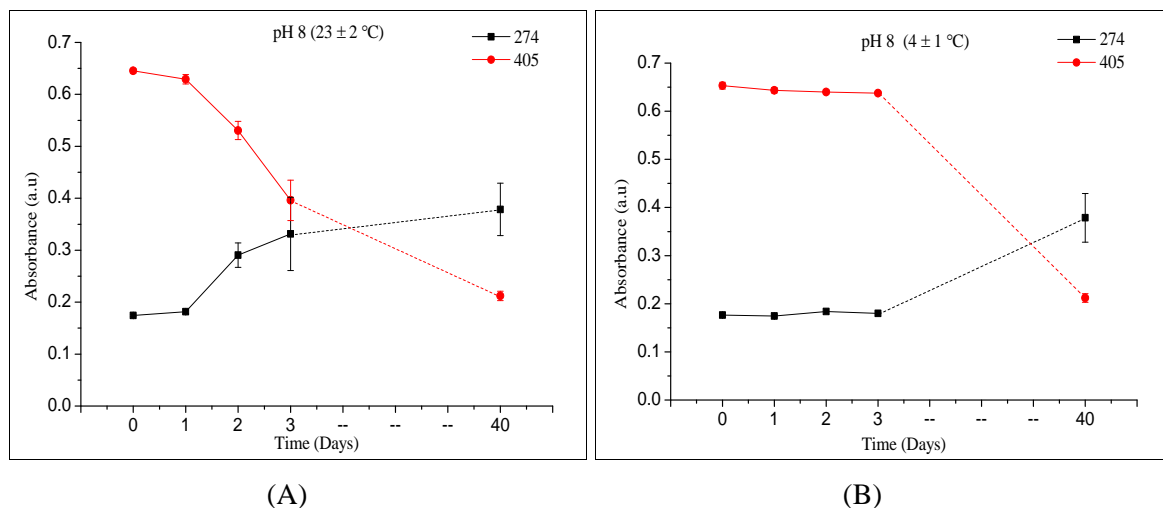


Figure 5.13: Inter-day stability of bHb at pH 8 stored at 23 °C (A) and 4 °C (B)

The instability of the protein molecule was also evident from the increase in absorbance at 274 nm (Figure 5.13 (A)) which was also quicker and higher in comparison to pH 6 and 7. Similar to pH 6 and 7, the absorbance for the pH 8 sample stored at 4 °C remained unchanged for first 3 days. The absorbance peak at 405 nm was lost completely and a large hyperchromic shift was observed at 274 nm after day 40 at both temperatures as shown in Figure 5.13.

It was seen that for samples stored at 23 °C the absorbance values at 405 nm decreased with time and in the order of pH 6 < pH 7 < pH 8. Conversely, the absorbance values increased with time in the case of 274 nm and maximum increase was observed at pH 8. However, no change in absorbance values was observed for all 3 samples stored at 4 °C after first 3 days of storage. These experiments confirm that pH and temperature are important factors in the storage stability of bHb solution. These studies also suggest that samples prepared in pH 6 buffer can be stored at 23 °C for a considerable period of time but solutions must be either stored at low temperatures or freshly prepared to ensure protein's stability.

5.4.2 Analysis by CD spectroscopy

Similar to UV studies, the CD analysis was also performed on the protein samples. The complete CD spectra collected for all samples are shown in Appendix C.2. CD spectra were analysed by CDNN software and the fraction content of 5 different secondary

structures were plotted with respect to time and storage conditions. This section discusses the results of CD analysis on the protein solutions.

5.4.2.1 Procedure for inter-day stability of bHb

Refer to section 3.2.8

5.4.2.2 Results

CD spectra were collected in the far UV region (190 to 260 nm) for all samples and the secondary structures contents were calculated using CDNN software. Secondary structures content obtained for samples at pH 6 are presented in Figure 5.14.

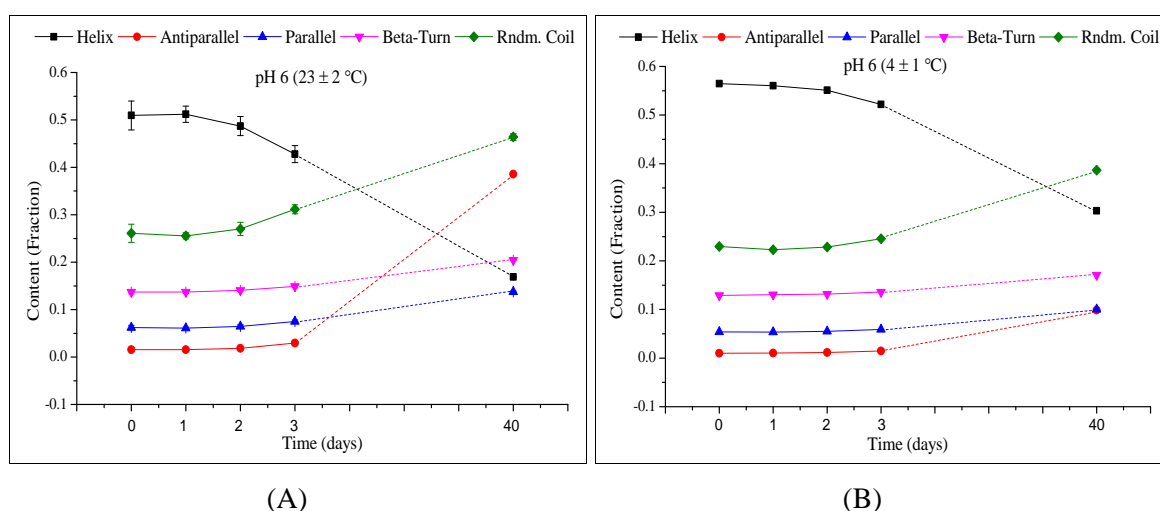


Figure 5.14: Secondary structure content of bHb at pH 6 stored at 23 °C (A) and 4 °C (B)

The alpha helix content of bHb samples stored at 23 °C decreased from the second day onwards, whereas the antiparallel, parallel, beta turns and random coil content increased. The decrease in alpha helix content was also observed in the 4 °C sample after first 2 days but it was less in comparison to the sample stored at higher temperature. Furthermore, the CD data suggested a complete loss of bHb conformation after 40 days of storage irrespective of the storage temperature. Similarly, a decrease in the alpha helix and an increase in the rest of the secondary structure content were observed for the protein samples prepared in pH 7 and stored at 23 °C.

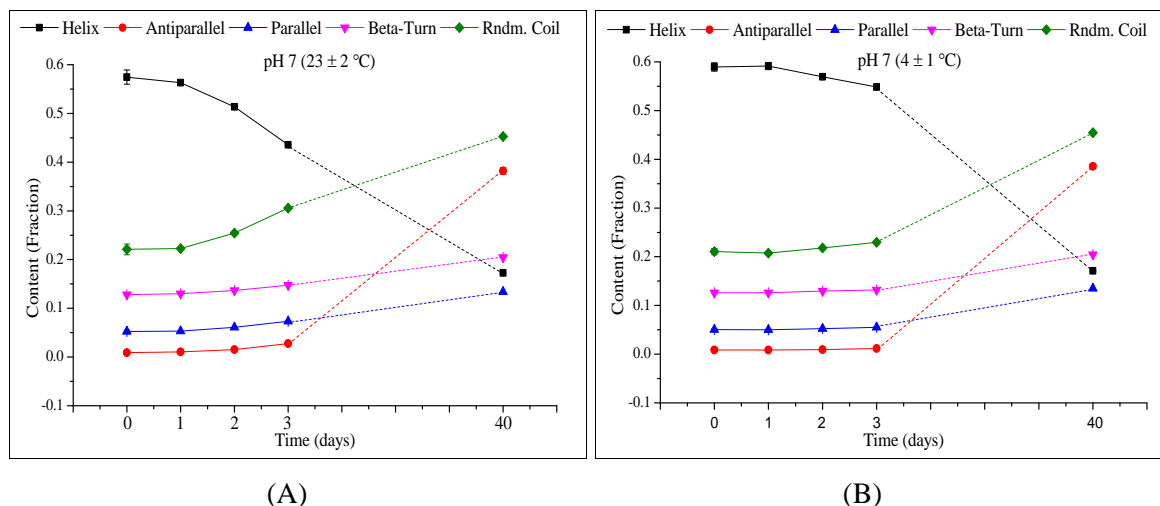


Figure 5.15: Secondary structure content of bHb at pH 7 stored at 23 °C (A) and 4 °C (B)

The decrease in alpha helix fraction was larger for the sample stored at 23 °C than the ones kept at 4 °C as shown in Figures 5.15. The initial decrease in the alpha-helicity was higher at pH 7 than pH 6 with a complete loss of the native structure of bHb after 40 days at both temperatures.

Figure 5.16 represents the secondary structures content of bHb in pH 8 at 23 and 4 °C respectively.

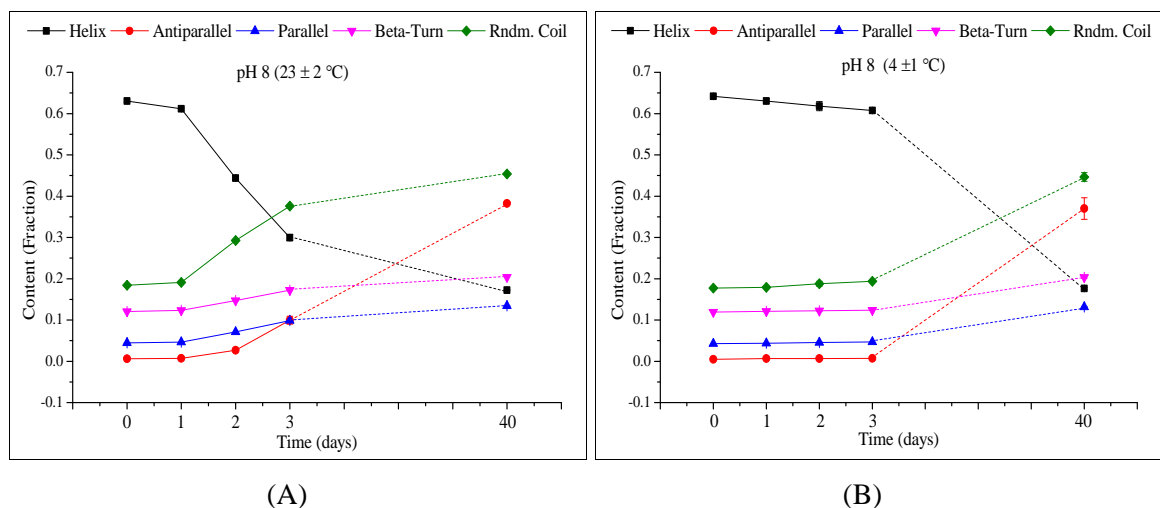


Figure 5.16: Secondary structure content of bHb at pH 8 stored at 23 °C (A) and 4 °C (B)

The data at pH 8 also showed a decrease in alpha helicity and increase in the rest of the secondary structures for both samples. However, the decrease in alpha helix content

was much faster at pH 8 in comparison with pH 6 and 7. Additionally, similar to previous cases the samples kept at 4 °C did not exhibit any change in the protein conformation for first 3 days but resulted in complete loss of native structure after 40 days.

5.4.3 Discussion

A clear difference in the stability of samples kept at 23 and 4 °C could be seen in these studies. The UV results of bHb samples prepared in pH 6 and 7 phosphate buffers were found to be similar during the storage at 23 °C. A small decrease in absorbance of soret band (405 nm) and similar increase at 274 nm was observed over the period of 3 days in both cases. However, a substantial decrease in absorbance at 405 nm and increase at 274 nm was observed in the case of pH 8 samples maintained at 23 °C. The hypochromic shift observed at 405 nm indicated the loss of haem moiety from the bHb molecule and the hyperchromic shift at 274 nm suggested the exposure of aromatic side chains of the protein to the solvent [10], [11]. The results of samples kept at 4 °C were similar with no changes in the UV spectrum for the first 3 days of storage. This indicated the stability of the bHb to be higher at lower temperatures. However, the results obtained after 40 days showed a complete loss of soret band in all samples irrespective of the temperature and pH which indicated that lower temperature only slowed the rate of protein denaturation rather than completely preventing it.

It is known that the proteins are amphoteric in nature and acquire a net positive charge below and overall negative charge above their isoelectric point (pI). [12]. The pI of bHb is 7.1 [13] which promotes electrostatic repulsion between protein molecules below and above this pH. Furthermore, the areas of large charge density within a single protein molecule can also result in intra-molecular repulsions and protein unfolding in a conducive atmosphere [10]. The rate of configuration loss according to UV results was highest for bHb in pH 8 buffer which suggested that the negatively charged groups in the protein molecule were more closely arranged and experienced stronger repulsive forces in comparison to the positively charged groups at pH 6. It is also widely accepted that the interaction between different charge groups can be accelerated at higher temperatures which was evident from the results obtained in this work. The instability

of protein solution was higher at 23 °C compared to 4 °C for first 3 days at all studied pH. This means that the storage temperature and pH are both important factors in the solution stability of bHb.

Similarly, the results obtained from CD analysis supported the observations made by UV spectroscopy. The main difference between UV and CD spectroscopy is that UV measures the absorption of monochromatic light by the molecules whereas CD measures the difference between the absorption of left and right circularly polarised light [14]. Moreover, unlike UV spectroscopy CD provides information on the precise changes in the conformation of proteins and other biomolecules. The majority of the bHb molecule (60-70%) exists in alpha helix form and rest (20-30%) of it consists of beta-turns, parallel, antiparallel and random coils [15]. The results indicated that changes in secondary structure, especially the loss of alpha helix followed a similar trend for samples stored at room temperature at pH 6 and 7. However, a rapid loss of alpha helix and gain in random coil was observed for bHb at pH 8. Additionally, the results obtained from samples stored at 4 °C were similar irrespective of the pH. All samples were found to be stable and only slight decrease in alpha helicity (3-4%) was observed over the period of 3 days. Also, there were no marked changes in the rest of the secondary structures. As discussed earlier, changes in the alpha-helicity were the result of the loss in hydrogen bonding between amide hydrogen and carbonyl oxygen in bHb molecule [8]. It is reported in the literature that haem stabilises the intact haemoglobin and its loss results in the decrease in the alpha helicity [16]. This phenomenon holds true in the present study where simultaneous loss of both haem (reduction in absorbance at 405 nm) and alpha helix was observed. Additionally, the bHb was completely denatured after 40 days irrespective of storage temperature which suggested that bHb is not stable in solution state and lower temperature only reduced the rate of denaturation.

Overall, the stability of proteins in the solution is a complex phenomenon which is affected by the changes in temperature, pH, ionic strength, solvent and other solutes [8], [17], [18]. Hence, in the present study factors such as temperature, pH and protein

concentration potentially played an important role individually or in combination towards the unfolding of bHb during its storage period.

5.5 Agitation stability

In addition to pH and temperature, vigorous agitation of protein solutions may also result in the change in conformation of a protein and loss of biological activity [19]. The agitation stability of bHb in pH 6 phosphate buffer was studied while stirring it at 250 rpm for 5 hours. The results obtained are discussed in the following section.

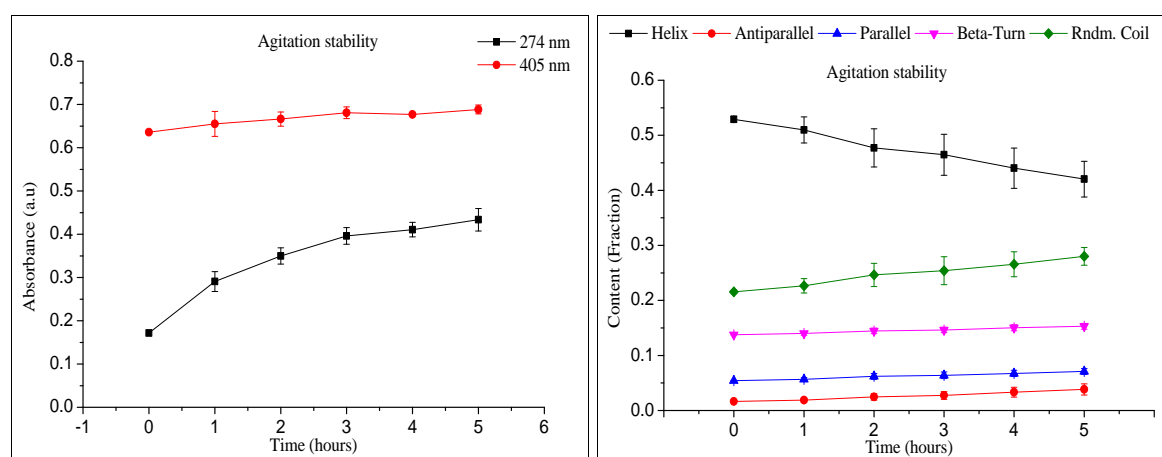
5.5.1 Procedure for agitation stability of bHb

Refer to section 3.3.9.

5.5.2 Results and discussion

The aim of this experiment was to observe any changes in bHb conformation caused by continuous stirring. The bHb solutions in this study were stirred at 250 rpm at (23 ± 2) °C for 5 hours. The UV and CD spectra were collected after every 60 minutes and compared to understand the effect of continuous mixing for the given duration.

Figure 5.17 (A) presents changes in the absorbance during the experiment at 274 and 405 nm. The bHb spectra were seen to change considerably over the period of 5 hours with substantial increase in the absorbance at 274 nm.



(A) UV absorbance at 274 and 405 nm

(B) Secondary structure content

Figure 5.17: Agitation stability of bHb

A hyperchromic shift of this peak suggested that turbulence caused by stirring affected the protein conformation and disrupted the native structure of the protein.

Similarly, CD analysis also confirmed changes in the secondary structure content as shown in Figure 5.17 (B). A continuous decrease from 55% to 45% in the alpha helix content and 7% increase in random coil fractions could be seen from the outset of the experiment. It is important to note that these results are different to the pH 6 stability study presented in section 5.4.2.2 where changes to the secondary structures occurred only after 48 hours. This indicated that physical agitation or shear stress provided enough energy to overcome the stabilising forces inside the protein molecule and led to conformational changes in bHb [17], [20].

5.6 Conclusions

It was found that bHb solution can withstand higher temperatures up to 50 °C during thermal degradation studies. Short term storage stability studies showed that there was no change in bHb conformation after 6 hours at 23 °C irrespective of solution pH. Inter-day stability studies demonstrated that bHb solution was more stable at 4 °C compared to 23 °C. Additionally, it was also observed that bHb was more stable at pH 6 and 7 than at pH 8 when stored at 23 °C. Therefore, it was concluded that the bHb in pH 6, 7 and 8 buffers must be prepared freshly before starting the experiment and essentially be used within 2 days if stored at 4 °C. Additionally, the agitation stability of bHb in pH 6 buffer illustrated that protein was sensitive towards stirring and changes in conformations were evident from the beginning of the experiment. Considering the results obtained from these studies the bHb solution was freshly prepared before all the further experiments. In addition to that, adsorption studies were performed in pH 6 phosphate buffer at 23 °C and for a duration of 4 hours.

References

- [1] E. J. McNally and J. E. Hastedt, *Protein formulation and delivery*, 2nd ed. New York, USA: informa helthcare, 2007.
- [2] S. Kelly and N. Price, “The Use of Circular Dichroism in the Investigation of Protein Structure and Function,” *Curr. Protein Pept. Sci.*, vol. 1, no. 4, pp. 349–384, 2000.
- [3] J. E. Noble and M. J. A. Bailey, “Quantitation of protein,” in *Methods in enzymology*, 1st ed., vol. 463, no. 09, Elsevier Inc., 2009, pp. 73–95.
- [4] C. Rimington, “Spectral-absorption coefficients of some porphyrins in the soret-band region,” *Biochem. J.*, vol. 75, no. 3, pp. 620–623, 1960.
- [5] E. A. Lapshina, I. B. Zavodnik, V. A. Ignatenko, and I. I. Stepuro, “Thermal stability and functional properties of human hemoglobin in the presence of aliphatic alcohols.,” *Mol. Biol. (Mosk)*., vol. 26, no. 2, pp. 315–320, 1992.
- [6] A. Michnik, Z. Drzazga, A. Kluczevska, and K. Michalik, “Differential scanning microcalorimetry study of the thermal denaturation of haemoglobin.,” *Biophys. Chem.*, vol. 118, no. 2–3, pp. 93–101, 2005.
- [7] G. M. Artmann, L. Burns, J. M. Canaves, A. Temiz-Artmann, G. W. Schmid-Schönbein, S. Chien, and C. Maggakis-Kelemen, “Circular dichroism spectra of human hemoglobin reveal a reversible structural transition at body temperature.,” *Eur. Biophys. J.*, vol. 33, no. 6, pp. 490–496, 2004.
- [8] E. Y. Chi, S. Krishnan, T. W. Randolph, and J. F. Carpenter, “Physical stability of proteins in aqueous solution: mechanism and driving forces in nonnative protein aggregation,” *Pharm. Res.*, vol. 20, no. 9, pp. 1325–1336, 2003.
- [9] C. N. Pace, B. A. Shirley, M. McNutt, and K. Gajiwala, “Forces contributing to the conformational stability of proteins.,” *FASEB J.*, pp. 75–83, 1996.

- [10] M. Mangino, "Protein Denaturation," *Ohio state university food science lectures*, 2007. [Online]. Available: <http://class.fst.ohio-state.edu/FST822/lectures/Denat.htm>. [Accessed: 07-Aug-2013].
- [11] E. C. Liang, Y. Dou, E. E. Scott, J. S. Olson, and G. N. Phillips, "Waterproofing the heme pocket: role of proximal amino acid side chains in preventing heme loss from myoglobin.," *J. Biol. Chem.*, vol. 276, no. 12, pp. 9093–9100, 2001.
- [12] T. Arakawa, S. J. Prestrelski, W. C. Kenney, and J. F. Carpenter, "Factors affecting short-term and long-term stabilities of proteins.," *Adv. Drug Deliv. Rev.*, vol. 46, pp. 307–326, 2001.
- [13] G. Zhan, C. Li, and D. Luo, "Electrochemical investigation of bovine hemoglobin at an acetylene black paste electrode in the presence of sodium dodecyl sulfate," *Bull. Chem. Soc.*, vol. 28, no. 10, pp. 1720–1724, 2007.
- [14] S. M. Kelly, T. J. Jess, and N. C. Price, "How to study proteins by circular dichroism.," *Biochim. Biophys. Acta*, vol. 1751, no. 2, pp. 119–39, 2005.
- [15] S. De and A. Girigoswami, "A fluorimetric and circular dichroism study of hemoglobin--effect of pH and anionic amphiphiles.," *J. Colloid Interface Sci.*, vol. 296, no. 1, pp. 324–31, 2006.
- [16] M. S. Hargrove and J. S. Olson, "The stability of holomyoglobin is determined by heme affinity," *Biochemistry*, vol. 35, no. 35, pp. 11310–11318, 1996.
- [17] W. Wang, S. Nema, and D. Teagarden, "Protein aggregation--pathways and influencing factors.," *Int. J. Pharm.*, vol. 390, no. 2, pp. 89–99, 2010.
- [18] C. P. Schneider, D. Shukla, and B. L. Trout, "Effects of solute-solute interactions on protein stability studied using various counterions and dendrimers.," *PLoS One*, vol. 6, no. 11, p. e27665, 2011.

- [19] P. L. Wang and T. P. Johnston, “Enhanced stability of two model proteins in an agitated solution environment using poloxamer 407,” *J. Parenter. Sci. Technol.*, vol. 47, no. 4, pp. 183–9, 1993.
- [20] H. C. Mahler, W. Friess, U. Grauschopf, and S. Kiese, “Protein aggregation: Pathways, induction factors and analysis,” *Journal of Pharmaceutical Sciences*, vol. 98, no. 9, pp. 2909–2934, 2009.

CHAPTER 6

Characterisation of silica particles & adsorption of bovine haemoglobin

6.1 Introduction

The aim of this chapter was to characterise silica used in the development of SCDDS and study adsorption (quantity and kinetics) of bHb on these particles. The information about the adsorption behaviour of bHb on silica is of utmost importance as the first step in the formulation of SCDDS is to adsorb/immobilise protein onto the core material. The inorganic cores used in this study were three morphologically different silica particles which were characterised by nitrogen sorption (BET) and scanning electron microscopy (SEM).

6.2 Characterisation of silica particles

The size, shape and porosity of silica particles were studied by BET and SEM. Specific surface area of silica particles with complete adsorption-desorption isotherm was determined using BET model. The pore size distribution and cumulative pore volumes were calculated according to Barrett-Joyner-Halenda (BJH) model and SEM was used to understand the surface morphology of these particles.

6.2.1 Materials and methods

This section discusses the materials and methods used in this study. Three morphologically different silica studied in this work were large particle silica (S_{LP}), spherical silica (S_S) and FP-244 silica (S_{FP}).

6.2.1.1 Materials

Refer to table 3.1

6.2.1.2 BET studies on silica particles

Refer to section 3.2.11

6.2.1.3 Analysis of silica particles by SEM

Refer to section 3.2.12

6.2.2 Results and discussion

In order to understand the surface of the particles, a complete BET isotherm of all 3 different silica was obtained. Figure 6.1 shows the adsorption and desorption of nitrogen from the surface of S_{LP} with respect to increase or decrease in relative pressure of nitrogen.

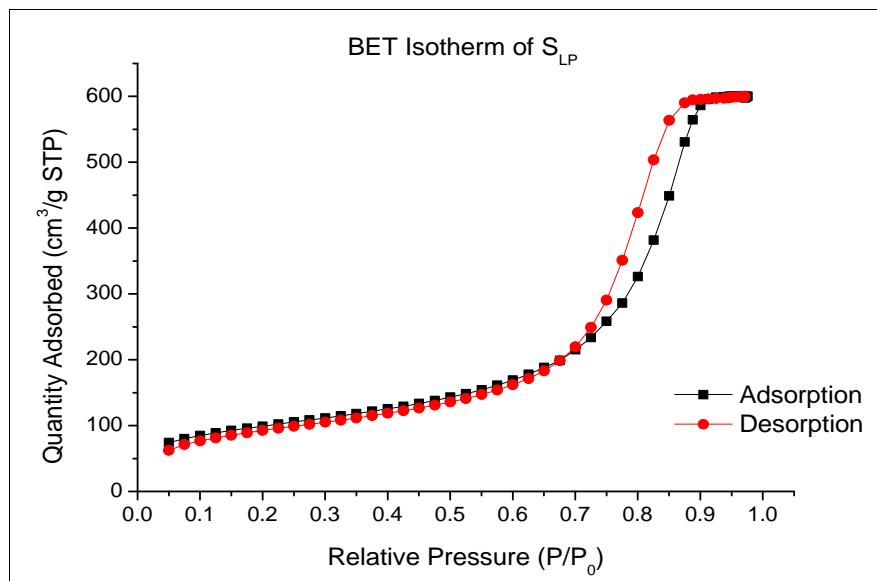


Figure 6.1: Complete BET isotherm of S_{LP}

The isotherm presented in Figure 6.1 was a BDDT (Brauner-Deming-Deming-Teller) Type IV isotherm characterised by its hysteresis which indicated that the particles were mesoporous *i.e.* they had pores with a diameter of 2-50 nm [1]. The appearance of hysteresis in a physisorption isotherm is usually associated with capillary condensation in mesopores and generally exhibit wide variety of shapes. IUPAC classification of various types of physisorption isotherms and hysteresis loops are shown in Figure 6.2.

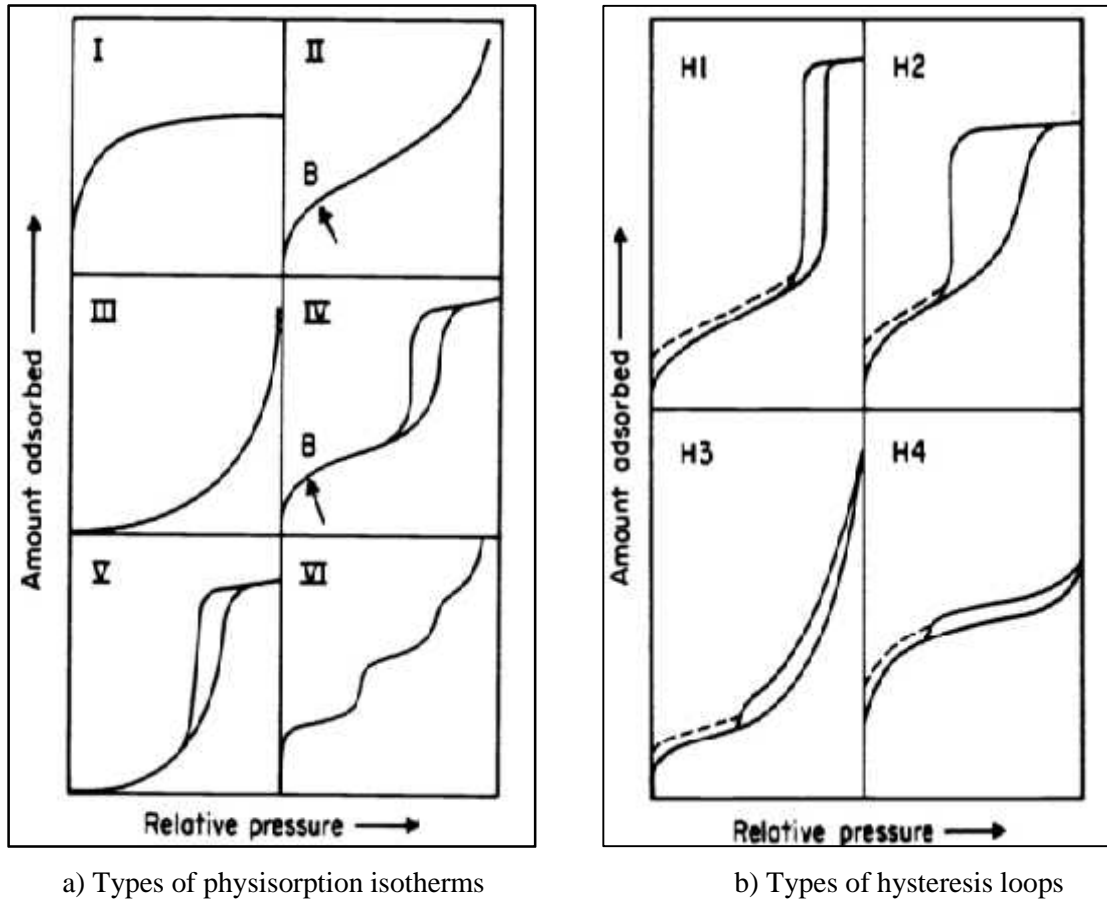


Figure 6.2: Types of sorption isotherms and hysteresis loops [1]

The Type I isotherm is given by microporous solids (pore size below 2 nm) which have relatively small external surfaces compared to its pore volume *e.g.* activated carbon and molecular sieve zeolites. Type II isotherm represents unrestricted monolayer-multilayer adsorption and is shown by a non-porous or macroporous (pore size above 50 nm) adsorbents. The point B in the isotherm indicates the stage at which monolayer coverage is complete. Type III isotherm is generally uncommon and does not exhibit a point B. Type IV isotherm is the most common isotherm and is characterised by its hysteresis loops as shown in Figure 6.2 (b). The shapes of these loops can be related with specific pore structures such as Type H1 is shown by porous materials which consist of agglomerates or compacts of spheres and have a narrow distribution of pore size. Type H2 loops are shown by many adsorbents which do not have well defined pore size and shape such as inorganic oxide gels and porous glasses. Type H3 loop is shown by aggregates of plate-like particles having slit-shaped pores. Similarly, Type

H4 is associated with narrow slit-like pores. Type V isotherm is uncommon and occurs when the adsorbate-adsorbent interactions are weak. The Type VI isotherms are characterised by the appearance of steps which shows multilayer adsorption on a uniform non-porous surface. Type VI isotherms are generally obtained with Argon or Krypton on graphitised carbon blacks.

Hysteresis in Figure 6.1 was intermediate to Type H1 and H2 which suggested cylindrical pores with opening at one or both ends. BJH model was applied to estimate the pore size (Figure 6.3) and pore volume distribution (Figure 6.4) in these particles. The average pore diameter and cumulative pore volume of S_{LP} were 95 Å (9.5 nm) and 0.92 ml/g respectively.

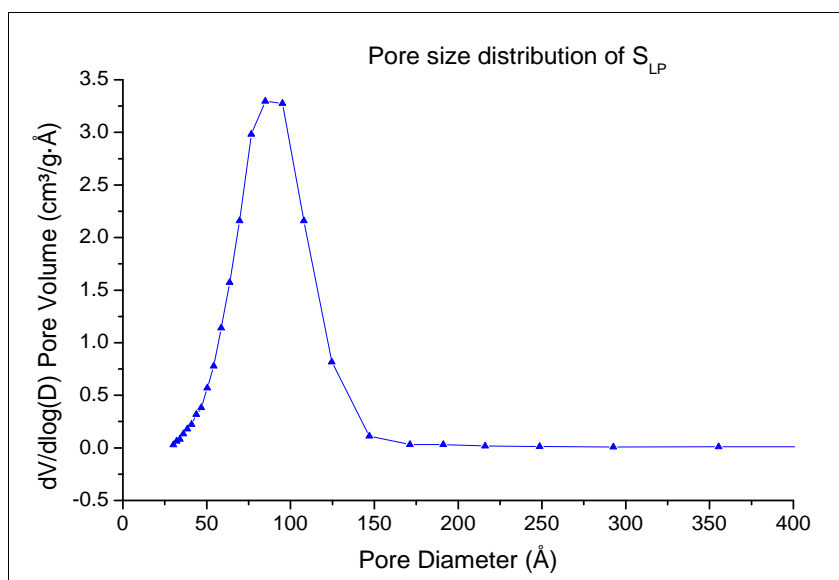


Figure 6.3: Pore size distribution of S_{LP}

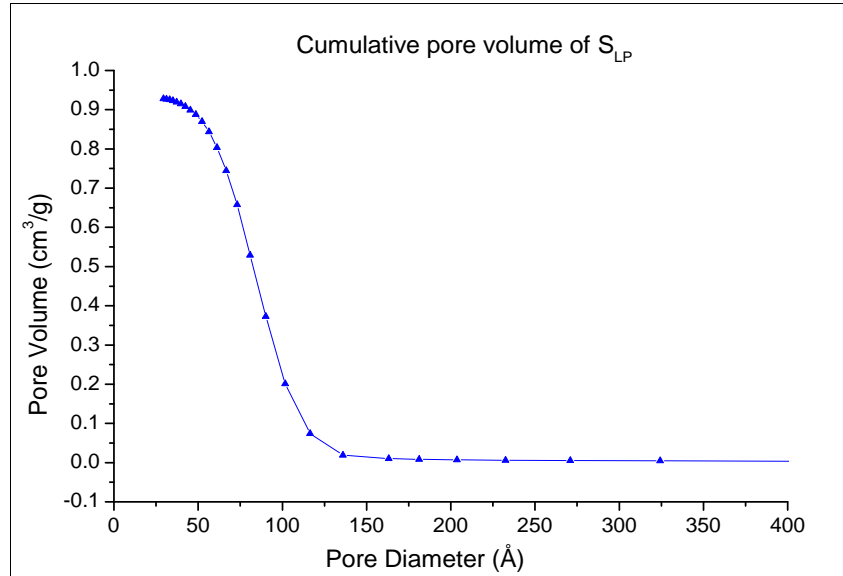


Figure 6.4: Cumulative pore volume of S_{LP}

Similarly, the complete BET isotherm for S_S was also obtained as shown in Figure 6.5. Similar to S_{LP} , the isotherm of S_S resembled to a BDDT Type IV isotherm indicating that the S_S particles were also mesoporous in nature.

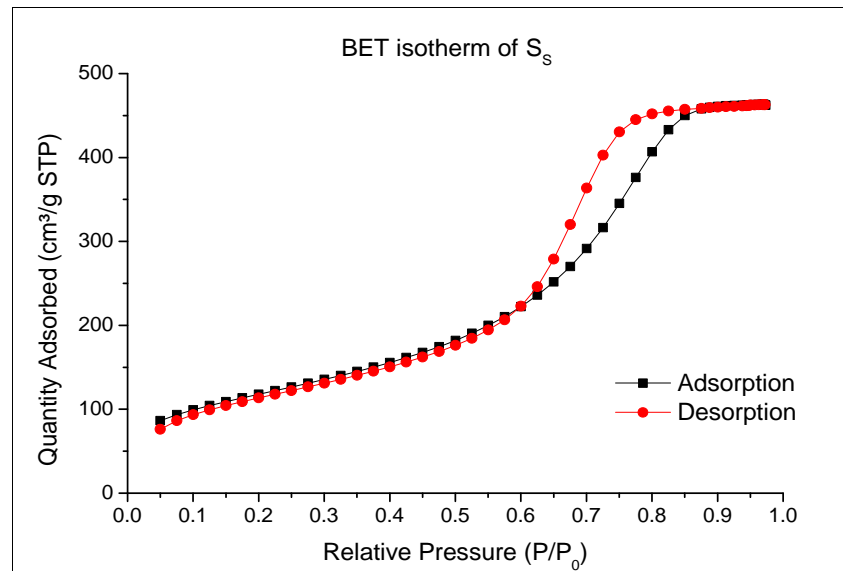


Figure 6.5: BET isotherm of S_S

The mesoporous nature was also confirmed by the BJH model where the average pore diameter of S_S was found to be approximately 55 Å (5.5 nm). Similar to S_{LP} particles,

the type of hysteresis obtained for S_S was intermediate to Type H1 and H2 as evident from the Figure 6.6.

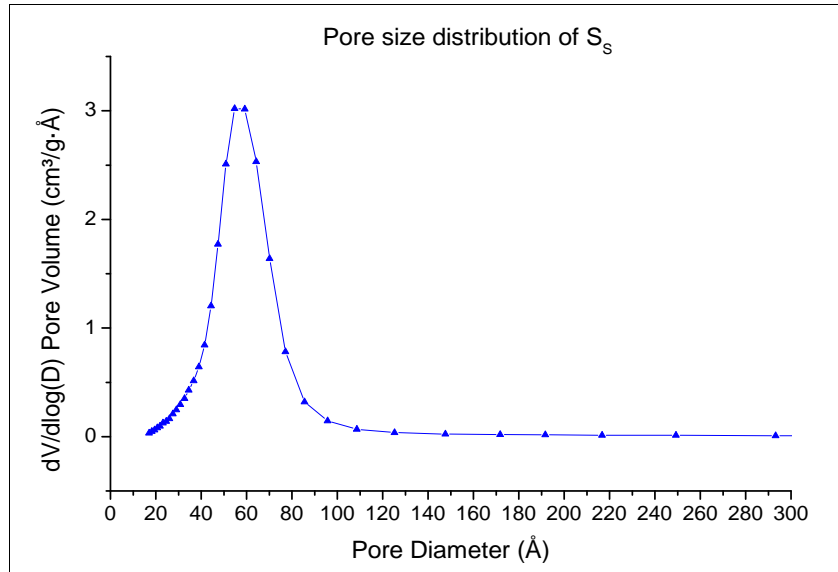


Figure 6.6: Pore size distribution of S_S by BJH model.

The cumulative pore volume of S_S calculated by BJH model was 0.7 ml/g as shown in Figure 6.7 which was lower than the pore volume of S_{LP} particles (0.9 ml/g).

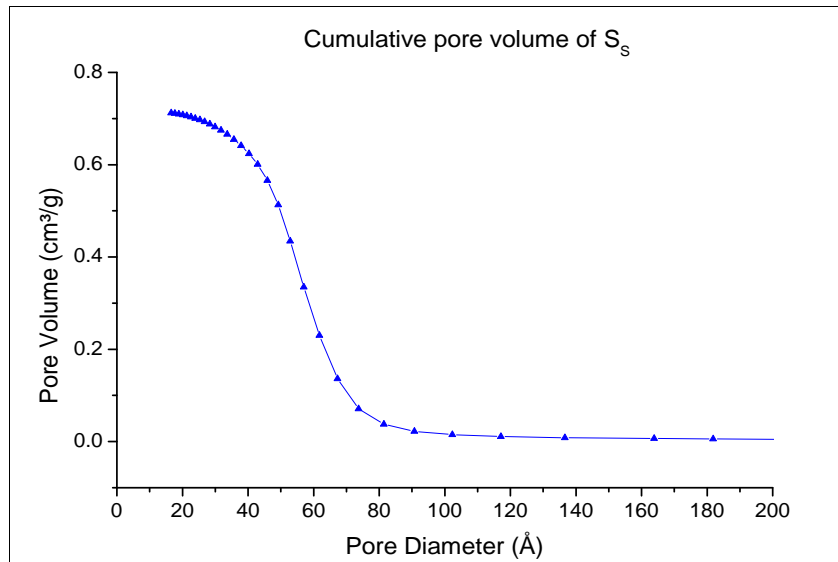


Figure 6.7: Cumulative pore volume of S_S by BJH model.

The complete nitrogen adsorption and desorption isotherm for S_{FP} is presented in Figure 6.8 which also resembled to the BDDT Type IV indicative of the mesoporous nature of the particles. The hysteresis in this isotherm resembled Type H1 meaning these particles consisted of agglomerates or compacts of approximately uniform spheres in a regular array [1].

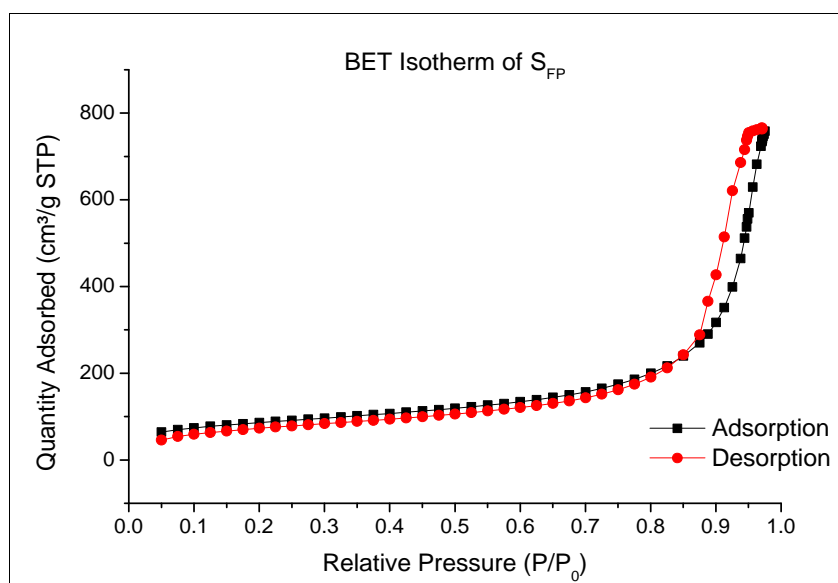


Figure 6.8: Complete BET isotherm of S_{FP}

The pore diameter and cumulative pore volume of S_{FP} calculated by BJH model were 160 Å (16 nm) and 1.1 ml/g respectively, as shown in Figures 6.9 and 6.10. The pore diameter and pore volume of S_{FP} were largest amongst all three silica particles studied here.

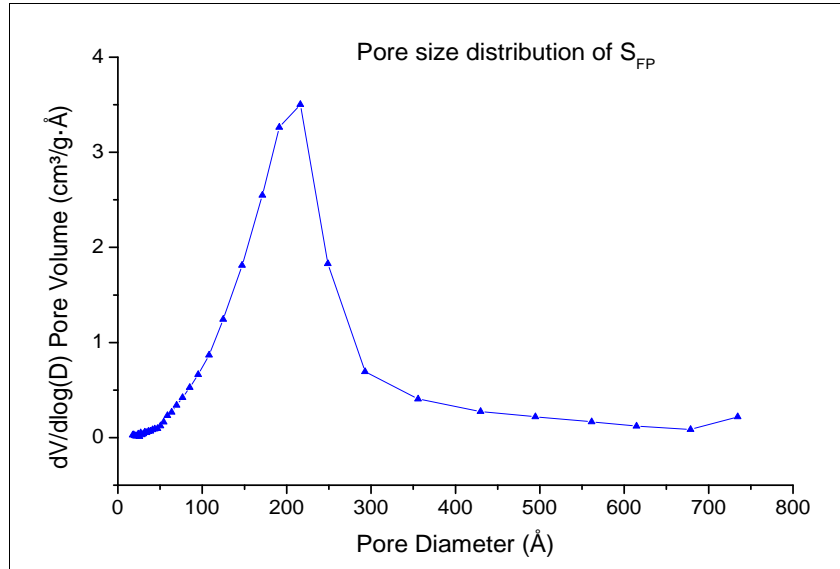


Figure 6.9: Pore size distribution of S_{FP} by BJH method

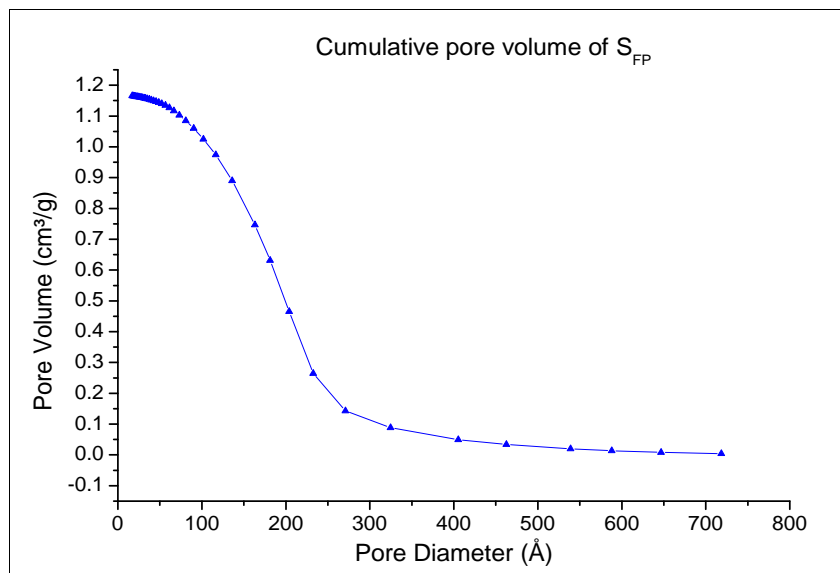


Figure 6.10: Cumulative pore volume of S_{FP} by BJH method

The specific surface area, cumulative pore volume and average pore diameter of different silica particles are summarised in Table 6.1.

Silica	Average particle size (µm)	BET surface area (m ² /g)	BJH Cumulative Pore Volume (ml/g)	BJH Pore Diameter (Å)
S _{LP}	300	353.5 ± 1.8	0.92	94.4
S _S	60	426.9 ± 0.8	0.71	58.3
S _{FP}	3	306.7 ± 2.0	1.16	159.2

Table 6.1 Characteristics of silica particles by nitrogen sorption

The data obtained from nitrogen adsorption method using BET model suggested that S_S had the highest specific surface area followed by S_{LP} and S_{FP} particles. Similarly, highest pore volume and pore size was obtained for S_{FP} as calculated by BJH model. The S_S particles had the smallest pore size and volume and the S_{LP} particles showed results intermediate to S_{FP} and S_S. The SEM analysis was also performed to further understand the surface morphology of these silica particles.

Electron micrographs were collected at lower and higher magnifications in order to observe the surface features of the particles. The micrograph at lower magnification showed discrete spherical particles with a narrow size distribution for S_S as presented in Figure 6.11 (A). The average size of S_S as determined by the labelling of a number of particles was 52.78 µm (n=15) which was similar to the supplier's reported value (approximately 60 µm).

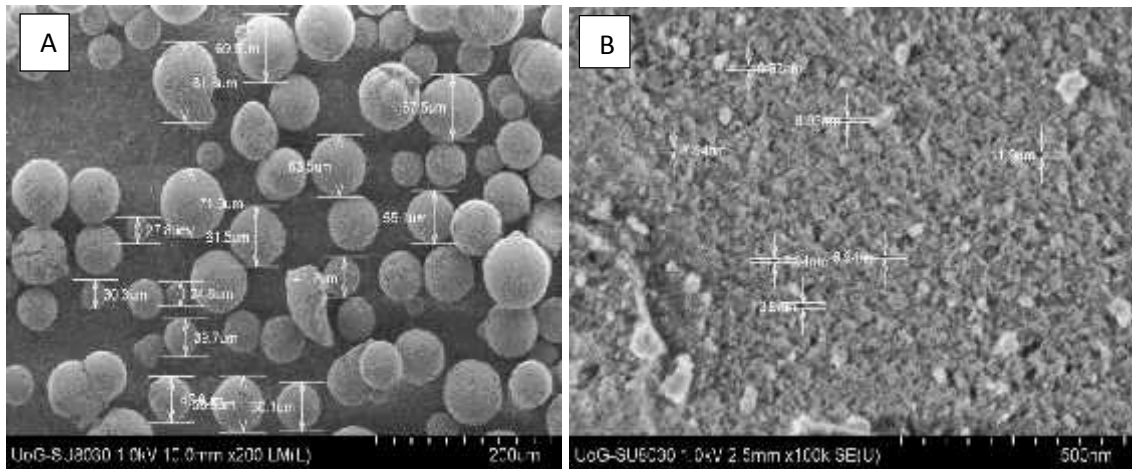


Figure 6.11: SEM micrographs of S_S at low (200) and high (100,000) magnification

A high magnification image (100,000X) of the particle surface is presented in Figure 6.11 (B). The pore diameter according to the micrographs was 9.63 nm (n=7) which was slightly larger than 5.83 nm calculated using BET. This difference in the pore diameter could be due to the smaller sample size in SEM or the parallax associated with the size measurement at high magnification.

Similarly, individual particles of S_{LP} could be seen in the micrograph presented in Figure 6.12 (A). Unlike S_S these particles were of irregular shapes and sizes. The mean particle size of 283.3 μm (n=9) as determined by SEM was slightly lower than the labelled value ($\sim 300 \mu\text{m}$).

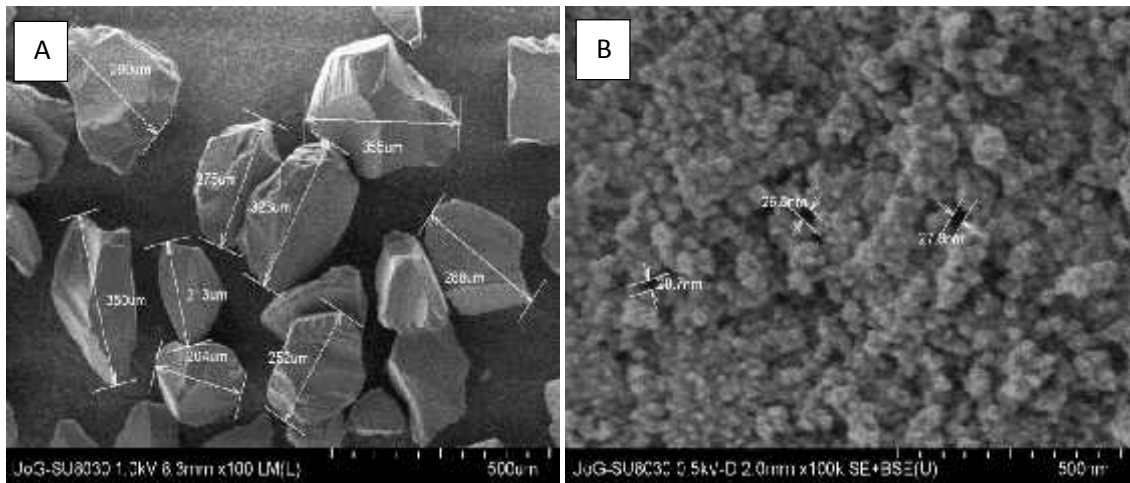


Figure 6.12: SEM micrograph of S_{LP} at low (100) and high (100,000) magnification

The surface of a single particle along with some of the pores is shown in Figure 6.12 (B). It was difficult to measure the exact pore diameter from the micrographs of S_{LP} because of their irregular surface morphology.

Likewise, the S_{FP} particles were also analysed by SEM and the micrographs collected are presented in Figure 6.13. The micrographs of S_{FP} were collected only under high magnification (25,000 and 100,000X) due to their comparatively low particle size of approximately 3 μm .

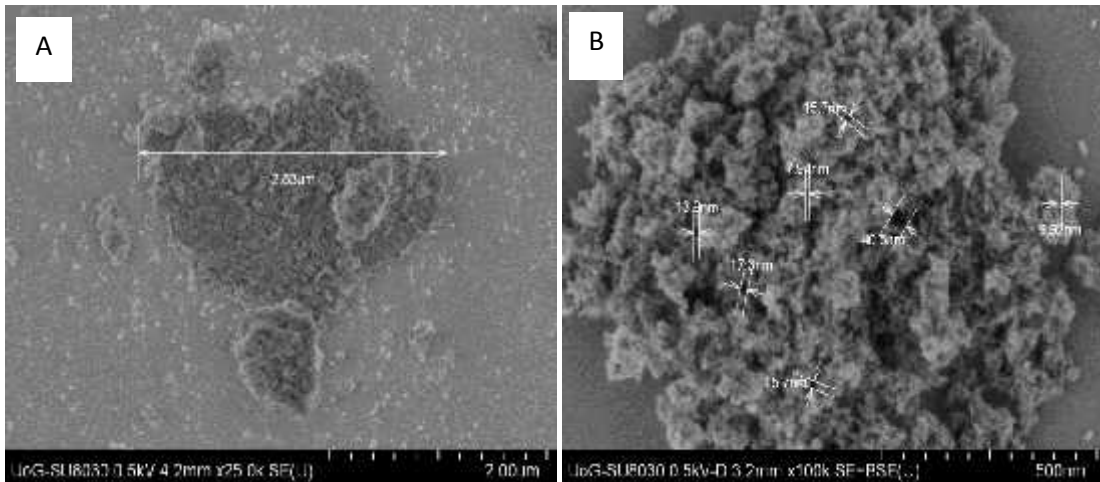


Figure 6.13: SEM micrographs of S_{FP} particle at 25,000 and 100,000 magnification.

Micrographs of S_{FP} particles confirmed that they were compacts or agglomerates of irregular shapes as suggested by BET analysis. The surface morphology of S_{FP} particles as presented in Figure 6.13 (B) further validated presence of large volume of empty spaces and interconnected pores. These findings supported the BET results which showed that the S_{FP} had the largest pore volume and diameter among all 3 silica particles studied here.

After the characterisation of all three silica particles by BET and SEM it could be stated that the specific surface area was highest for S_S followed by S_{LP} and S_{FP} . Furthermore, S_{FP} particles had the largest pore diameter and pore volume followed by S_{LP} and S_S . Therefore, if only the specific surface area of particles was considered then S_S should potentially adsorb the highest amount of protein and if only the pore features were taken in account then the maximum adsorption should be seen for S_{FP} . The following section discusses adsorption experiments conducted to test this hypothesis and find maximum amount of bHb adsorbed on each type of silica particles.

6.3 Adsorption of bovine haemoglobin (bHb) on silica particles

Protein adsorption is a very common phenomenon as they are highly likely to adsorb on a solid surface upon contact [2]. Protein molecules do not behave like rigid particles and exist in variety of sizes, shapes and structural conformations. It is important to note that adsorption of protein is different from small molecules because unlike small

molecules, proteins are folded into secondary and tertiary structures and have a unique distribution of hydrophilic and hydrophobic side chains which affect their adsorption characteristics [3]. The extent of protein adsorption is affected by various factors such as properties of proteins (charge, size, stability of structure and amino acid composition), type of adsorbent and adsorption conditions (temperature, pH, ionic strength and buffer composition) [3].

bHb is a large molecule and can interact with silica in different ways such as ionic interactions, hydrophobic interactions, hydrogen bonding, van der Waals interaction and hydration forces [3][4]. The ionic and hydrophobic interactions along with the gain in conformational entropy of proteins are considered to be the most prominent driving forces for its adsorption onto a solid surface [5]–[7].

The adsorption of haemoglobin has been reported on various materials *viz.* silica nanoparticles [8], porous glasses, silichromes, silica gels [9], molecular sieves, mesoporous alumina [10], biporous silica [11], hydroxyapatite [12] and chitosan [13] where the amount of haemoglobin adsorbed was found to vary from 20 to 2000 mg/g of the adsorbent [14].

There are a number of methods available for protein adsorption on solid surfaces but physical adsorption is the most commonly used method for this purpose. The other methods include covalent/chemical binding and entrapment. The advantages of physical adsorption are as follows [15]

- a) It is economical, rapid and requires simple experimental procedures
- b) Functionalisation of the carrier material is not required and
- c) Usage of toxic solvents can be avoided.

Hence, physisorption was the preferred method for the bHb immobilisation on the three types of silica particles described in section 6.2. The agitation stability studies detailed in section 5.5 confirmed that prolonged stirring of bHb solution leads to changes in the protein conformation, therefore, the duration of experiments was fixed to 4 hours throughout the adsorption studies. These experiments to determine maximum protein

adsorption along with the kinetics also helped to understand the effect of surface morphology of core materials in this process.

6.3.1 Materials and methods

Materials used here are listed in Table 3.1 and the methods used for bHb adsorption on silica particles and its kinetics have been discussed in this section.

6.3.1.1 Adsorption of bHb on silica particles

Refer to section 3.2.10.1

6.3.1.2 Kinetic measurements of bHb adsorption on silica

Refer to section 3.2.10.2

6.3.2 Results and Discussion

It is known that proteins are positively charged at low pH (*i.e.* $\text{pH} < \text{pI}$) and negatively charged at high pH (*i.e.* $\text{pH} > \text{pI}$) conditions [2]. The rate of protein adsorption is likely to be high when the adsorbent surface and protein bear opposite charges. This higher rate of adsorption is primarily driven by the electrostatic attractions which accelerates the protein migration towards the oppositely charged surface [3]. The adsorption studies presented in this section were performed in pH 6 phosphate buffer (0.13 M) due to the overall positive charge on bHb and a negative charge on silica particles such that the ionic interactions could be encouraged. Another reason towards the selection of this pH was the higher protein stability compared to pH 7 and 8 as discussed in chapter 5.

The results of bHb adsorption on S_{LP} , S_{S} , and S_{FP} are shown in Figures 6.14, 6.15 and 6.16 respectively.

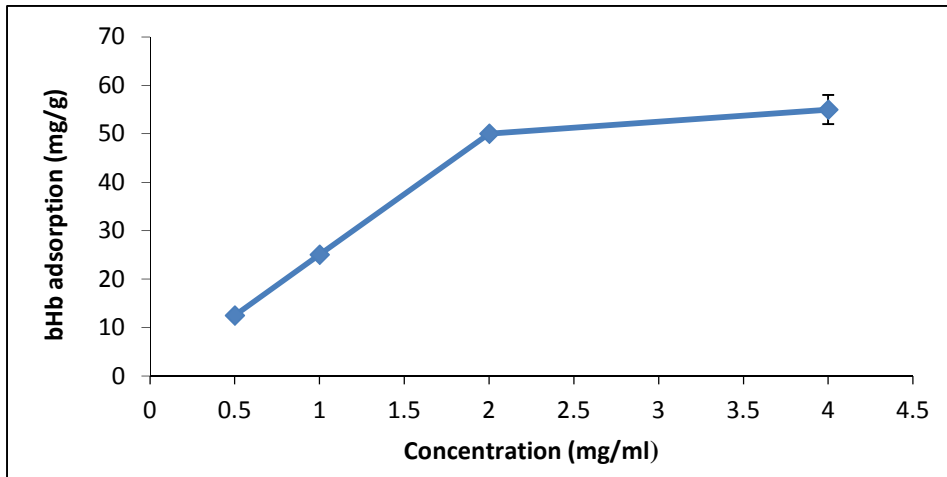


Figure 6.14: Adsorption isotherm of bHb on S_{LP}

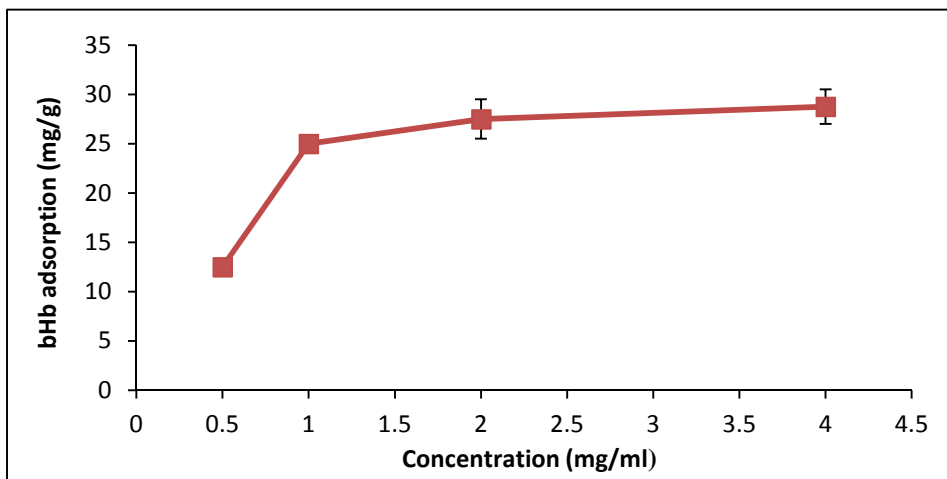


Figure 6.15: Adsorption isotherm of bHb on S_s

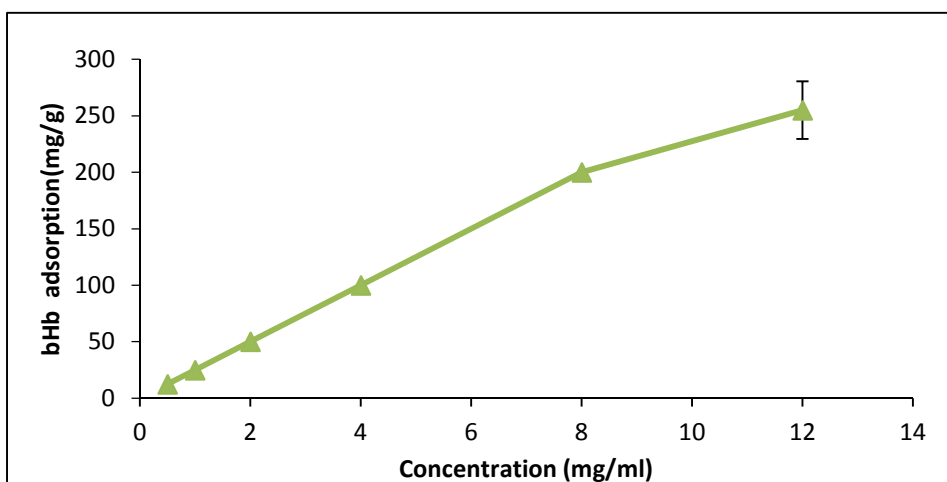


Figure 6.16: Adsorption isotherm of bHb on S_{FP}

A continuous increase of bHb adsorption on S_{LP} with the increase in protein concentration could be observed in Figure 6.14. The adsorption limit was achieved at 2 mg/ml with the maximum adsorption of 50 mg/g of protein on silica. A further increase in the concentration to 4 mg/ml did not lead to higher adsorption of bHb. Similarly, the adsorption limit for S_S was achieved at lower concentration than for S_{LP} as evident from Figure 6.15 where an increase in the bHb concentration above 1 mg/ml did not lead to any further increase in the adsorption. The maximum quantity of bHb adsorbed on S_S was determined to be 25 mg/g which was 50% less than S_{LP} particles. The protein adsorption on S_{FP} was significantly higher in comparison to S_S and S_{LP} as evident from Figure 6.16. The bHb adsorption increased with the increase in concentration and the maximum adsorbed amount was found to be 200 mg/g. This was 4 times higher to the adsorbed amount on S_{LP} and 8 times higher than S_S .

The adsorption kinetics of bHb was also determined on these three silica particles. The concentration of 2 mg/ml was used to determine adsorption kinetics of bHb on S_{LP} . The results presented in Figure 6.17 clearly show that almost 80% of bHb was adsorbed on S_{LP} in the first 2 hours. The isotherm was almost linear between 0-2 hours denoting high affinity of bHb for S_{LP} in pH 6 phosphate buffer. The slope of the isotherm provided the rate of adsorption of protein on silica and was found to be 0.14 mg/min for S_{LP} particles. Similar to S_{LP} , the adsorption kinetics (Figure 6.18) of bHb on S_S was studied at the concentration of 1 mg/ml. It could be seen that the adsorption of protein was comparatively slower on S_S as it took 4 hours to attain maxima with an adsorption rate of 0.04 mg/min for these particles. This slow rate of adsorption on S_S suggested low affinity of protein for these particles and weak protein-silica interactions in comparison to S_{LP} . The adsorption concentration of 8 mg/ml was used for the kinetics experiment for S_{FP} . The results presented in Figure 6.19 indicated high affinity of protein to S_{FP} particles. Similar to S_{LP} , it took only 2 hours for almost 80-85% of protein adsorption to occur on these particles. The rate of adsorption was determined by calculating the slope of the curve, which was found to be 0.58 mg/min confirming bHb's high affinity towards S_{FP} at studied conditions.

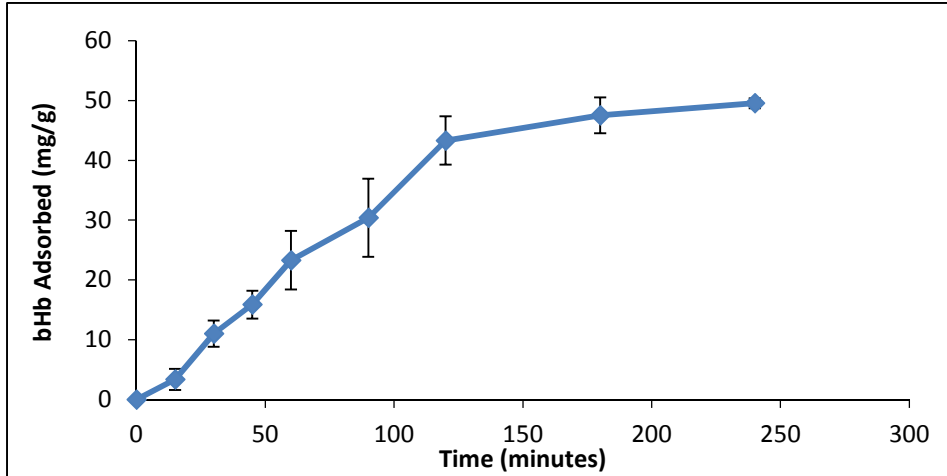


Figure 6.17: Adsorption kinetics of 2 mg/ml bHb solution on S_{LP}

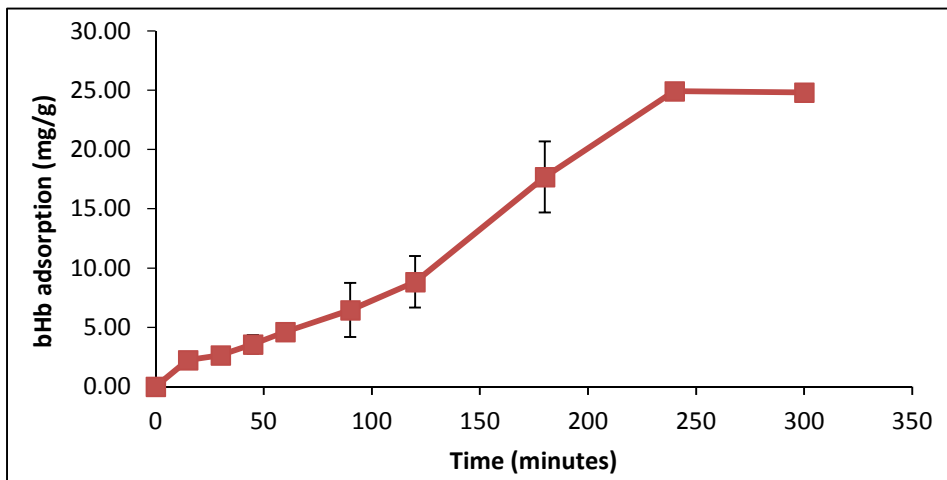


Figure 6.18: Adsorption kinetics of 1 mg/ml bHb solution on S_s

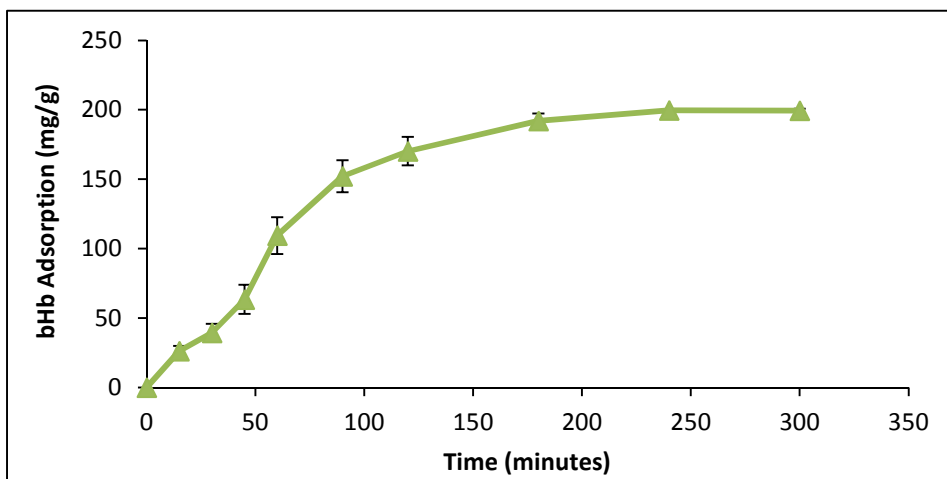


Figure 6.19: Adsorption kinetics of 8 mg/ml bHb solution on S_{FP}

The results from the adsorption studies showed that a gram of S_S , S_{LP} and S_{FP} particles adsorbed 25, 50 and 200 mg of bHb respectively. The adsorption kinetics data also suggested significantly different affinity of protein for different silica particles. The S_{FP} particles once again had highest rate of adsorption followed by S_{LP} and S_S .

In general, it can be expected that larger surface area will lead to higher protein adsorption but present study suggests otherwise. A comparison of the specific surface area and the total protein adsorbed by 3 different silica particles is presented in the Figure 6.20. Interestingly, the amount of protein adsorbed had an inverse relation to the specific surface area of the silica particles as calculated by BET.

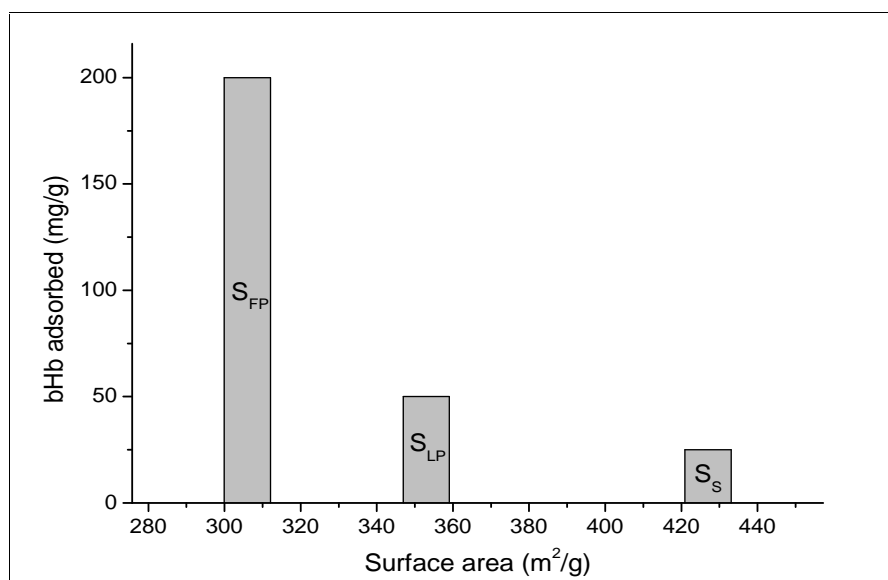


Figure 6.20: Inverse relationship between surface area and protein adsorption

The surface area of S_S particles was largest but the quantity of bHb adsorbed was lowest. Conversely, the amount of protein adsorbed on S_{FP} particles was highest but its specific surface area was the lowest amongst all studied core materials. This difference in the protein adsorption could be related to the pore morphology/features of the adsorbent material [16]. The comparison between pore volume and pore diameter with total protein adsorbed is presented in Figure 6.21 where a positive correlation can be observed between the pore characteristics of the adsorbent material and the total bHb adsorption.

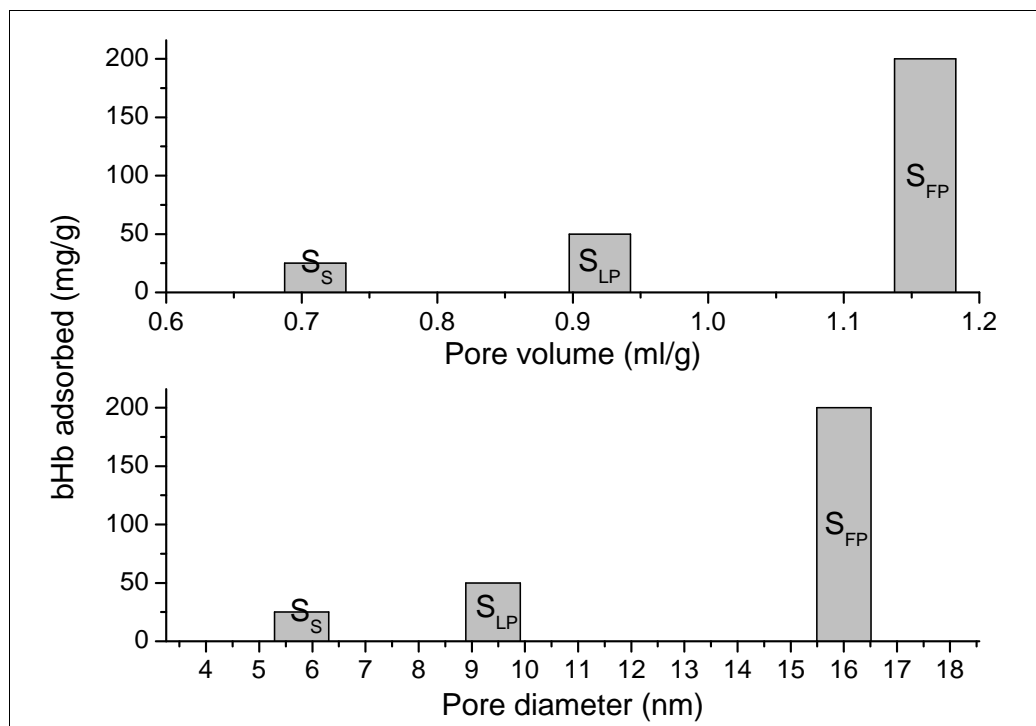


Figure 6.21: Comparison of adsorbed protein with pore volume and pore diameter

The protein adsorption increased with the increase in the pore diameter and volume of silica particles. The low protein adsorption on S_S particles despite its large surface area can be explained by the presence of smaller pores. It is important to remember that the smaller pores which were easily accessible to nitrogen molecules during BET analysis could be completely inaccessible to large molecules such as bHb. The average pore diameter (~5.8 nm) of S_S was less than the size of bHb molecule (6.2 nm) [14]. Thus, majority of these pores present on the surface of S_S would be inaccessible to the protein molecules leading to low adsorption of bHb [16], [17]. Conversely, an average pore size of 16 nm on S_{FP} particles could easily accommodate up to two bHb molecules and result in the overall increase in the quantity of protein adsorbed on these particles. The protein adsorption on S_{LP} was intermediate to S_S and S_{FP} which can also be explained by studying its pore diameter and pore volume. The pore diameter of S_{LP} (9.5 nm) was larger than both the pore size of S_S and the protein which permitted higher bHb adsorption on these particles than S_S. However, the protein adsorption on S_{LP} was 4 times lower in comparison to S_{FP} because of its comparative low pore size and volume. This confirmed that the presence of larger pore size and pore volume plays an important

role in the protein adsorption in comparison to the overall specific surface area as determined by BET. As stated earlier, BET surface area doesn't always translate into the available surface area for protein adsorption primarily due to size of the probe molecule used in this method. However, it provides important information and theoretical background to study these processes further.

BET analysis was also performed on bHb adsorbed silica which indicated that the specific surface area and pore volume decreased after adsorption of bHb for all three silica. A comparison between BET results of silica before and after bHb adsorption is presented in Table 6.2.

Silica type	Silica		bHb adsorbed silica	
	Surface area (m ² /g)	Pore volume (ml/g)	Surface area (m ² /g)	Pore volume (ml/g)
S_{LP}	353.5 ± 1.8	0.92	231.7 ± 0.8	0.63
S_S	426.9 ± 0.8	0.71	322.0 ± 0.6	0.57
S_{FP}	306.7 ± 2.0	1.16	226.2 ± 0.7	0.93

Table 6.2: Comparison of BET results before and after adsorption of bHb

The results presented in Table 6.2 showed a decrease in pore volume and surface area after adsorption of bHb. The pore volume decreased from 0.92 ml/g to 0.63 ml/g for S_{LP}, 0.71 to 0.57 ml/g for S_S and 1.16 to 0.93 ml/g for S_{FP}. This can be expected as the presence of bHb inside the pores or the blockage of pore openings by protein molecule will lead to the decrease in the pore volume. These results further confirmed the findings from adsorption experiments that bHb was adsorbed inside the pores of these silica particles.

6.4 Conclusions

The protein adsorption is a complex phenomenon and factors such as available surface area, average pore volume and pore diameter of adsorbent are also important along with

adsorption conditions (temperature, pH and ionic strength). It was found that 1 g of S_{FP} adsorbed the highest amount of protein (200 mg) followed by S_{LP} (50 mg) and S_S (25 mg). The reason to this phenomenon was accredited to the available surface area for adsorption, which was dependent upon the pore volume and pore diameter. Adsorption kinetics suggested that the adsorption of bHb on S_{FP} was quickest and slowest on S_S silica.

The main aim of these experiments was to quantify bHb that can be immobilised on these three morphologically different silica particles and it was found that highly porous systems such as S_{FP} can be potentially used as a carrier in protein delivery.

References

- [1] K. Sing, D. Everett, R. Haul, L. Moscou, R. Pierotti, J. Rouquerol, and T. Siemieniewska, 'Reporting physisorption data for gas/solid systems with special reference to the determination of surface area and porosity (Recommendations 1984)', *Pure Appl. Chem.*, vol. 57, no. 4, pp. 603–619, 1985.
- [2] K. Nakanishi, T. Sakiyama, and K. Imamura, 'On the adsorption of proteins on solid surfaces, a common but very complicated phenomenon.', *J. Biosci. Bioeng.*, vol. 91, no. 3, pp. 233–44, 2001.
- [3] M. Rabe, D. Verdes, and S. Seeger, 'Understanding protein adsorption phenomena at solid surfaces.', *Adv. Colloid Interface Sci.*, vol. 162, no. 1–2, pp. 87–106, 2011.
- [4] R. A. Hartvig, M. Van De Weert, J. Østergaard, L. Jorgensen, and H. Jensen, 'Protein adsorption at charged surfaces: The role of electrostatic interactions and interfacial charge regulation', *Langmuir*, vol. 27, no. 6, pp. 2634–2643, 2011.
- [5] W. Norde and A. C. I. Anusiem, 'Adsorption, desorption and re-adsorption of proteins on solid surfaces', *Colloids and Surfaces*, vol. 66, no. 1, pp. 73–80, 1992.
- [6] F. Fang and I. Szleifer, 'Kinetics and thermodynamics of protein adsorption: a generalized molecular theoretical approach.', *Biophys. J.*, vol. 80, no. 6, pp. 2568–89, 2001.
- [7] J. J. Gray, 'The interaction of proteins with solid surfaces.', *Curr. Opin. Struct. Biol.*, vol. 14, no. 1, pp. 110–5, 2004.
- [8] Z. Xu, S. L. Wang, and H. W. Gao, 'Effects of nano-sized silicon dioxide on the structures and activities of three functional proteins.', *J. Hazard. Mater.*, vol. 180, no. 1–3, pp. 375–83, 2010.

- [9] E. S. Chukhrai, L. F. Atyaksheva, and O. S. Pilipenko, 'The special features of protein adsorption isotherms on silica adsorbents', *Russ. J. Phys. Chem. A*, vol. 85, no. 5, pp. 890–896, 2011.
- [10] J. Yu, J. Ma, F. Zhao, and B. Zeng, 'Direct electron-transfer and electrochemical catalysis of hemoglobin immobilized on mesoporous Al₂O₃', *Electrochim. Acta*, vol. 53, no. 4, pp. 1995–2001, 2007.
- [11] L. Zhang, Q. Zhang, and J. Li, 'Direct electrochemistry and electrocatalysis of hemoglobin immobilized in bimodal mesoporous silica and chitosan inorganic–organic hybrid film', *Electrochem. commun.*, vol. 9, no. 7, pp. 1530–1535, 2007.
- [12] C. Fargues, M. Bailly, and G. Grevillot, 'Adsorption of BSA and hemoglobin on hydroxyapatite support: equilibria and multicomponent dynamic adsorption', *Adsorption*, vol. 4, no. 1, pp. 5–16, 1998.
- [13] Y.-Q. Xia, T.-Y. Guo, H.-L. Zhao, M.-D. Song, B.-H. Zhang, and B.-L. Zhang, 'Protein recognition onto silica particles using chitosan as intermedium substrate.', *J. Biomed. Mater. Res. A*, vol. 90, no. 2, pp. 326–32, 2009.
- [14] L. F. Atyaksheva, I. V. Dobryakova, I. I. Ivanova, E. E. Knyazeva, R. a. Ovsyannikov, and E. S. Chukhrai, 'Adsorption properties of hemoglobin', *Russ. J. Phys. Chem. A*, vol. 86, no. 3, pp. 468–474, 2012.
- [15] M. Hartmann and X. Kostrov, 'Immobilization of enzymes on porous silicas-- benefits and challenges.', *Chem. Soc. Rev.*, vol. 42, no. 15, pp. 6277–89, 2013.
- [16] Z. Ma, J. Bai, Y. Wang, and X. Jiang, 'Impact of shape and pore size of mesoporous silica nanoparticles on serum protein adsorption and RBCS hemolysis', *ACS Appl. Mater. Interfaces*, vol. 6, no. 4, pp. 2431–2438, 2014.
- [17] D. M. Schlipf, S. E. Rankin, and B. L. Knutson, 'Pore-size dependent protein adsorption and protection from proteolytic hydrolysis in tailored mesoporous

silica particles', *ACS Appl. Mater. Interfaces*, vol. 5, no. 20, pp. 10111–10117, 2013.

CHAPTER 7

Effect of pluronics on desorption of bHb from silica particle

Proteins are known to adsorb irreversibly on a solid surface hence determination of bHb's desorption behaviour is essential to successfully develop SCDDS. The aim of this chapter was to study and delineate desorption parameters for bHb from silica. This chapter also investigates the use of a displacer such as non-ionic surfactants to achieve maximum release without causing any conformational changes to the protein.

7.1 Introduction

Protein adsorption on hydrophobic solid surfaces is generally irreversible due to the increase in the free energy, whereas, hydrophilic surfaces show both reversible and irreversible adsorption [1]. The desorption of bHb from silica plays a major role in the development of SCDDS, where drug release is expected to be achieved by changes in solvent ionic strength, pH and/ or use of surfactants [2]–[7]. It is shown by Norde *et.al* that human plasma albumin can be desorbed partly from different surfaces by adjusting the ionic strength and pH or by addition of a displacer (morpholine) [3]. Similarly, it has been reported that approximately 80% of fibrinogen can be desorbed from borosilicate glass just by increasing the ionic strength of the buffer [4]. Likewise, the rate of desorption of proteins from alumina surface by various desorbing agents such as buffers, surfactants, urea and sodium chloride was described by Sarkar *et.al* [8].

A displacer (surfactant) is commonly used in the desorption of proteins from solid surfaces and the extent of protein desorbed along with the desorption mechanism is mainly dependent upon the type of protein, adsorbent surface and surfactant [9]. Desorption of bHb from silica particles in the studied system was minimal. Hence, the effect of non-ionic surfactants on desorption and protein conformation was investigated. The displacers used in the current work were a number of tri-block copolymers (pluronics) with varying molecular weights and concentrations. The role of pluronics as a displacer and their effect on the release and conformation of protein is detailed in this chapter.

7.2 Materials and methods

This section discusses the adsorption protocol and desorption procedure used to study the effect of pluronics on bHb desorption.

7.2.1 Materials

Refer to table 3.1

7.2.2 Adsorption protocol

Refer to section 3.2.10.3

7.2.3. Desorption procedure

A fixed quantity of bHb adsorbed silica particles (bHb-Si) were taken into a 250 ml beaker. Weight corresponding to 0.5, 1.0, 5.0 and 10 mg/ml of pluronic was added in 100 ml of pH 6.8 phosphate buffer (0.2 M). Contents were stirred at 250 rpm and desorbed amount of bHb was measured by UV spectroscopy after 15, 30, 45, 60, 90, 120, 180, 240 and 1440 minutes. 400 mg of bHb-Si was used for S_{LP} and S_S, whereas, for S_{FP} only 100 mg of silica was used due to 4 times higher amount of bHb on these particles. All experiments were conducted in triplicate and at room temperature.

7.2.4 Effect of pluronics on bHb conformation

The effect of various pluronics on the conformation of bHb was studied by UV and CD spectroscopy. The concentrations used (*viz.* 1, 5, 10 and 20 mg/ml) covered the full range that has been used for desorption experiments. 0.1 mg/ml of bHb was prepared in pH 6.8 phosphate buffer along with each of the above mentioned pluronic concentrations and the readings were taken in UV and CD spectrophotometer after 4 hours.

7.3 Results

The effect of various concentrations and molecular weights of pluronics on protein desorption from three types of silica is discussed in the following sections.

7.3.1 Desorption from S_{LP} particles

Desorption of bHb from S_{LP} by different concentrations of pluronic F-38 is presented in Figure 7.1. The desorption profiles of bHb with 0.5 and 1.0 mg/ml pluronic were similar where the maximum release was around 60%. The final desorbed amount for 5 and 10 mg/ml concentrations was slightly higher to 70%.

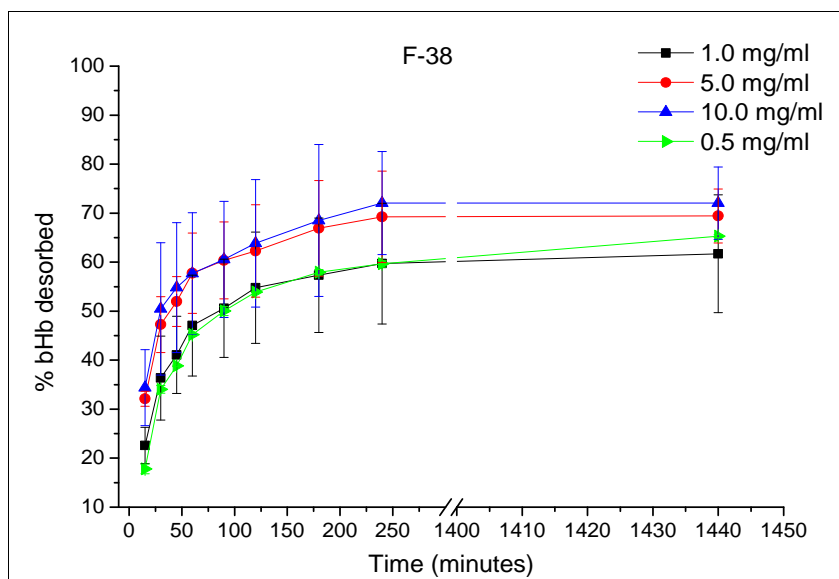


Figure 7.1: bHb desorption from S_{LP} particles using F-38 as a displacer

The graph of all four concentrations followed the same trend with only difference in the initial release. It is also important to note that increasing the surfactant concentration from 5 to 10 mg/ml did not result in a clear increase in the protein desorption. It was also observed that almost 80% of total protein desorption took place within the first 120 minutes indicating stronger silica-pluronic interactions compared to silica-protein attractions. Additionally the error associated with the bHb desorption in this case was large which led to the overlapping release profiles for example, 0.5 and 1 mg/ml F-38 concentrations showed similar trends for bHb desorption. This phenomenon can be attributed to the irregular size and shape of S_{LP} particles which resulted in variations in protein release from the silica surface.

Similarly, desorption isotherm of bHb from S_{LP} particles by different concentrations of pluronic F-68 is presented in Figure 7.2. The bHb desorbed by 0.5 mg/ml concentration of F-68 was nearly 58% whereas; desorption by 1, 5 and 10 mg/ml was between 75-80%.

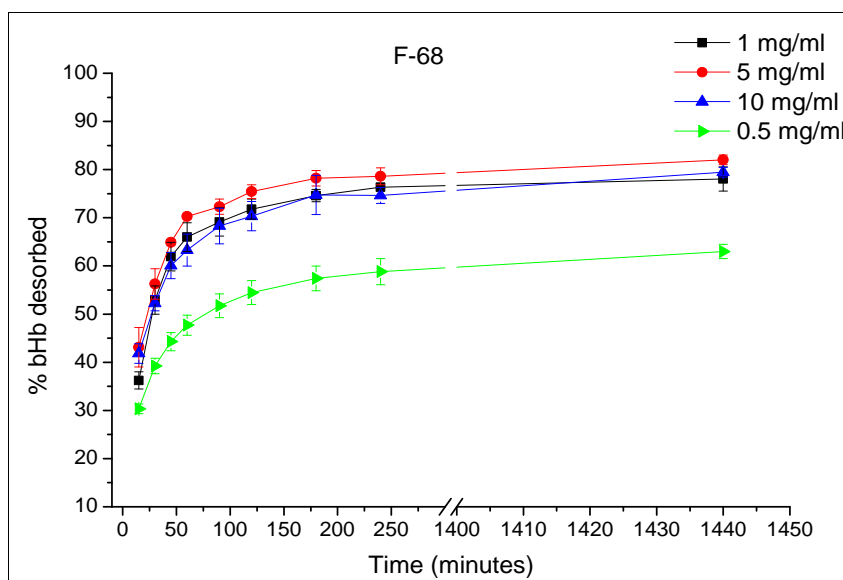


Figure 7.2: bHb desorption from S_{LP} particles using F-68 as a displacer

The total bHb release using pluronic F-68 was comparatively higher than F-38. This could be due to the presence of higher number of hydrophilic PEO (polyethylene) units in F-68 which are known to interact with silica surface by hydrogen bonding [10].

Similarly, desorption of bHb by F-77 at concentrations of 0.5, 1, 5 and 10 mg/ml is presented in Figure 7.3. Unlike F-38 and F-68, the desorption curve of bHb shifted upwards as the concentration of F-77 was increased. The minimum desorption of 67% was once again shown by 0.5 mg/ml pluronic concentration. Interestingly, the increase in concentration to 10 mg/ml resulted in slightly higher release of bHb which was not the case with previously studied pluronics. The total bHb release from S_{LP} using F-77 was 85% with majority of protein desorbing within the first 120 minutes.

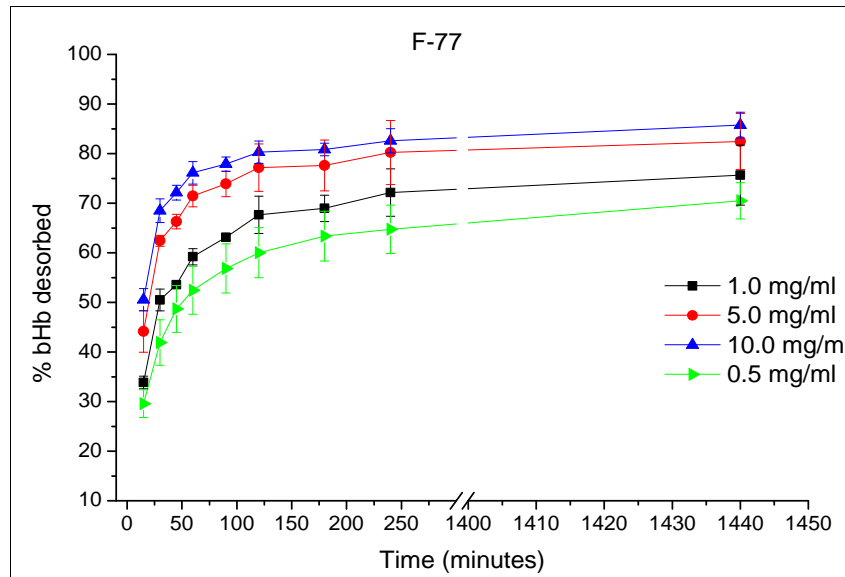


Figure 7.3: bHb desorption from S_{LP} particles using F-77 as a displacer

Desorption results of F-127 as a displacer are presented in Figure 7.4. Similar to other pluronics, the minimum release was obtained by 0.5 mg/ml, whereas, 1, 5 and 10 mg/ml concentrations showed desorption of 83%. It was also evident from the isotherms that higher F-127 concentrations (*i.e.* 5 and 10 mg/ml) had minimal effect on protein desorption. Interestingly, for F-127 the majority of protein desorption occurred in 60 minutes instead of 120 minutes as seen for other pluronics.

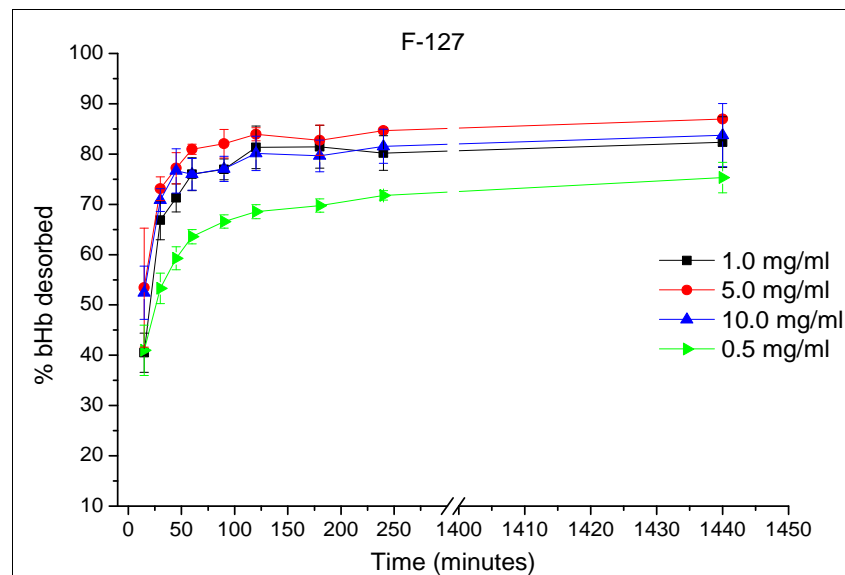


Figure 7.4: bHb desorption from S_{LP} particles using F-127 as a displacer

The pluronic F-108 induced desorption profiles of bHb are presented in Figure 7.5. Similar to F-127, the higher concentrations of displacer *viz.* 1, 5 and 10 mg/ml did not result in significantly different protein desorption isotherms. The total protein release with 0.5 mg/ml of F-108 was approximately 70%, whereas, higher concentrations provided 88% of bHb desorption.

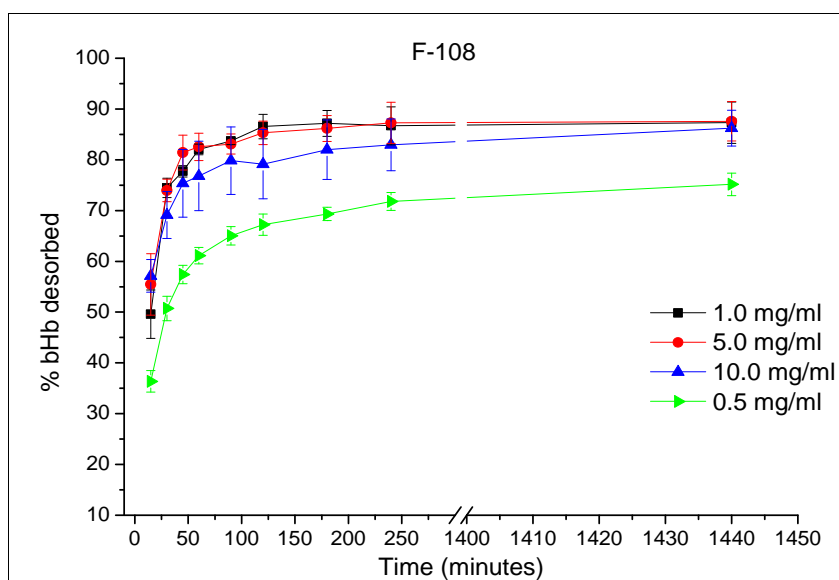


Figure 7.5: bHb desorption from S_{LP} particles using F-108 as a displacer

It must be noted that without the displacer desorption of bHb was minimal due to the strong protein-silica interactions. The use of pluronics as displacer was promising as all studied polymers resulted in higher release of protein. These results also suggested that higher molecular weight pluronics such as F-127 and F-108 were better displacers for the protein desorption from S_{LP} than their lower molecular weight counterparts *i.e.* F-38, F-68 and F-77.

7.3.2 Desorption from S_s particles

Similar to S_{LP} silica, desorption of bHb by different concentrations of pluronics was also studied for S_s particles. The profiles of pluronic F-38 induced desorption are presented in Figure 7.6. Unlike S_{LP} , pluronic F-38 concentrations of 1, 5 and 10 mg/ml showed similar desorption profiles which means that increase in pluronic concentration from 1 to 10 mg/ml had no or negligible effect on desorption of bHb from S_s particles.

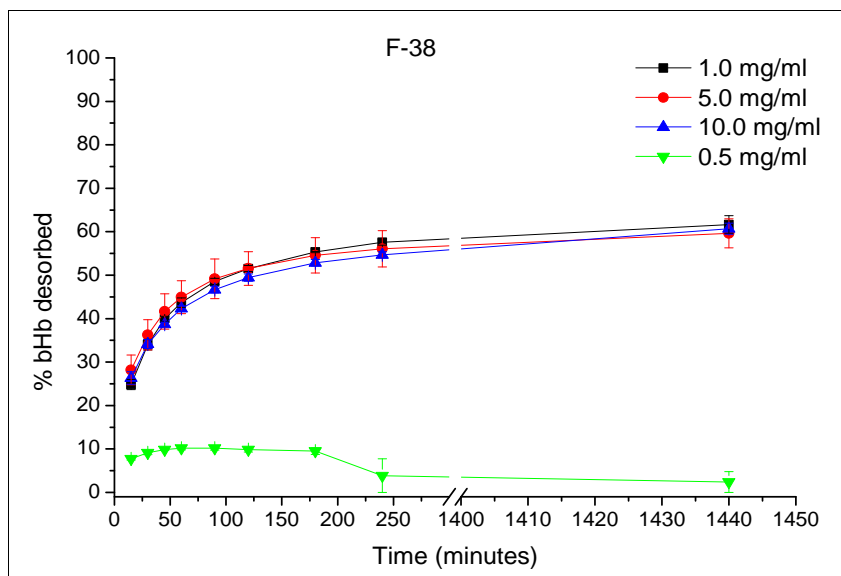


Figure 7.6: bHb desorption from S_s particles using F-38 as a displacer

The bHb release at 0.5 mg/ml F-38 concentration was only 10% which was very low in comparison to S_{LP} particles. It was also observed that protein concentration decreased in desorption media after 240 minutes presumably due to the readsorption because of prolonged stirring.

Desorption profile of bHb by pluronic F-68 from S_s is shown in Figure 7.7.

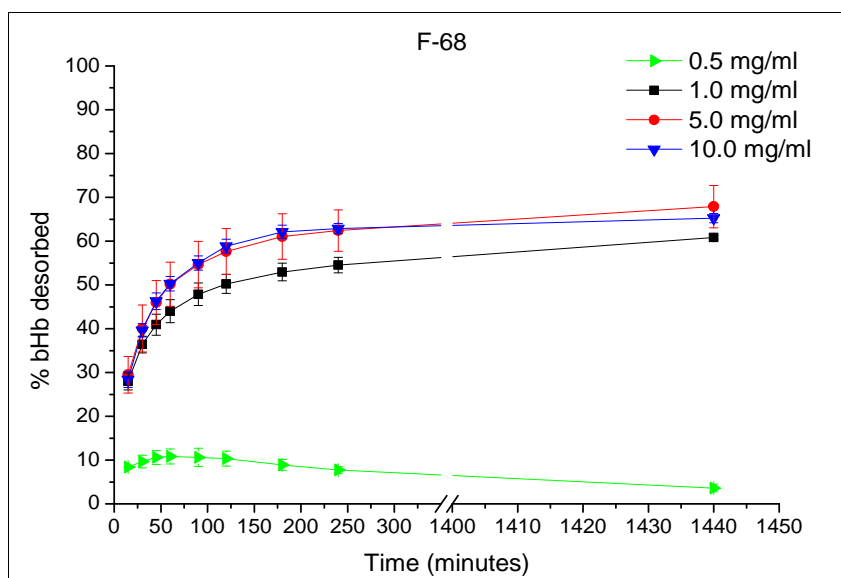


Figure 7.7: bHb desorption from S_s particles using F-68 as a displacer

Similar results were obtained for pluronic F-68 where 0.5 mg/ml concentration showed approximately 10% protein release with possible readsorption of bHb onto silica after 24 hours. The bHb desorption was highest (65%) for 5 and 10 mg/ml followed by 1 mg/ml concentration which showed a slightly lower release of 59%. Similar to S_{LP} silica, majority of protein was desorbed in first 120 minutes and only slight increase in bHb release was seen thereafter.

The desorption profile of bHb from S_s using pluronic F-77 as a displacer is presented in Figure 7.8. The bHb release profiles matched with F-68 where protein release by 5 and 10 mg/ml pluronic concentrations was similar (approximately 65%) and 1 mg/ml showed a slightly lower desorption.

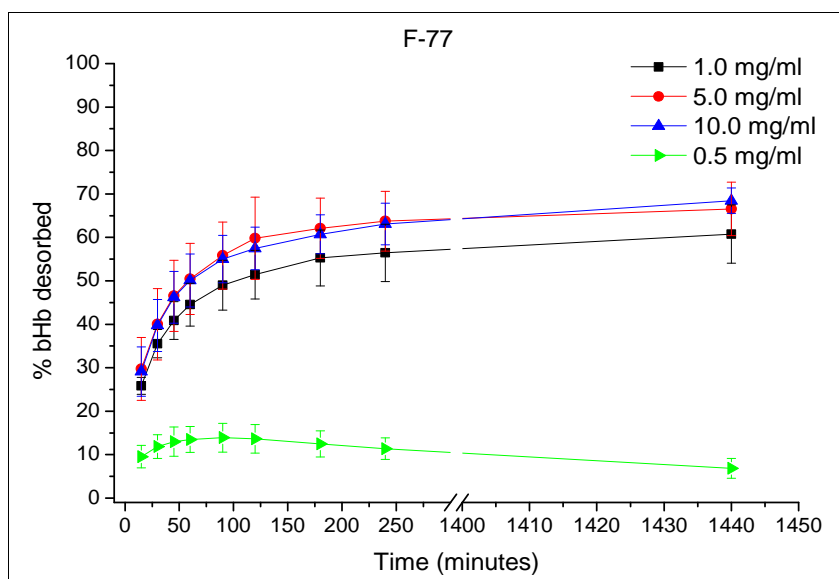


Figure 7.8: bHb desorption from S_s particles using F-77 as a displacer

Also, release at lower concentration (0.5 mg/ml) resulted in approximately 10% protein desorption with possible readsorption on silica surface during 24 hours.

Desorption of bHb by higher molecular weight pluronics *i.e.* F-127 and F-108 from the surface of S_s is presented in Figures 7.9 and 7.10. Desorption profiles of bHb for F-127 and F-108 were similar to each other but very different from previously discussed pluronics. The maximum protein desorption of 60% was obtained with 1 mg/ml concentrations of higher molecular weight pluronics. Protein desorption at 0.5 mg/ml of

F-127 was similar (< 10%) to the smaller pluronics but unlike previous studies increase in pluronics concentration above 1 mg/ml resulted in the decreased desorption.

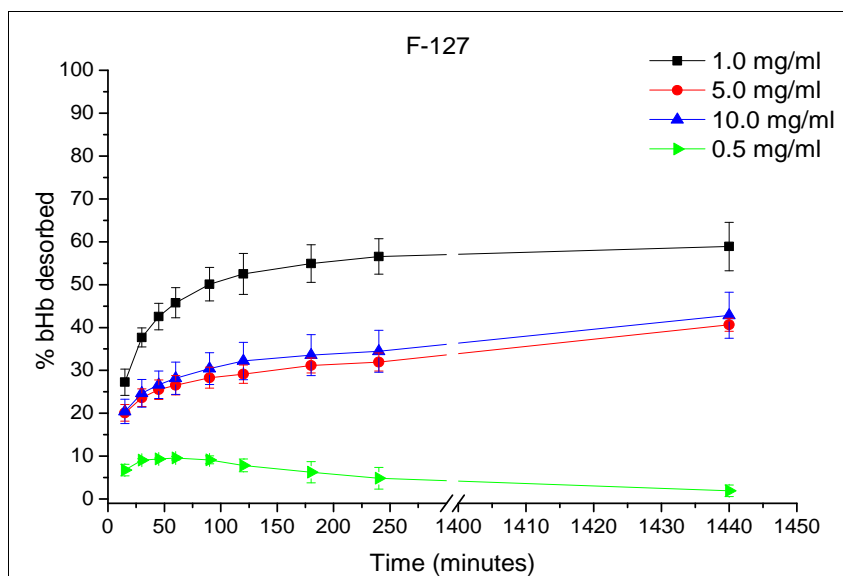


Figure 7.9: bHb desorption from S_s particles using F-127 as a displacer

The F-108 induced desorption profiles of bHb (Figure 7.10) were similar to F-127 except no re-adsorption of protein was observed in the case of 0.5 mg/ml concentration.

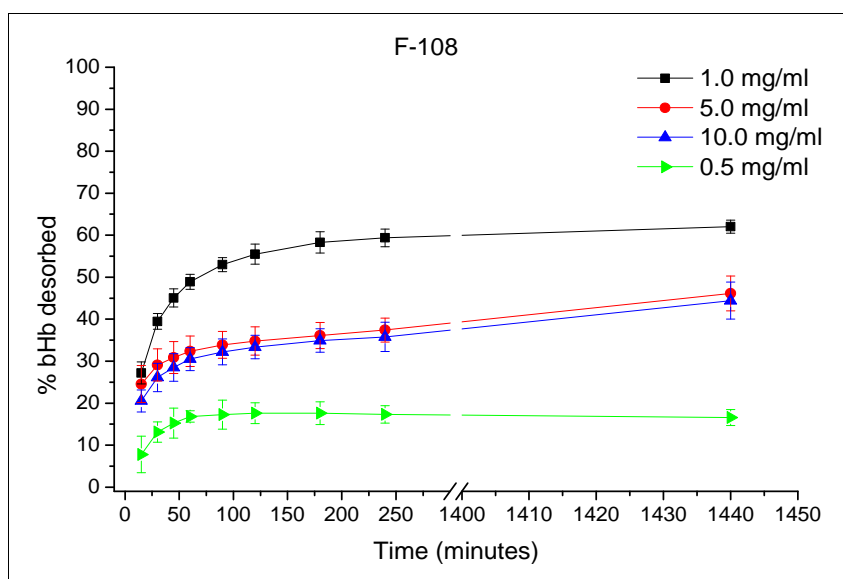


Figure 7.10: bHb desorption from S_s particles using F-108 as a displacer

7.3.3 Desorption from S_{FP} particles

Similar to S_{LP} and S_S, desorption of bHb from S_{FP} particles by pluronics was also studied and the results obtained are reported in this section. Desorption profiles of bHb with 10 mg/ml of pluronics was similar to 5 mg/ml in all previous cases hence, it was omitted from S_{FP} studies. However, another data set with 0.125 mg/ml was collected to understand the effect of reduced amount of displacer on bHb desorption.

The desorption profile of bHb by F-38 from S_{FP} particles in pH 6.8 phosphate buffer is shown in Figure 7.11.

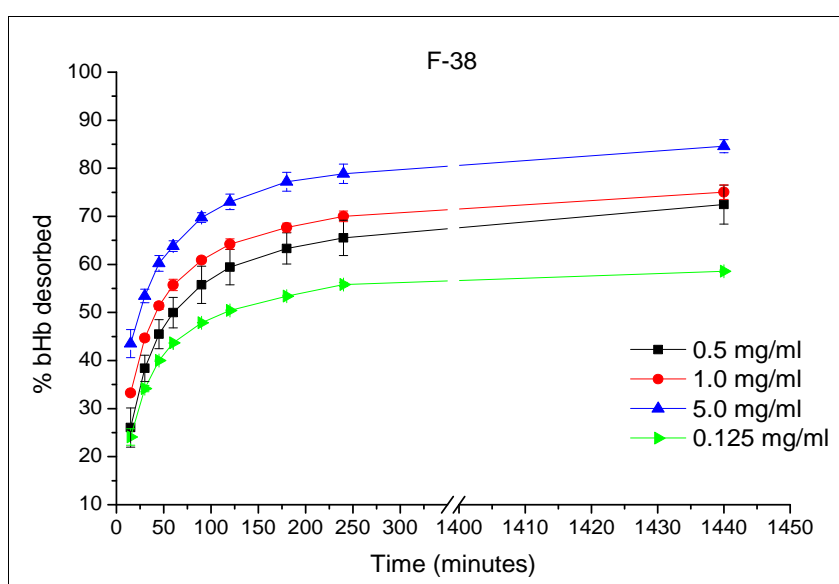


Figure 7.11: bHb desorption from S_{FP} particles using F-38 as a displacer

The protein desorption increased with the increase in pluronic concentration where 5 mg/ml showed the highest release of 85% and 0.125 mg/ml showed a release of only 56%. It was also observed that it took 240 minutes for maximum desorption to occur and no further release was detected thereafter.

Desorption profiles of bHb with F-68 are shown in Figure 7.12. The bHb released by 0.5, 1 and 5 mg/ml was between 75 to 90% whereas 0.125 mg/ml showed a release of 60%. Moreover, the bHb release using F-68 was also higher in comparison to F-38.

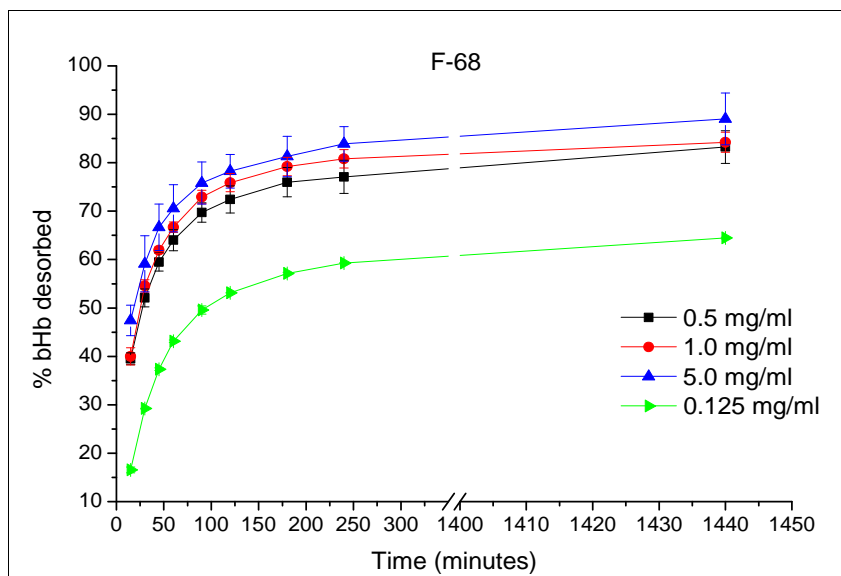


Figure 7.12: bHb desorption from S_{FP} particles using F-68 as a displacer

Desorption profiles of bHb by pluronic F-77 (Figure 7.13) followed the same trend as shown by F-68.

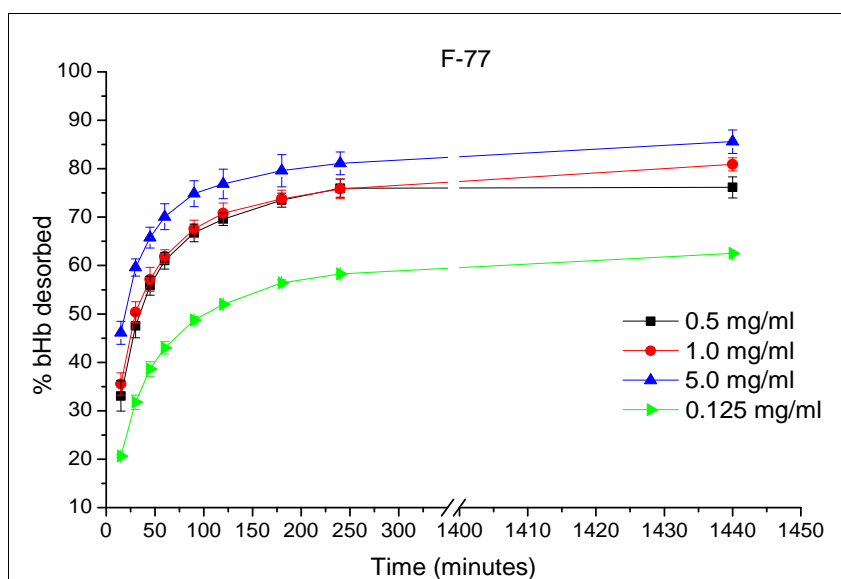


Figure 7.13: bHb desorption from S_{FP} particles using F-77 as a displacer

The release was lowest (62%) with the pluronic concentration of 0.125 mg/ml which increased with the increase in concentration of displacer. Desorption profiles of 0.5 and 1 mg/ml were similar and differed only after 240 minutes where a slight decrease in

protein concentration was observed at 0.5 mg/ml. The maximum protein release with pluronics F-77 as a displacer was 85%.

The bHb desorption using F-127 as a displacer is presented in Figure 7.14. The trend in desorption was akin to F-68 and F-77 with the lowest and least release with 0.125 mg/ml followed by increase in desorption at higher concentrations. However, the release was found to be quicker with F-127 than previously studied pluronics. It took only 60 to 90 minutes for maximum desorption in comparison to 120 min for F-68 and F-77. This indicated the relatively higher affinity of F-127 towards S_{FP} particles in comparison to previously discussed pluronics.

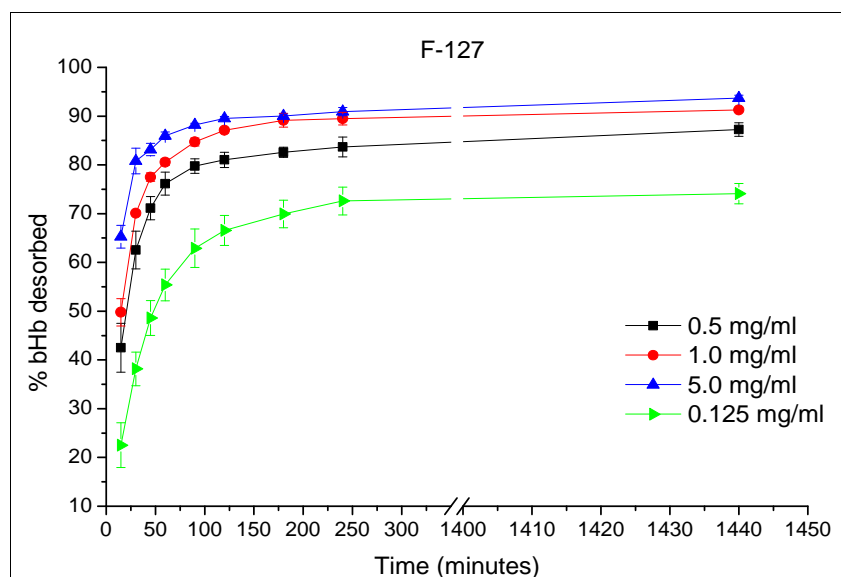


Figure 7.14: bHb desorption from S_{FP} particles using F-127 as a displacer

The desorption profiles of bHb by various concentrations of pluronic F-108 are shown in Figure 7.15. The concentrations of 0.5, 1 and 10 mg/ml exhibited no significant difference in the protein desorption with a final release of 80-85%. The pluronic concentration of 0.125 mg/ml resulted in the lowest percentage release of only 73%.

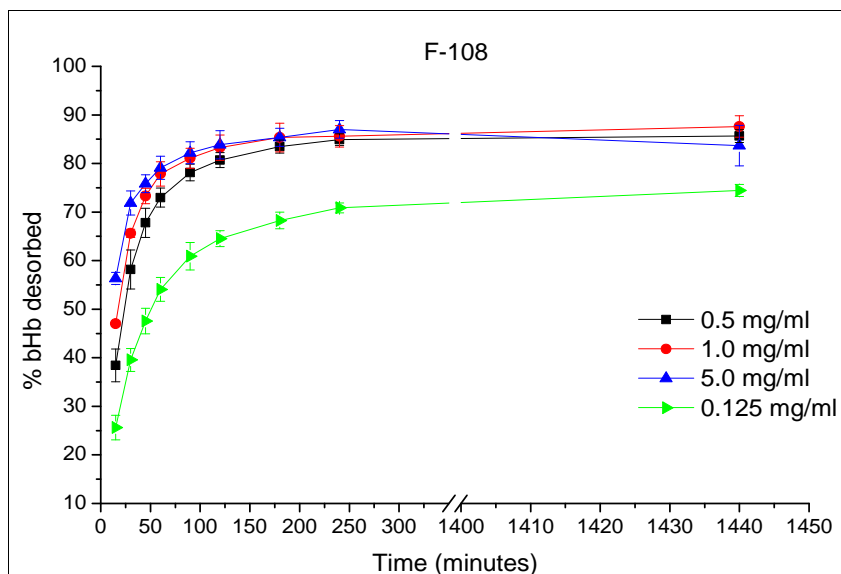


Figure 7.15: bHb desorption from S_{FP} particles using F-108 as a displacer

Similar to F-127, the desorption using F-108 was also faster and took only 60 to 90 minutes instead of 120 minutes in the case of F-36, F-68 and F-77. Figures 7.16 to 7.18 presents desorption of bHb from different silica particles by 1 mg/ml of various pluronics. It can be observed from Figures 7.16 and 7.17 that the protein desorption increased with increase in number of EO (ethylene oxide) units in pluronics in the case of S_{LP} and S_{FP} silica particles.

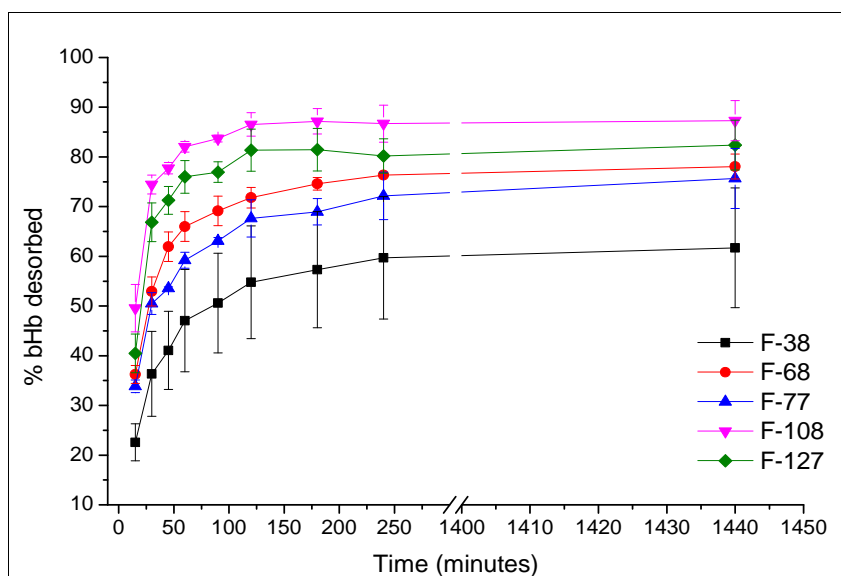


Figure 7.16: bHb desorption from S_{LP} particles by 1 mg/ml of pluronics

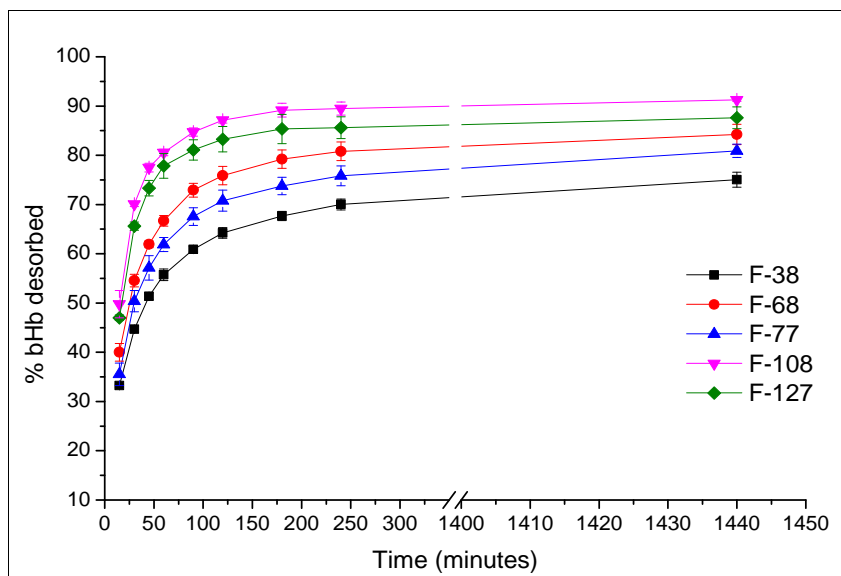


Figure 7.17: bHb desorption from S_{FP} particles by 1 mg/ml of pluronics

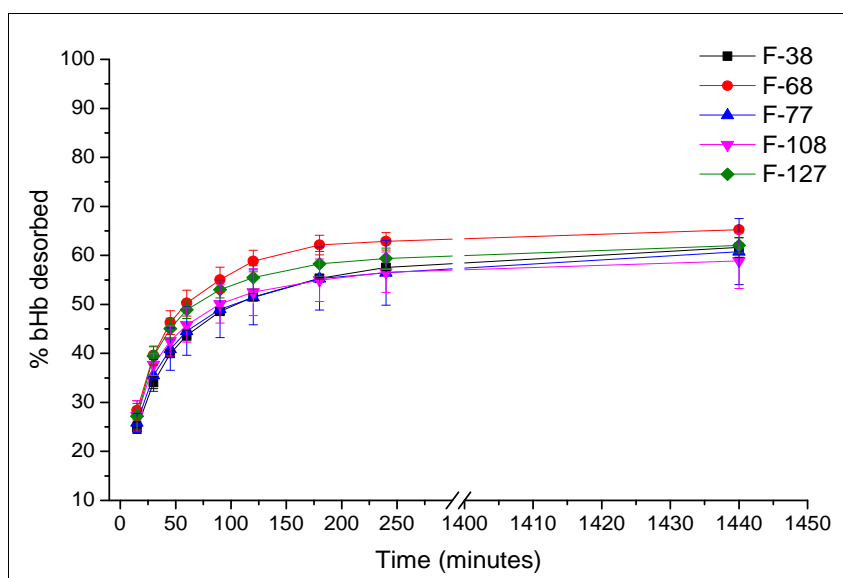


Figure 7.18: bHb desorption from S_s particles by 1 mg/ml of pluronics

However, no such trend in desorption with respect to EO content of pluronics was observed for S_s particles.

7.3.4 Effect of pluronics on bHb conformation

The effect of different concentrations *viz.* 1, 5, 10 and 20 mg/ml of pluronics on the conformation of bHb in pH 6.8 phosphate buffer was studied by CD and UV

spectroscopy. The effect of pluronic F-127 on protein conformation is presented in Figures 7.19 and 7.20 as an example. Results for other pluronics were omitted to avoid repetition as same results were obtained for all studied displacers.

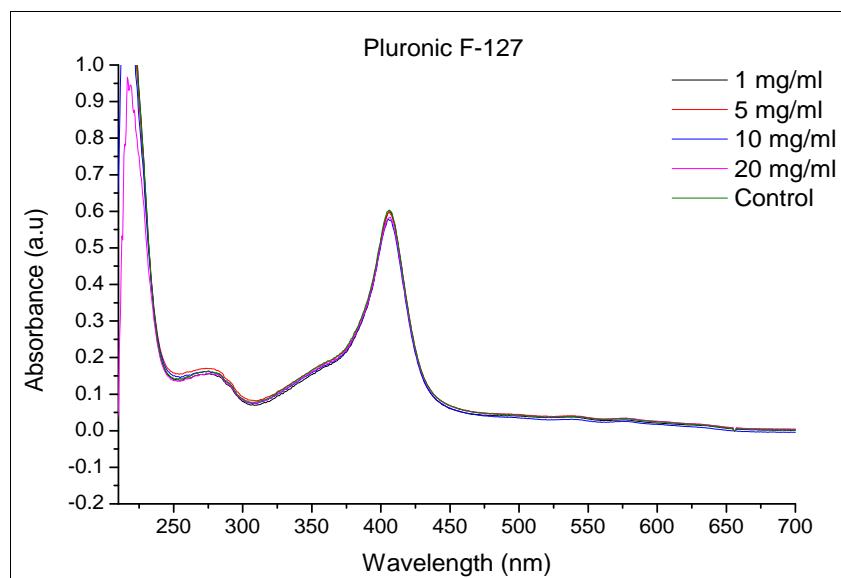


Figure 7.19: UV spectra of bHb with various concentrations of pluronic F-127

The UV spectrum of bHb remained unchanged with the increase in F-127 content which shows that the addition of pluronic to the protein solution had no or minimal effect on the conformation of bHb at the studied concentrations.

Figure 7.20 shows the percentage content of five different secondary structures present in bHb at various concentrations of F-127. The protein solution in pH 6.8 phosphate buffer without surfactant was used as a control and compared with pluronic containing bHb solutions to ascertain any changes in its conformation. In general, the protein conformation remained the same and did not change with the increase in pluronic concentration. An increase of approximately 2% in helix content was observed at higher surfactant concentrations of 10 and 20 mg/ml. This increase was not significant and did not suggest any major interactions between protein and pluronics.

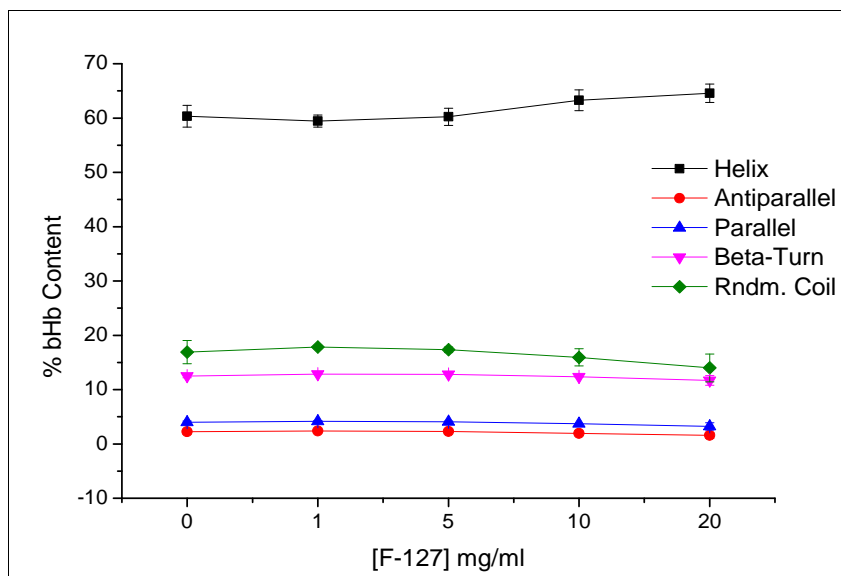


Figure 7.20: Effect of F-127 concentration on bHb secondary structures

It could be concluded from the UV and CD results presented here that pluronics studied in this work showed no or minimal interaction with bHb.

7.4 Discussion

As mentioned in section 7.1, protein adsorption on hydrophilic surfaces can be reversible or non-reversible depending upon the type of protein and adsorbent. It must be noted that during adsorption, the protein molecule attaches to a surface by a large number of segments and potentially rearranges its structure to optimise the interaction with the adsorbent. Therefore, desorption process requires a higher free energy to overcome the binding forces between the protein and adsorbent surface [3]. This free energy can be provided to the system in many ways *e.g.* by change in pH, ionic strength, use of a displacer *etc.* Surfactants are commonly used displacers to desorb strongly adsorbed proteins where factors such as type of surfactant, protein and adsorbent play an important role in desorption. Wahlgren and Arnebrant have suggested two mechanisms of protein desorption by surfactant [11].

- a) Desorption by replacement of protein with surfactant and
- b) Desorption by surfactant assisted solubilisation of protein.

Desorption by replacement mechanism is more likely to occur due to strong surfactant-adsorbent and weak surfactant-protein interactions [9]. Non-ionic surfactants (pluronics) used in the present study achieve higher desorption because of their weak interactions with proteins and higher interactions with hydrophilic silica [12]. The highest bHb desorption was obtained from S_{FP} followed by S_{LP} and S_S in the present study. This confirmed that the protein-silica interactions were strongest in the case of S_S and weakest in S_{FP}. It must be noted that these findings were contrary to results obtained from adsorption studies where it was observed that protein had highest affinity towards S_{FP} particles and least affinity to S_S. This was accredited to the smaller surface area available for protein adsorption due to the presence of pores which had smaller openings than the protein diameter. However, bHb could potentially have undergone structural changes after adsorption on S_S which can lead to stronger protein-silica interactions. This is supported by the results where only 60% desorption was achieved in comparison with 85-95% from S_{LP} and S_{FP} particles. Additionally, the adsorption concentration also played a role in the extent of protein desorption by the surfactant. The concentrations used for adsorption on S_S, S_{LP} and S_{FP} were 1, 2 and 8 mg/ml respectively which were selected from protein adsorption studies as discussed in chapter 6. It is known that proteins adsorbed from dilute solutions attain a more spread out conformation on a solid surface and hence require a higher surfactant concentration for desorption [13]. This supported the results where low desorption was observed from S_S even with higher concentrations of pluronics (*i.e.* 5 and 10 mg/ml) whereas, this was not the case with other two silica particles. Interestingly, as the pluronic concentration was increased the amount of protein desorption from S_S either remained same or decreased. The decrease was found to be dependent on the molecular weight of the pluronic. The high concentrations of large molecular weight pluronics *i.e.* F-127 and F-108 resulted in decreased protein desorption which could be attributed to stronger polymer-polymer interactions than polymer-silica interactions.

In general, desorption of bHb increased with the increase in pluronic concentration for S_{LP} and S_{FP}. Moreover, the amount of protein desorbed was also dependent on the EO content of pluronic *i.e.* higher desorption by the surfactant containing larger numbers of EO units in the molecule. This can be explained by the fact that pluronics adsorb on the

hydrophilic silica particles by hydrogen bond formation between their EO subunits and silanol groups on the silica surface [12]. Therefore, pluronics with more EO subunits are expected to displace larger amounts of adsorbed protein from the silica surface. Figures 7.16 to 7.18 presents desorption of bHb from different silica particles by 1 mg/ml concentration of various pluronics. It could be seen that the total amount of protein released from S_{LP} and S_{FP} increased with the increase in EO units *i.e.* F-108 > F-127 > F-68 > F-77 > F-38. Therefore, it can be suggested that as the number of EO units increased they occupied larger area on the silica surface and replaced previously adsorbed bHb molecules. This also implies stronger pluronic-silica interactions than bHb-silica without which protein desorption cannot be achieved. However, higher concentrations of pluronics (*i.e.* 5 and 10 mg/ml) for S_{LP} and (1 and 5 mg/ml) for S_{FP} resulted in similar desorption profiles. In other words, no substantial increase in protein release was observed by increasing the pluronics concentrations from 5 to 10 mg/ml in the case of S_{LP} and from 1 to 5 mg/ml for S_{FP} . This can be accredited to the saturation of silica surface with pluronic molecules and hence further increase in surfactant concentration led to surface micellisation and had no or minimal effect on desorption [10], [12].

Interestingly, results obtained for S_S did not follow the same trend. The desorption profiles of bHb in the presence of 1 mg/ml pluronic is presented in Figure 7.18. In contrast to S_{LP} and S_{FP} , no direct correlation between the number of EO units and extent of protein desorbed could be drawn for S_S particles. The trend and final amount of protein released from S_S was similar (60 ± 5 %) for all studied pluronics. This could be related to stronger protein-silica interactions in the case of S_S in comparison to other two silica particles.

After studying above results, it could be concluded that desorption of protein is primarily caused by the displacement of bHb by pluronic molecules. The pluronic adsorption on a solid surface has been studied extensively where these were thought to adsorb on hydrophilic surfaces in a pancake like formation (Figure 7.21) due to the higher affinity of EO units towards silica [14].



Figure 7.21: Pluronic adsorbed at hydrophilic surface in a pancake formation

However, recent findings propose that this is probably not true and critical surface micellisation is more likely to attribute to the adsorption of pluronic on a solid surface. It is known that pluronics adsorb on protonated silica and form surface micelles at/above certain concentrations. The surface micellisation occurs at critical surface micelle concentration (CSMC) which is much lower than the actual critical micelle concentration (CMC) of pluronics [10]. The schematic diagram presented in Figure 7.22 shows how surface micellisation of pluronics could promote protein displacement from the silica surface in the present study.

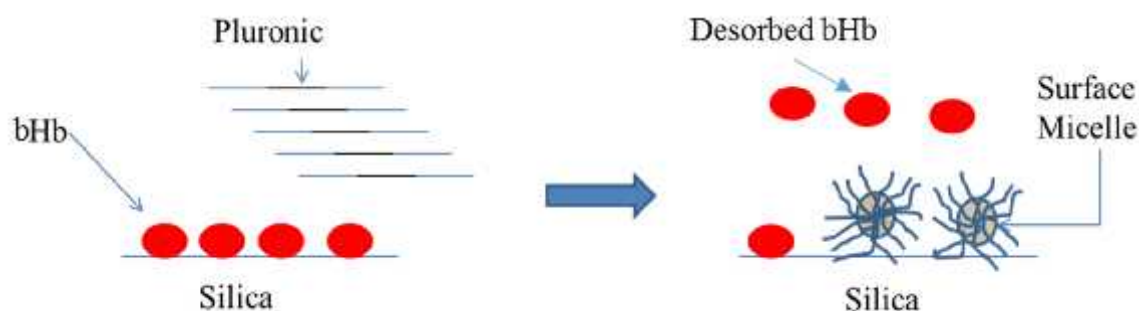


Figure 7.22: Schematics of protein desorption by pluronics

The CMC and CSMC of F-127 at 22 °C are reported in literature as approximately 20 and 0.2 mg/ml respectively [10]. Therefore, in the case of F-127 all the concentrations used were below its CMC and above CSMC. Hence, F-127 adsorption and surface micellisation can be attributed to the subsequent displacement /desorption of protein molecules from silica surface. This hypothesis can also be extended to other surfactants used in this work but further studies are required to determine the CSMC of these pluronics. It can be inferred from the present study that the interactions between pluronics and silica surface were stronger than the protein-silica interactions. However,

the interactions between pluronics and bHb are of equal importance as it may alter the protein's conformation [15], [16]. Therefore, effect of different concentrations of pluronics on the conformation of bHb was also studied and discussed in the following section.

7.5 Conclusions

The role of various pluronics on desorption was studied as the adsorption of bHb on silica particles was irreversible. The pluronics namely; F-38, F-68, F-77, F-127 and F-108 were studied to act as a displacer for SCDDS. The concentrations used were 0.5, 1, 5 and 10 mg/ml for S_{LP} and S_S . However, highest pluronic concentration was omitted for S_{FP} particles and a concentration of 0.125 mg/ml was added. In general, it was observed that as the concentration of pluronic was increased the amount of bHb desorbed from silica surface also increased. This could be attributed to the higher number of pluronic molecules displacing the protein from the surface. Additionally, in the case of S_{LP} and S_{FP} it was observed that amount of bHb desorbed was different for each pluronic which increased with the increase in number of EO units. However, all studied pluronics desorbed almost similar amount of protein from the silica surface in the case of S_S indicating that there was no effect of EO units on desorption. It was also observed that the minimum pluronic concentration that can be used to desorb the maximum protein from all three silica was 1 mg/ml.

The effect of pluronics on conformation of bHb was also studied by UV and CD spectroscopy and it was concluded that pluronics concentration used in this study had no effect on protein's conformation.

References

- [1] C. M. Alves, R. L. Reis, and J. A. Hunt, 'The dynamics, kinetics and reversibility of protein adsorption onto the surface of biodegradable materials', *Soft Matter*, vol. 6, no. 17, p. 4135, 2010.
- [2] B. K. Lok, Y. Cheng, and C. R. Robertson, 'Protein adsorption on crosslinked polydimethylsiloxane using total internal reflection fluorescence', *J. Colloid Interface Sci.*, vol. 91, no. 1, pp. 104–116, 1983.
- [3] W. Norde, F. MacRitchie, G. Nowicka, and J. Lyklema, 'Protein adsorption at solid-liquid interfaces: Reversibility and conformation aspects', *J. Colloid Interface Sci.*, vol. 112, no. 2, pp. 447–456, 1986.
- [4] B. M. C. Chan and J. L. Brash, 'Adsorption of fibrinogen on glass: reversibility aspects', *J. Colloid Interface Sci.*, vol. 82, no. 1, pp. 217–225, 1981.
- [5] R. J. Rapoza and T. A. Horbett, 'The effects of concentration and adsorption time on the elutability of adsorbed proteins in surfactant solutions of varying structures and concentrations', *J. Colloid Interface Sci.*, vol. 136, no. 2, pp. 480–493, 1990.
- [6] J. L. Bohnert and T. A. Horbett, 'Changes in adsorbed fibrinogen and albumin interactions with polymers indicated by decreases in detergent elutability', *J. Colloid Interface Sci.*, vol. 111, no. 2, pp. 363–377, 1986.
- [7] H. Elwing, A. Askendal, and I. Lundström, 'Desorption of fibrinogen and - globulin from solid surfaces induced by a nonionic detergent', *J. Colloid Interface Sci.*, vol. 128, no. 1, pp. 296–300, 1989.
- [8] D. Sarkar and D. K. Chattoraj, 'Kinetics of Desorption of Proteins from the Surface of Protein-Coated Alumina by Various Desorbing Reagents', *J. Colloid Interface Sci.*, vol. 178, no. 2, pp. 606–613, 1996.

- [9] M. Wahlgren and T. Arnebrant, 'Removal of lysozyme from methylated silicon oxide surfaces by a non-ionic surfactant, pentaethylene glycol mono n-dodecyl ether (C12E5)', *Colloids Surfaces B Biointerfaces*, vol. 6, no. 2, pp. 63–69, 1996.
- [10] B. Sarkar, V. Venugopal, M. Tsianou, and P. Alexandridis, 'Adsorption of Pluronic block copolymers on silica nanoparticles', *Colloids Surfaces A Physicochem. Eng. Asp.*, vol. 422, pp. 155–164, 2013.
- [11] M. Wahlgren, 'Protein adsorption to solid surfaces', *Trends Biotechnol.*, vol. 9, no. 1, pp. 201–208, 1991.
- [12] M. Malmsten, P. Linse, and T. Cosgrove, 'Adsorption of PEO-PPO-PEO block copolymers at silica', *Macromolecules*, vol. 25, no. 9, pp. 2474–2481, 1992.
- [13] S. Welin-Klintström, A. Askendal, and H. Elwing, 'Surfactant and Protein Interactions on Wettability Gradient Surfaces', *J. Colloid Interface Sci.*, vol. 158, no. 1, pp. 188–194, 1993.
- [14] C. G. P. H. Schroen, M. A. C. Stuart, K. V. Maarschalk, A. Vanderpadt, and K. Vantriet, 'Influence of Preadsorbed Block-Copolymers on Protein Adsorption: Surface Properties, Layer Thickness, and Surface Coverage', *Langmuir*, vol. 11, no. 8, pp. 3068–3074, 1995.
- [15] E. Y. Chi, S. Krishnan, T. W. Randolph, and J. F. Carpenter, 'Physical stability of proteins in aqueous solution: mechanism and driving forces in nonnative protein aggregation', *Pharm. Res.*, vol. 20, no. 9, pp. 1325–1336, 2003.
- [16] D. Otzen, 'Protein-surfactant interactions: a tale of many states.', *Biochim. Biophys. Acta*, vol. 1814, no. 5, pp. 562–91, 2011.

CHAPTER 8

Coating and release studies

8.1 Introduction

The process by which tiny droplets or particles of liquid or solid are coated with a material is generally termed as microencapsulation [1]. The material inside a microcapsule is known as the core, internal phase, active, payload, nucleus or fill, whereas coating material is referred as a wall, shell or membrane. Microencapsulation of a core material can provide sustained or prolonged drug release, taste masking and improved stability amongst various other desirable properties [2]. Encapsulation is achieved by a wide range of processes such as spray-drying, solvent evaporation, extrusion, coacervation etc. However, these processes require the use of organic solvents and subject the drug to high stress and/or temperature. Therefore, processing of certain materials which are sensitive to these conditions *e.g.* proteins and peptides can be difficult using conventional techniques.

Supercritical fluid technology (SCFT) can provide a solution to the problems associated with conventional encapsulation methods. The advantages of SCFT include; avoiding the use of organic solvent, operation at low temperatures and the ability to work in oxygen free environment to prevent thermal, oxidative and solvent induced degradation of a material [3]. SCCO₂ is the most commonly employed solvent for the particle engineering and encapsulation purposes as it is chemically inert, easily available, environmentally benign and easy to remove in comparison to many organic solvents [4].

8.2 Coating of silica particles with FAs

The protein adsorbed silica particles (bHb-Si) were coated with saturated FAs by SCF processing and a conventional solvent evaporation method. FAs used were LA, MA, PA and SA. Pentane was used as an organic solvent in the evaporation method. The two coating methods were then compared by studying the protein release in pH 6.8 phosphate buffer (USP) containing a surfactant.

8.2.1 Materials and methods

The experimental procedures for coating silica particles by SCF processing and solvent evaporation method are discussed in this section.

8.2.1.1 Materials

Refer to Table 3.1

8.2.1.2 Coating of silica particles by SCF processing

The bHb immobilised silica particles (S_{LP} , S_S , and S_{FP}) were coated by SCF processing with LA, MA, PA and SA using temperature and pressure conditions determined and discussed in chapter 4. The ratios of silica to FAs (w/w) used were 1:0.5 and 1:1. These ratios were selected after estimating the quantity of FA required to cover the surface of 1 g of silica. The calculations showed that surface area of 300 m^2 on silica particles will require 0.2 to 2.3 g of FAs to form a single layer. The upper and lower limit relies upon the orientation of the FA molecule on the silica surface. For example, if LA molecules interact with the silica surface in head-on position then the amount needed to form a single layer on the silica with a surface area of 300 m^2 is 2.3 g, whereas in the case of side-on interaction the required amount is 0.2 g. The supercritical fluid instrument used for coating experiments has been detailed in section 2.9 and the schematic diagram of coating procedure is presented in Figure 8.1.

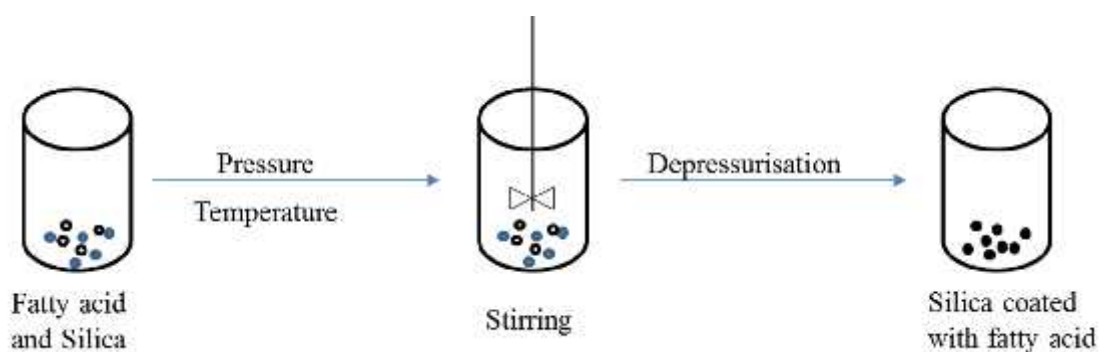


Figure 8.1: Schematic diagram of coating by SCF processing

Required weights of silica and FA to achieve desired ratios were introduced into the reaction vessel. The vessel was then closed and liquid CO_2 was pumped to a

predetermined pressure value. The temperature of the system was increased to 27-60 °C depending upon the FA used. The system was left stirring for 15 minutes after equilibration before depressurisation at a rate of 8 bar/minute. The processing parameters used to coat bHb adsorbed silica particles are summarised in Table 8.1.

Fatty acid	Pressure (bar)	Temperature (°C)	Time (min)
LA	70	27	15
MA	100	43	15
PA	150	53	15
SA	150	60	15

Table 8.1: Parameters for silica coating by SCF processing

The above experiment was performed on all 3 silica particles at two different FA: silica ratios.

8.2.1.3 Coating of silica particles by solvent evaporation

The silica particles were also coated with FAs by solvent evaporation method. The required amount of FA was dissolved in approximately 15-20 ml of pentane and the silica particles were added to it. The beaker was then shaken in a fume hood for 15 minutes at room temperature in order to evaporate the solvent. FA coated silica particles were obtained after the evaporation of pentane. SA was excluded from these experiments due to its extremely low solubility in pentane [5].

8.2.1.4 Protein release from coated particles

The aim of this study was to identify the most suitable core and compare both coating methods *viz.* SCF coating and solvent evaporation for the formulation of SCDDS. The release studies were conducted in duplicates in pH 6.8 phosphate buffer (USP) with 1 mg/ml pluronic F-127 at the room temperature.

Phosphate buffer was prepared as described in section 3.2.14. 400 mg of FA coated silica particles were added in 100 ml of phosphate buffer containing F-127 and stirred at 250 rpm. 1 ml of supernatant was taken after 15, 60, 120, 240 and 1440 minutes and

filtered through 0.45 μm syringe filter for UV absorbance. The volume of the dissolution media was kept constant for the duration of the experiment.

8.2.1.5 *In-vitro* release studies at pH 1.2 and 6.8

The conventional USP method for extended release formulations was difficult to use for the SCDDS because of the sensitivity of protein and small particulate nature of the formulation. Hence, the method was slightly modified and two containers were used for separate pH conditions instead of one. The equal amount of formulation was taken in two beakers which also contained 100 mg F-127 as displacer. Beaker A had 100 ml of 0.1 M HCl (pH 1.2) to represent gastric environment and beaker B had 100 ml of phosphate buffer (pH 6.8) to simulate intestinal conditions. The contents of beaker A were stirred at 100 rpm for 2 hours before switching to beaker B. The readings were recorded after 15, 60 and 120 minutes for beaker A and after 135, 180, 240, 360 and 1440 minutes for beaker B. The experiments were performed in duplicates and at room temperature.

8.3 Results

Following sections contain release profiles of SCDDS prepared using different cores, shell materials and coating methods to understand their suitability as a delivery system.

8.3.1 *In-vitro* release studies at pH 6.8

This section discusses bHb release from SCDDS in pH 6.8 phosphate buffer containing 1 mg/ml pluronic F-127. The phosphate buffer in this study was used as simulated intestinal fluid (USP) without pancreatin and the role of F-127 was to act as a displacer for bHb from the silica surface. The protein conformation after the release from SCDDS was also determined by CD spectroscopy. Legends/nomenclature used in this study includes information on type of silica followed by FA name/ratio and processing technique. For example, $S_{LP}:LA_{0.5}$ -PEN refers to SCDDS prepared with S_{LP} silica where coating was performed using LA in a ratio of 1:0.5 ($S_{LP}:LA$) by solvent evaporation method (PEN).

8.3.1.1 Release studies from S_{LP} based SCDDS

The release profiles of protein from LA coated bHb-S_{LP} particles are presented in Figure 8.2. The highest release of 80% was observed from uncoated particles and used as control for protein release experiments.

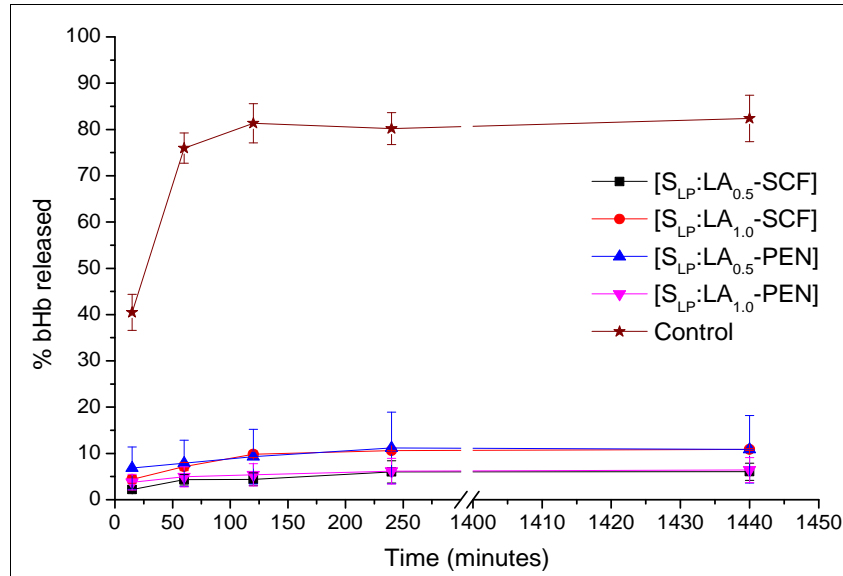
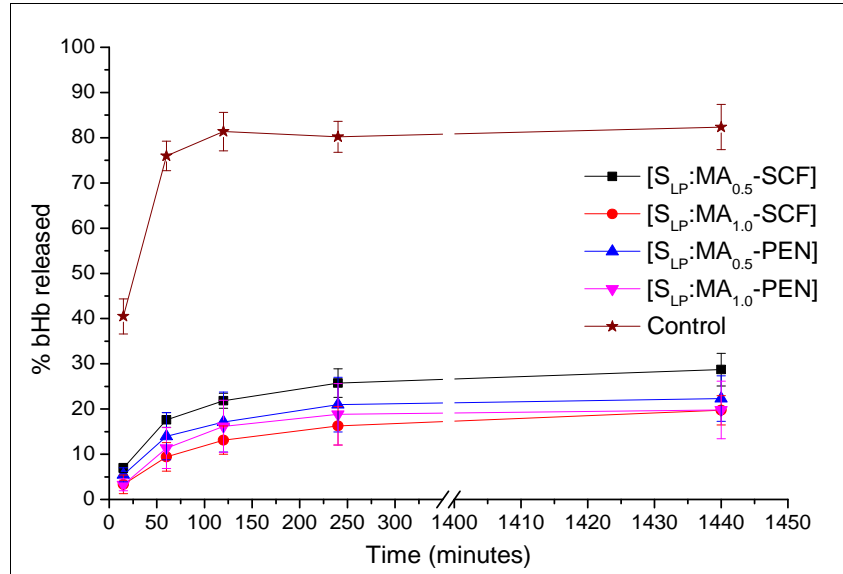


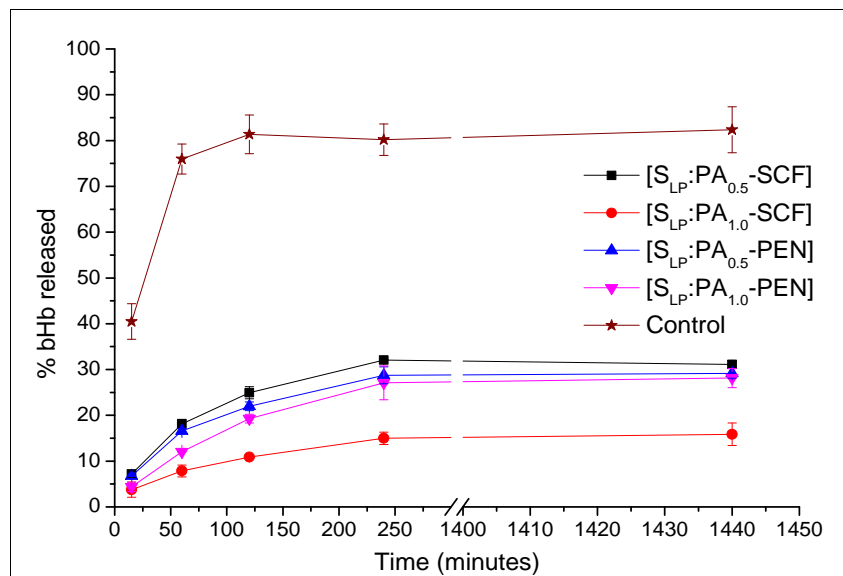
Figure 8.2: bHb release from S_{LP} based SCDDS with LA coating

All LA coated bHb-S_{LP} formulations showed a release of less than 20% which was independent of FA/silica ratio and the method of coating. This low release indicated the formation of multi-layered LA coating which did not dissolve and/or erode completely at the studied conditions and in turn prevented the protein release. The possible release mechanism of bHb from SCDDS is discussed in detail later in this chapter.

The release profiles of bHb from MA based SCDDS are presented in Figure 8.3. The bHb release (30%) from MA based formulations was comparatively higher to the LA coated SCDDS. The highest release of 30% was shown by S_{LP}:MA_{0.5}-SCF followed by S_{LP}:MA_{0.5}-PEN with a 23% total protein release. The release profiles of 1:1 formulations were similar for both coating methods with a total protein release of 19%.

Figure 8.3: bHb release from S_{LP} based SCDDS with MA coating

The release profiles of the protein from S_{LP} based SCDDS coated with PA are presented in Figure 8.4.

Figure 8.4: bHb release from S_{LP} based SCDDS with PA coating

The release from these formulations (~30%) was similar to MA based SCDDS but higher than LA coated bHb-S_{LP} (20%). Interestingly, S_{LP}:PA_{0.5}-PEN and S_{LP}:PA_{1.0}-PEN formulations prepared by solvent evaporation showed similar release profiles with a

final bHb release of nearly 25%. This could be attributed to the partial coating of particles or possibly due to the limited solubility of PA in pentane. Whereas, clear difference was observed in the case of PA coated bHb- S_{LP} particles by SCF processing. The total bHb released after 24 hours from $S_{LP}:PA_{0.5}$ -SCF was 30% which was twice in comparison to 15% desorption achieved from $S_{LP}:PA_{1.0}$ -SCF.

Similarly, the release profiles of bHb from SA coated S_{LP} based SCDDS are presented in Figure 8.5. The coating by solvent evaporation was omitted for SA due to its limited solubility in pentane.

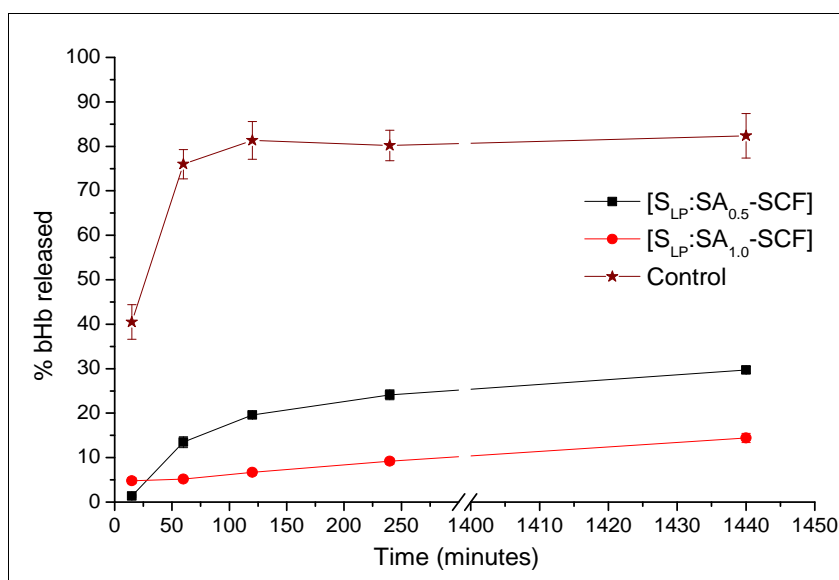


Figure 8.5: bHb release from S_{LP} based SCDDS with SA coating

Similar to PA and MA based formulations, bHb release from $S_{LP}:SA_{0.5}$ -SCF was nearly 30% and almost twice in comparison to 15% from $S_{LP}:SA_{1.0}$ -SCF.

8.3.1.2 Release studies from S_S based SCDDS

Similar to S_{LP} , the release studies were also performed on FA coated S_S formulations and the results obtained are discussed in this section.

The release profiles of protein from LA coated bHb- S_S particles are presented in Figure 8.6.

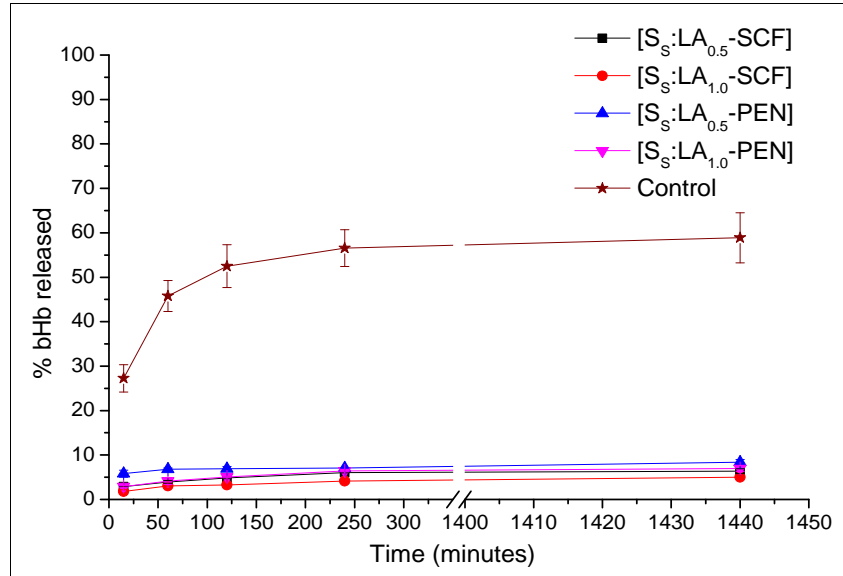


Figure 8.6: bHb release from S_s based SCDDS with LA coating

The uncoated bHb-S_s (control) showed a release of nearly 60% which was almost 20% lower than S_{LP} and could be due to the higher affinity of protein towards these particles. The total release of < 10% from all LA coated formulations could also be attributed to higher protein-S_s interactions along with the multi-layered coating.

The release profiles of bHb from MA based formulations are presented in Figure 8.7.

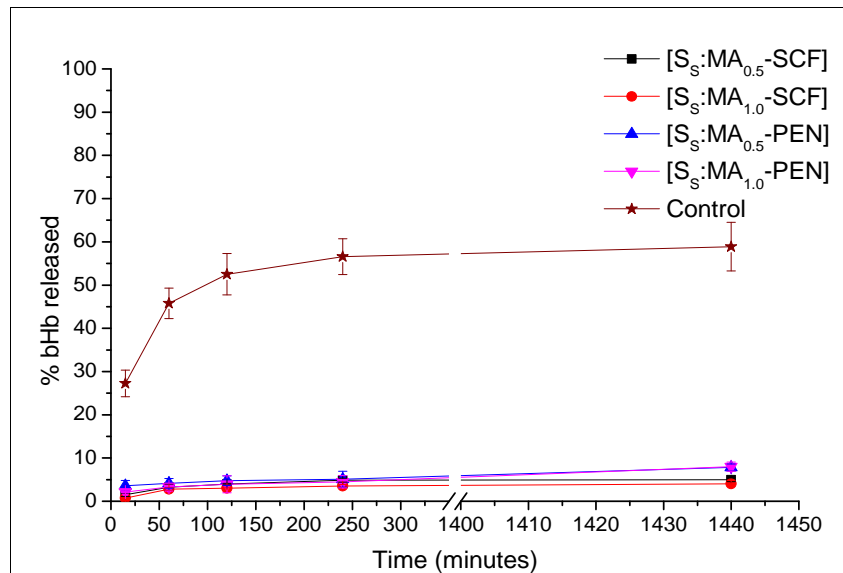


Figure 8.7: bHb release from S_s based SCDDS with MA coating

The release of bHb (< 10%) was also minimal from these formulations similar to SCDDS prepared by LA coating.

The maximum release of 24% was obtained from $S_S:PA_{0.5}$ -PEN amongst all PA based SCDDS (Figure 8.8) whereas, rest of the PA coated formulations released only 5-16% of total bHb. The release from the PA coated formulations prepared by solvent evaporation was slightly higher than LA and MA based SCDDS. This can be attributed to the partial or non-uniform coating of these particles due to comparatively low solubility of PA in pentane.

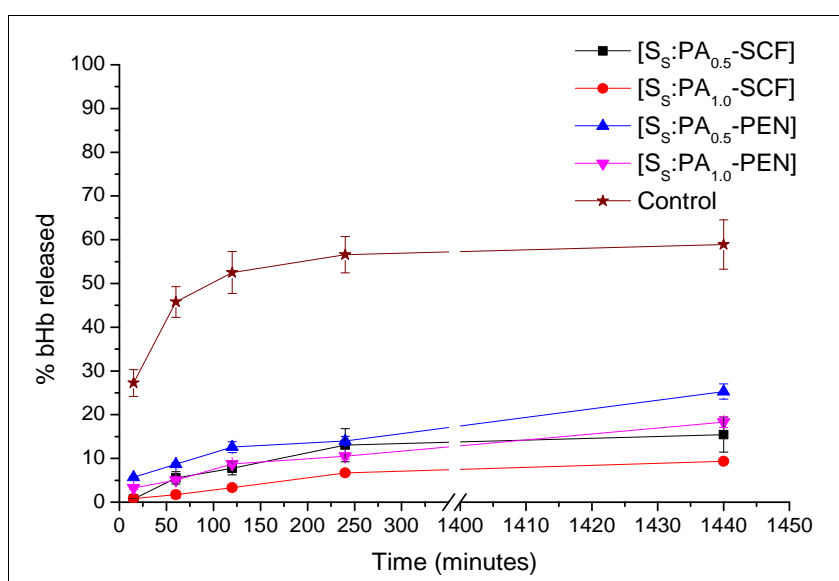


Figure 8.8: bHb release from S_S based SCDDS with PA coating

The release studies performed on the SA coated S_S based SCDDS are presented in Figure 8.9. The maximum bHb release of 15% was obtained from $S_S:SA_{0.5}$ -SCF whereas, $S_S:SA_{1.0}$ -SCF released only 5% of total protein. Particles were only coated by SCF processing due to the limited solubility of SA in pentane.

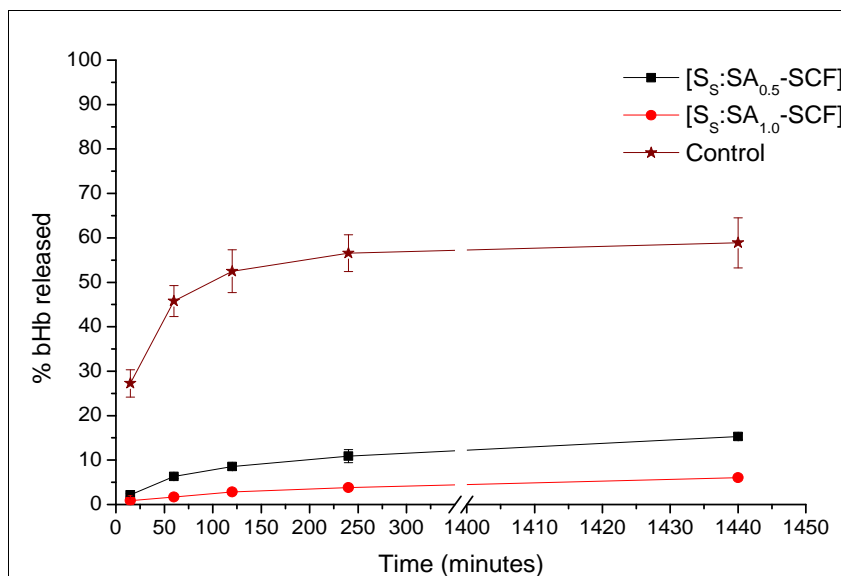


Figure 8.9: bHb release from S_S based SCDDS with SA coating

All S_S based formulations showed extremely low release of bHb in comparison to S_{LP} SCDDS. This could be due to the combination of factors such as saturation solubility of FAs in the given media and enhanced S_S-protein interactions. Also, a slightly higher release from PA and SA coated formulations could be attributed to the partial coating of bHb-S_S particles.

8.3.1.3 Release studies from S_{FP} based SCDDS

Similar to the S_{LP} and S_S the release studies were also performed on the FA coated S_{FP} formulations. A change in the bHb conformation was observed in LA based SCDDS, hence it was discontinued and release studies were conducted only on MA, PA and SA coated formulations.

The bHb release profiles from MA coated formulations are shown in Figure 8.10.

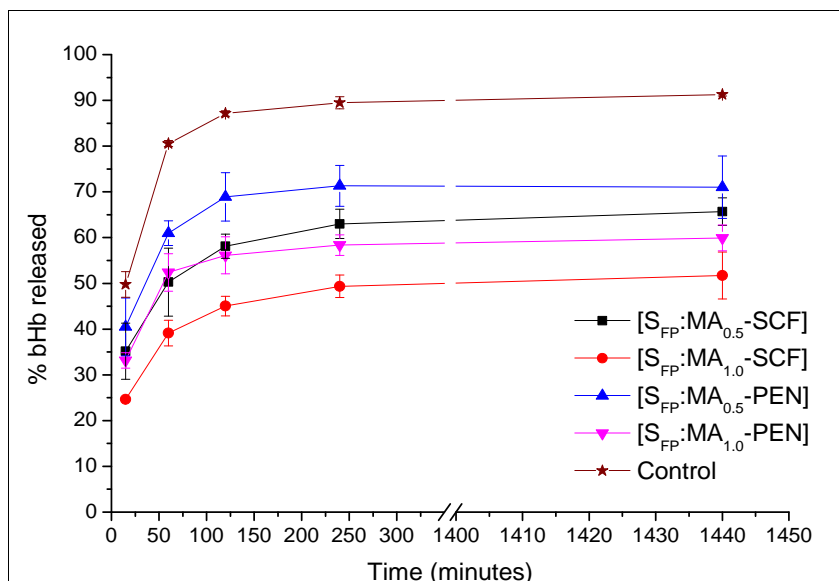


Figure 8.10: bHb release from S_{FP} based SCDDS with MA coating

Similar to S_{LP} and S_S studies, the uncoated particles with a total release of 91% were treated as control for these studies. It is evident from the data presented in Figure 8.10 that the release from S_{FP} based formulations was highest amongst all three types of cores studied in this work. Also, S_{FP} based SCDDS prepared by SCF processing showed slightly lower release when compared to the particles coated by solvent evaporation. For example, S_{FP}:MA_{0.5}-PEN showed a release of 70% in comparison to 65% from S_{FP}:MA_{0.5}-SCF. Additionally, if the FA/silica ratios were compared then 0.5:1 showed higher release compared to 1:1 for both coating methods. For instance, S_{FP}:MA_{0.5}-SCF released a total of 65% bHb which was 14% higher than the formulation containing 1:1 MA/silica ratio. Similarly, the total release from SCCDS prepared by solvent evaporation was 55% (1:1) and 70% (0.5:1).

The release profiles of bHb from PA coated formulations are presented in Figure 8.11. The highest protein release of 65% was obtained from S_{FP}:PA_{0.5}-PEN which was approximately 6% less than the corresponding formulation of MA. In addition to that, the lowest bHb release of 47% was obtained from S_{FP}:PA_{1.0}-SCF which indicated that coating by SCF processing led to a lower protein release from the formulation. This could be due to the better coating and improved surface coverage in comparison with solvent evaporation method.

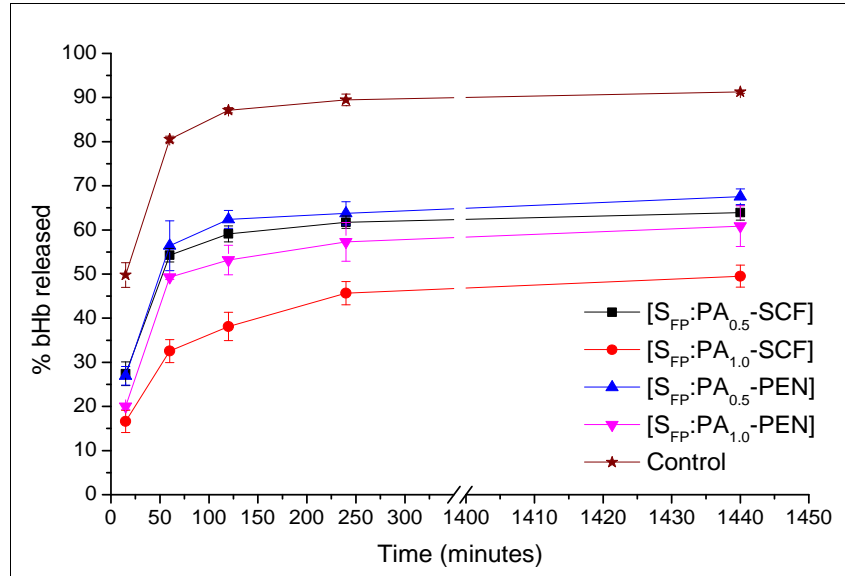


Figure 8.11: bHb release from S_{FP} based SCDDS with PA coating

The other three PA coated formulations *viz.* S_{FP}:PA_{0.5}-PEN, S_{FP}:PA_{0.5}-SCF and S_{FP}:PA_{1.0}-PEN showed a total bHb release of 63, 60 and 56% respectively.

Similar to the MA and PA, S_{FP} based SCDDS were also prepared using SA and the release profiles of bHb from these formulations are presented in Figure 8.12.

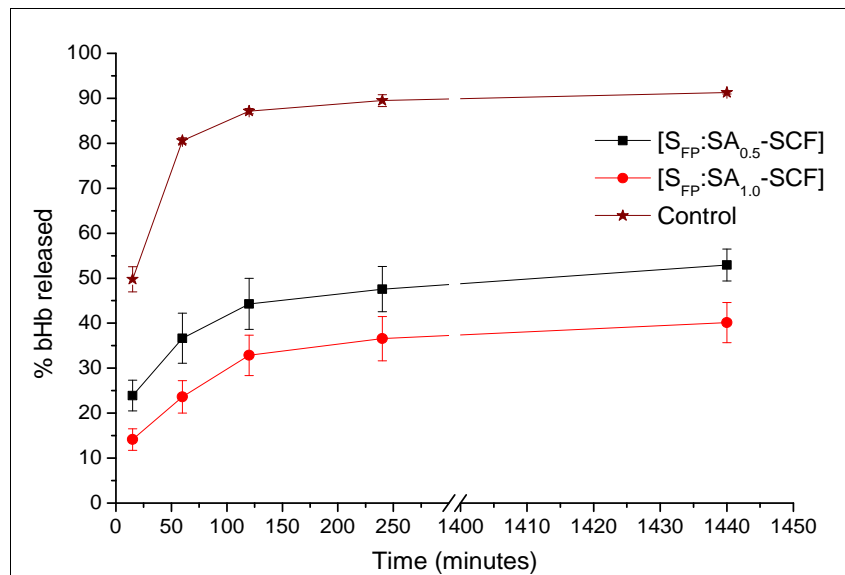


Figure 8.12: bHb release from S_{FP} based SCDDS with SA coating

The percent protein release from $S_{FP}:SA_{0.5}$ -SCF formulation was approximately 52%. It was 12% higher in comparison to $S_{FP}:SA_{1.0}$ -SCF which showed a total bHb release of 40%. Additionally, the amount of bHb released was lowest for SA coated formulations in comparison with PA and MA coated SCDDS. The order of bHb release with respect to the FA coating for S_{FP} based systems was found to be MA > PA > SA.

8.3.2. *In-vitro* release studies at pH 1.2 and 6.8

The S_{FP} based SCDDS with MA coating were selected for *in-vitro* release studies in simulated gastric fluid (SGF) and simulated intestinal fluid (SIF). This was primarily due to the higher release of bHb under given conditions along with the mild processing requirements for the preparation of MA based SCDDS in comparison to PA or SA.

The percentage release of bHb from MA based formulations at pH 1.2 and 6.8 are shown in Figure 8.13.

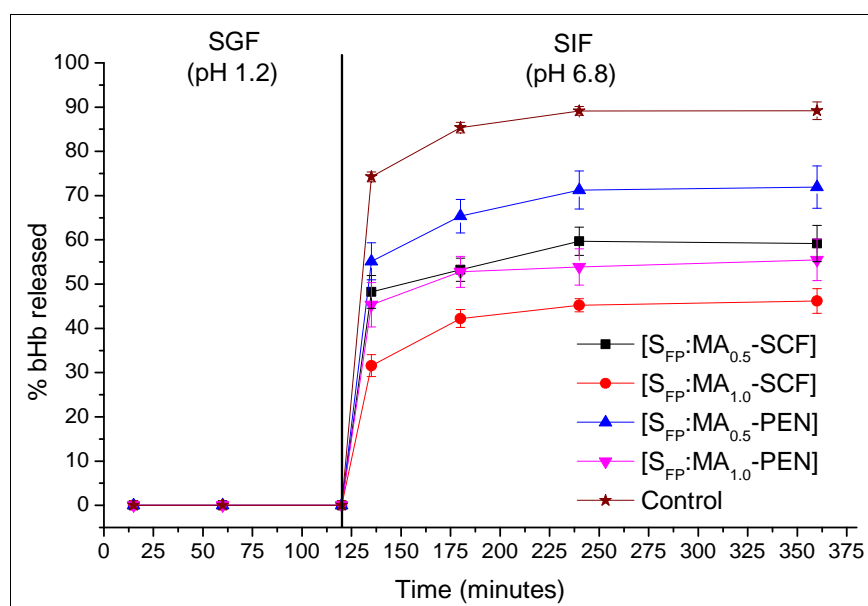


Figure 8.13: Release of bHb from MA coated S_{FP} based SCDDS at pH 1.2 and 6.8

The MA coated S_{FP} based SCDDS did not show any protein release in the first 120 minutes at pH 1.2. This suggests SCDDS prepared by MA coating has enteric properties to provide sufficient protection to protein from the gastric environment.

These findings were in agreement with the results from other researchers where Pettit *et al* showed 15% release of adsorbed protein from MA coated silica nanoparticles at intestinal pH and Cerchiara *et al* also showed that FA coating imparted enteric properties to vancomycin loaded chitosan particles prepared by freeze drying [6], [7]. However, loss of chromophore at gastric pH due to the denaturation of the released protein could not be rejected which would make quantification by UV spectroscopy difficult. The bHb release at higher pH was similar to previously (Figure 8.11) presented results, where highest bHb release of 71% was shown by S_{FP}:MA_{0.5}-PEN followed by S_{FP}:MA_{0.5}-SCF, S_{FP}:MA_{1.0}-PEN, and S_{FP}:MA_{1.0}-SCF with a release of 62, 56 and 48% respectively.

The F1 (dissimilarity factor) and F2 (similarity factor) comparison was made between control (uncoated particles) and various formulations in SIF. The results obtained are shown in Table 8.2.

Time (mins)	% Mean bHb released \pm S.D				
	Control	S _{FP} :MA _{0.5} -SCF	S _{FP} :MA _{1.0} -SCF	S _{FP} :MA _{0.5} -PEN	S _{FP} :MA _{1.0} -SCF
135	74.25 \pm 1.1	48.23 \pm 3.7	31.58 \pm 2.5	55.15 \pm 4.2	45.32 \pm 5.0
180	85.38 \pm 1.2	53.25 \pm 2.6	42.23 \pm 2.0	65.36 \pm 3.8	52.78 \pm 3.5
240	89.15 \pm 1.0	59.68 \pm 3.2	45.23 \pm 1.5	71.25 \pm 4.3	53.87 \pm 4.1
360	89.20 \pm 2.0	59.17 \pm 4.1	46.18 \pm 2.8	71.93 \pm 4.8	55.48 \pm 4.7
F1		35	51	22	39
F2		27	18	36	24

Table 8.2: Dissolution data for F1 and F2 calculations

Two dissolution profiles can be considered similar when F1 is between 0 - 15 and F2 is between 50 and 100 [8]. For all the above formulations, F1 was higher than 15 and F2 was lower than 50. Hence, it was established that these formulations were not similar to the control (uncoated particles).

8.3.3 bHb conformation after the release from S_{FP} based formulations

The conformation of bHb after the release from formulations was studied and compared with freshly prepared protein solution. Only S_{FP} based formulations were included in this study as the bHb release from other two silica particles was limited. The protein conformation was analysed after the 24 hours of release study at the room temperature. The UV spectra of untreated bHb and protein released from the LA coated S_{FP} formulations are presented in Figure 8.14. Significant differences in the UV spectra were observed between the bHb in the release media and untreated sample. This change in the spectra indicated alteration in the bHb conformation and also meant that concentration calculations of the released protein could not be relied upon. CD analysis was omitted for LA based systems as deconvolution of the spectrum would have also resulted in erroneous results.

It could be seen from the Figure 8.14 that the signature peaks of bHb at 405 and 285 nm in the spectra of released protein appeared either shifted or elevated when compared to the untreated sample. A bathochromic shift of 7 nm was observed for the absorption maxima of soret band, whereas the peak at 285 nm shifted upwards and appeared as a shoulder in the spectra of released protein.

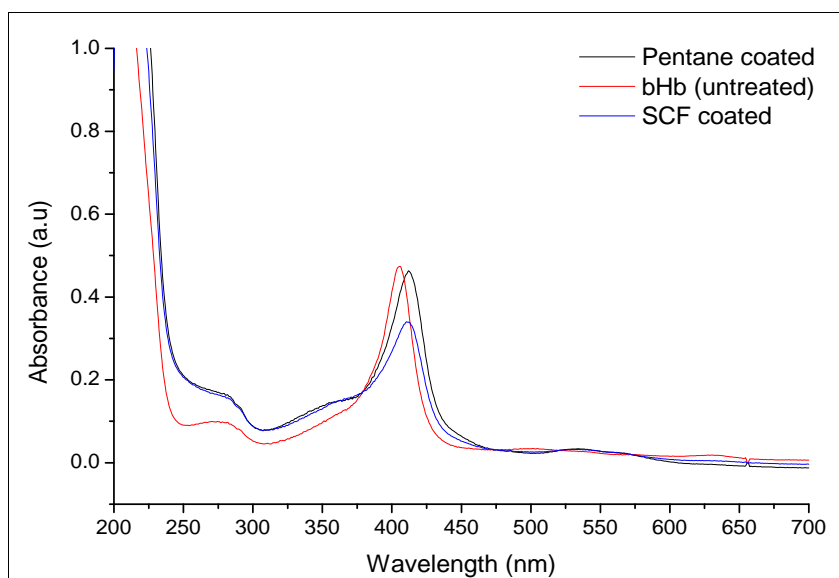


Figure 8.14: UV spectra of untreated bHb and bHb released from LA coated S_{FP} formulations

Formulations prepared by both coating methods resulted in conformational changes of the protein when LA was used as coating material. However, coating with other FAs (MA, PA and SA) had shown no changes in bHb conformation. An example of UV spectra of bHb released from MA coated formulations is shown in Figure 8.15.

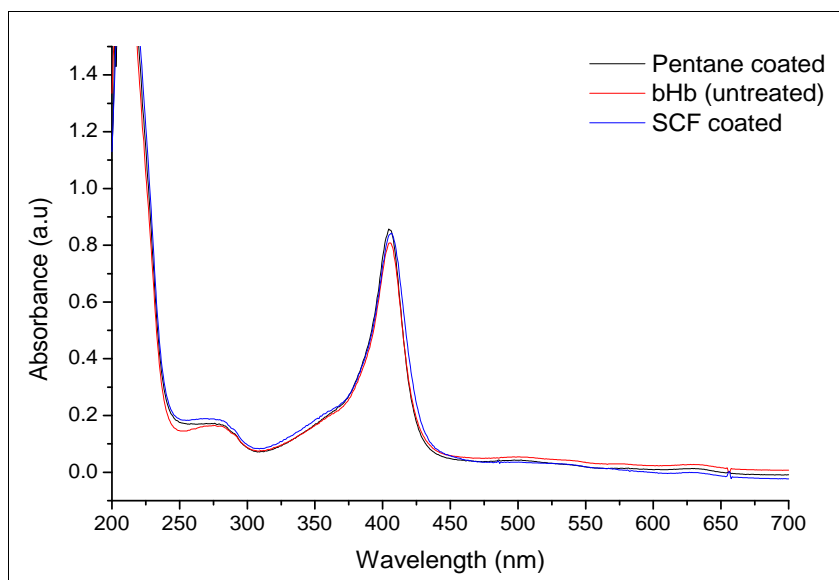


Figure 8.15: UV spectra of untreated bHb and bHb released from MA coated S_{FP} formulations

The CD analysis was also performed on the bHb released from S_{FP} based SCDDS prepared by MA, PA and SA coating. The percentage content of secondary structures determined by CD for protein released from MA coated formulations is shown in Table 8.3 as an example.

Secondary structure	bHb (untreated)	bHb released from S_{FP} formulation	
		CO ₂ coated	Pentane coated
Helix	60.5 ± 1.5 %	59.1 ± 0.4 %	60.7 ± 0.9 %
Antiparallel	0.7 ± 0.1 %	0.8 ± 0.0 %	0.7 ± 0.1 %
Parallel	4.9 ± 0.2 %	5.1 ± 0.1 %	4.9 ± 0.2 %
Beta turns	12.4 ± 0.2 %	12.5 ± 0.1 %	12.3 ± 0.1 %
Random coil	20.7 ± 1.0 %	21.2 ± 0.1 %	20.6 ± 0.7 %

Table 8.3: Percentage content of secondary structures [mean ± SE (n=2)] of untreated bHb and bHb released from MA coated S_{FP} formulations

Results supported the UV data and confirmed absence of any changes in the bHb conformation. The alpha helix content of the protein released from formulations was the same as the freshly prepared bHb solution *i.e.* approximately 60%. Similarly, the rest of the secondary structures content was also comparable to the untreated sample confirming the absence of any conformational changes in the bHb molecules.

8.4 Discussion

Ideally, the formulations coated with smaller FAs such as LA and MA should potentially show higher release compared to PA and SA owing to their better solubility in the release medium [7]. The release studies of protein from S_{LP} based SCDDS showed no specific trend with respect to the dissolution or erosion of FA coating in pH 6.8 buffer. The overall release was found to be below 30% and can be attributed to various factors such as large particle size, irregular shape, partial, non-uniform and/or multi-layered coating of these particles. The theoretical quantity of FA for a monolayer formation on 1 g of S_{LP} particles would be between 0.2 to 2.3 g depending upon the orientation of the FA molecules on the surface. The FA ratios used in the coating experiments correspond to 1 and 0.5 g of FA per 1 g of S_{LP} . However, the actual surface area available to FA molecules would be much less than the area calculated by the BET due to the factors such as inaccessible surface features on the particles and adsorbed protein molecules. Therefore, it is entirely possible that the amount of FA present in the formulation is higher than the quantity required to form a mono-layer. This will result in the multi-layer formation and low protein release due to the restricted access to the solvent and displacer molecules. The lower bHb release at higher FA ratio also suggests the same where 1:1 formulation showed nearly 50% less bHb release in comparison to 0.5:1 S_{LP} based SCDDS.

The S_S based formulations showed less than 10% protein release most probably due to the strong silica–protein interactions. It was established in previous chapters that S_S particles resulted in limited protein desorption even in the presence of a displacer which was lowest amongst all three types of silica. This low protein adsorption/desorption can be attributed to the presence of smaller pores on the silica surfaces. It is known that the pore diameter plays an important role in the protein adsorption on mesoporous materials

where large pore size and volume allow higher protein adsorption and *vice versa* [9], [10]. This was found true in the present study where S_S adsorbed least protein compared to other two silica particles which had larger pores as shown in Table 8.4.

Silica	SLP	S _S	S _{FP}
Average particle size (µm)	300	60	3
BET surface area (m²/g)	353.54 ± 1.84	426.97 ± 0.81	306.74 ± 2.08
BJH Pore Volume (ml/g)	0.92	0.71	1.16
BJH Pore Diameter (Å)	94.4	58.3	159.8
bHb adsorbed (mg/g)	50	25	200
bHb desorbed from uncoated particles (mg/g)	40	15	180

Table 8.4: Adsorbed and desorbed amount of bHb from different silica particles with their physical characteristics

The bHb release from the FA coated formulations was found to be <10% which was considerably lower than the 60% of protein desorption from uncoated particles. This showed that the FA coating prevented the release of adsorbed protein from the silica surface at studied conditions irrespective of the coating method. The main reason behind this phenomenon could be the inaccessibility of silica surface to the displacer because of FA coating. Similar to S_{LP}, the calculated quantity of FA required to form a monolayer on the surface of 1 g of S_S was found to be between 0.3 to 2.7 g. The FA to silica ratios used in the coating experiments were 1:1 and 0.5:1 (w/w). Therefore, there is a high probability that the quantity of FA present in the encapsulation process is higher than the amount required to form a mono-layer. The presence of extra FA molecules might have resulted in the formation of multi layered FA coating and prevented the protein release at the studied conditions.

The highest adsorption (200 mg/g) and desorption (180 mg/g) of bHb was obtained from S_{FP} particles. The higher adsorption can be assigned to the large pore diameter and pore volume whereas, 90% of bHb desorption from these particles can be accredited to the ease of availability of silica surface to the displacer.

The release from S_{FP} based SCDDS followed an expected trend where MA coated formulations showed highest release followed by PA and SA coated systems. LA was found to alter the conformation of bHb on S_{FP} and was excluded from this study. The reason for this is not exactly known but this may be due to the various factors affecting the conformation either alone or in combination such as pore diameter, surface crowding of protein molecules and polarity of LA. Further studies with various combinations of above mentioned parameters are required to understand this phenomenon in detail. The bHb release from S_{FP}:MA_{0.5}-SCF, S_{FP}:PA_{0.5}-SCF, and S_{FP}:SA_{0.5}-SCF was 66, 61 and 52% respectively. The trend in release profiles can be explained by the differences in the solubility of FAs in water and buffer which decreases with the increase in carbon chain length [11]–[13] as shown in Table 8.5.

Fatty Acid	Solubility (mg/l) water at 20 °C
LA	55
MA	2.4
PA	0.83
SA	0.34

Table 8.5: Solubility of FAs in water at 20 °C [14]

Moreover, according to Vorum *et al* solubility of FAs especially of LA and MA increases at higher pH [12]. It was found that solubility of LA increased to 200 mg/l in pH 7.4 phosphate buffer whereas, MA solubility increased 3 times to 7 mg/l. The solubility of PA and SA was not quantified by the authors but it was suggested that though PA and SA may not exist as true solution in the media but can form liposomes up to the concentrations of 6-7 mg/ml which means that slow erosion of FA coating can take place above their solubility limits. The release pattern of bHb from S_{FP} formulations is supported by solubility behaviour of FAs where MA coated formulations showed highest release followed by PA and SA.

It can be observed from the Figure 8.13 that as the FA ratio in the formulation increased the total bHb release decreased which could be expected due to the slow erosion of the

FA layer above the solubility limit. Moreover, the quantity of MA used in the S_{FP} based SCDDS corresponded to a final concentration of 0.4 (1:1) and 0.2 (0.5:1) mg/ml upon complete dissolution which was closer to its solubility limits. Whereas, PA and SA amounts used in the formulations were significantly higher than their solubility limits but lower than the liposomal concentration. Hence, if solubility is the primary factor behind the release of bHb from these systems then a trend of $MA > PA > SA$ could be expected. The SCF processed FA: S_{FP} (1:1) based SCDDS showed 52, 48 and 40% of protein release from MA, PA and SA coated formulations respectively. This confirms that the protein release from SCDDS takes place principally due to the continuous erosion of FA coating at studied conditions. This phenomenon of providing enteric properties to formulations by FA coating and release of the drug at higher pH has also been reported by various other researchers [5], [6].

Additionally, there were also clear differences between the proteins released from the samples coated by two different methods. The SCF coating resulted in slightly lower release for all FAs in comparison to the solvent evaporation method. For instance, $S_{FP}:MA_{0.5}$ -PEN released 71% of bHb in comparison with 66% by $S_{FP}:MA_{0.5}$ -SCF. This suggests incomplete surface coverage on the particles coated by solvent evaporation method. It could also be due to the need of high operating pressures for SCF coating (70-150 bar) which may assist FA molecules to penetrate into the pores instead of remaining only on the surface.

The S_{FP} based MA formulations performed better in terms of protein release and were chosen for *in-vitro* release studies at simulated gastric and intestinal fluids. The results showed that either there was no protein release at pH 1.2 or it was not quantifiable by UV spectroscopy. However, a significant bHb release at pH 6.8 proved that FA coating provided a protective layer to the immobilised protein. The protein released from the formulations was also analysed by CD and secondary structure contents were calculated which confirmed that bHb remained in its native conformation after the release from SCDDS.

8.5 Conclusions

Coating of bHb adsorbed silica particles was performed by SCF processing and a conventional solvent evaporation method. FAs were used as coating materials because of their pH dependent solubility. Release studies of bHb from S_{LP} based formulations displayed no specific trend with respect to the solubility of FAs and were attributed to the factors such as incomplete coating and irregular size & shape of the silica particles. The amount of bHb released in the case of S_S was $\leq 10\%$ which was probably due to the strong protein-silica interactions and multi-layered FA coating. S_{FP} formulations provided highest release with MA coated particles followed by PA and SA. The trend in protein release was in accordance to the FAs solubility in pH 6.8 buffer. The MA coated S_{FP} based SCDDS were subjected to *in-vitro* release at gastric and intestinal pH which resulted in 50-70% protein release from the formulations. CD analysis on the protein released from SCDDS did not show any changes in the secondary structures which proved that SCF processing or exposure to pentane had no/minimal effect on the conformation of bHb.

This study proved that S_{FP} can be used as a core to develop SCDDS for large therapeutic molecules such as proteins/ peptides and FAs can be used as effective coating materials for pH dependent release of the drug from the formulation.

References

- [1] H. Umer, H. Nigam, A. M. Tamboli, and M. S. M. Nainar, 'Microencapsulation : Process , Techniques and Applications.', *Int. J. Res. Pharm. Biomed. Sci.*, vol. 2, no. 2, pp. 474–481, 2011.
- [2] S. S. Bansode, S. K. Banarjee, D. D. Gaikwad, S. L. Jadhav, and R. M. Thorat, 'Microencapsulation: a review', *Int. J. Pharm. Sci. Rev. Res.*, vol. 1, no. 2, pp. 38–43, 2010.
- [3] A. Taberero, E. M. Martín del Valle, and M. A. Galán, 'Supercritical fluids for pharmaceutical particle engineering: Methods, basic fundamentals and modelling', *Chem. Eng. Process. Process Intensif.*, vol. 60, pp. 9–25, 2012.
- [4] Ž. Knez, E. Marko i , M. Leitgeb, M. Primoži , M. Knez Hrn i , and M. Škerget, 'Industrial applications of supercritical fluids: A review', *Energy*, pp. 1–9, 2014.
- [5] B. Calvo and E. A. Cepeda, 'Solubilities of Stearic Acid in Organic Solvents and in Azeotropic Solvent Mixtures', *J. Chem. Eng. Data*, vol. 53, no. 3, pp. 628–633, 2008.
- [6] M. W. Pettit, P. D. R. Dyer, J. C. Mitchell, P. C. Griffiths, B. Alexander, B. Cattoz, R. K. Heenan, S. M. King, R. Schweins, F. Pullen, S. R. Wicks, and S. C. W. Richardson, 'Construction and physiochemical characterisation of a multi-composite, potential oral vaccine delivery system (VDS).', *Int. J. Pharm.*, vol. 468, no. 1–2, pp. 264–71, 2014.
- [7] T. Cerchiara, B. Luppi, F. Bigucci, M. Petrachi, I. Orienti, and V. Zecchi, 'Controlled release of vancomycin from freeze-dried chitosan salts coated with different fatty acids by spray-drying.', *J. Microencapsul.*, vol. 20, no. 4, pp. 473–478, 2003.

- [8] L. Kassaye and G. Genete, 'Evaluation and comparison of in-vitro dissolution profiles for different brands of amoxicillin capsules', *Afr. Health Sci.*, vol. 13, no. 2, pp. 369–375, 2013.
- [9] D. M. Schlipf, S. E. Rankin, and B. L. Knutson, 'Pore-size dependent protein adsorption and protection from proteolytic hydrolysis in tailored mesoporous silica particles', *ACS Appl. Mater. Interfaces*, vol. 5, no. 20, pp. 10111–10117, 2013.
- [10] Z. Ma, J. Bai, Y. Wang, and X. Jiang, 'Impact of shape and pore size of mesoporous silica nanoparticles on serum protein adsorption and RBCS hemolysis', *ACS Appl. Mater. Interfaces*, vol. 6, no. 4, pp. 2431–2438, 2014.
- [11] P. Khuwijitjaru, S. Adachi, and R. Matsuno, 'Solubility of saturated fatty acids in water at elevated temperatures.', *Biosci. Biotechnol. Biochem.*, vol. 66, no. 8, pp. 1723–6, 2002.
- [12] H. Vorum, R. Brodersen, U. Kragh-Hansen, and A. O. Pedersen, 'Solubility of long-chain fatty acids in phosphate buffer at pH 7.4', *Biochim. Biophys. Acta - Lipids Lipid Metab.*, vol. 1126, no. 2, pp. 135–142, 1992.
- [13] C. W. Hoerr, R. S. Sedgwick, and A. W. Ralston, 'The solubilities of the normal saturated fatty acids. III', *J. Org. Chem.*, vol. 11, no. 5, pp. 603–609, 1946.
- [14] K. S. Markley, 'Lipids', in *Practical Handbook of Biochemistry and Molecular Biology*, G. D. Fasman, Ed. Boca raton, USA: CRC Press, 1989.

CHAPTER 9

Summary and future work

9.1 Summary (Key findings)

- a) The melting point of excipients (FAs and pluronics) was lowered under pressurised CO₂. It was observed that FAs melted at 10.7 to 19.5 °C below their actual melting point and this decrease was found to be inversely proportional to the carbon chain length of FAs. Similarly, the pluronics also showed a decrease of 18.1 to 19.3 °C in melting temperature. However, this decrease was independent of the molecular weight and polypropylene oxide (PPO) content of the polymers. The similar decrease in melting point of pluronics was assigned to their high cohesive energy density and presence of large CO₂-philic PPO units. Additionally, this depression in melting point was found to be dependent upon pressure. In the case of FAs, melting point decreased initially with increase in pressure and then increased after reaching a minimum whereas, the melting point of all pluronics decreased with initial increase in pressure and then remained constant. It was also established that there was no change in crystal structure upon CO₂ processing of these excipients. These findings were very useful during the coating of bHb adsorbed silica. FAs were chosen as coating materials over pluronics for the development of SCDDS because of their pH dependent solubility.

- b) The stability of bHb was studied in order to determine the key parameters for the formulation of SCDDS. The thermal stability studies showed that irreversible conformational changes occur in bHb structure above 50 °C. Hence, it was established that exposure of protein solution to higher temperatures must be discouraged at any step while formulating SCDDS. Storage stability studies indicated that protein was relatively more stable at mildly acidic conditions (pH 6) and at lower temperature (4 °C). This helped in identifying the conditions for adsorption experiments. The agitation stability performed also suggested

changes in the protein conformation with time due to the shear stress; hence the duration of adsorption was fixed to 4 hours.

- c) bHb adsorption studies onto three morphologically different silica particles indicated that the total amount of protein adsorption was dependent upon size and shape of pores present in these particles. Therefore, the silica particles having larger pores allowed the higher protein adsorption and could be used in delivering higher dose. It was also observed that the adsorption of bHb on silica was irreversible, hence application of pluronics (non-ionic surfactants) as displacer was explored for protein desorption. Positive correlations between desorption and the number of polyethylene units and concentration of pluronics were observed for all studied polymers. It was established that minimum pluronic concentration of 1 mg/ml was required to obtain maximum bHb desorption from these studies. Pluronic F-127 was the preferred choice of displacer during *in-vitro* dissolution studies in simulated gastric and intestinal fluids as it is well characterised and easily available.
- d) The SCDDS formulations were prepared using silica as core and FAs as shell materials and subjected to *in-vitro* release studies. S_{LP} and S_S based SCDDS showed a release of maximum 30 and 15% respectively in the media. Whereas, protein release from S_{FP} was in the range of 45-75% depending upon the type and ratio of fatty acid in the formulations. The low release of bHb shown by S_{LP} was attributed to its irregular size, shape and incomplete and/or multi-layered coating. Similarly, the low ($\leq 10\%$) release in the case of S_S was believed to be due to the strong protein-silica attractions and multi-layer FA coating. The release from S_{FP} based formulations was dependent on the aqueous solubility of FAs and followed a trend of $MA > PA > SA$. The protein release was also dependent on the ratio of FAs where 1:1 (silica: FA) ratio always showed lower and slower release in comparison to 0.5:1 formulations. The protein release in SGF from MA coated S_{FP} based formulations were also analysed which resulted

in no or minimal protein release. Furthermore, up to 60% protein release was observed when SIF was used as release media.

- e) The conformation of bHb released from SCDDS was analysed and compared with the freshly prepared bHb solution. Both UV and CD results confirmed that bHb remained in its native conformation after the dissolution studies except in the case of LA based S_{FP} formulations prepared using S_{FP} as core. This shows that the steps involved in the formulation of SCDDS have minimum or no effect on protein's conformation. This confirmed that S_{FP} can be used as carrier material for large proteins, FAs as coating material and supercritical fluid as processing technique for the formulation of SCDDS.

9.2 Future work

- a) It has been established in this work that mesoporous silica can be used as a carrier material in the preparation of SCDDS for protein drug delivery. Other core materials such as polymer particles, zeolites, inorganic particles with well-defined pore size and volume can be studied in order to identify their potential use. Commonly used biodegradable polymeric nanoparticles such as poly-lactic acid, poly-D-L-glycolide, poly-D-L-lactide-co-glycolide, poly-cyanoacrylate, polycaprolactone, gelatine and chitosan can also be investigated as carrier materials [1].
- b) FAs were studied as the coating material in this work to provide enteric properties to the formulation. The pH dependent solubility of FAs can be further investigated in a broader pH range *i.e.* from 4 to 10. Other pH sensitive polymers including cellulose acetate phthalate, cellulose acetate trimellitate, hydroxyl propylmethyl cellulose phthalate, and Eudragit S can also be studied for their coating capabilities with supercritical processing. These materials have already shown good results when used with small molecules [2]. Slight

modification can be done in the current supercritical instrument to obtain more uniformly coated and less aggregated particles.

- c) bHb was used as a model drug in this project and in the future this strategy can be extended to therapeutically active proteins/peptides. It is reported in literature that surfactants can potentially prevent the protein denaturation in aqueous environment [3], [4]. Therefore, use of surfactants as an excipient in the formulation can also be investigated.
- d) Pluronics were used as displacing agents in this work and to further understand the protein desorption by pluronics, their CSMC on silica particles can also be examined.
- e) Furthermore, SCF instrument can be modified in order to achieve uniform coating and reduced agglomeration. For example, addition of a larger expansion vessel through a nozzle with a temperature controlled system will allow the utilisation of the fundamentals of the PGSS process.
- f) The release studies conducted here can be extended to biorelevant gastric and intestinal fluids to understand the protection provided by coating material. The studies herein were conducted at room temperature and it will be important to analyse the results obtained from experiments conducted at physiological temperature (37 °C).

References

- [1] A. Kumari, S. K. Yadav, and S. C. Yadav, “Biodegradable polymeric nanoparticles based drug delivery systems.,” *Colloids Surf. B. Biointerfaces*, vol. 75, no. 1, pp. 1–18, 2010.
- [2] G. F. Palmieri, S. Michelini, P. Di Martino, and S. Martelli, “Polymers with pH-dependent solubility: possibility of use in the formulation of gastroresistant and controlled-release matrix tablets.,” *Drug Dev. Ind. Pharm.*, vol. 26, no. 8, pp. 837–45, 2000.
- [3] D. Otzen, “Protein-surfactant interactions: a tale of many states.,” *Biochim. Biophys. Acta*, vol. 1814, no. 5, pp. 562–91, 2011.
- [4] P. L. Wang and T. P. Johnston, “Enhanced stability of two model proteins in an agitated solution environment using poloxamer 407,” *J. Parenter. Sci. Technol.*, vol. 47, no. 4, pp. 183–9, 1993.

APPENDIX

A) Thermal stability of bHb

A.1) UV Spectra

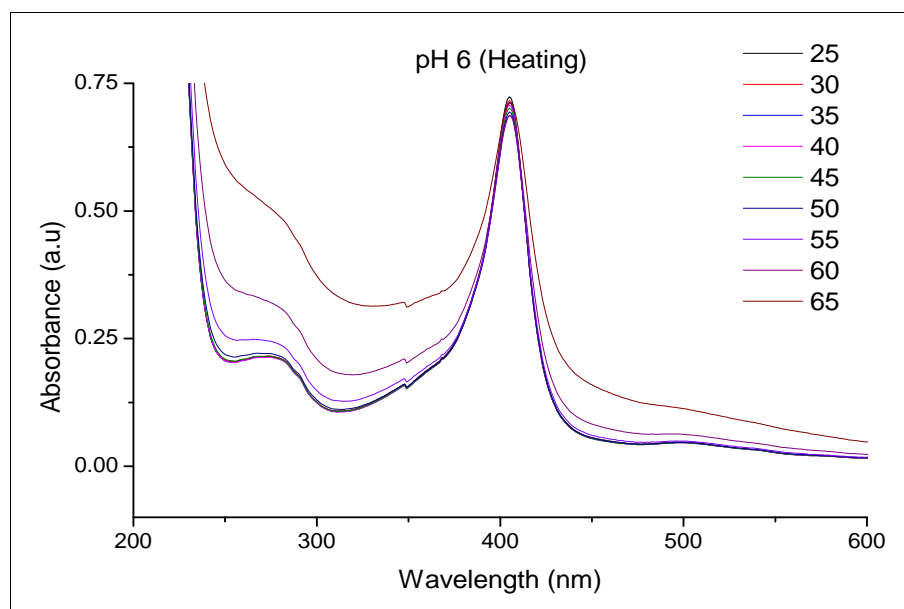


Figure 1: UV spectra of bHb at pH 6 from 25 to 65°C

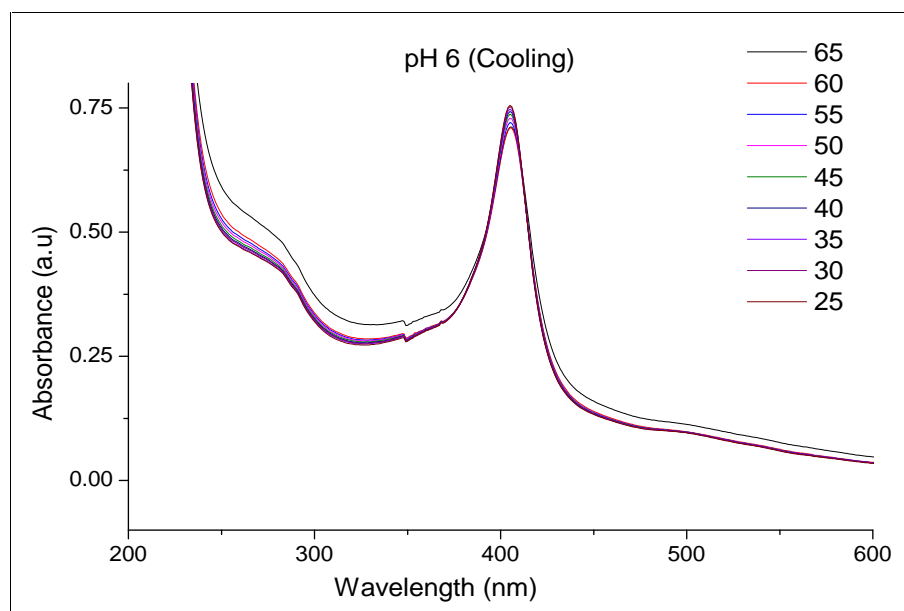


Figure 2: UV spectra of bHb at pH 6 from 65 to 25 °C

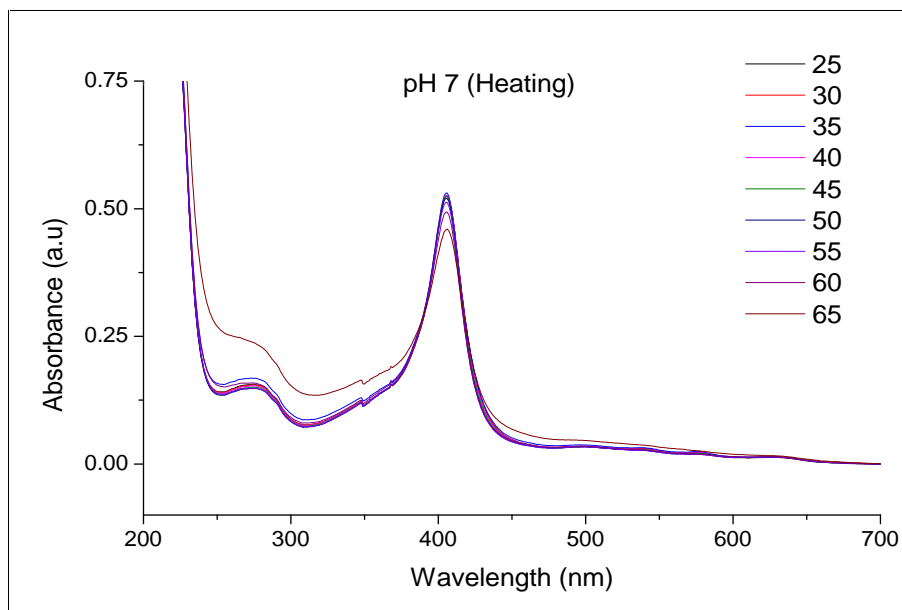


Figure 3: UV spectra of bHb at pH 7 from 25 to 65 °C

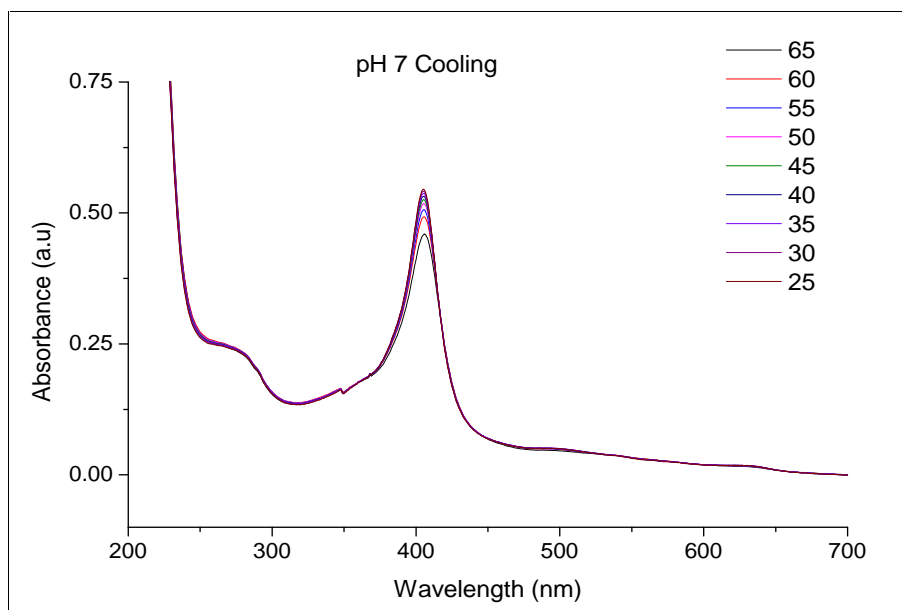


Figure 4: UV spectra of bHb at pH 7 from 65 to 25 °C

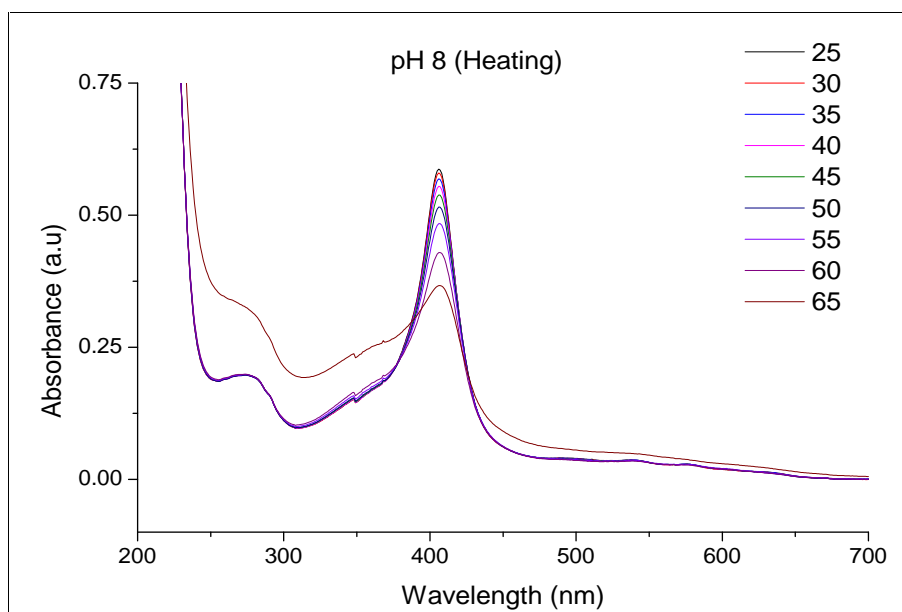


Figure 5: UV spectra of bHb at pH 8 from 25 to 65 °C

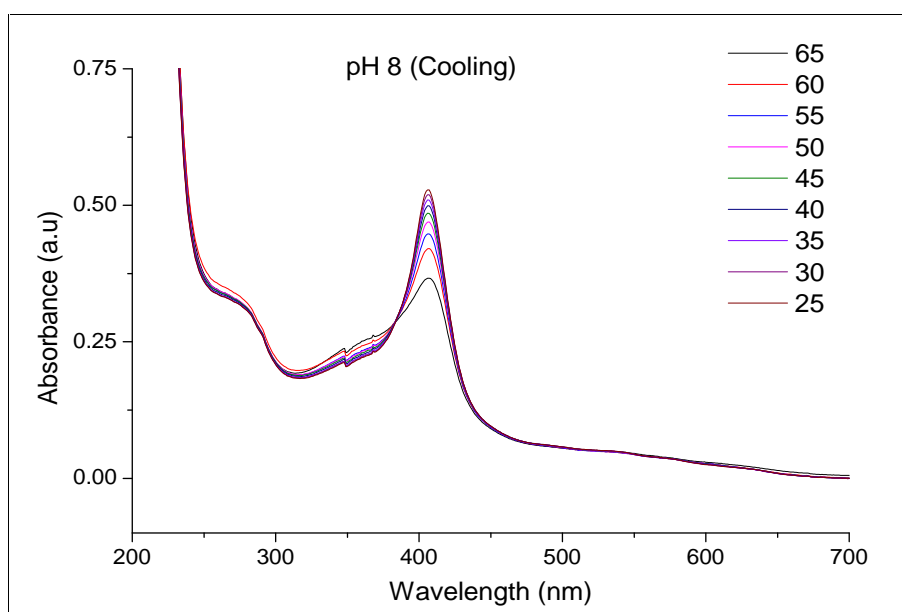


Figure 6: UV spectra of bHb at pH 8 from 65 to 25 °C

A.2) CD Spectra

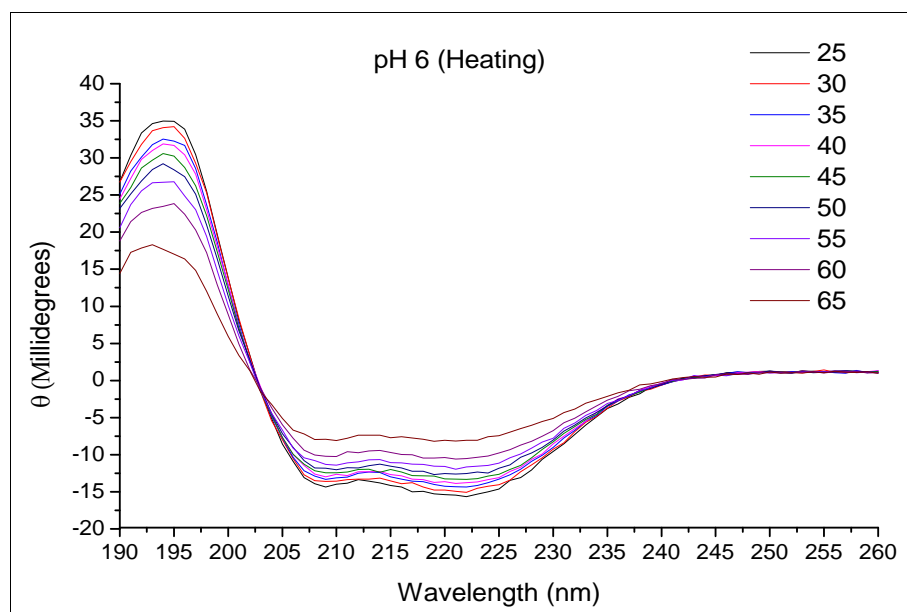


Figure 7: CD spectra of bHb at pH 6 from 25 to 65 °C

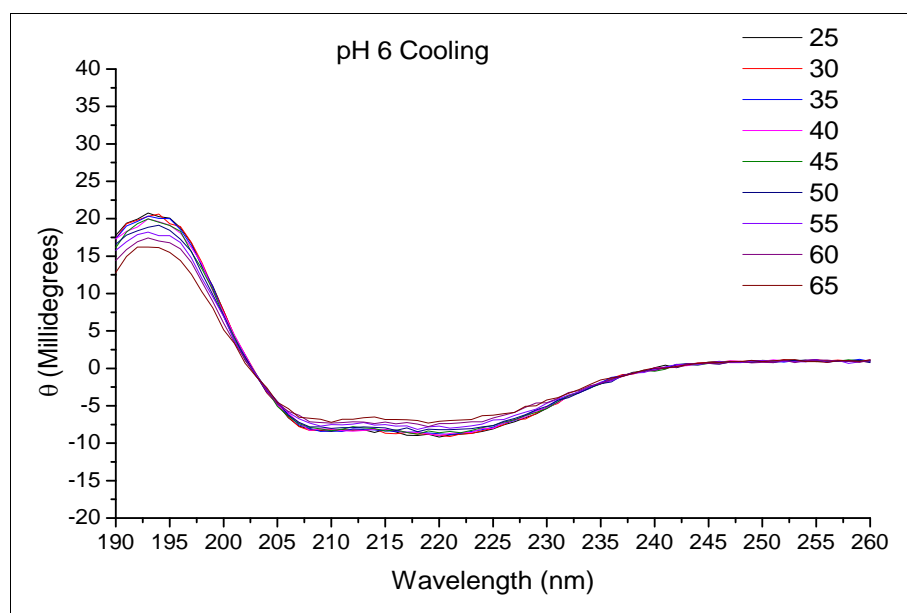


Figure 8: CD spectra of bHb at pH 6 from 65 to 25 °C

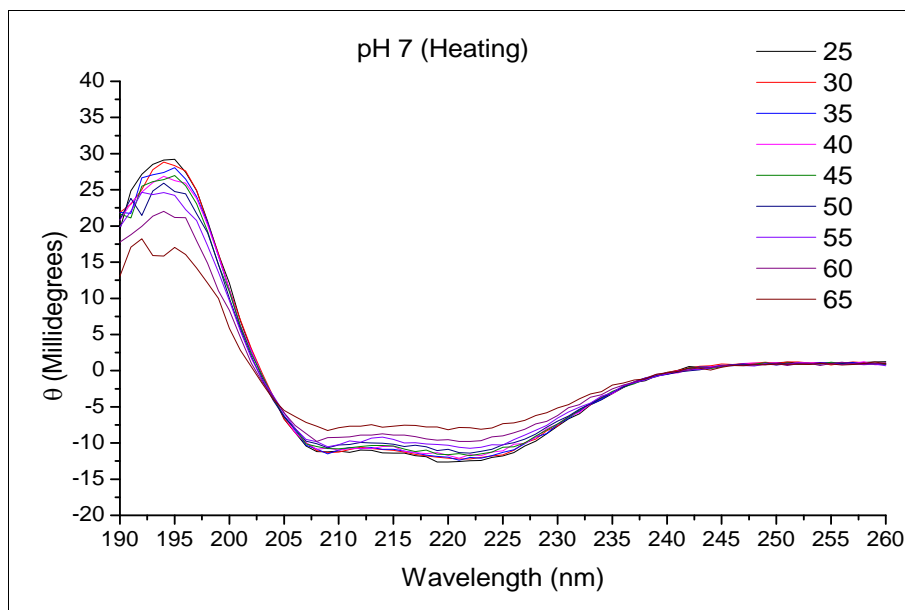


Figure 9: CD spectra of bHb at pH 7 from 25 to 65 °C

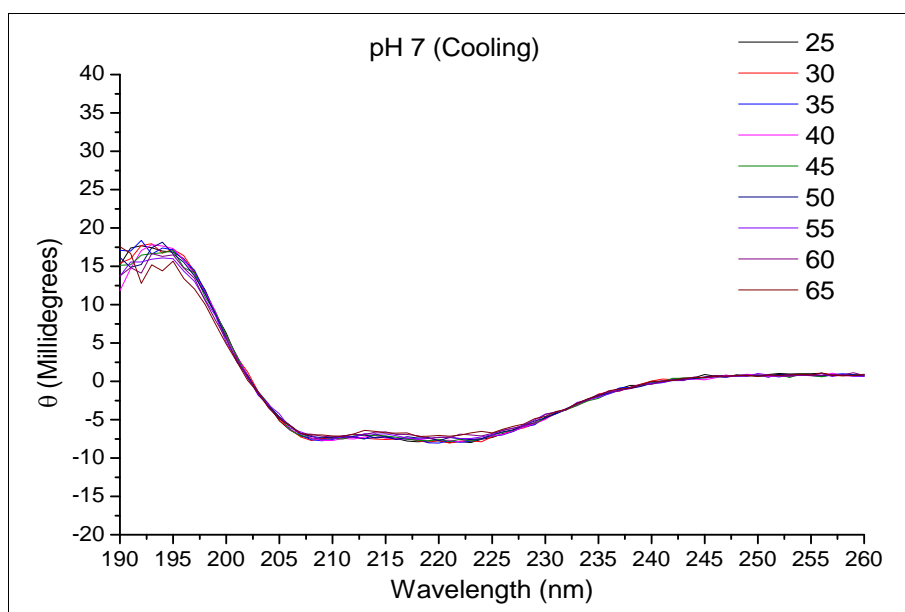


Figure 10: CD spectra of bHb at pH 7 from 65 to 25 °C

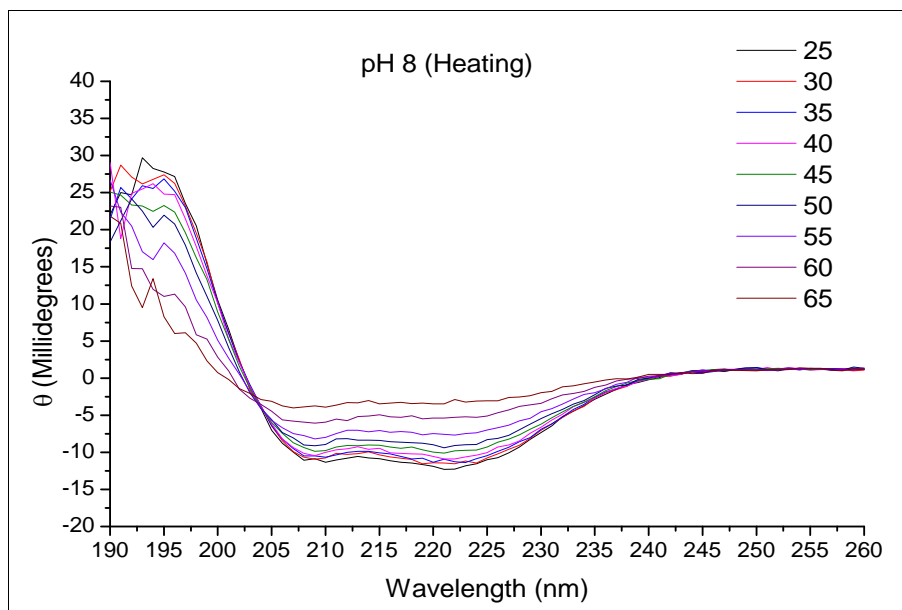


Figure 11: CD spectra of bHb at pH8 from 25 to 65 °C

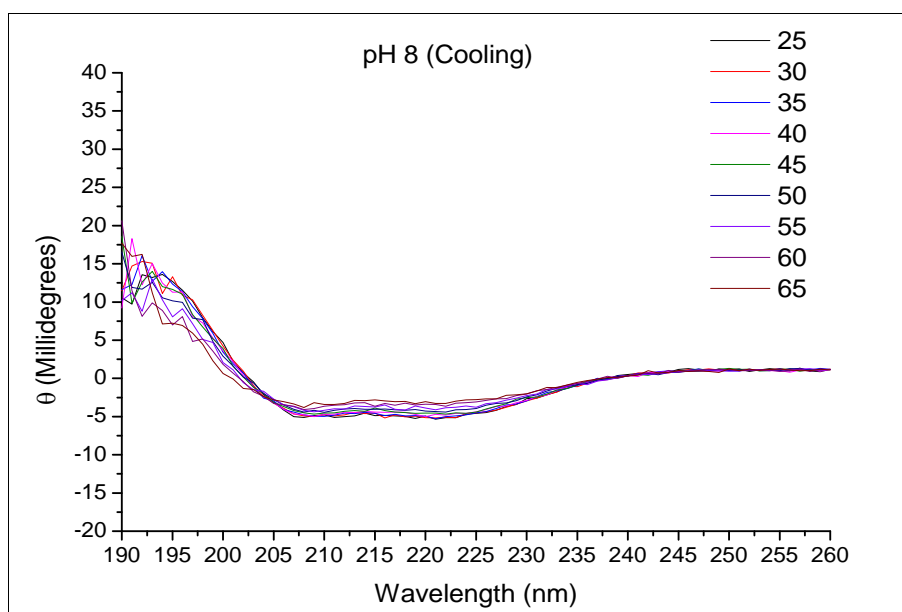


Figure 12: CD spectra of bHb at pH 8 from 65 to 25 °C

B) Six hours stability of bHb

B.1) UV Spectra

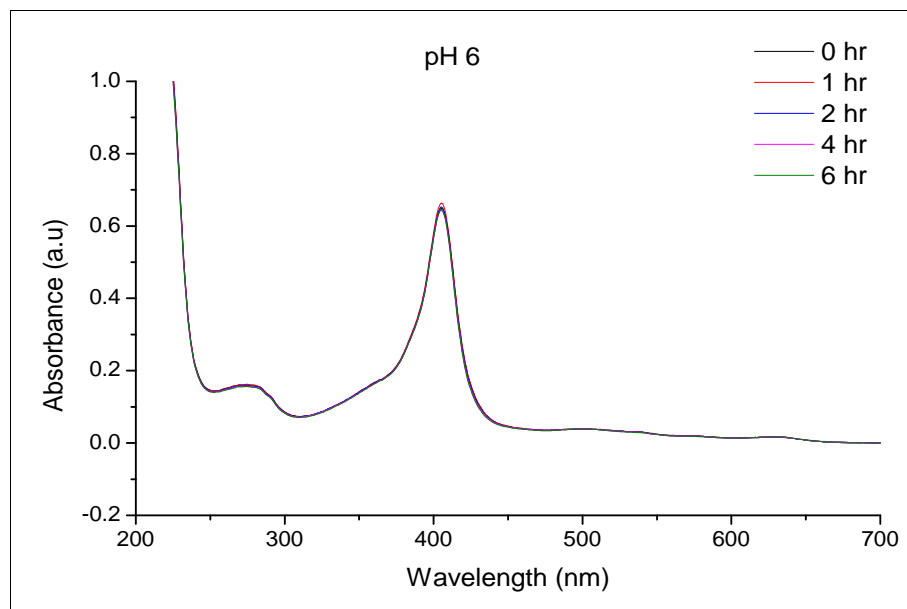


Figure 13: UV spectra of bHb at pH 6

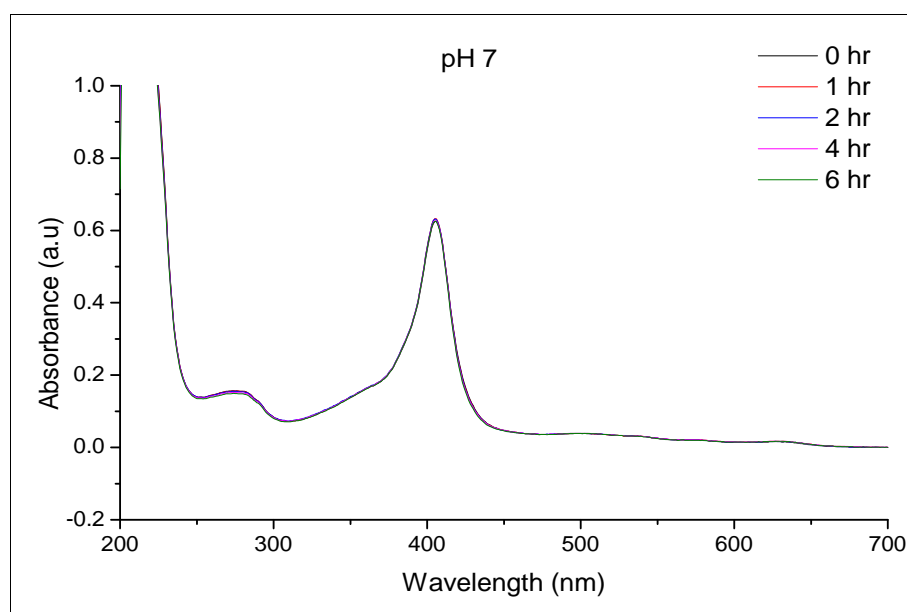


Figure 14: UV spectra of bHb at pH 7

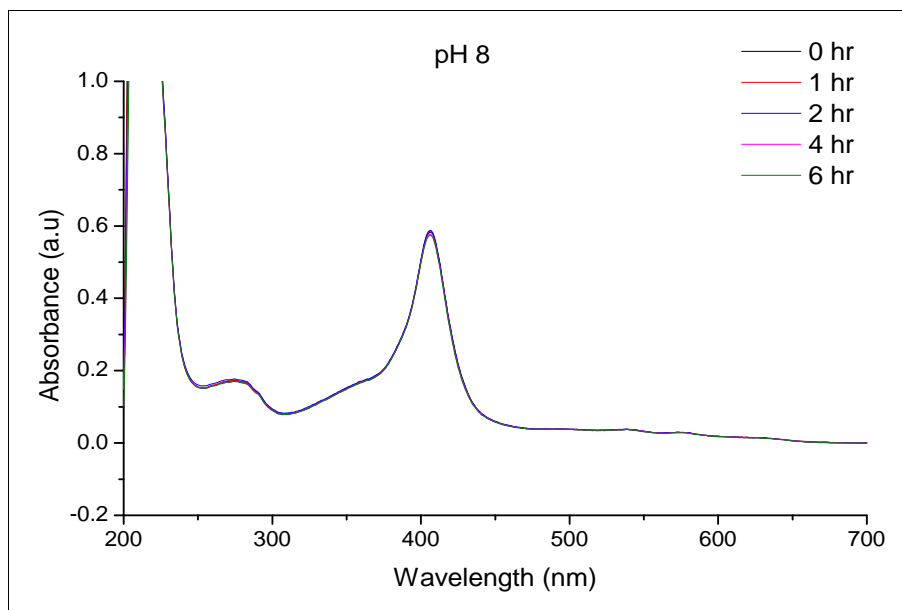


Figure 15: UV spectra of bHb at pH 8

B.2) CD Spectra

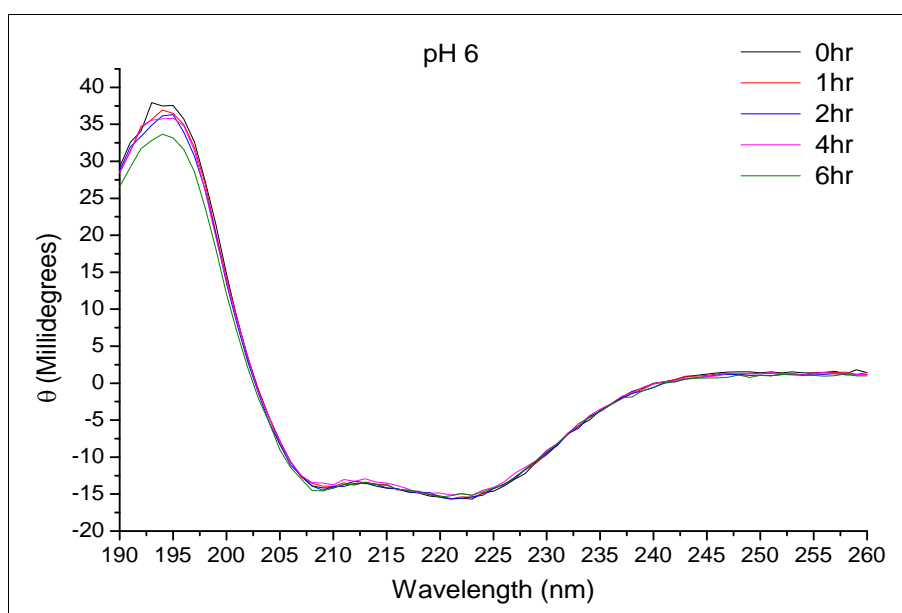


Figure 16: CD spectra of bHb at pH 6

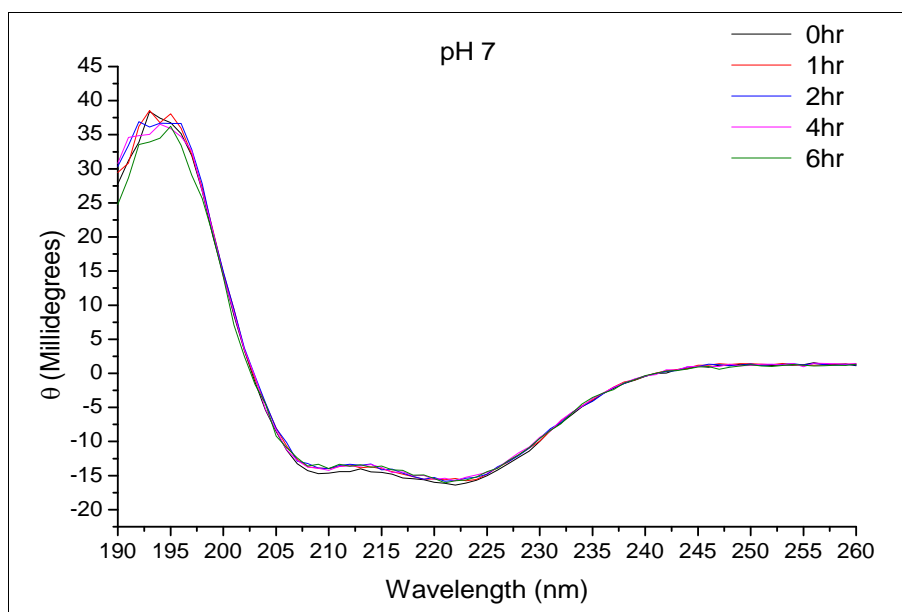


Figure 17: CD spectra of bHb at pH 7

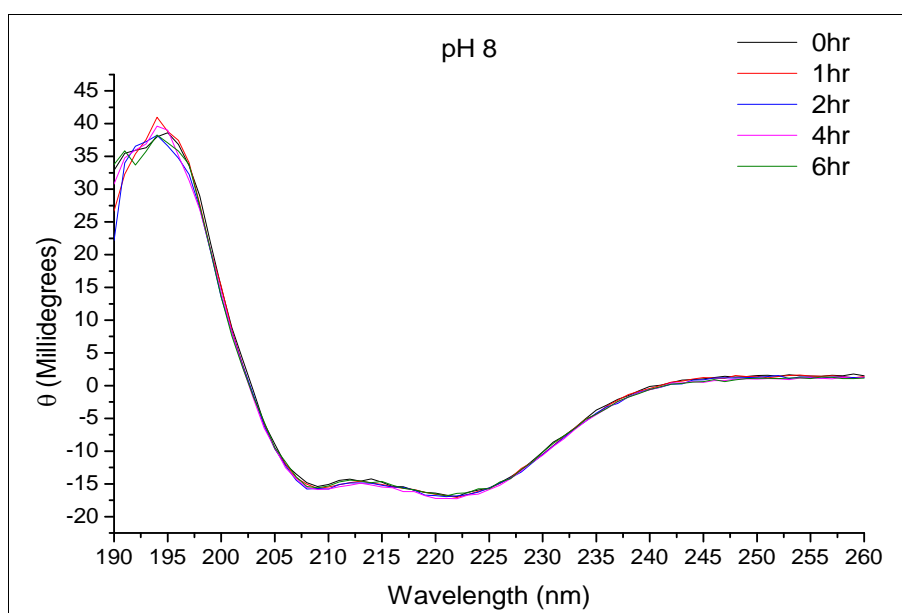


Figure 18: CD spectra of bHb at pH 8

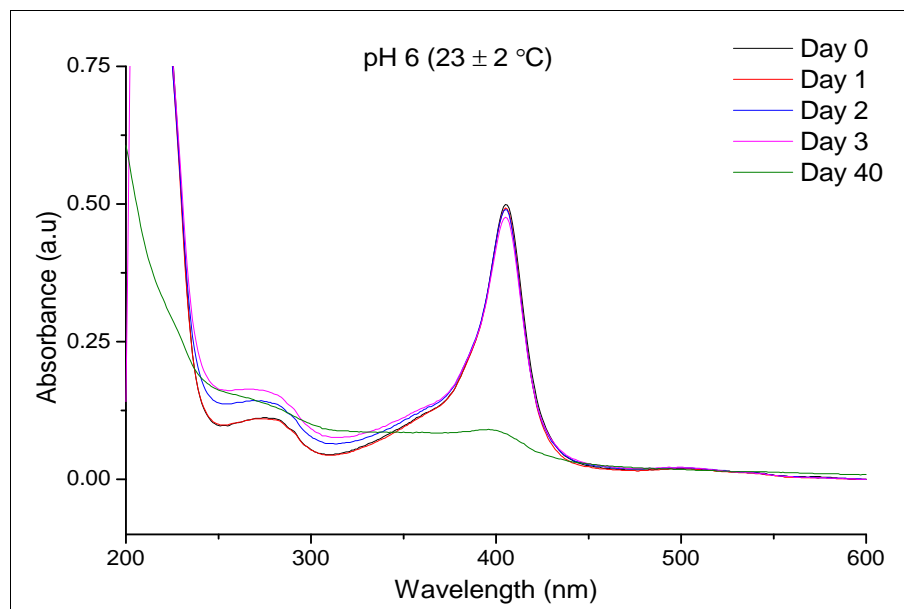
C) Inter-day stability of bHb**C.1) UV Spectra**

Figure 19: UV spectra of bHb at pH 6 stored at 23 °C

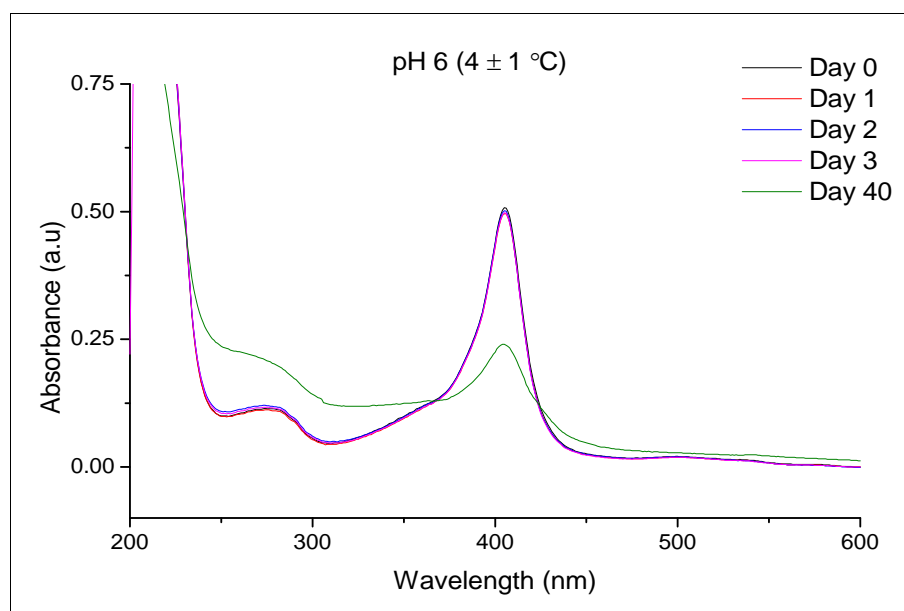


Figure 20: UV spectra of bHb at pH 6 stored at 4 °C

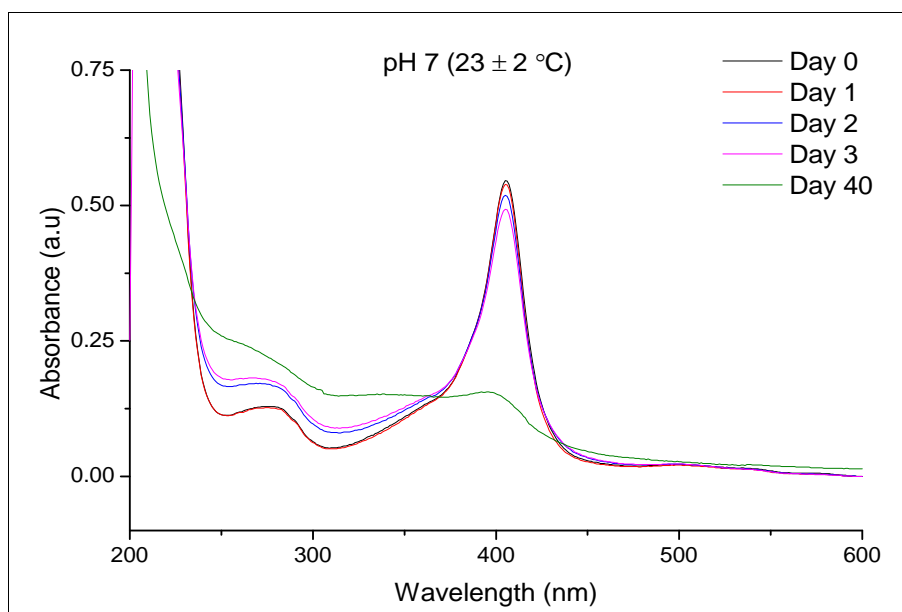


Figure 21: UV spectra of bHb at pH 7 stored at 23 °C

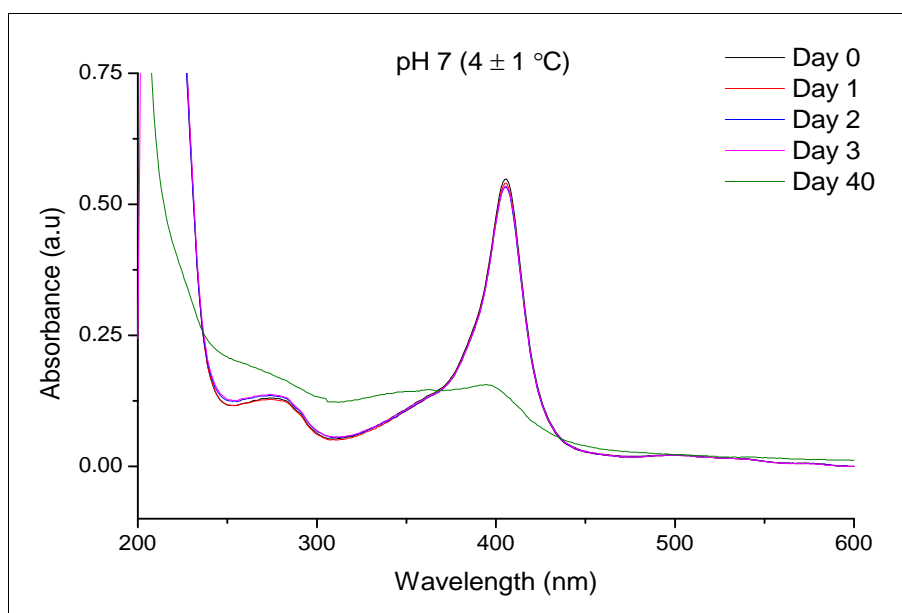


Figure 22: UV spectra of bHb at pH 7 stored at 4 °C

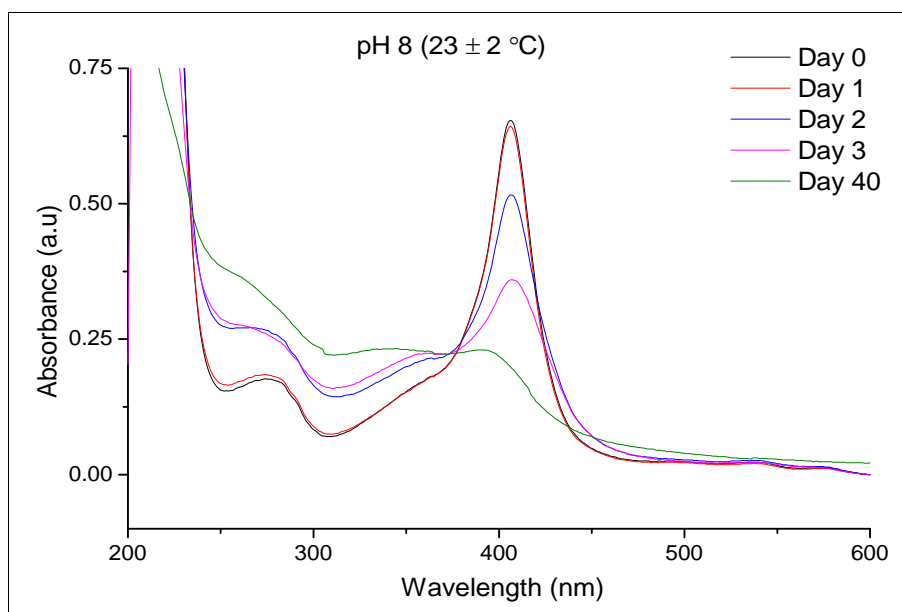


Figure 23: UV spectra of bHb at pH 8 stored at 23 °C

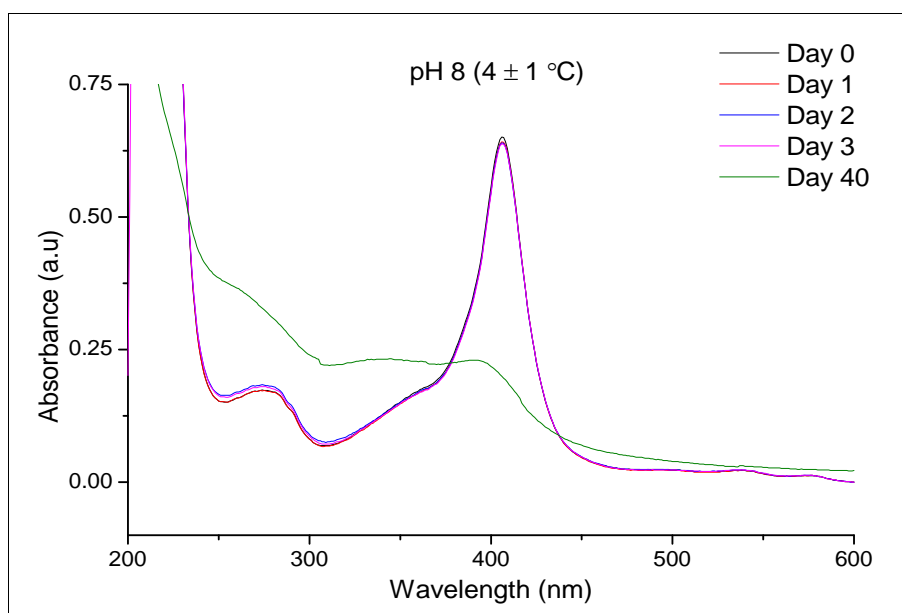


Figure 24: UV spectra of bHb at pH 8 stored at 4 °C

C.2) CD Spectra

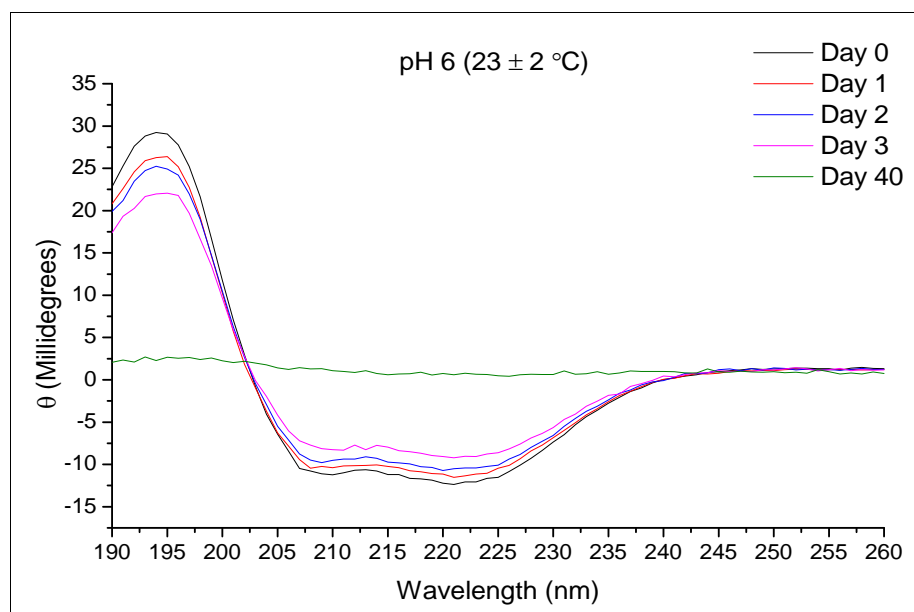


Figure 25: CD spectra of bHb at pH 6 stored at 23 °C

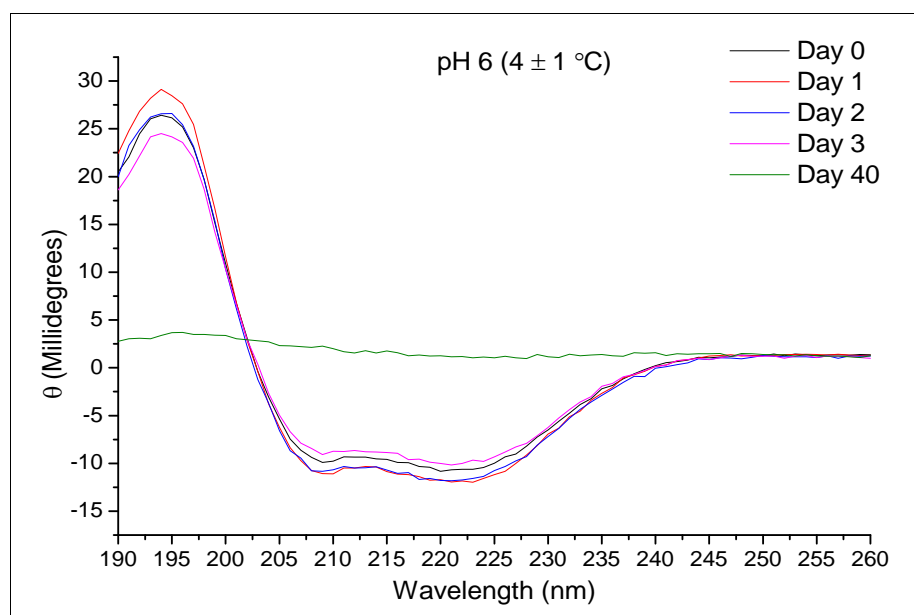


Figure 26: CD spectra of bHb at pH 6 stored at 4 °C

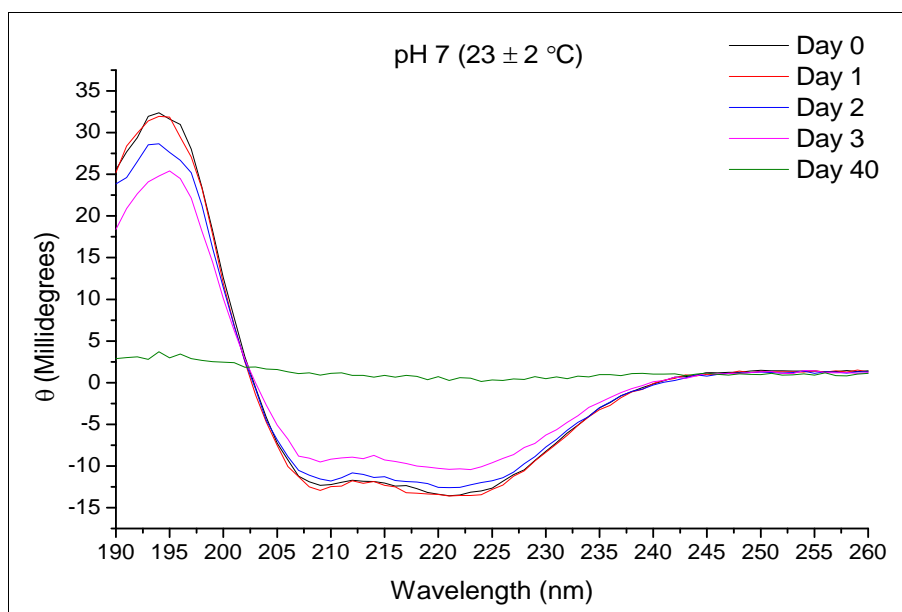


Figure 27: CD spectra of bHb at pH 7 stored at 23 °C

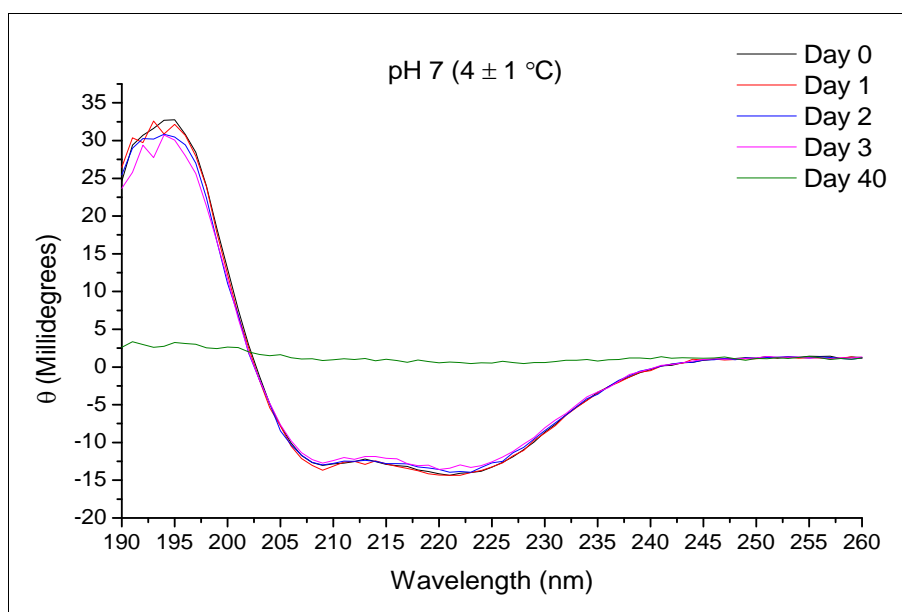


Figure 28: CD spectra of bHb at pH 6 stored at 4 °C

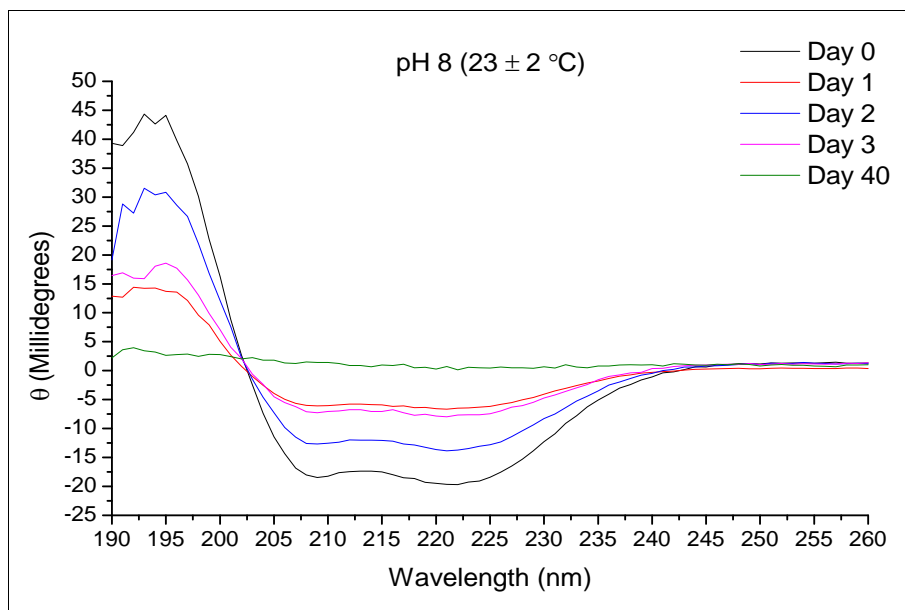


Figure 29: CD spectra of bHb at pH 8 stored at 23 °C

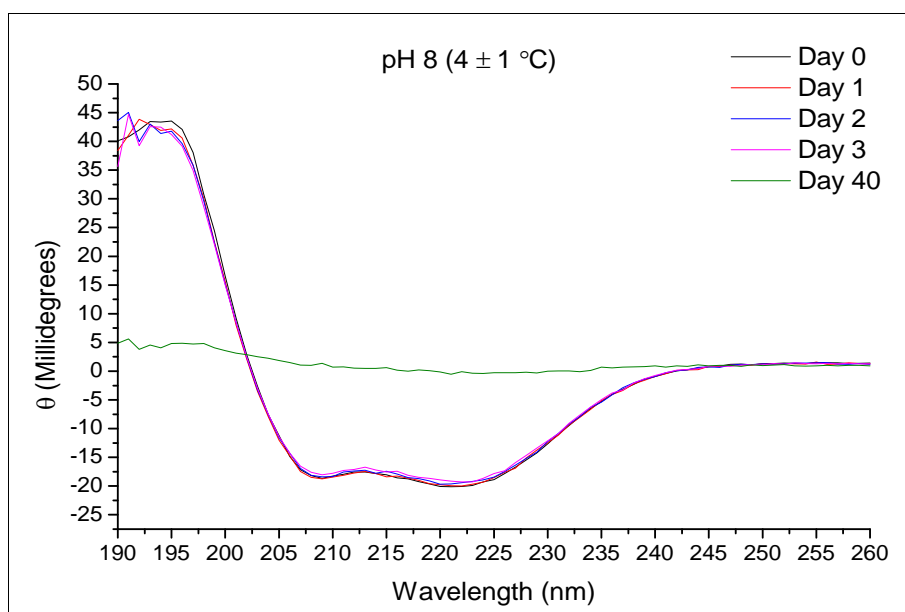


Figure 30: CD spectra of bHb at pH 8 stored at 4 °C

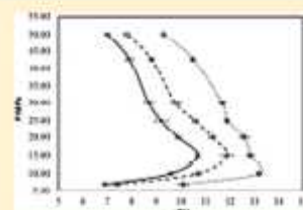
D.) Publications

Study of the Effect of Pressure on Melting Behavior of Saturated Fatty Acids in Liquid or Supercritical Carbon Dioxide

Vivek Trivedi,* Ruchir Bhomia, John C Mitchell, Nichola J Coleman, Dennis Douroumis, and Martin J Snowden

School of Science, University of Greenwich, Medway Campus, Central Avenue, Chatham Maritime, Kent, ME4 4TB United Kingdom

ABSTRACT: The melting point depression of saturated fatty acids (C_{12} – C_{18}) was investigated in liquid or supercritical carbon dioxide. The pressure and temperature melting point ranges were determined for each excipient in liquid or supercritical CO_2 . Additionally, the effect of pressure on the melting point of fatty acids was also more closely studied in the (7.0 to 50.0) MPa range. Untreated and CO_2 -treated samples were analyzed by differential scanning calorimetry (DSC) and X-ray diffraction (XRD). A melting point depression in the range (10.8 to 19.5) K was observed for the fatty acids studied in this work. The melting behavior of fatty acids in CO_2 was found to be dependent on pressure and carbon chain length. Melting temperature curves for each of the fatty acids in CO_2 exhibited a minimum as a function of pressure. Analysis by DSC and XRD indicated that CO_2 treatment had no impact on the morphological or crystallographic properties of these excipients under the selected experimental conditions.



INTRODUCTION

The development of new tools for materials processing and the substitution of traditional methods based on the use of organic solvents has intensified in the past decade. Since this time, the application of supercritical fluids has received increasing attention from the pharmaceutical, food, and biotechnology industries.

Supercritical fluids (SCFs) are defined as substances above their critical pressure (P_c) and temperature (T_c).¹ SCFs exist as a single phase which possesses properties of both liquids and gases. For example, the density of SCFs resembles that of a liquid whereas the diffusivity is akin to that of a gas. Properties such as density, viscosity and diffusivity can be easily tuned by manipulating the operational pressure and temperature.² A number of different SCFs including water, nitrogen, short chain alkanes and acetone have been used in various applications such as organic synthesis, cleaning and materials processing. However, CO_2 is the most widely used because it is environmentally benign, nontoxic, nonflammable, noncorrosive, readily available, inexpensive, and easy to remove from the reaction systems in comparison with many organic solvents. Moreover, CO_2 with low T_c (304.3 K) and P_c (7.38 MPa) also presents exciting prospects in the processing of thermo-labile materials with relevance to pharmaceuticals and biotechnology.³

In general, supercritical carbon dioxide ($SCCO_2$) is an excellent solvent for many nonpolar (and some polar) low molecular weight compounds and selected polymers, such as amorphous fluoropolymers and silicones.^{4,5} However, the solubility of numerous pharmaceutically significant excipients such as fatty acids in liquid carbon dioxide (LCO_2) or $SCCO_2$ is very low and usually requires the addition of a cosolvent. Conversely, the solubility of $SCCO_2$ in many polymers, fats, and fat derivatives is substantial and it acts as a plasticizer which

causes a depression in melting (T_m) or glass transition (T_g) temperatures.^{5–7} The melting point of a pharmaceutical excipient is a crucial physical property which determines its appropriateness in various pharmaceutical processes and applications.⁸ LCO_2 and $SCCO_2$ are known to alter the melting points of various polymers and ionic salts.^{9,10} Dissolution of CO_2 increases the free volume of an excipient by dissolving into the intermolecular spaces and causing a substantial reduction in T_m or T_g . Dissolved CO_2 also reduces the viscosity of molten excipients which improves mixing, blending and flow characteristics of the melt.¹¹ Moreover, it can also alter various other physical properties such as density, diffusivity and swollen volume of an excipient.^{7,11} The depression in melting point allows organic solvent-free processing at low temperatures. Particles from gas saturated solution (PGSS) processes can be successfully performed at lower temperatures if the reduction in T_m or T_g of an excipient has been determined. There are currently a number of studies which discuss the solubility of fatty acids (FAs) in $SCCO_2$, although information on the melting behavior of these excipients in LCO_2 and $SCCO_2$ is scarce.^{12–14} FAs being biologically inert, biocompatible and nontoxic have numerous applications in the pharmaceutical industry.¹⁵ FAs have also been studied previously in the development of drug delivery systems for different routes of administration i.e. fatty acid implants containing insulin,¹⁶ cyclosporine A loaded stearic acid nanoparticles,¹⁷ and cetuximab axetil containing stearic acid microparticles.¹⁸ The purpose of the present study was to determine the melting point depression of lauric, myristic,

Received: March 18, 2013

Accepted: May 7, 2013

Effect of Pressure on the Melting Point of Pluronics in Pressurized Carbon Dioxide

Ruchir Bhomia, Vivek Trivedi,^{*} John C. Mitchell, Nichola J. Coleman, and Martin J. Snowden

Department of Pharmaceutical, Chemical and Environmental Science, University of Greenwich, Central Avenue, Chatham Maritime, Kent ME4 4TB, United Kingdom

ABSTRACT: The melting points of Pluronic F-77, F-127, F-68, F-38, and F-108 were investigated in pressurized CO₂ between a pressure range of 2.0–50.0 MPa. Unprocessed and CO₂-processed Pluronic samples were analyzed by differential scanning calorimetry (DSC) and powder X-ray diffraction (PXRD). A melting point depression in the range of 18.1 (± 0.5 K) to 19.3 (± 0.3 K) was observed for all Pluronics studied in this work. The melting point of Pluronics in pressurized CO₂ was found to be independent of their molecular weight and poly(propylene oxide) [PPO] content. Analysis by DSC and PXRD revealed that CO₂ processing had no impact on the morphology of Pluronics.

INTRODUCTION

Any substance above its critical temperature and pressure can be defined as a supercritical fluid.¹ A supercritical fluid has liquidlike density and gaslike diffusivity, which can also be tuned by varying the operational temperature and pressure.² Supercritical CO₂ (sCCO₂) is, by far, the most commonly used supercritical fluid, because of its low critical temperature (304.3 K) and critical pressure (7.33 MPa). Moreover, it is readily available, nontoxic, nonflammable, noncorrosive, inexpensive, environmentally benign, and easy to remove from reaction systems. sCCO₂ has found its use in the chemical industry as an alternative to organic solvents, and it is also considered to be desirable for the processing of thermolabile materials.^{3,4} Supercritical fluid technology has applications in a variety of fields, such as extraction, cleaning, synthesis, etc.⁵ One such application includes polymer processing. The interaction of CO₂ with polymers is an interesting phenomenon and plays a significant role in various polymer processing operations.^{6–8}

The depression in melting point (T_m) or glass-transition (T_g) temperature in polymers, because of the sorption of CO₂, is a well-known phenomenon that is dependent on various factors, such as crystallinity and presence of CO₂-philic moieties.^{9–14} Amorphous polymers are reported to show higher interactions with CO₂ than crystalline polymers.^{15,16} These interactions can be enhanced by the incorporation of functionalities, e.g., ether linkages, carbonyl, and fluoro groups.^{8,16–19} The reduction in T_m or T_g is a colligative property, which is simply not a hydrostatic pressure effect but is dependent on the CO₂-polymer interactions.⁸ This phenomenon provides an exciting opportunity for the processing of polymers at low temperatures in operations such as coating, impregnation, and particle engineering.

Pluronics or poloxomers (nonproprietary name) are block copolymers consisting of hydrophilic poly(ethylene oxide) [PEO] and hydrophobic poly(propylene oxide) [PPO] segments arranged in a PEO–PPO–PEO triblock structure (A–B–A). The structure of a pluronic block copolymer is presented in Figure 1.

Pluronics are synthesized by sequential polymerization, where the PPO block is synthesized followed by growth of

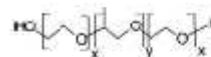


Figure 1. Generalized structure of a pluronic molecule, where x and y are positive integers.

PEO chains at both ends of PPO block. This reaction is generally carried out in the presence of an alkaline catalyst such as sodium hydroxide, which is then neutralized and removed.²⁰ Pluronics are semicrystalline in nature, where PEO units impart crystallinity to the polymer.^{21,22} The physical properties of Pluronics are dependent on their molecular weight and PPO–PEO ratios. Pluronics studied in this work are all solids at room temperature, and other properties such as molecular weight, melting point and PPO–PEO ratios are presented in Table 1. The polydispersity index of F-68 and F-127 has been reported in the literature to be 1.4.²³

Pluronics are generally regarded as safe (GRAS) and listed in the U.S. and British Pharmacopoeia.²⁵ They are widely used excipients as antifoaming agents, wetting agents, dispersants, thickeners, and emulsifiers.^{26–28} Pluronics interact with hydrophobic surfaces and biological membranes due to their amphiphilic nature and have been shown to modify the biological response by overcoming drug resistance in cancer and promoting drug transport across cellular barriers.^{20,29}

The solubility of low-molecular-weight Pluronics in CO₂ has been discussed in the literature; however, information on its interaction with higher-molecular-weight Pluronics is uncommon.^{3,19,30} The objective of this work was to study the effect of PPO–PEO ratio, molecular weight, and pressure on the melting behavior of higher-molecular-weight Pluronics in CO₂.

Received: March 31, 2014

Revised: June 11, 2014

Accepted: June 13, 2014

Published: June 13, 2014



Contents lists available at ScienceDirect

International Journal of Pharmaceutics

journal homepage: www.elsevier.com/locate/ijpharm

Influence of the preparation method on the physicochemical properties of indomethacin and methyl- β -cyclodextrin complexes



Shashi Kavi Suman Rudrangi^{*}, Ruchir Bhomia, Vivek Trivedi, George J. Vine, John C. Mitchell, Bruce David Alexander^{*}, Stephen Richard Wicks

Medway Centre for Pharmaceutical Sciences, University of Greenwich, Central Avenue, Chatham, Maritime, Kent, ME4 4TB, United Kingdom

ARTICLE INFO

Article history:

Received 7 November 2014

Received in revised form 6 January 2015

Accepted 7 January 2015

Available online 8 January 2015

Keywords:

Indomethacin

Methyl- β -cyclodextrin

Inclusion complexes

Spray drying

Supercritical carbon dioxide

ABSTRACT

The main objective of this study was to investigate different manufacturing processes claimed to promote inclusion complexation between indomethacin and cyclodextrins in order to enhance the apparent solubility and dissolution properties of indomethacin. Especially, the effectiveness of supercritical carbon dioxide processing for preparing solid drug-cyclodextrin inclusion complexes was investigated and compared to other preparation methods. The complexes were prepared by physical mixing, co-evaporation, freeze drying from aqueous solution, spray drying and supercritical carbon dioxide processing methods. The prepared complexes were then evaluated by scanning electron microscopy, differential scanning calorimetry, X-ray powder diffraction, solubility and dissolution studies. The method of preparation of the inclusion complexes was shown to influence the physicochemical properties of the formed complexes. Indomethacin exists in a highly crystalline solid form. Physical mixing of indomethacin and methyl- β -cyclodextrin appeared not to reduce the degree of crystallinity of the drug. The co-evaporated and freeze dried complexes had a lower degree of crystallinity than the physical mix; however the lowest degree of crystallinity was achieved in complexes prepared by spray drying and supercritical carbon dioxide processing methods. All systems based on methyl- β -cyclodextrin exhibited better dissolution properties than the drug alone. The greatest improvement in drug dissolution properties was obtained from complexes prepared using supercritical carbon dioxide processing, thereafter by spray drying, freeze drying, co-evaporation and finally by physical mixing.

Supercritical carbon dioxide processing is well known as an energy efficient alternative to other pharmaceutical processes and may have application for the preparation of solid-state drug-cyclodextrin inclusion complexes. It is an effective and economic method that allows the formation of solid complexes with a high yield, without the use of organic solvents and problems associated with their residues.

© 2015 Elsevier B.V. All rights reserved.

1. Introduction

Poor water solubility and the resulting low oral bioavailability of drugs is one of the major challenges encountered by drug discovery and development scientists (Lipinski et al., 1997; Leuner and Dressman, 2000). Various approaches to enhance the solubility and dissolution rate of drugs have been reported (Strickley, 2004; Vasconcelos et al., 2007). Inclusion complexation

of drug molecules with cyclodextrins has been extensively used to improve the solubility and dissolution rate of drugs (Mura et al., 1999; Nagase et al., 2001; Jain and Adeyeye, 2001; Bandi et al., 2004; Jambhekar et al., 2004).

Cyclodextrins are macrocyclic oligomers of α -D-glucose with a hydrophilic exterior and a lipophilic central cavity. The interior cavity of cyclodextrin can harbour a poorly water soluble drug, whilst the hydrophilic exterior increases its apparent solubility (Bodor, 1993).

Several processing methods have been developed to prepare drug-cyclodextrin inclusion complexes in the solid-state, e.g. grinding (Mura et al., 2001), kneading (Moyano et al., 1995; Saldústio et al., 2009), roll mixing (Nozawa et al., 1997), ultrasound compaction (Hiri et al., 1997), co-precipitation from various solvents (Montassier et al., 1997), freeze-drying (Pase-Vilanova et al., 2001) and spray drying (Moyano et al., 1997). Most of these

Abbreviation: Me- β -CD, methyl- β -cyclodextrin; SC-CO₂, supercritical carbon dioxide; SEM, scanning electron microscopy; DSC, differential scanning calorimetry; XRPD, X-ray powder diffraction; DP, percent drug dissolved; DE, dissolution efficiency.

^{*} Corresponding authors. Tel.: +44 2083318209; fax: +44 2083315805.

E-mail addresses: S.R.Rudrangi@greenwich.ac.uk (S.R.S. Rudrangi),

B.Alexander@greenwich.ac.uk (B.D. Alexander).

<http://dx.doi.org/10.1016/j.ijpharm.2015.01.010>

0378-5173/© 2015 Elsevier B.V. All rights reserved.